INVESTIGATION INTO INTERFACIAL TRANSPORTS AND EXCHANGE FLOWS FOR LAKE MODELS

by

© BASSEM M.F. EID, B.Sc., M.Eng.

A Thesis

Submitted to the School of Graduate Studies in

Partial Fulfillment of the Requirements

for the Degree

Doctor of Philosophy

McMaster University

February 1981

DOCTOR OF PHILOSOPHY (1984)
(Civil Engineering)

McMASTER UNIVERSITY
Hamilton, Ontario

TITLE: Investigation into Interfacial Transports and Exchange Flows for Lake Models

AUTHOR: Bassem M.F. Eid, B.Sc. (Cairo University)
M.Eng. (McMaster University)

SUPERVISOR: Dr. W. James

NUMBER OF PAGES: xvi, 208

To My Parents

ABSTRACT

Many lakes act as receiving waters for polluted runoff and other effluents. Water quality problems in lakes depend for their management on numerical lake transport models. Lake transport models have recently become quite detailed and realistic. However, a difficulty still facing this field is the determination of the interfacial transports at the boundaries and related model parameters. Numerical modeling of lake physics and bio-chemistry requires special treatment of the boundaries at the air-water interface, sediment-water interface at the bottom of the lake and horizontal densimetric fluxes of active materials across the lake boundaries into and out of the lake. This latter problem is particularly complex when two interconnected lake basins of dissimilar characteristics exchange flow via a communicating channel.

In this study, the following important parameters were derived and related to lake and flow conditions: surface drag coefficients, vertical eddy diffusion coefficients and bottom roughness.

At the air-water interface, momentum transfer is studied and the over-water wind stress is determined using the logarithmic wind velocity distribution and Von Karman's integral equation for turbulent flow over a rough movable surface of variable roughness. Thus the wind drag coefficient is determined as a function of wind-and-wave characteristics.

At the lake bottom, shear stress due to a very rough lake bed, with weed growth, is determined as a function of local parameters such

as weed length and distribution. The approach is particularly suitable for shallow lakes with considerable roughness. Also, vertical transports at the sediment-water interface and in the water column above the sediments is studied using two natural tracers: temperature and Radon-222 isotope. Vertical eddy diffusivity in the lower layers of a lake is determined as a function of depth and time by using the observed temperature and Radon profiles.

At the lateral boundary, exchange flow between two interconnected stratified bodies of water is investigated. The local exchange is modeled through a proper treatment of stratified flow at the open boundaries at the two ends of the "connecting channel" and proper presentation of the effect of the adjacent basins.

Numerical models are developed to study the above processes and boundary conditions. The computational algorithms are tested for theoretical and computational performance. Numerical models are tested against available field observations at Valens reservoir, Hamilton harbour, Baldeggersee (Switzerland) and Lake Erie.

A three-dimensional hydrodynamical model of lake currents is applied to two, non-stratified and stratified, lakes during summer periods where field observations were carried out: Valens reservoir and Hamilton harbour.

ACKNOWLEDGEMENTS

I wish to express my sincere gratitude to Dr. W. James for his invaluable guidance and encouragement during the course of this study. I would also like to acknowledge with gratitude the assistance and guidance of Farrell Boyce. Special thanks are due to Dr. A.A. Smith for the provision of his subroutine-library of stratified flow and for his continuous encouragement, and to Dr. T.J. Simons for the use of his three-dimensional hydrodynamic model. In addition, I wish to record with gratitude the assistance and encouragement of Drs. D. Lam, P. Hamblin, C.R. Murthy and H. Donelan of CCIW and Drs. W. Snodgrass and J. Vlachopoulos for their continuing interest in the work.

It has been a pleasure to work with Dr. D. Imboden of EAWAG, Switzerland and I wish to thank him for the use of the data we collected there in this study.

I would also like to show appreciation to my family and friends for the encouragement which they freely gave. Thanks also to Betty Petro of the Word Processing Centre for typing the thesis.

This work was made possible by the research grants to Dr. W. James from National Water Research Institute, CCIW, Ontario Ministry of the Environment, Science and Engineering Research Board of McMaster University and NSERC.

TABLE OF CONTENTS

CHAPTER V (cont.)

PART 2: PRACTICAL APPLICATIONS

CHAPTER VI: APPLICATION TO REAL LAKES: MODELING WIND-DRIVEN CURRENTS IN VALENS RESERVOIR AND HAMILTON HARBOUR

CHAPTER VI (Cont.)

PART 3: CONCLUSIONS AND REMARKS

LIST OF FIGURES

LIST OF FIGURES (Cont.)

LIST OF FIGURES (Cont.)

LIST OF TABLES

PART 1

BACKGROUND THEORY AND MODEL DEVELOPMENT

CHAPTER I

SCOPE AND OBJECTIVES OF THE STUDY

1. INTRODUCTION

Recently there has been increased interest in using numerical hydrodynamic models for scientific and practical purposes in order to explore lake processes. A large amount of field, laboratory and theoretical work has been done on the physical processes and their interaction with chemical and biological processes in a water body. Water quality problems in many lakes, especially in the Great Lakes, depend for their solution on lake transport models. In the last few years numerical models of lake transport have become quite detailed and realistic.

The dynamics of chemical and biological reactions in lakes are determined by the interplay of reaction kinetics and material transport mechanisms. The latter include "macro-processes" (i.e., advection, turbulence, particle settling, etc.) and "micro-processes" (i.e., molecular diffusion through boundary layers, transfer processes at cell membranes, etc.). This study deals with the "macro-processes", i.e., with transport mechanisms in lakes and the treatment of different boundary conditions which are necessary for modeling such transports. This is a classical problem of hydrodynamics for which, in fact, a set of differential equations exists. Yet, since the equations are nonlinear and have complex boundary conditions, analytical solutions can

only be found for special cases, where numerical solutions may be impossible to attain because they strongly depend on external forces and may require continuous or nearly continuous data collection. Under these circumstances, oceanographers and limnologists have developed some simplified concepts to approximate the hydrodynamical behaviour of their systems.

One simplification is introduced by describing the complex pattern of turbulence with a few empirical parameters; the coefficients of eddy diffusion. Another approach may be used in comparing typical time rates for mixing and reaction in order to select those mixing processes which are fast relative to in-situ reactions and thus can be replaced by the concept of homogeneous mixing. In fact, in many lakes and for most biological reactions horizontal mixing belongs to the class of fast processes. On the other hand, due to strong density gradients typical of stratified lakes, vertical mixing may be much slower than in-situ reactions and may result in large vertical gradients for those chemical species involved in the reaction. Therefore, the methods used in the analysis of homogeneous flows can be extended to some simple cases of multi-layer flow sytems.

Most models that include both friction and time-dependent flow have been applied to specific real basins; the modelers have not attempted to generalize their results. In other words, most of these models use constant values of certain parameters, such as wind drag coefficient, bottom friction and eddy diffusivities. Extensive research is required to establish more generalized and reliable approaches and to

relate these parameters to lake and flow characteristics. For example, the drag coefficient at water surface as a function of wind-and-wave characteristics, and bed friction may be described as a function of local roughness and currents near the bottom.

Numerical modeling of lake physics or bio-chemistry requires special treatment of the boundary conditions at the water surface and the bottom of the lake. In many cases, it is also necessary to account as fully as possible for all fluxes of the active materials across the lake boundaries. This problem is particularly complex when two interconnected lake basins of dissimilar characteristics exchange water through a communicating channel. A substantial portion of the interchange is wind induced, and therefore variable, and the flow is also influenced by bottom topography and stratification in both basins.

2. OBJECTIVES

The main objective as sketched out in Figure 1.1, is to study the different boundary conditions and related physical processes necessary in the modeling of lake transports. This includes the determination of the following important parameters: surface drag coefficients, vertical eddy diffusion coefficients and bottom roughness, and relate them to the lake and flow characteristics. The momentum transfer at the air-water interface, shear stress due to very rough lake bed, vertical transports at the sediment-water interface and in the water column above the sediments as well as the exchange flow between two interconnected stratified basins are considered. Numerical models are developed to

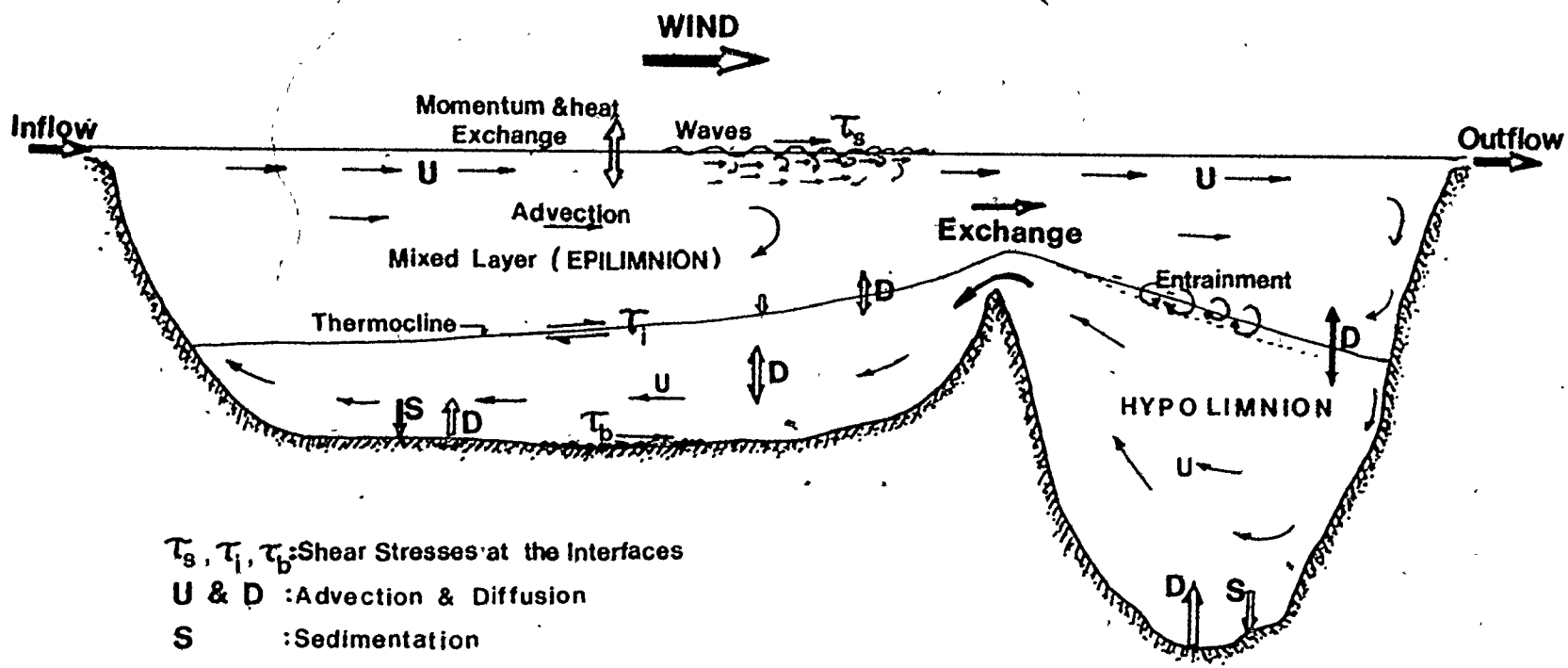

Figure 1.1 Schematic Diagram of Interfacial Transports and Exchange Flow in a Lake

study these processes and boundary conditions. The models are applied to real lakes of various sizes and characteristics.

In order to attain the above objectives, the processes and their interactions in the hydrodynamical equations listed below are studied.

(1) Wind-induced surface shear stresses

A preliminary attempt is carried out to calculate the drag coefficient at the air-water interface as a function of wind-and-wave conditions. Thus temporal and spatial variations of the shear stresses over the lake surface can be considered when solving the lake transport hydrodynamical equations. The mechanism of momentum transfer from the air to the water surface is studied. A numerical model is developed and applied to Hamilton Harbour, at the western end of Lake Ontario (about 4.8 x 8 km; maximum depth of 24 m) and Valens reservoir; a recreational small lake (about 0.75 km^2 and maximum depth of 4 m).

(2) Bottom roughness due to very rough - flexible elements

Formulation of the boundary conditions at the bed, for a three-dimensional transport model, is another important task to be considered especially for small shallow lakes with considerable bed roughness and more especially for lakes with weed growth. In such lakes bottom roughness becomes an important term in the hydrodynamical equations. The local bottom roughness is related to the roughness parameters, i.e., weed length and density. The model was developed by the author in a previous study (Eid, 1976) and applied to study

wind-driven currents in Valens reservior, a small shallow man-made lake suffering from extensive weed growth. The work is revised using the results obtained in the present study.

(3) Vertical mixing in stratified lakes

The application of observed temperature and natural radon-222 isotope to the determination of vertical eddy diffusion in lakes is studied. Radon-222 isotope is applied as a natural tracer for studying vertical transports at the water-sediment interface. Vertical eddy diffusion coefficient is determined as a function of depth and time by using the traditional "temperature method". The results may be used for the prediction of the distribution of a dissolved substance in the hypolimnion waters of a lake. The model is applied to a "typical" small Swiss lake (1.5 x 4.5 km; maximum depth 66 m).

(4) Interbasin exchange flow

The main thrust of the present study is to lay the groundwork for numerical modeling of the exchange flow between two interconnected stratified basins. A literature survey of possible hydrodynamic models is presented. The application of the model is centered on the interchange of water between the shallower Central Basin and the deeper Eastern Basin of Lake Erie during stratification periods, but, the model is general enough to treat similar problems. The philosophy here is to develop a rather simple model of the local exchange flow at the "channel" connecting two lakes or two basins of a lake. The main

difficulty here is the treatment of the open boundaries at the two ends of the communicating channel and the proper presentation of the effect of adjacent basins. In the present attempt, several assumptions are made based on field observations. A two-layer, one-dimensional, steady-state model is developed. Such a model is helpful in studying the relative importance of the different terms in the dynamic equations of the exchange flow. Solutions of initial-value and boundary-value problems are presented for channels of arbitrary geometry. Special treatment of critical flow and the singular solution for stratified flow is considered.

Each of the above topics is treated as a computational algorithm; the theoretical background is laid out and a numerical model is developed. These models are applied to different lakes and the models' predictions are then compared to the available field observations or to data collected from other studies in the literature.

Since the present study aims at developing computer models to determine different parameters and boundary conditions which are necessary for modeling of lake transports, it is advantageous to apply each model to a different lake where this particular parameter or process is dominant. The effect of this particular process or boundary condition on the lake transports can then be examined. Thus, an important aspect of the present study is the practical application of these new computer models to a variety of real lakes of various sizes and characteristics.

In the following section, a general background reivew of related

hydrodynamic models is presented. The next four chapters (II to V) include a review, definition, analysis and development of numerical solutions of the four topics listed above. Part 2 presents the applications of these models to real lakes; this includes sensitivity analysis and model verification. Finally, the summary and conclusions are presented in Part 3.

3. REVIEW OF RELATED HYDRODYNAMICAL MODELS

3.1 Introduction

This section furnishes the groundwork for the numerical modeling studies on the topics previously mentioned. A background review of lake hydrodynamic models is presented. A literature survey of related studies is also included.

3.2 Lake Transport Models

Lake Modeling proceeded from relatively simple models in which the lake is represented by one homogeneous layer, eg. Wellander (1959), Platzman (1963), and Liggett and Hadjitheodoron (1969). Such models assume steady-state conditions. The steady-state theories have largely been confined to a study of the linearized, vertically integrated equations for flow in homogeneous lakes. These methods are useful in studying winter average currents in lakes.

Most observers believe that the time history of the wind is at least as important as the instantaneous value. However most of the existing theories assume steady-state flow or quasi-steady state, e.g.,

Wellander (1957), Gedney and Lick (1972).

Much of the inviscid time-dependent theory is due to G.T. Csanady (1967, 1968 a,b). He studied the response of a two-layer lake of constant depth to a uniform wind stress.

Several three-dimensional, time-dependent models of lake currents have been developed. The more sophisticated of these include variable density effects. Such models require large computer storage and they are very expensive to run.

An alternative approach in the study of the three-dimensional circulation structure is the use of well known multi-layer models, e.g. Simons (1971, 1972, 1973), Leendertse (1973, 1975) and Lick (1976). In these models the lake is divided into several horizontal layers and the interfaces between layers (except at the free surface), are assumed to be permeable and of fixed position in space, through which the fluid moves vertically. The free surface (or thermocline) is treated as an impermeable movable surface. Integration of the hydrodynamic equations of motion and continuity is performed for each layer to arrive at a system of equations in terms of the layer-average variables. Interlayer stresses and the bottom resistance are expressed as functions of the layer-averaged velocity. These hydrodynamic equations are solved using finite-differences method.

The study of water quality of near-shore shallow areas of the Great Lakes is very important because of locally introduced contaminants and also due to the particular importance of the near shore region for recreation. Lick (1976) used different numerical grid sizes; finer size

near the shore, when modeling currents in Lake Erie. Csanady (1972) and Bennett (1974) found that the currents in the shore region differ markedly from those in the central region of Lake Ontario. They suggested that stratification, inertial acceleration (non-linear advection), bottom topography and friction may all be important in the boundary region of large lakes, or throughout small shallow lakes.

Although there are a large number of studies on the Great Lakes, e.g., Csanady (1967, 68, 72), Lick (1976) and Simons (1973, 76), there are a surprisingly small number of studies regarding circulation in basins of much smaller dimensions, e.g., recreational lakes in North America. Lith and Bengtsson (1971), and Bengtsson (1973) studied wind-driven currents in small lakes in Sweden. In the author's previous study on wind-driven currents in a recreational small lake (Valens reservoir), Eid (1976), it was found that bottom topography and roughness, shore configuration, and vertical eddy viscosity are all important in modeling such lakes. Coriolis forces should also be considered even for such small lakes.

The study of water quality in such lakes is very important as many of these lakes suffer from extensive nutrient loading and the quality of water is often not satisfactory for recreation purposes. More emphasis should be made on the determination of model parameters in a more general and rational way.

3.2.1 General considerations in modeling lake transports

The currents in enclosed lakes (e.g., Great Lakes) are primarily driven by the wind. Currents due to through flows are comparatively small except locally near the mouths of the rivers. In addition, temperature, and hence density, gradients cause currents or modify the existing currents. This effect must be considered in a study of lake circulation during the late spring, summer, and early fall when stratification occurs and the density gradients are large.

The model developed by T.J. Simons (1973), for circulation in Lake Ontario, has been modified and used in the present study. The common hydrodynamic equations for lake currents have been used. The flow is assumed to be incompressible and in hydrostatic equilibrium. The lake is considered to consist of a number of horizontal layers. This concept of the "layers" is a geometrical concept only, and should not be confused with the layers in stratified flow. Layer thickness may be taken to be a function of temperature or density gradient. The hydrodynamic equations (conservation of mass and momentum or energy) are integrated over each layer. This system of partial differential equations are numerically solved using a suitable finite-difference scheme in time and space (for more details, see Simons 1973 and Eid 1976).

3.2.2 Basic Model Equations

The integrated non-linear equations of motion, continuity and heat flux for a multi-layered lake system with U, V, P and T representing the layer averages of particular layer k, and k ± 1/2 as a subscript designating interface values of the layer, are:

1. Momentum equations:

$$\frac{\partial U_k}{\partial t} = fV_k - \frac{h}{\rho}\frac{\partial P}{\partial x} + (\tau^{xz}/\rho)_{k+1/2} - (\tau^{xz}/\rho)_{k-1/2} + A_h\left(\frac{\partial^2 U}{\partial x^2} + \frac{\partial^2 U}{\partial y^2}\right)_k \tag{1.1}$$

$$\frac{\partial V_k}{\partial t} = -fU_k - \frac{h}{\rho}\frac{\partial P}{\partial y} + (\tau^{yz}/\rho)_{k+1/2} - (\tau^{yz}/\rho)_{k-1/2} + A_h\left(\frac{\partial^2 V}{\partial x^2} + \frac{\partial^2 V}{\partial y^2}\right)_k \tag{1.2}$$

2. Continuity equation, integrated from the bottom to the water surface:

$$\frac{\partial \xi}{\partial t} + \sum_{L=1}^{b}\left(\frac{\partial U}{\partial x} + \frac{\partial V}{\partial y}\right)_L = 0 \tag{1.3}$$

3. Heat balance equation, neglecting sources and sinks of heat:

$$\frac{\partial (hT)_k}{\partial t} + \frac{\partial (UT)_k}{\partial x} + \frac{\partial (VT)_k}{\partial y} + (wT)_{k-1/2} - (wT)_{k+1/2}$$

$$= hK_x\left(\frac{\partial^2 T}{\partial x^2} + \frac{\partial^2 T}{\partial y^2}\right)_k + \left(K_z\frac{\partial T}{\partial z}\right)_{k+1/2} - \left(K_z\frac{\partial T}{\partial z}\right)_{k-1/2} \tag{1.4}$$

4. The integrated hydrostatic pressure equation:

$$P = \rho_o g(\xi - z) + \int_{-z}^{\xi} \sigma dz \qquad (1.5)$$

and $\sigma = (\rho - \rho_o)$ is a measure of the density anomaly.

From the equation of state:

$$\sigma = -\varepsilon (T - T_o)^2 \qquad (1.6)$$

where U and V are the integrated layer transport components in x and y directions,

x, y are horizontal coordinates, positive to the east and north, respectively,

z is the vertical coordinate, positive upward from the mean still water level,

u, v, and w are the average layer velocity components along these axes, respectively,

t is time (sec),

f is Coriolis parameter (for Hamilton harbour = 10^{-4} radians/sec.),

ρ is the water density for a given layer at a given temperature,

ρ_o is the maximum density of the water (at 4^oC),

ξ is the fluctuation of the free-surface elevation measured from the still water level,

P is the pressure at any point,

T is the temperature at any level,

T_o is the temperature of maximum water density = 4^oC,

τ^{xz}, τ^{yz} are the interfacial shear stress components in x and y directions,

A_v and A_h are the vertical and horizontal eddy viscosities,

K_z and K_x are the vertical and horizontal eddy diffusivities of heat,

h is a layer thickness,

g is the gravitational acceleration, and

ϵ is a constant and has a value = $-6.8 \times 10^{-6}{}^{o}C$ (Simons 1973).

L is the layer number

b is the total number of layers

The above system of differential equations is used to compute three-dimensional lake transport for given initial and boundary conditions. These boundary conditions are:

at the free surface; $z = \xi$:

$$\tau^{xz} = \tau_{sx} \; ; \; \tau^{yz} = \tau_{sy} \tag{1.7}$$

where τ_{sx} and τ_{sy} are the wind shear stresses in x and y directions. This stress is discussed in more detail Chapter II of this thesis (see also, James and Eid 1978a). As a preliminary simplification of the model, the heat flux at the water surface as well as other sources and losses of heat are set equal to a constant or to zero. This is acceptable for non-continuous simulation. At an interface between any two layers:

$$\tau^{xz} = \rho A_v \frac{\partial U}{\partial z} \; ; \; \tau^{yz} = \rho A_v \frac{\partial V}{\partial z} \tag{1.8}$$

Bengtsson (1973) suggested that vertical eddy viscosity (A_v) is related to the depth of the lake and wind speed through the relation:

$$A_v = C.H.W_a \tag{1.9}$$

where C is a constant, H is the lake depth (cm) or the depth of the mixed layer and W_a is the wind speed (cm/s). this equation is valid for shallow lakes (H < 15 m). the author (Eid 1976) has successfully applied (1.9) in previous study on small shallow lakes (H = 4 m); C was taken to be 2×10^{-5}.

In Chapter IV of the thesis, the vertical eddy diffusivities (K_z) are determined as a function of the depth and time using the measured temperature profiles and radon-222 concentration near the lake bottom (Imboden, Eid and Joller 1979).

At the bottom where z = -H:

$$\tau^{xz} = \tau_{bx} = \rho K_b \frac{(U_b^2 + V_b^2)^{1/2}}{h_b^2} U_b$$

$$\tau^{yz} = \tau_{by} = \rho K_b \frac{(U_b^2 + V_b^2)^{1/2}}{h_b^2} V_b \qquad (1.10)$$

where

τ_{bx} and τ_{by} are bottom shear stress components in x and y directions,

U_b and V_b are the integrated bottom layer transport components,

h_b is the thickness of bottom layer, and

K_b is a non-dimensional skin friction coefficient.

In most lake models the skin friction coefficient has been taken to be constant throughout the lake. In Chapter III of this study the bottom friction coefficient has been expressed as a function of local large scale roughness due to weed growth. Thus, the bottom shear stress can be varied spatially and temporally in the solution scheme for the

hydrodynamic equations for such lake models (James and Eid 1978b). In addition to the above boundary conditions, the components of velocity and heat flux normal to the solid boundary vanish at that boundary. Surface currents can be determined by extrapolation of the layers' horizontal velocity components to the water surface.

3.2.3 Numerical Solution

The numerical method developed by Simons (1973) is the basis of the transport model which is used in this study, but of course modifications are necessary to calculate wind-driven currents in small lakes, such as Valens reservoir and Hamilton harbour (Chapter VI). Details of the finite-difference scheme can be found elsewhere (Eid 1976; James and Eid 1978a,b).

3.2.4 Numerical Stability

In the numerical calculation of space and time-dependent lake problems, for efficiency one would like to use as large space and time steps as are consistent with accuracy and the physical details desired. However, there are usually other restrictions on the allowable space and time steps which might affect the stability of the numerical method used in the calculation. For example, consider the explicit, forward-time, central-space scheme used in the numerical solution in this study. Simple theory indicates that limits on the time step Δt and space steps Δz and Δx in the vertical and horizontal directions are approximately given by (Lick 1976):

(a) $$\Delta t < \frac{\Delta x}{\sqrt{gH_{max}}}$$

where H_{max} is the maximum water depth.

This means that the numerical time step must be less than the time it takes a surface gravity wave (of celerity = $\sqrt{gH}$) to travel a grid distance Δx. For Hamilton harbour $\Delta t < 20$ seconds.

(b) $$\Delta t < \frac{(\Delta z)^2}{2A_v}$$

i.e. the time step must be less than the time for diffusion in the vertical. For example, assuming minimum $\Delta z = 1.0$ m and average A_v of order of 10 to 20 cm^2/sec, thus Δt should be of the order of 500 to 250 sec.

In the method used herein, the external (vertically averaged) and internal modes of the flow field are treated separately. The time step used in the calculation of the external modes is limited by the stability condition (a) (i.e. $\Delta t \leq 20$ sec.); for the internal structure it is limited by the second stability requirement (i.e. $\Delta t \leq 250$ sec.).

CHAPTER II

MODELING OF WIND-INDUCED DRAG AT THE AIR-WATER INTERFACE

1. INTRODUCTION

It is necessary to determine the shear stresses imposed as a boundary condition at a lake surface when solving the hydrodynamic equations of lake circulation mentioned in previous chapter. The total transfer of momentum from air to water is clearly the consequence of wind action. This wind stress locally has an important influence on the wind-wave interaction (including the generation of water surface setup, drift currents, and surface waves) as well as on the transfer of heat and mass through the air-water interface. The relation between wind stress and wind velocity is rather complicated as it depends on mean speed, gustiness, fetch and duration of the wind; on the degree of roughness of the water surface; on the previous history of waves and wave development; and on the stability state of the air flow. It is not surprising, therefore, that the treatment of turbulent energy transfer at the air-water interface, must still rely on empirical or semi-empirical relationships, often very difficult to verify experimentally.

One of the objectives of this study is to develop an algorithm to determine the wind drag coefficient C_d and consequently wind stress τ_o at the water surface as function of wind-and-water surface

characteristics to be used in the numerical modeling of lake transports.

A considerable amount of laboratory and field work has been carried out on wind-wave interaction. Most of the commonly used equations were developed for open sea conditions, where a number of investigators have concluded that the drag coefficient C_d is independent of wind fetch and duration and wave characteristics. They found that C_d is slightly dependent on wind speed and average values were used in most of the studies (see Kraus 1972; Garratt 1977). In enclosed bodies of water, however, this may not be the case, as lakes are subject to slower winds and the effect of the lake size (i.e. wind fetch and water depth) may play an important role in determining the drag coefficient (Donelan 1975; Graf and Prost 1980).

Many different values of the drag coefficient have been used in numerical modeling of oceans and lakes. In these studies, the drag coefficient was usually considered constant and its value was chosen to bring the model results into close agreement with the observations (e.g. Platzman 1963, Simons 1973, 1976; Leendertse 1973, 1975; Eid 1976).

It is interesting to notice that from many studies in both micrometeorology and oceanography or limnology, the micrometeorologists, through wind profile observations, have found that the drag coefficient is nearly constant and less than that used in numerical models of ocean and lakes by a factor of two or so. Because micrometeorologists measure drag for a fully developed wave field and for nearly steady wind conditions, the resulting values are low. Numerical models, on the other hand, do not use steady conditions and thus the roughness is not

fully developed. They usually use higher drag coefficients (Donelan 1975).

Thus the need to develop the functional dependence of the drag at the air-water interface on wind-and-surface conditions is obviously important. In this chapter, a literature review of recent studies is presented. Then, the methodology and model development are discussed. The model results are compared to some data obtained from literature, and results of model applications to two small lakes are presented in Chapter VI.

2. BACKGROUND REVIEW

Taylor (1916) reasoned that the horizontal reaction between the earth's surface and the moving atmosphere might be represented by a velocity-square law involving a non-dimensional factor known as the coefficient of skin friction or drag coefficient. The knowledge of this coefficient would allow the rate at which horizontal momentum is transferred from the atmosphere to a surface to be calculated. In succeeding years, comprehensive observations have indeed verified this law over land and sea (e.g. Deacon 1957; Phillips 1966; Kraus 1972; Dunckel et al. 1974, etc.). The quadratic relationship which has commonly been used in the bulk of the literature, is written:

$$\tau_o = \rho_a C_d |U_z| U_z \qquad (2.1)$$

where τ_o is the shear stress at water surface (or rate of momentum transfer), C_d is the surface drag coefficient, ρ_a is the air density and

U_z is the mean wind speed at a certain distance z above the water surface (usually taken to be 10 m).

Considerable advances made in turbulence theories and the advent of similarity theories for both atmospheric surface and boundary layers, allow the drag coefficient to be explicitly defined in terms of aerodynamic roughness, atmospheric thermal stability and other relevant physical parameters such as those connected with wind-wave generation (Deardorff 1972).

The wind velocity near the air-sea interface was reported by a great majorty of investigators to follow the Von Karman-Prandtl logarithmic distribution (Schlichting 1955; Charnock 1955; Phillips 1966; Wu 1968; Kraus 1972). For neutral stability case, the logarithmic profile is written:

$$U_z/U_* = 1/k \ln(Z/Z_o) \qquad (2.2)$$

where $U_*^2 = \tau_o/\rho_a$, k is the Von Karman universal constant = 0.4, and Z_o is the so-called "roughness length" or dynamic roughness.

The quantity Z_o can be defined vigorously only as a parameter which specifies a logarithmic profile some distance above the surface. It may be interpreted physically in a manner such that it specifies the scale of the turbulent eddies that are generated by the surface roughness elements (Kraus 1972). In flows over solid surfaces, the roughness length is usually determined by the nature of the surface. However, for stress over the sea, surface roughness itself is largely determined as part of the problem, rather than externally imposed.

Charnock (1955) suggested, on the basis of dimensional consideration, that Z_o, in aerodynamically rough flow, should depend only upon the shear velocity U_*, giving:

$$Z_o = \alpha U_*^2/g \tag{2.3}$$

where g is the gravitational acceleration and α is assumed to be constant. This equation has been used in various theoretical models. Several values of α were assigned in different studies (i.e. Charnock 1955; Wu 1969 and Garratt 1977; α = 0.012, 0.016 and 0.0144 respectively). More recently Kitaigorodskii (1968); Kitaigorodskii and Zaslavskii (1974), Hsu (1974) and Stewart (1974) considered the case of transitional flow, where α is not constant but exhibits variations dependent on the characteristics of the water surface and stability of the boundary layer such that:

$$Z_o\, g/U_*^2 = f(C/U_*,\ Z/L) \tag{2.4}$$

where C is the phase velocity of the dominant wave, C/U_* then describing the degree of wave development, or "wave age". The function Q(Z/L) represents the influence of the thermal stratification on the wind profiles (e.g. stability parameter; where L is the Monion-Oboukov length, see Deacon 1962; Kraus 1972). Davidson (1974) has shown that the momentum transfer is found to be influenced by both stability and wind-wave coupling. He studied the separate influences of stability and wind-wave coupling on the value of the drag coefficient. In most studies, however, neutral conditions were assumed where the stability

term vanished.

The wind speed dependence of C_d has been sought based on the prediction of equations (2.2) and (2.3); Equation (2.4) on the other hand, suggests that the dependence upon other parameters such as wind fetch and duration should be looked for. Perhaps because these seem to be of secondary importance for wind-wave interaction in open sea, the most of the published sources of C_d data (shown in Table 2.1) do not classify C_d accordingly; there is little or no quantitative information on fetch, wind duration, sea state, etc., with which we can categorize C_d in the present analysis. Their effects remain obscured in the data scatter of individual data sets (see Table 2.1 and Figures 2.1 and 2.2) and overall mean values determined by Garratt (1977) (Figure 2.3).

Kraus (1972, Chap. 5) argued that the data scatter, in part, may be due to the nonlinear nature of equation (2.1) and the effect of wind speed variance, while Garratt (1977) in his critical review of the drag coefficients over oceans and continents, suspected that much of the data scatter and systematic differences between data sets in Table (2.1) and Figure 2.3 are due to insufficiently long averaging periods and technical difficulties of making the measurements. On the other hand, as suggested by Stewart (1974), there may very well be some external parameters which have not yet been closely examined but which contribute importantly to this scatter; this will be discussed in following sections.

It is obvious from Table 2.1 and Figures 2.1, 2.2, and 2.3 that the observed values of the drag coefficients are much smaller, as

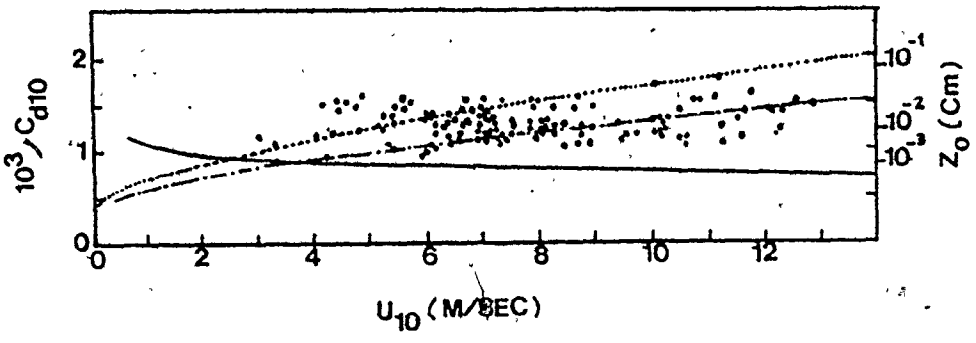

Figure 2.1 Drag coefficient and roughness length as a function of wind speed. The data were obtained under neutral conditions. The solid line is the smooth surface result. The other two curves correspond to Charnock formula $Z_o = U_*^2/g$ with α = 28.5 for the dotted line and α = 81 for dash-dot line (Redrawn from Brocks and Krugermeyer 1970, after Stewart 1974).

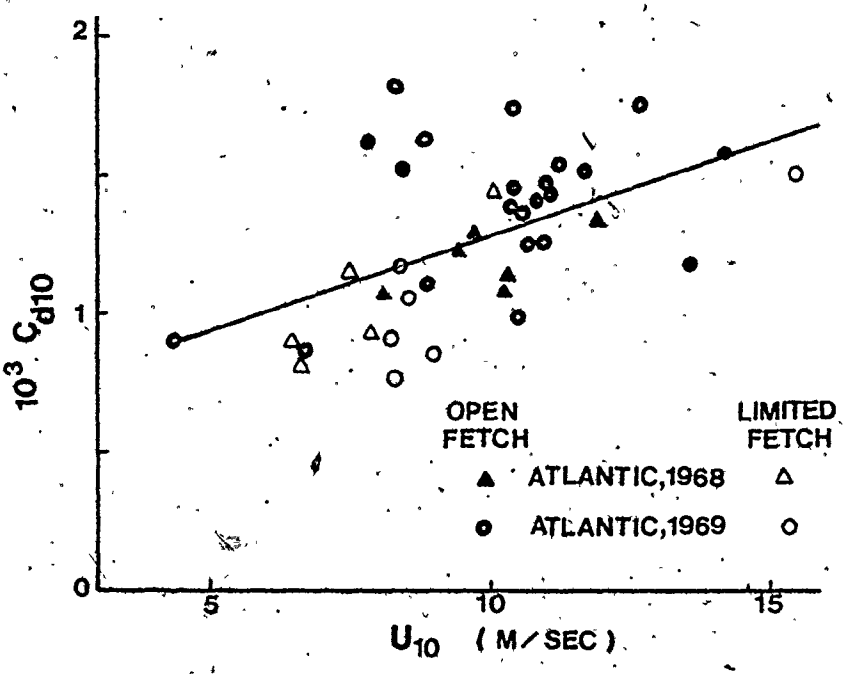

Figure 2.2 Drag coefficient versus wind speed observed at different sites (After Smith 1973)

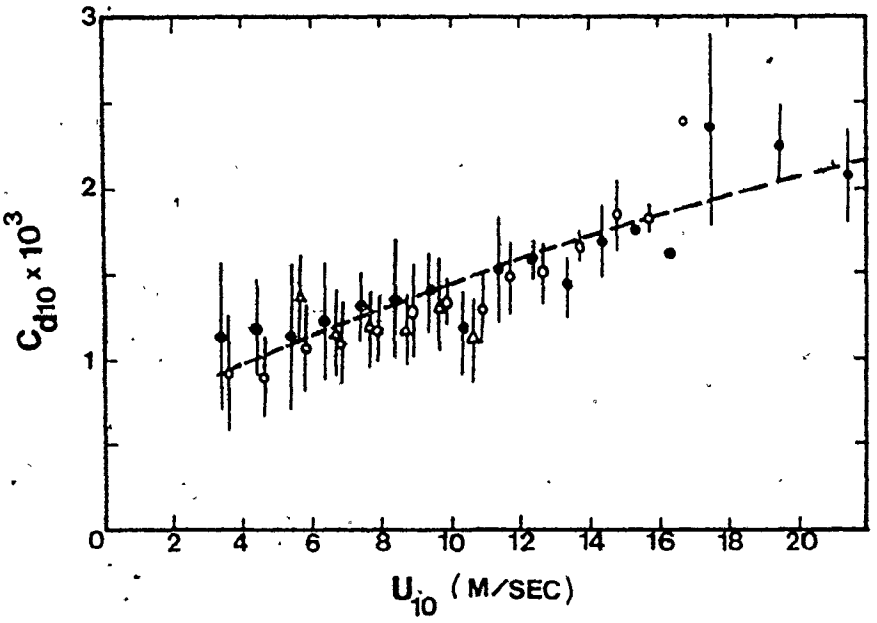

Figure 2.3 Neutral drag coefficient values as a function of wind speed at 10 m height, based on individual data taken from the recent literature (see Table 2 and text). Mean values are shown for 1 m s^{-1} intervals based on the eddy correlation method (•) and wind profile method (0); wind profile data are also shown (Δ) with Hoeber's (1969) [see Kraus (1972)] data included. Vertical bars refer to the standard deviation of individual data for each mean. The dashed curve represents the variation of $C_{DN}(10)$ with U_{10} based on $z_o = \alpha U_*^2/g$ with $\alpha = 0.0144$.

Table 2.1: Drag Coefficients for wind at 10 m level over water collected from the recent literature

Investigator	Wind Speed range (m/s)	$10^3 \times C_d$	Variability σ (%)	Method
1. Garratt (1977)	4-21	$0.51U^{0.46}$ or $0.75 + 0.067U$	-	summary of others observations
2. Smith and Banke (1975)	2.5-21	$0.63 + 0.066U$	$\pm$ 23	eddy correlation (ec)
3. Smith (1973)	2.5-21	$0.63 + 0.066U$	$\pm$ 23	thrust & sonic anemometers
4. Kondo (1975)	3-16	$1.2 + 0.025U$	$\pm$ 15	waves data
5. Davidson (1974)	5-12	1.44	?	eddy correlation (ec)
6. Dunckel et al. (1974)	2-12 2-12	1.39 1.26	? ?	wind profile (wp) Dissipation Method
7. Kitaigorodskii et al (1973)	3-11	0.9 (at 3 m/s) to 1.6 (at 11 m/s)	?	eddy correlation (ec)
8. Hicks (1972)	4-10	$0.5U^{0.5}$	$\pm$ 25	eddy correlation (ec)
9. Sheppard et al (1972)	2.5-16	$0.36 + 0.1U$	$\pm$ 20	wind prifile (wp)
10. Smith (1970)	3-20	1.35	$\pm$ 34	eddy correlation (ec)
11. Brocks and Krugermeyer (1970)	3-13	$1.18 + 0.016U$	$\pm$ 15	wind profile (wp) North Sea
12. Miyake et al (1970)	a. 4-9 b. 4-9	1.09 1.13	$\pm$ 20 $\pm$ 20	eddy correlation (ec) wind prifile (wp)
13. Wu (1969)	3-15 15-21	$0.5U^{0.5}$ 2.6	$\pm$ 30 $\pm$ 10	Charnock relation with $\alpha = 0.016$
14. Hoeber (1969)	3-15	1.23	$\pm$ 16	wind prifile Atlantic Ocean
15. Zubkovskii and Kravchenko (1967)	3-9	$0.72 + 0.12U$	$\pm$ 15	eddy correlation (ec)
16. Deacon (1962)	3-14	1.2	$\pm$ 25	w p (fetch 12-30km)

mentioned previously, than those used in numerical modeling.

3. DYNAMIC ANALYSIS

The mechanism of momentum transfer from the air to the water is very complex and still requires a great deal of research. It should also be realized that further progress in our understanding of the laws governing the drag of the sea surface should be associated with the study not only of the momentum transfer to the waves but also the momentum transfer to the drift currents. To understand this mechanism, let us consider first the turbulent flow over a rigid surface. This surface is described as aerodynamically smooth or rough depending on the value of the roughness length, Z_o. In aerodynamically smooth flow, there is a viscous sublayer near the wall. In this region of the flow, the Reynolds shear stress is negligible, vanishing entirely at the wall and the total shear stress, τ_o, is supported by the molecular viscosity (i.e. $\tau_o = \tau_\nu$), and Z_o is given by (Phillips 1966):

$$Z_o = 0.1\ \nu/U_*$$

where ν is the kinematic viscosity of the air.

At the other extreme, the surface is sufficiently rough that the wall stress is supported primarily by "form drag" of the individual roughness elements, in which molecular viscosity is unimportant. In this case Z_o is found to be proportional to (and usually small fraction of) the chracteristic height of the roughness elements.

In the air flow over the sea, however, the interchange of

momentum has been shown to be dominated by processes taking place very close to the surface, whether by molecular viscosity or by the induced drag on the short wave components (of celerity or phase velocity $C<5U_*$). At low values of U_* (i.e. low wind velocities), when few or no ripples are presented, the turbulent air flow must correspond to that over an aerodynamically smooth surface. As U_* increases, the density of short gravity and capillary waves increases, and the momentum flux to these waves grows. Evidently the momentum flux to these shorter waves accounts for a substantial fraction of the total stress. At this stage one might expect that the molecular viscous stress at the surface becomes small compared to the momentum flux to short waves, though it may be an important source of momentum transfer to the drift currents. The water surface is then described as aerodynamically rough. This argument represents the basis for a widely held belief, that long wave components cannot contribute significantly to surface drag and the momentum transfer is mostly determined by short waves. This is the basis of Charnock's Equation (2.3). However, the evidence for this seems to be thin and, as mentioned by Stewart (1974); "the notion may itself be wrong". The principal argument for this belief is that most observations have shown that drag coefficient depends rather little upon such features as fetch and duration of wind and wave age (e.g. Wu 1968; Hicks 1972, 1974; Smith and Banke 1976). The long waves depend rather critically upon these features while the short waves much less so.

On the other hand, Stewart (1974) discussed the observations of Dobson (1971) and those obtained in the "JONSWAP" (Joint North Sea Wave

Project) (Barnett et al 1973), as evidence for momentum transfer into both short gravity waves and longer waves with phase velocities less than air velocity.

Many investigators have considered the way in which the total stress on the water surface may be divided between "skin friction" and momentum flux to the dominant waves "form drag" (e.g., Kitaigorodskii et al 1974; Donelan 1978, Taylor and Gent 1978). There is disagreement, however, on quite how the separation should be made, and on how much of the stress is carried by each mechanism. The division made by Longuet-Higgins (1977) is:

$$\tau_o = \tau_w + \tau_s \qquad (2.5)$$

where

$$\tau_w = \rho_a C_d |U_z| U_z \quad \text{and} \quad \tau_s = \rho_a C_s |U_z| U_z \ ,$$

where τ_o is the total shear stress, τ_w is the form drag or wave-induced Reynolds stress and τ_s is the tangent shear stress or "skin friction" which may include normal stresses on the "small-scale elements". In our use of this concept we will evaluate the form drag, τ_w, from the dominant waves (i.e. around the peak of the spectrum) as shown in the next section. The contributions to τ_s will come partly from viscous shear stress of the water surface and partly from form drag on short waves in the capillary range. Based on the analysis made by Taylor and Gent (1978), Donelan (1978) suggested that skin friction coefficient C_s may be taken to be of the order of 0.7×10^{-3}. The relation between τ_w and the momentum flux to the waves and consequently the determination of the form drag coefficient are the central questions in the present problem.

4. MODEL DEVELOPMENT

4.1 Methodology

In thermally neutral conditions, the equilibrium wind profile is approximately logarithmic and equation (2.2) may be rewritten (Phillips 1966):

$$U_z - C/\text{Cos}\ \theta = U_*/k\ \ \ln z/z_m \qquad (2.6)$$

where Z_m is the height of the "matched layer" where U Cosθ = C, and θ is the angle between average wind direction and dominant wave direction. In most practical purposes θ is set equal to zero. If Z_o is the virtual origin of the logarithmic profile (the roughness length) such that $U(Z_o)$ = 0, then from equation (2.6) setting θ = 0 we get:

$$Z_o = Z_m \exp(-k\ C/U_*) \qquad (2.7)$$

Assuming that the height of the matched layer, Z_m, is a function of the significant wave height (H_s), thus:

$$Z_o = \beta H_s \exp(-k\ C/U_*) \qquad (2.8)$$

Equation (2.8) is similar to that developed by Kitaigorodskii (1968) and Kitaigorodskii and Zaslavskii (1974). Where β is a dimensionless numerical factor to be determined. For Kitaigorodskii's data, β was found to be in the order of 0.12 while, when applying the same model for Lake Geneva observations, Graf et al. (1980) found much smaller value (β = 0.01). Graf argued that the reason for this disagreement is due to the choice of the representative wave height; Graf used significant wave

height, H_s, while Kitaigorodskii used the considerably smaller mean-square height of the waves. On the other hand Donelan (1978) found that $Z_o = 0.05\ H_s$ gives best fit to his data on Lake Ontario.

From equations (2.1), (2.6) and (2.8), one can arrive at the following relationship which may be used to determine the value of the drag coefficient:

$$C_d = \left(\frac{U_*}{U_z}\right)^2 = \left[\frac{k}{\ln(Z/\beta H_s)}\right]^2 \left(1.0 - \frac{C}{U_z}\right)^2 \qquad (2.9)$$

The above equation implies that the drag coefficient is a function of the mean wind speed at distance Z (usually 10 m) above water surface as well as wave height and wave age (C/U_* or C/U). This relation is similar to that proposed by Donelan (1975) through his wind-wave coupling model.

The Sverdrup-Munk-Bretschneider, "SMB" wave prediction method is used to determine wave characteristics in both deep and shallow waters as shown in the Appendix.

4.2 Analysis and Model Results

4.2.1 Variation of the form drag coefficient C_d with wind speed

For different wind speeds, the significant wave heights and phase velocities are determined using "SMB" wave prediction method for given wind fetches. Wind fetches were chosen in the range of 1 to 20 km, which are typical fetches for small lakes. The form drag coefficients are then evaluated for these values using equation (2.9) setting β =

0.05 (Figure 2.4).

It is clear from Figure 2.4 that the drag coefficient increases with increasing wind velocity. This agrees with the field observations carried out by many researchers as mentioned previously in section 2.

4.2.2 The drag coefficient versus wind fetch:

Figures 2.4 and 2.5 show this effect; as the fetch increases the drag coefficient decreases. We notice that at short fetches the drag coefficient rises to more than three times its value for fully developed waves at longer fetches. This contradicts the published observations in which the drag coefficient was assumed to be independent of the fetch. For example Figure 2.3, taken from Smith (1973) shows that C_d does not vary significantly when it was measured in open and limited fetch conditions.

One, however, can argue that the larger value of the drag coefficient associated with shorter fetches is due to the fact that wave field is undeveloped near the upwind shore (short fetches) and more developed near the downwind shore. Equation (2.9) explains this clearly; C_d is proportional to $(1 - C/U_{10})^2$. It appears that when the waves are fully developed most of the drag is supported by the short slow-moving waves riding on the top of long gravity waves (C/U becomes close to unity and C_d is small), whereas when waves are "young" most of the drag is supported by waves near the peak of the spectrum (i.e. the dominant gravity waves). More experimental effort is still required to study such relationships for different lake sizes.

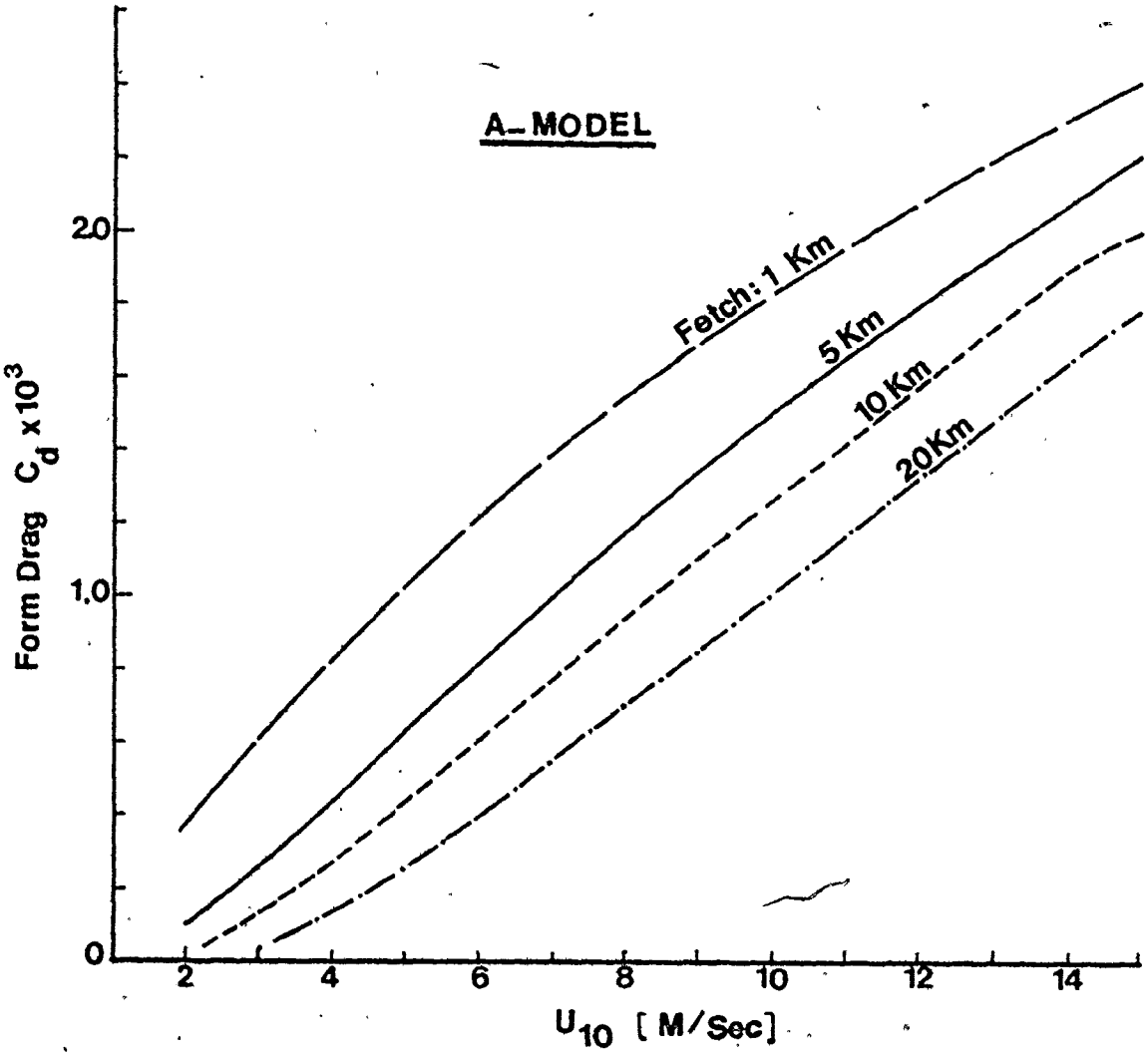

Figure 2.4 Form Drag as a function of Wind Speed & Fetch

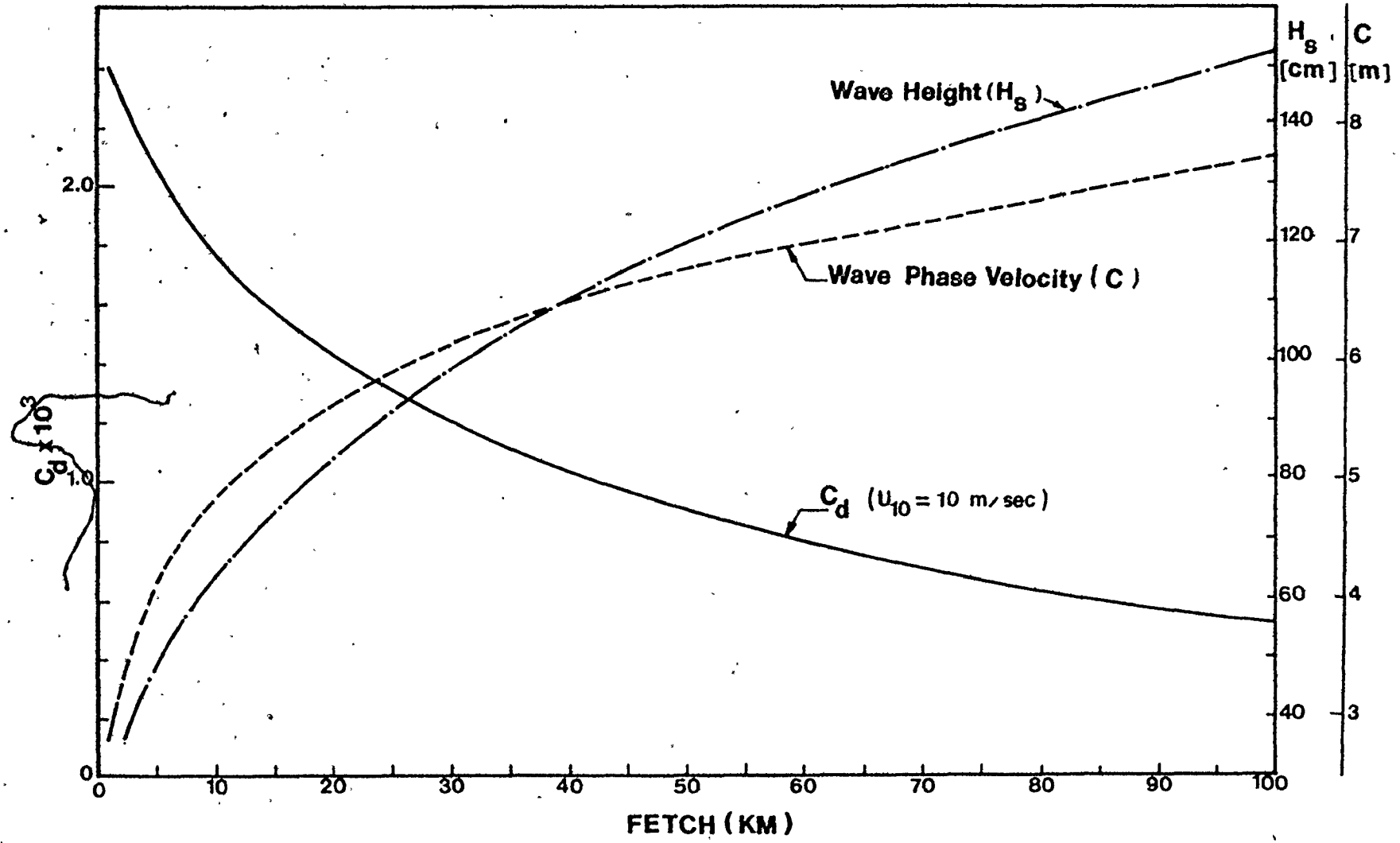

Figure 2.5 Drag Coefficient Versus Wind Fetch, Wave Height & Phase Velocity

4.2.3 Variation of C_d with C/U_* and H_s

Keeping the amplitude and wave length, and hence phase velocity C of the waves fixed and varying C/U_* by choosing different values of U_* or equivalently U_{10}, Figure (2.6) shows that the drag coefficient decreases as the wave age (C/U_*) increases. This agrees with the results obtained in several studies (e.g. Davidson 1974; Taylor et al. 1978). Similarly, for a constant value of $C/U_* = 10$, C_d is determined for different values of H_s. Figure (2.7) shows that as H_s increases, the drag coefficient increases. It was found that the effect of wave age, in the present model, is more pronounced than the effect of changing wave height.

4.2.4 Comparison with data obtained fom other studies:

Comparing the present model results (Figure 2.4) to the measured values of the drag coefficient collected from other studies (Figures 2.1, 2.2 and 2.3) one can find that for low wind speeds, the computed values of C_d are less than that found in the literature, while for high wind speeds, computed C_d are higher than the observed values.

Although the model results are consistent with those obtained by Donelan 1975 and some other scattered studies (Dunckel et al. 1974; Davidson 1974), considerable experimental effort is required to validate the above model.

Another approach is suggested in next section, in which the concept of Charnock (1955) is used after being modified to include the dpendence of the dynamic roughness Z_o on wave characteristics. The

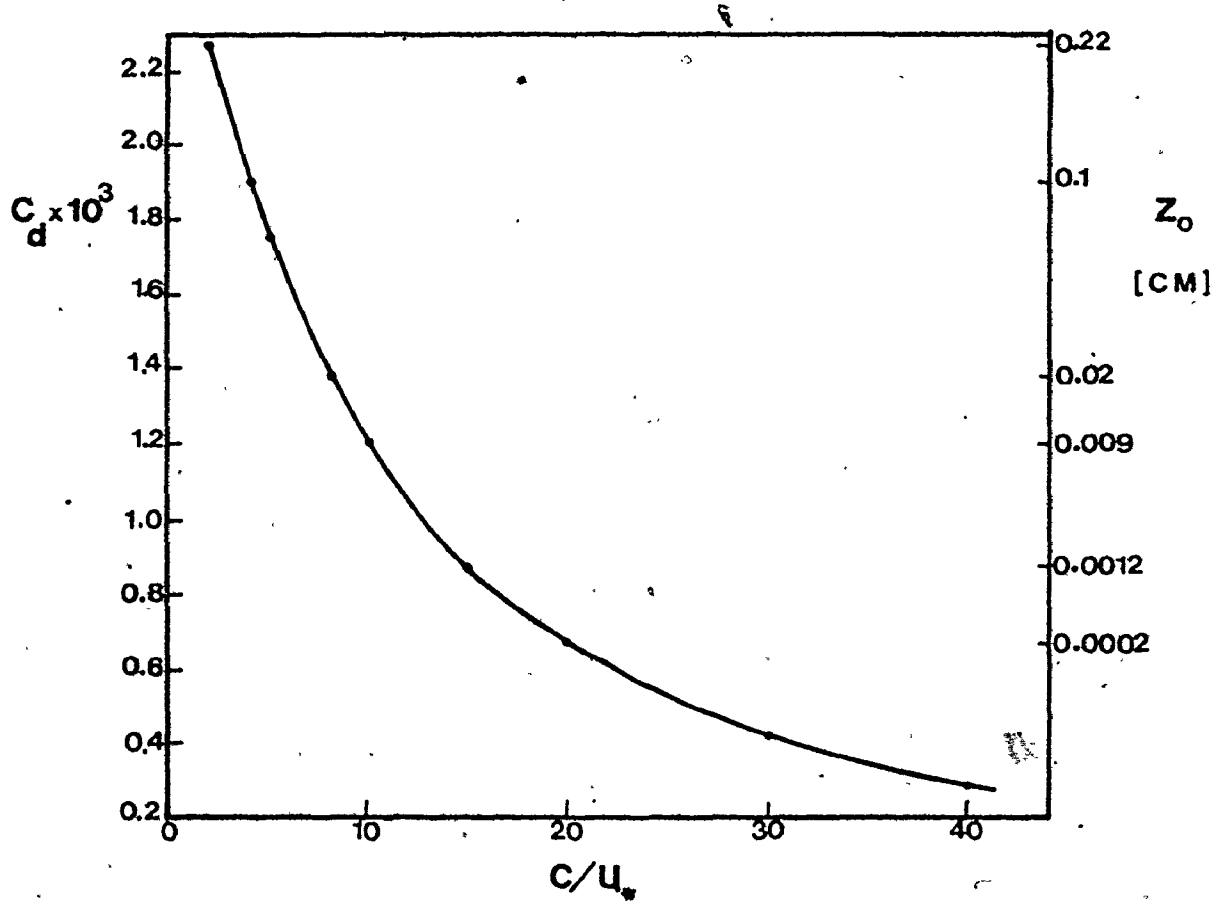

Figure 2.6 Drag Coefficient vs. Wave Age

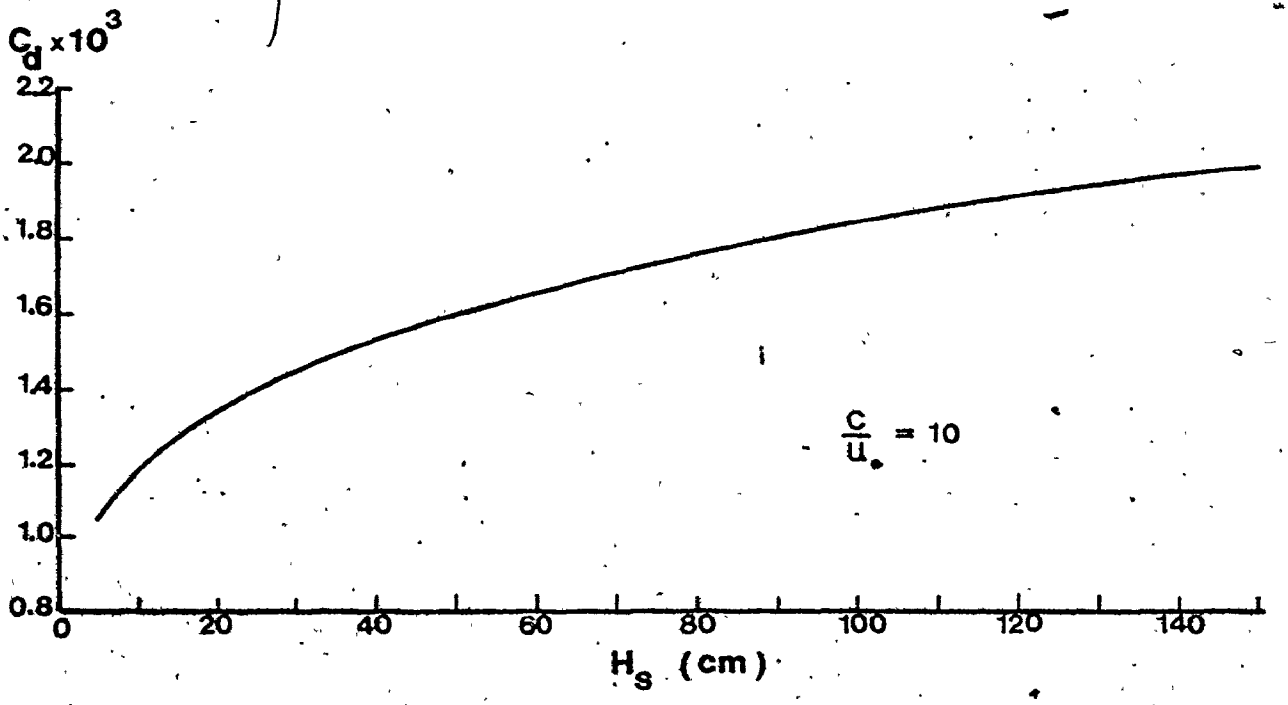

Figure 2.7 Drag Coefficient vs. Significant Wave Height

model developed above will be referred to as A-model, while the next model will be called B-model.

4.3 The B-Model

It is worth-while to examine the relationship between the dynamic roughness Z_o and shear velocity U_* based on Charnock's (1955) hypothesis (equation 2.3). The fact that α in Equation (2.3) is not constant, but exhibits variations dependent on the characteristics of the water surface has led investigators, as mentioned before, to postulate an added dependence of Z_o on wave height and phase velocity. As argued by Taylor and Gent (1976, 1977 and 1978), the roughness length depends rather critically on the wave slope (or wave steepness H/L) and wave age C/U_*. Therefore, as suggested by Hsu (1974), it is proposed from dimensional considerations that

$$Z_o \propto H/L \cdot U_*^2/g \qquad (2.10)$$

where H/L is the wave steepness of the dominant waves. As $C \propto (gL/2\pi)^{0.5}$ (see the appendix), (2.10) may be written as:

$$Z_o = \gamma/2\pi \, [H_s/(C/U_*)^2] \qquad (2.11)$$

where γ is constant to be determined. Hsu (1974) found (using deep water observations) that γ is close to unity. The values of γ will be examined later.

Substituting (2.11) into (2.2) and with the aid of Equation (2.1) we arrive at:

$$C_d \exp(k/\sqrt{C_d}) = 2\pi Z/\gamma H_s (C/U_z)^2 \qquad (2.12)$$

the above implicit equation is solved to determine C_d for given wind speed U_z at elevation Z (say 10 m), wave height H_s and phase velocity C. Wave characteristics are again determined by the "SMB" method (see the Appendix).

4.3.1 Analysis and results of the B-model

Similar analysis were carried out to study the behaviour of the above model under different wind-and-wave conditions.

4.3.1.1 Variation of C_d with wind speed U_{10} and fetch

Equation (2.12) is solved for different wind speeds (3-15 m/s) (γ=1.0). As shown in Figure (2.8), C_d increases as wind speed increases. The computed values of C_d are generally higher than those obtained from the previous approach (A-model) especially for low wind speeds.

The model was run for different fetches (ranging from 1 km to 300 km). Figure (2.8) shows that, increasing the fetch would slightly decrease the computed drag coefficients, especially under higher wind velocities (U > 10 m/s). One may conclude that the drag coefficient C_d is practically fetch independent. This agrees with the results of many studies in the literature as discussed previously.

When compared to the data collected and compiled by Wu (1969) and Garratt (1977), the present B-model gives better agreement than that obtained by the A-model. However C_d values obtained by the B-model are

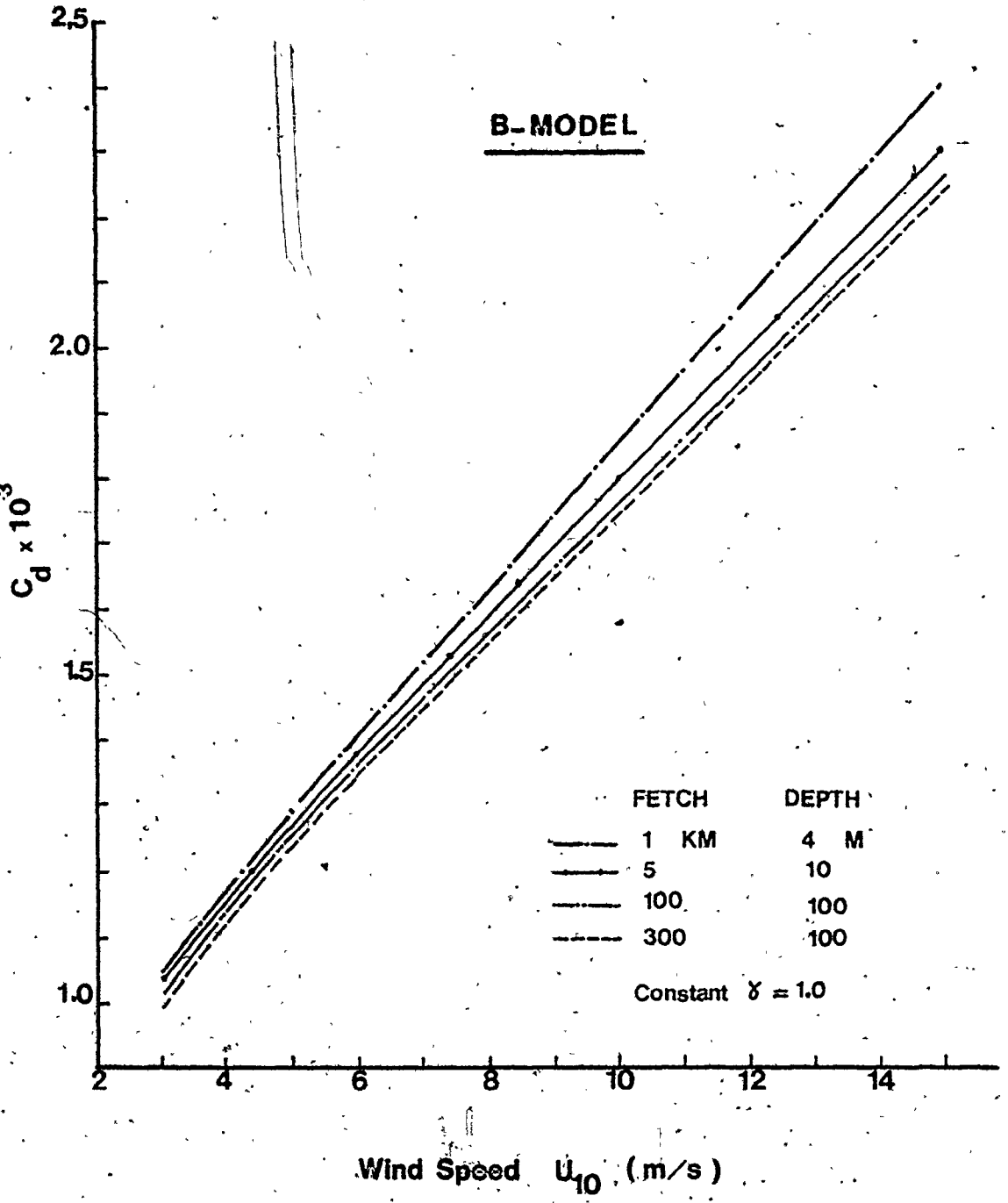

Figure 2.8 Form Drag Coefficient vs. Wind Speed at Different Fetches

slightly higher than that found in other studies (see Figures 2.8 and 2.9). This may be due to the choice of the constant γ in Equation 2.12. Figure 2.9 shows the model results for different values of γ. A value of γ in the order of 0.5 gives closer agreement with other studies.

Comparing equation (2.11) with Charnock's equation (2.3) we find that

$$Z_o = \alpha(U_*^2/g) = \gamma/2\pi(H_s U_*^2/C^2) \tag{2.13}$$

thus

$$\alpha = \gamma/2\pi\ (gH_s/C^2) \tag{2.14}$$

the dimensionless quantity (gH_s/C^2) is calculated for different fetches and variable wind speeds, and the results are presented in Table 2.2. Surprisingly, we found that for a given fetch, this quantity (and thus α) is almost constant for the given range of wind speeds (3-15 m/s).

On the other hand, the quantity (gH_s/C^2) decreases slightly as fetch increases. This clearly indicates that, under steady wind where an equilibrium state between the wind profile and the water surface condition is reached (i.e., wind duration is longer than wave period) at any given fetch, even though the shear velocity U_* (or wind stress coefficient) and the surface roughness (or average wave height) both dependent very much on the fetch, the equilibrium state at any particular fetch can well be characterized by Charnock's expression. The present modified Charnock's equation (2.13), however, can be used to determine the value of α (Equation 2.14) for a given fetch. This, as claimed by Wu (1968 and 1969) reveals the practicality of relating laboratory measurements to oceanic observations. We also found that, a

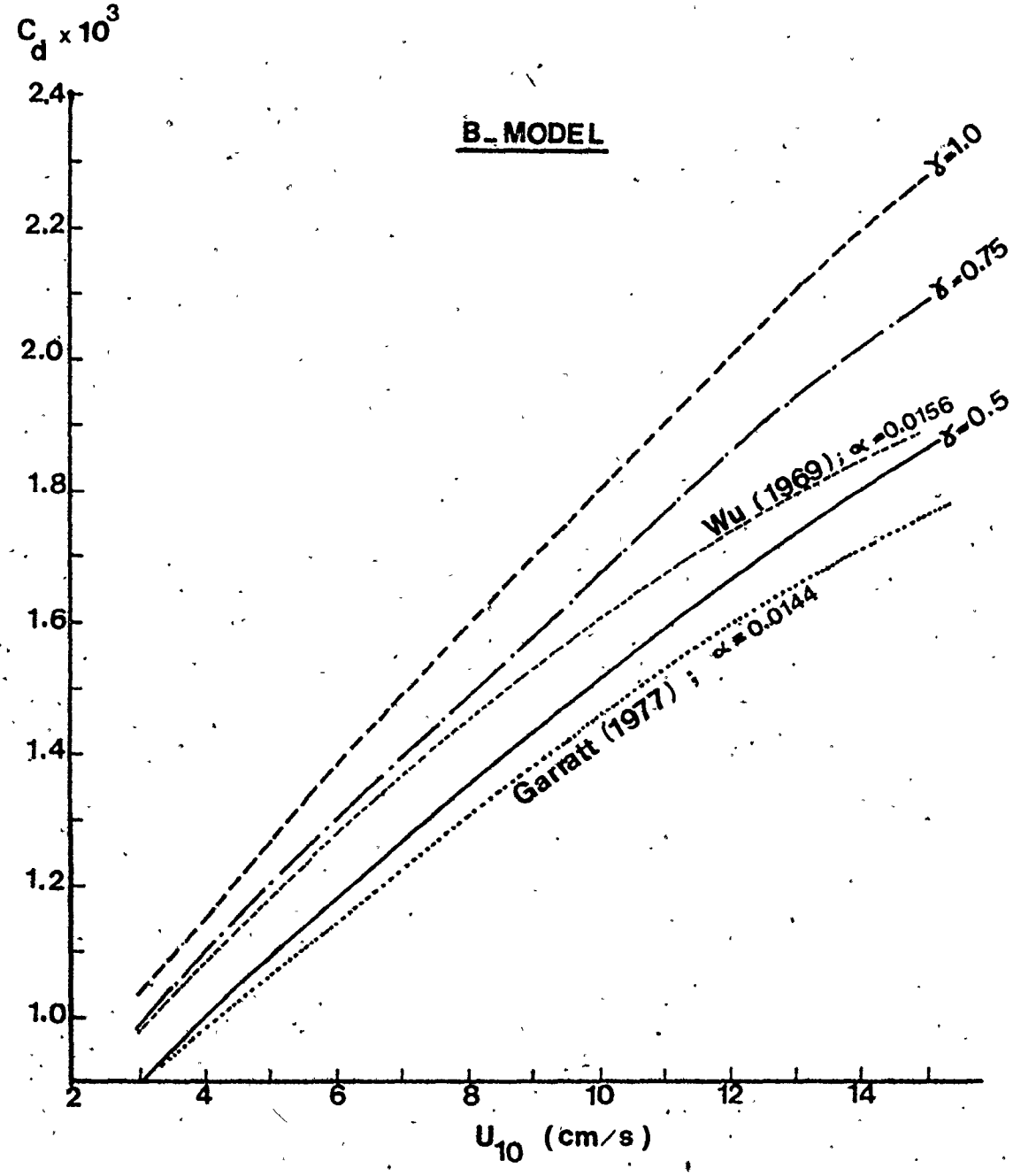

Figure 2.9 C_d versus U_{10} For Different Values of γ (Eq. 2.12)

value of γ in the order of 0.5 would result in a value of Charnock's constant α (for large fetches) close to those obtained by Wu (1969) and Garratt (1977).

Thus we may use the above approach (B-model) to determine the "form" drag coefficients for a given lake under different wind and surface conditions and compare the results with those observed elsewhere (as we do not have observations to verify the present model). By trial, a value of γ, in equation (2.12) of the order of 0.4-0.5 was found to bring the present model results into close agreement with data collected from other studies (Figure 2.9).

4.4 Discussion and Conclusion

Two models are proposed in which the drag coefficient is determined as function of wind speed at certain elevation (Z = 10 m) and water surface characteristics represented by significant wave height and wave age C/U_*. The first model (A-model) produces values of C_d which were found to be much smaller than those obtained from observations especially for longer fetches. The computed C_d using the A-model was found to be very much dependent on the fetch and consequently on wave age and wave height. This conflicts with many studies based on observations carried out on oceans and open seas, where the researchers concluded that the form drag is practically independent of wind fetch. The second approach (B-model) however, produces results which are more consistent with the observations reported in several studies.

Overall there is considerable evidence that C_d increases with

Table 2.2: B-Model predictions for different fetches and variable Wind speeds

U_{10}	Fetch = 5 km			Fetch = 100 km			Fetch = 300 km		
m/s	H_s cm	C cm/s	Q*	H_s	C	Q	H_s	C	Q
3.0	11.3	208.5	0.255	24.1	318.6	0.233	25.7	342.3	0.215
4.0	15.1	248.3	0.255	39.6	401.7	0.241	44.6	441.9	0.224
5.0	21.2	283.0	0.263	56.8	476.6	0.245	67.4	534.4	0.231
6.0	26.3	314.1	0.261	75.0	544.9	0.248	93.0	620.7	0.236
7.5	34.3	355.9	0.265	103.7	637.8	0.250	135.3	740.1	0.242
10.0	48.2	416.6	0.272	153.7	773.5	0.251	212.5	917.9	0.247
15.0	77.5	516.7	0.284	259.0	998.8	0.254	379.8	1218.1	0.250
average			Q = 0.265			Q = 0.246			Q = 0.235
for $\gamma = 0.5$;			$\alpha = 0.021$			$\alpha = 0.019$			$\alpha = 0.018$

* $Q = g\, H_s / C^2$

Note that deep water wave prediction was used to determine H_s and C.

wind speed, a little evidence that C_d remains constant over certain wind speed ranges, with transitions related to changes in sea state. The results of the two models support this conclusion. The present study is to be considered as a preliminary attempt to calculate the drag coefficient as a function of wind speed, fetch, wave height and phase velocity. Thus temporal and spatial variations of the drag coefficient, and consequently surface shear stresses over the lake surface can be determined when applying the hydrodynamic equations of lake circulation. The procedure is as follows:

a) Assume that a steady wind blows for a sufficient duration. The spatial variations of the wind, for example, observed in Hamilton Harbour (see Chapter VI), could be taken into account by interpolation of records from the wind stations around the lake, by using weight factors inversely proportional to the square of the distance between in-water locations and onshore wind stations.

b) Wind fetch is determined at each node on the numerical grid (distance from the upwind shore to that point along wind direction). For small lakes subject to a uniform wind distribution, an average fetch and water depth may be assumed to represent the whole lake, and consequently an average value of C_d may be used.

c) Use the Sverdrup-Munk-Bretschneider (SMB) method (U.S. Army Engineering Research Center 1973) to determine wave characteristics as shown in the Appendix.

d) Calculate the form drag coefficient C_d using either or both models developed in the previous sections. Add to this value the skin drag coefficient $C_s = 0.7 \times 10^{-3}$, to get the total drag coefficient $C_D = C_d + C_s$

e) Substitute C_D calculated in the previous step into equation (2.1) to get surface shear stress at each grid node to be used in the hydrodynamic equations at each time step.

The new models have been applied to two small lakes (Valens reservoir; average fetch of 0.3 km, and Hamilton Harbour, average fetch of about 3 km) and the results are presented in Chapter VI.

CHAPTER III

SPATIAL VARIATION OF INTERFACIAL SHEAR STRESS FOR BOTTOM WEEDS

1. INTRODUCTION

Another important term in the hydrodynamical equations of lake transport is the shear stress at the lake bottom. This chapter presents the formulation of bed boundary conditions for the three-dimensional transport model described in Chapter I. The approach is particularly suitable for shallow lakes with considerable roughness due to weed growth. The approach is similar to that of previous chapter: the bed roughness is determined using the Von Karman-Prandtl logarithmic velocity distribution for turbulent flow near the rough surface.

To account for spatial variation of the roughness elements, local bottom roughness is taken to be related to local parameters such as weed length and density. The model was applied to a study of wind-driven currents in Valens reservoir, a small, shallow, recreational lake suffering extensive weed growth. The application of the model and the results obtained are presented in Chapter VI.

2. MODELING OF BOTTOM ROUGHNESS DUE TO WEED GROWTH

The determination of flow within a three-dimensional vegetated shallow lake or coastal zone is a complicated problem, and one which requires considerable research before the phenomena involved are

completely understood. Very little has been published on flow resistance inside and around aquatic weeds. The approach here is similar to that used to calculate one-dimensional flow resistance in vegetated open channels.

A literature survey has been reported in an earlier work (Eid 1976). Only the main highlights are summarized here. Boundary layer theory (Prandtl 1904) has opened the way toward a rational understanding of some of the flow phenomena involving boundary roughness (Schlichting 1963). The application by G.H. Keulegan and others (ASCE 1963) of Von Karman-Prandtl concepts and Nikuradse roughness to open channels has been quite successful in describing grain-type roughness in wide channels. However, it is not adequate for describing flow over long flexible roughness elements. Recently, studies using flexible plastic strips attached to the bed of laboratory flumes have been carried out (Kouwen et al 1969; Kouwen and Unny 1973).

In meteorology, wind profiles inside and above vegetal cover (tall plants) have been studied in both laboratory and field (Cionco, 1965, 1972; Pernir et al. 1972; Plate and Quraishi 1965). No investigations have been done to determine the velocity distribution inside and around an aquatic plant canopy. There exists a definite need for field measurements for different types of aquatic weed commonly found in shallow lakes. For example, no velocity or turbulence measurements are available at the top of a flexing plant canopy. Indeed, in view of the small velocities and probable large eddies in and around flexing weeds of varying length, such measurements would appear

to be difficult to accomplish.

2.1 Methodology

The background theory and method are covered in detail in an earlier thesis (Eid 1976). Main points and concepts relevant to later work are reviewed herein. H. Rouse (1965) summarized much of the reported work in open channel resistance using Karman-Prandtl concepts of turbulent flow near a rough boundary. Meteorologists have assumed that many of the parameters found to affect flow resistance in channels with rigid roughness could also be applied to flexible roughness such as that represented by grass and other vegetation (Plate and Quraishi 1965).

The velocity profile of a fluid moving near a rough boundary can be described, as mentioned in the previous chapter, by the logarithmic law:

$$\frac{V}{U_*} = \frac{1}{k} \ln\left(\frac{z}{z'}\right) \qquad (3.1)$$

where:

- V is the velocity at distance z above the boundary (bed)
- U_* is the shear velocity = $(\tau_b/\rho)^{1/2}$
- τ_b is the average boundary shear stress
- k is Karman-universal constant (= 0.4)
- z' is the magnitude of z at $v=0$, i.e. the intercept of the velocity profile on the z-axis, as shown in Fig. 3.1, also known as roughness parameter (Rouse 1965; Sayre et al 1961).

Plate and Quraishi (1965) and others (Cionico 1965; Pernir et al. 1972) applied the logarithmic velocity distribution some distance above the plant cover. This distance is called the "zero plane displacement". There is no evidence, and it appears unlikely that the velocity inside and around the plant cover can be defined by the logarithmic law. Derivation of an equation describing the velocity distribution both inside and above the weeds would require field and laboratory investigations (which were not available for this study). We will not deal herein with the transverse velocity profile around locally high plants. We thus assume that flow within the submerged weeds is similar to meteorologic data for the velocity distribution of wind inside certain crops. These data have been summarised by Plate and Quraishi (1965). As the aquatic weeds generally formed a dense, flexible growth, the velocity distribution is assumed to have a similar shape to that for wind within wheat (the most flexible of the crops used) but of course with smaller velocities.

The approach used in this study is based on the assumption that the logarithmic law, Equation (3.1), can be applied at a distance z' inside the weed canopy. This distance is calculated, such that the area under the logarithmic velocity profile inside the weeds (from z' to d) is equal to that given by the wind data, as shown in Figure 3.2. In other words, the discharge resulting from integrating the logarithmic velocity distribution (from z' to the weeds height d) is set equal to the discharge (within the plants) given by the empirical data. This yields an equivalent sublayer of zero discharge with depth z', denoted

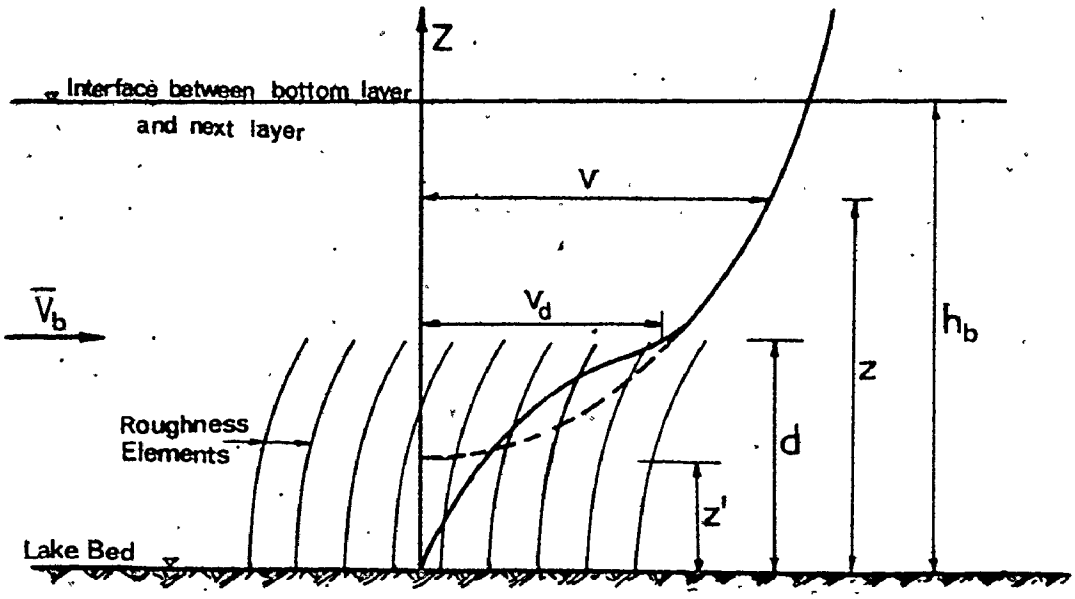

Figure 3.1: Velocity Profile Inside and Above Plant Canopy

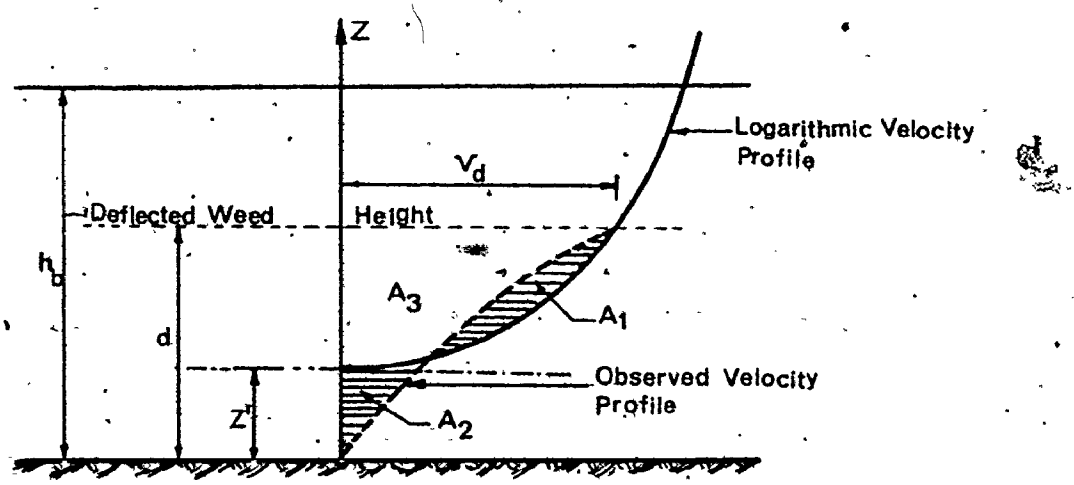

Figure 3.2: Empirical and Theoretical Velocity Distributions Inside the Canopy

the "boundary layer displacement thickness". This is equivalent to an imaginary new solid boundary, over which the logarithmic velocity distribution is applied.

Now, applying equation (3.1) at the tip of the vegetation:

$$\frac{V_d}{U_*} = \frac{1}{k} \ln \frac{d}{z'} \tag{3.2}$$

where d is the deflected height of the weeds (Figures 3.1 and 3.2).

z' can be determined from:

$$A_1 + A_3 = A_2 + A_3 \tag{3.3}$$

where $$A_1 + A_3 = \int_{z'}^{d} v \, dz = \frac{U_*}{k} \int_{z'}^{d} \ln \frac{z}{z'} \, dz$$

Thus

$$A_1 + A_3 = \frac{U_*}{k} [d \ln \frac{d}{z'} - (d - z')] \tag{3.4}$$

A non-dimensional presentation of field data for wind profiles inside plant cover (wheat and corn) obtained by Tan and Ling together with the wind tunnel results obtained by Plate and Quraishi (1965) is given in Figure 3.3.

Assuming the dimensionless area under the observed profile (Figure 3.3) is A, then

$$A_2 + A_3 = A \, d \, V_d = A \, d \, \frac{U_*}{k} \ln \frac{d}{z'} \tag{3.5}$$

From equations (3.4) and (3.5), equation (3.3) becomes:

$$(1 - \frac{z'}{d}) - (1 - A) \ln \frac{d}{z'} = 0 \qquad (3.6)$$

For a given velocity distribution inside the plant cover, the boundary layer displacement thickness (z') can be obtained from the dimensionless equation (3.6).

It is evident from equation (3.6) that the boundary layer displacement thickness (z') depends on the local roughness conditions, i.e. size, shape and spacing of the roughness elements which are represented by the dimensionless area A and the height d. In other words, z' should completely describe the boundary roughness, in a similar way to that used by Sayre and Albertson (1961). This includes the effect of turbulence at the interface. One may notice that the parameter z' is analogous to the "roughness length" z_o described in previous chapter.

Rewrite equation (3.6) with $z'/d = c$ as follows:

$$(1 - c) - (1 - A) \ln \frac{1}{c} = 0 \qquad (3.7)$$

By solving equation (3.7), c is obtained as function of the normalized area A, which, in turn depends on the type of vegetation and its density. This relation is represented in Figure 3.4. Then, once the velocity distribution inside the weeds is known, the roughness parameter ($z' = c.d$) can be obtained from Figure 3.4. Substituting back into equation (3.1) we can calculate the velocity distribution above the boundary layer displacement thickness in the bottom layer.

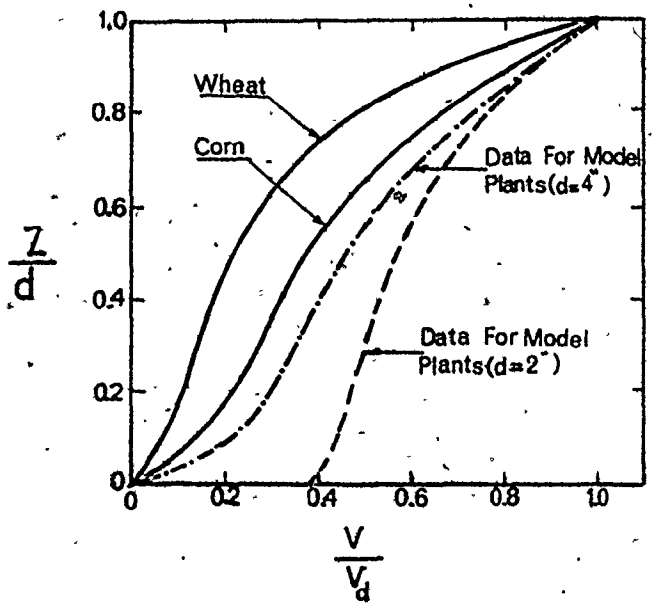

Figure 3.3: Field and Experimental Velocity Profiles in Canopy (After Plate and Quraishi, 1965)

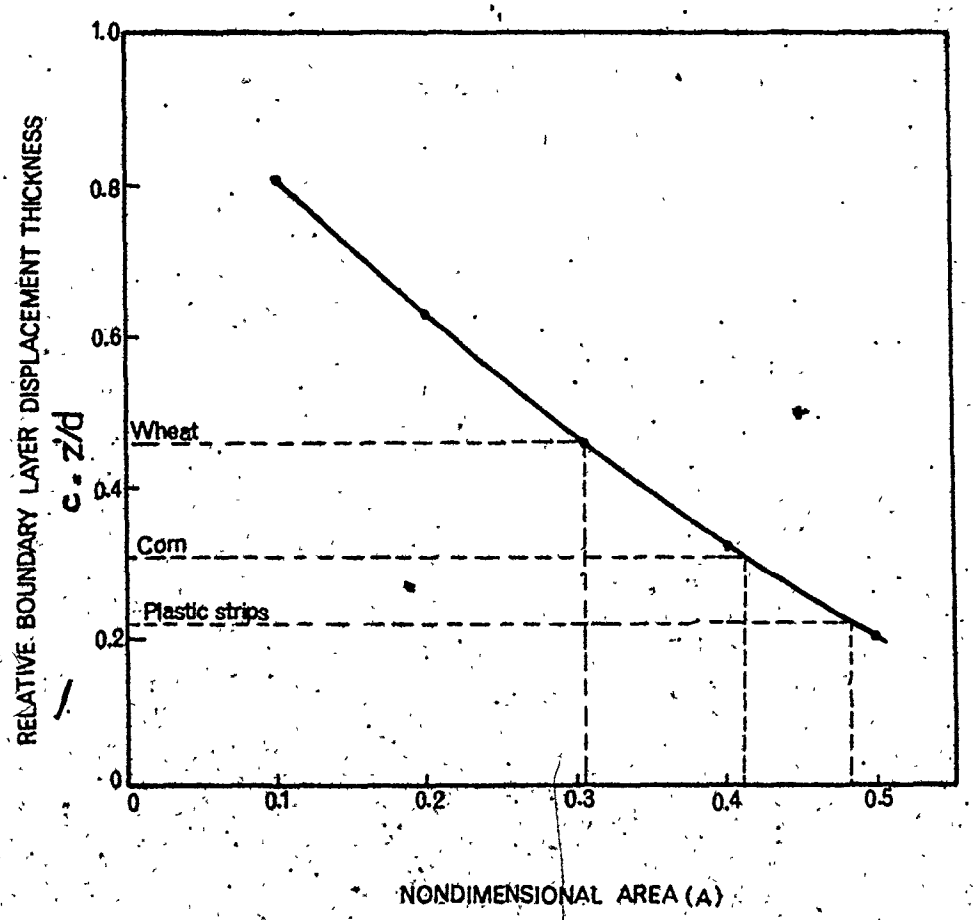

Figure 3.4: Determination of Boundary Layer Displacement Thickness

2.2 Calculation of Bottom Shear Stress (τ_b)

For the flow in the bottom layer, the discharge per unit width is:

$$\bar{V}_b\,(h_b - z') = \int_{z'}^{h_b} v\,dz \qquad (3.8)$$

Substituting Equation (3.1) into the right hand side of equation (3.8) and integrating gives

$$\frac{\bar{V}_b}{U_*} = \frac{1}{k}\,\frac{h_b}{h_b - z'}\,\ln\frac{h_b}{d} + \frac{1}{k}\left[\frac{h_b}{h_b - z'}\,\ln\left(\frac{d}{z'}\right) - 1\right] \qquad (3.9)$$

where, as shown in Figure 3.1:

$\bar{V}_b(\bar{u}_b, \bar{v}_b)$ is the average velocity in the bottom layer

h_b is the depth of the bottom layer

z' is the boundary layer displacement thickness (=c.d)

Equation (3.9) can be rewrtten in the simple form:

$$U_* = \frac{1}{c_2}\,\bar{V}_b$$

$$\frac{\tau_b}{\rho} = \left(\frac{1}{c_2}\right)^2 \bar{V}_b^2$$

Thus:

$$\frac{\tau_b}{\rho} = K_b\,\bar{V}_b^2 \qquad (3.10)$$

where $$c_2 = 2.5\,\frac{h_b}{h_b - z'}\left(\ln\frac{h_b}{d}\right) + 2.5\left[\frac{h_b}{h_b - z'}\left(\ln\frac{d}{z'}\right) - 1\right]$$

and $K_b = (1/c_2)^2$ is called (Simons 1973) the non-dimensional skin friction coefficient. In a study on Lake Ontario (Simons 1975), it was assumed to be a constant of the order of 2.5×10^{-3}. In the present study K_b is assumed to have this same value (2.5×10^{-3}) for the case of no weeds. It is convenient to rewrite equation (3.10):

$$\tau_b = \rho K_b |\bar{V}_b| \bar{V}_b \tag{3.11}$$

The shear stress components in x and y directions are calculated from:

$$\tau_{bx} = \rho K_b |\bar{u}_b| \bar{u}_b \tag{3.12a}$$

$$\tau_{by} = \rho K_b |\bar{v}_b| \bar{v}_b \tag{3.12b}$$

Substituting back into the equations of motion (1.1) and (1.2) yields the complete set of equations to be used for calculating wind-driven currents in shallow lakes with prolific weeds. These equations are solved using a finite differences technique in time and space.

3. DISCUSSION

The model has been applied to a shallow lake with very rough bed due to vegetation, where the shear stress term is very important in the force balance equations. The model determines local roughnesss by incorporating the effect of weed height and distribution throughout the lake.

In the present approach, the standard logarithmic boundary layer equation is modified to account for the effect of bed weeds. The

roughness parameter z' is used as a measure of the effects of the boundary on the profile and is not only a measure of the displacement from the true geometric boundary. Due to the absence of field measurements of the velocity distribution inside the weeds, data collected from the meteorological-hydrodynamical literature was used. z' is thus calculated using a match of logarithmic and observed nondimensional velocity profiles, and this same large value of z' is applied directly to the velocity profile in the numerical model. This may describe a turbulence field with relatively large scale eddies at the top of the weed field, which seems to accord with the prototype mechanism.

The model was used to study the effect of spatial distribution and time-dependent growth of weeds on the wind-driven surface current patterns in Valens reservoir (Eid 1976). The algorithm described in this chapter together with that developed previously in Chapter II are included in the hydrodynamical model described in Chapter I, and the results are presented in Chapter VI.

CHAPTER IV

VERTICAL MIXING NEAR THE SEDIMENT-WATER INTERFACE

1. INTRODUCTION

In previous chapters, the transfer of momentum from the air to the water and flow resistance at the bed of a lake were discussed. This chapter covers the dynamics of vertical exchange processes under stratified conditions, basically in the hypolimnion and especially at the water-sediment interface. The fundamental problem examined is the quantitative description of vertical motions as they affect the vertical distribution of nutrients, such as phosphorous and dissolved gases, such as oxygen. Of course, mass transport terms through both the sediment-water interface and the thermocline are important in such models.

Vertical transport may be described by the coefficient of vertical eddy-diffusion, K_z, which itself may depend on time and depth (Schmidt 1917). An excellent review of the theories and fundamentals of vertical mixing and physical limnology has been carried out by Mortimer (1972). Theoretical modeling of the vertical exchange coefficients in lakes and seas has been discussed by Wellander (1968).

We should distinguish between two different diffusion coefficients: a) eddy-diffusion of momentum A_v or eddy-viscosity, and b) diffusion of a dissolved substance (or temperature) K_z which we will refer to as eddy-diffusivity. The former is usually larger than the latter because momentum can be transferred by both pressure fluctuations

and translation of water particles, whereas the diffusion of transported materials is accomplished only by the latter (Boyce 1974).

During the stratification period, and in the absence of strong winds and cold water inflow into the hypolimnion, the main mechanism of heat transfer into lower waters is due to turbulent diffusion. Generally, in a thermally stable lake, the thermocline is a barrier to the direct transmission of epilimnetic waters into the lower layers. In most cases, turbulence in the hypolimnion is much weaker than that in the epilimnion.

In the case of the vertical transport of heat, time-series of temperature profiles, suitably time-averaged to remove short-term fluctuations and space-averaged to be representative of the whole lake basin, may be used to evaluate vertical diffusivity K_z (McEwen 1929; Hutchinson 1957). The values of K_z determined by this method are useful in a study of chemical or biological processes, but only if the results are interpreted in the same time-scale averages of the original data. In the present study, observed temperature profiles are used to determine time and depth variations of the eddy diffusion coefficients in the hypolimnion of a stably stratified lake.

Study of vertical mixing mechanism at the water-sediment interface is essential to determine the flux of a solute from the sediments into the overlaying waters. This flux often originates from the sediment surface (or the top few millimeters of the sediment column). It is thus very difficult if not impossible to estimate this flux from chemical analysis of sediment cores. However, concentration

profiles in the overlaying lake waters, together with some knowledge of the mixing processes (e.g., vertical eddy diffusivities) would make such calculations feasible. The Radium-226/Radon-222 isotope pair has been successfully applied as a tracer for vertical eddy diffusion near the bottom in the ocean (Broecker 1967, 1968; Chung and Craig 1972). The radium/radon isotope pair has rarely been used as a tracer for mixing in lakes (except in artificially added quantities; Hesslein and Quay 1973) due to certain complexities which do not arise in ocean (lake bottom topography, small concentrations of radon-222, etc.). Imboden and Emerson (1976, 1978) described the analysis of naturally occurring radon-222 isotope data to the determination of vertical eddy diffusion in lakes and applied the results to the interpretation of phosphorous flux to the hypolimnion.

In the following sections, two methods (temperature and radon) are used to evaluate vertical eddy diffusions and mixing in the hypolimnion. The resulting model is applied to a small "test" lake in Switzerland in Chapter VII.

2. THE CONCEPT OF VERTICAL EDDY DIFFUSION

In an open body of water turbulence leads to an irregular pattern of advection velocities, whereas molecular diffusion is too slow to play a significant role in material transport. Due to the conservation of mass the arithmetic sum of all fluxes through a horizontal plane (of cross-sectional area A) is zero provided that no subsurface sources or sinks exist. Following Schmidt (1917) (Figure 4.1), the net flux of

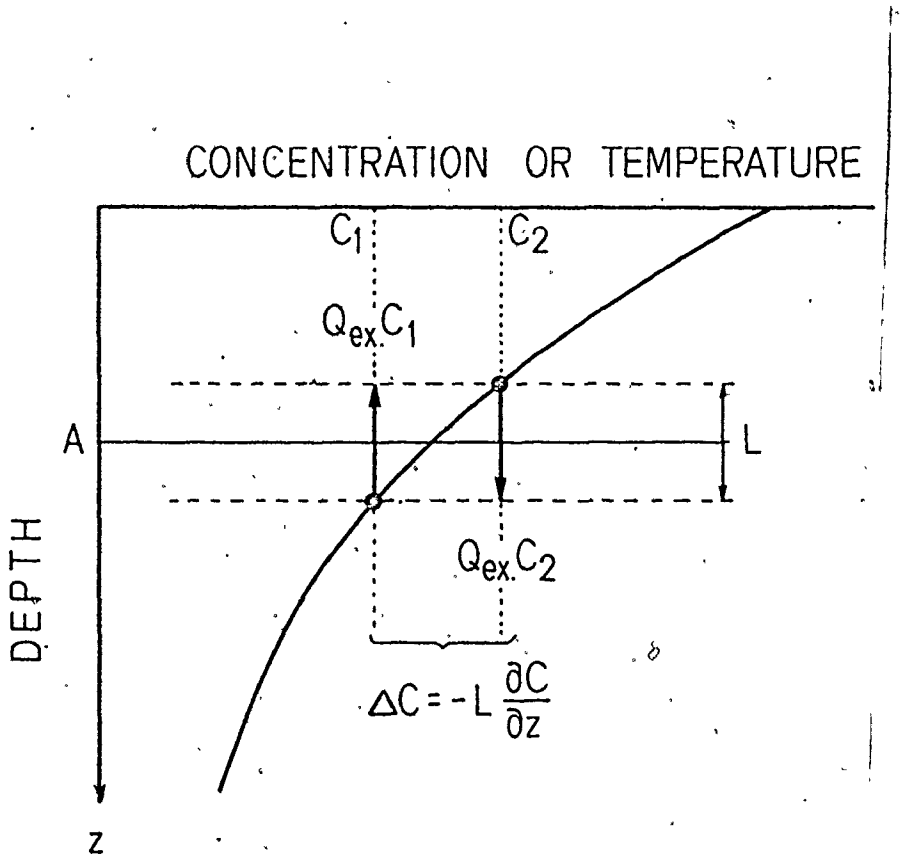

Figure 4.1 Vertical Exchange of a Substance (Q_{ex}) across Plane A as a function of concentration gradient

dissolved material through the cross-sectional area A is given by

$$F.A = Q_{ex}\Delta C = -Q_{ex}L(\partial C/\partial z) \qquad (4.1)$$

where $Q_{ex} = |Q_{up}| - |Q_{down}|$ is the vertical exchange of water per unit time across A, and L is a typical vertical transport distance of the water (mixing length, analogous to the mean free path of molecular diffusion theory). C is the concentration of a substance and z is the depth coordinate (positive downward).

In the right-hand side of equation (4.1) ($Q_{ex}L$) describes the

hydrodynamic properties of the system, and $(\partial C/\partial z)$ depends on the spatial distribution of the chemical or physical species under consideration. Writing the coefficient of vertical eddy diffusion

$$K_z = \frac{Q_{ex} L}{A} \qquad \text{(dimension } L^2T^{-1}\text{)} \tag{4.2}$$

Thus flux per unit area, F, is given by:

$$F = - K_z \frac{\partial C}{\partial z} \tag{4.3}$$

3. THE TEMPERATURE METHOD

The temperature method for calculating coefficients of vertical eddy diffusion K_z was introduced by McEwen (1929) and later used by Hutchinson (1957). It is based on the assumption that heat is transported by vertical eddy diffusion from the warm surface water into the colder hypolimnion. Thus, its application is restricted to the thermocline and hypolimnion waters during the stagnation period. Situations typical in autumn, when parcels of cool surface water sink into the deeper part of the lake (convective mixing), cannot be treated this way.

As Li (1973) pointed out, a precise, absolute calibration and stability of field thermometers is necessary to detect the extremely small temporal temperature variations during the stagnation period and to calculate the change of hypolimnetic heat content.

We start with the classical theory of advection and diffusion in

continuous media:

$$\frac{\partial C}{\partial t} = -\frac{\partial}{\partial z}(\omega C) + \frac{\partial}{\partial z}\left(K_z \frac{\partial C}{\partial z}\right) + S \qquad (4.4)$$

The mean vertical velocity ω is usually small and especially so in stratified lakes within the hypolimnion near the thermocline. However, of course, significant mean vertical velocities may occur near the shore where they are associated with upwelling and downwelling. In this study we are concerned with processes occurring beyond the influence of lateral boundaries and thus ω is set equal to zero in equation (4.4). In the above equation, C is concentration and S is a source or sink. The last term (S) in the above equation is neglected. This assumption is discussed later.

Based on the above assumptions, equation (4.4) is used to relate time and space derivatives of temperature:

$$A_z \frac{\partial T(z,t)}{\partial t} = + \frac{\partial}{\partial z}\left(K_z A_z \frac{\partial T(z,t)}{\partial z}\right) \qquad (4.5)$$

where A_z is the horizontal cross-sectional area of the lake at level z, and T(z,t) is the average temperature profile.

Equation (4.5) can be expressed in finite difference form to yield estimates of K_z at various depths and times; T(z,t) is typically determined from synoptic temperature surveys (Blanton 1973). Integration of equation (4.5) yields an equation expressing K_z as a function of depth z and time t taking into account the variation of the horizontal cross-sectional area A_z with depth (Figure 4.2)

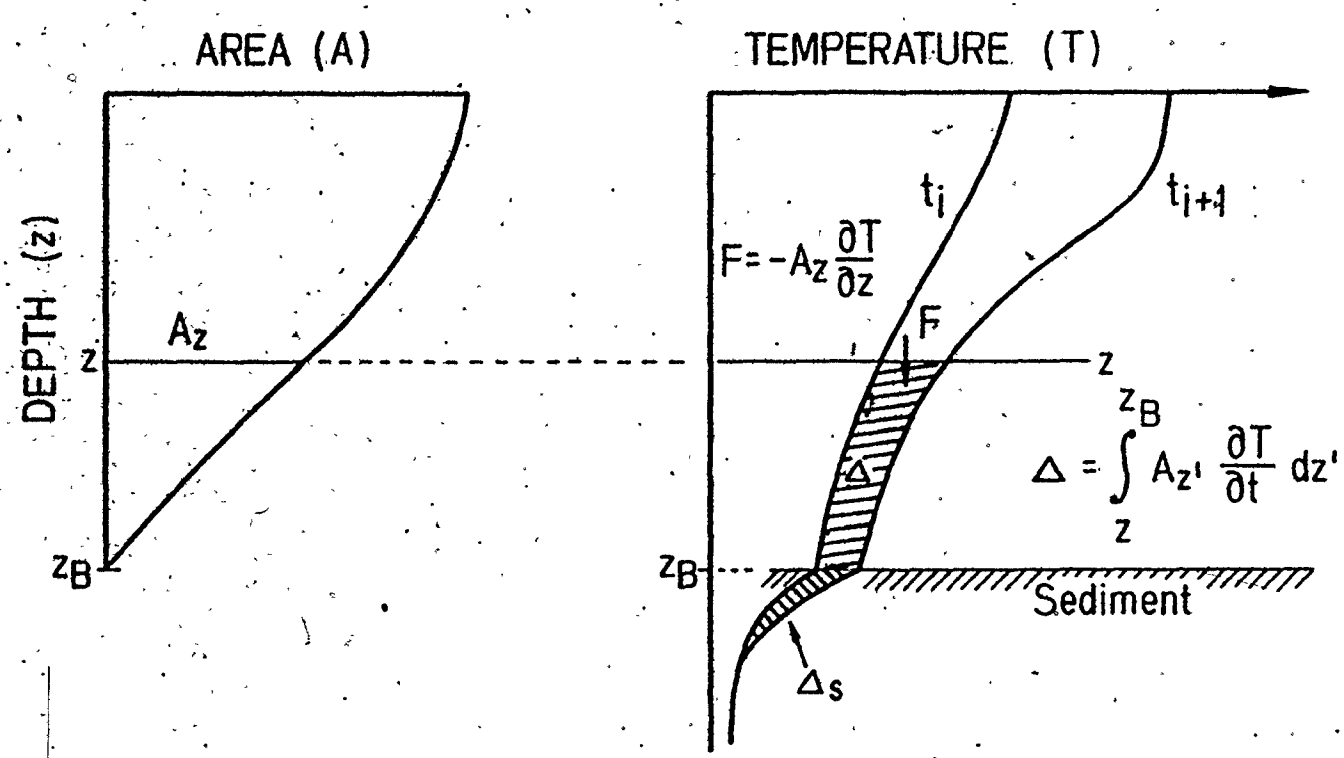

Figure 4.2 Calculation of Vertical Eddy Diffusion Using Temperature Profiles

$$K_z(z,t) = - \frac{\int_z^{z_B} A_{z'} \frac{\partial T}{\partial t}\Big|_{z',t} dz'}{A_z \frac{\partial T}{\partial z}\Big|_{z,t}} \qquad (4.6)$$

Equation (4.6) is solved numerically, using a finite-difference method, by the FORTRAN program VERDI (VERtical DIffusion). The program calculates the vertical eddy diffusion coefficient K_z as a function of depth and time for given temperature profiles measured at consecutive times t_1, t_2, ..., t_n. The program is flexible with respect to the required input data. Besides lake morphometry (given by A_z) a series of temperature profiles are given at arbitrary times, and each profile consisting of an arbitrary number of pairs (z_i, T_i) where the depths z_i can be different from one profile to the next. The program yields values for K_z at selected depths $z_1^* \ldots z_m^*$ valid for the periods between consecutive sampling times t_i and t_{i+1}. It also calculates the Brunt-Vaisala (stability) frequencies N^2:

$$N^2 = (g/\rho)(d\rho/dz) \qquad (4.7)$$

Where ρ is the water density and g is the gravitational acceleration. The exponential correlation

$$K_z = a\,(N^2)^{-b} \qquad (4.8)$$

is often used as an empirical model for K_z (Jassby and Powell 1975).

With a slight modification to the program VERDI, the flux of heat across the sediment-water interface or across thermocline due to penetration of short wave solar radiation can also be taken into account. This leads to an additional term (Δs) in the numerator of equation

(4.6). Heat flux in the pore water of the sediment column is modelled by molecular diffusion into a semi-infinite media for a given temperature of sediment-water interface (Broecker 1965). In most cases, however, the thermal "sediment memory" may have insignificant influence on the evaluation of K_z (Imboden, et al 1979). Commonly, though not universally, the solar radiation input at the base of the thermocline is negligible. In particular, in the study lake (Baldeggersee), this assumption is justified, as a typical average water transparency is about 1.2 m (Gächter 1979).

4. THE RADON METHOD

To evaluate the potential benefit of this technique, it is important to know which parameters influence sediment radon flux and where "excess" radon can be found. The short half-life (3.83 days) of radon-222 makes it ideal as a geochemical tracer with a "memory" of about one week. The parent nuclide, radium-226 (Half-life = 1620 years) occurs in far greater quantities in sediments than in the water column; thus providing a boundary source for emanation of radon-222.

Radon activity in the epilmnion and thermocline is influenced by the continually changing patterns of surface mixing, thus creating a varying source for the top portion of the profiles. Radon increase near the bottom, on the other hand, reveals the sediments as the other source area, which remains reasonably constant for nearly the entire stagnation period. The two sources are sufficiently far apart that there is very little or no excess radon in samples in intermediate was

confirmed by observation in the study lake. Thus bottom radon may be treated as diffusion into semi-infinite space.

Broecker (1965) first used vertical radon profiles to calculate eddy diffusion in the deep sea. The same method can be applied to lakes (Imboden and Emerson 1978), though complications may arise due to the relatively narrow bottom topography when horizontal currents may require three-dimensional diffusion/advection models. In the present study, the model was applied to vertical mixing in a limno-corral, an ideal system for the one-dimensional radon diffusion model (Imboden et al. 1979).

4.1 Modeling of Vertical Transport at the Sediment-Water Interface

Radon profiles are first interpreted in terms of a one-dimensional vertical eddy diffusion flux. The flux of radon from sediment (F) as well as the mixing regime (K_z) are commonly assumed to be constant for time periods of the order of the half-life time of radon. Thus the steady state, one-dimensional diffusion equation becomes:

$$0 = K_z (\partial^2 R'/\partial Z^2) - \lambda R' \qquad (4.9)$$

where R' is the "excess" radon activity (i.e. R' = R_n activity - R_a activity in dpm/liter; dpm = decays per minute) and $\lambda = 0.181$ days^{-1} is the radon decay constant. The solution of the above equation is:

$$R'(\xi) = R'_o \exp(-\alpha \xi) \quad , \quad \alpha = (\lambda \quad)^{1/2} \qquad (4.10)$$

interface and at a vertical distance ξ above the interface, respectively (Fig. 4.3).

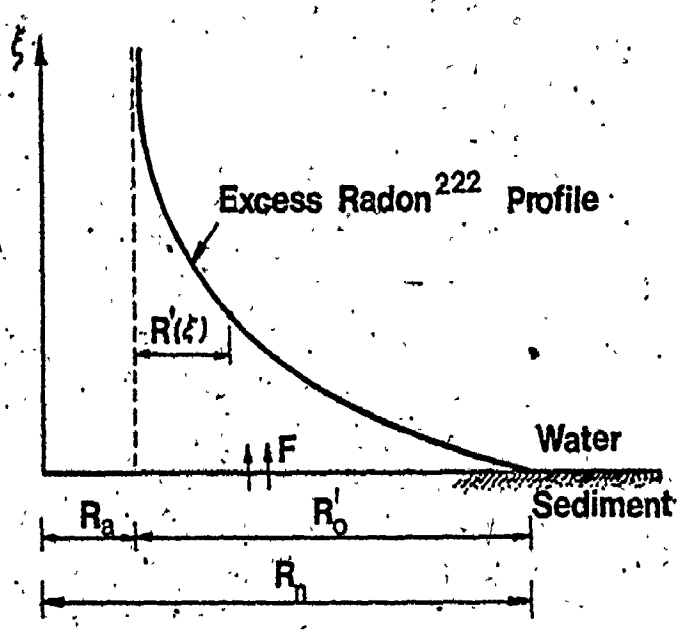

Figure 4.3 One-Dimensional diffusion Model of Radon-222

The flux of radon through the interface is determined from equation (4.10):

$$F = -K_z (\partial R'/\partial \xi)\big|_{\xi=0} = (\lambda K_z)^{1/2} R'_o \qquad (4.11)$$

For steady state, the standing crop of excess radon

$$\Sigma R' = \int_0^\infty R'(\xi)\, d\xi$$

is related to the flux F:

profiles of excess radon, which in turn are confined to the lowest few meters of the water column. In order to do this, a first estimate (and a test of the validity of the one-dimensional model) is the fit of the measured excess radon activities to the exponential relationship of equation 4.10. The resulting parameters K_z and R_o' are, in this case determined as apparent vertical eddy diffusivity and apparent boundary value. An alternative solution to equation (4.10) for K_z may be obtained by determining radon flux (F) from the sediments directly; i.e. by measuring radon flux from samples taken from the sediment core (Imboden and Emerson 1976). The boundary value R_o' of radon activity is then determined from equation (4.11).

Standing crops of excess radon (R_o') in the ocean vary between 0.2 and 20 dpm/cm^2 (Borecker et al. 1978). Since K_z near the bottom of oceans is usually larger than 1 cm^2/sec, excess radon can be detected up to 100 or more meters above the bottom, thus providing information on the average mixing regime in this layer. In lakes, on the other hand, K_z is significantly smaller, thus compressing the profile of R_n to a layer of a few meters thickness. Thus the technique provides information on the average mixing in the lower few meters of the water column. It can also be used to determine the flux of a substance from the sediments to the overlaying waters.

5. DISCUSSION

Temperature and radon models can provide much insight into the transport and thermal structure in the lower layers. However, such

models incorporate some serious limitations when applied to real lakes. These limitations arise from the simplifying assumptions, time averaging involved in the measurements of temperature or radon, and because the models are essentially one-dimensional whereas the lake is not. Perhaps their principal limitation is that they do not include the effect of lateral boundaries and advection.

The above limitations do not apply to the hypolimnion of many stably stratified lakes. The models have been successfully applied to relatively deep and thermally stable Swiss lakes (Imboden and Emerson 1978) and to vertical mixing in a limno-corral (in Baldeggersee; Switzerland). The results of the latter application are presented in Chapter VI.

Successful application of these methods requires precise measurements of temperature and radon activity.

CHAPTER V

EXCHANGE FLOW BETWEEN TWO INTERCONNECTED STRATIFIED BODIES OF WATER

1. INTRODUCTION

Exchange flow between two interconnected, stratified basins may be considered an interfacial transport or flux on the lateral boundary; such flow often produces considerable effects in both basins. Present oceanographic techniques for stratified exchange flow in sea straits or straits connecting two lakes are only of limited value. The main outlines and typical features of such flow are known but many details remain to be explained.

Limnological models of lake physics and biochemistry require an account of all fluxes of the active materials across the basin boundaries. This problem is complex when two interconnected lake basins of dissimilar characteristics exchange water via a communicating channel, especially where the wind is a major driving force.

The direct measurement of interbasin flow using current meters and/or similar supporting equipment can yield at best only approximate order-of-magnitude answers. Such measurements are very expensive. Numerical hydrodynamical modeling, on the other hand, would appear to hold out some hope for estimating interbasin flow using more readily available wind and temperature data. In any case numerical modeling may be the "best" way of describing our understanding of the complexities of

such flows even if the models are still unsatisfactory as operational predictors.

The goal of the present study is to prepare the groundwork for a numerical model of interbasins exchange flows. The next section presents a brief literature review of various potential approaches. In the following sections, a numerical model is developed. The application of the model to the Central and Eastern basins of Lake Erie at Pennsylvania Ridge is presented in Chapter VIII.

1.1 Literature Review of Related Models

A comprehensive literature survey was recently published (Eid; Internal report submitted to NWRI, Canada Centre for Inland Waters, March 1979). Various approaches suggested in that report, were subsequently discussed in a recent paper (Boyce, Chiocchio, Eid, Penicka and Rosa 1980). The paper reviews the physical processes of exchange flow between the two basins of Lake Erie based on field observations carried out in summer of 1977.

Only a summary of this literature survey is presented here.

a) Two-layer Models

The basic assumptions are that the flow consists of two distinct layers separated by a well-defined interface and that the dynamics can be simulated by assigning an average velocity and density to each layer. Recently, several authors have applied the so-called "streamtube" models to deep water underflows in fjords and straits (e.g., Whitehead, Leetman

and Knox 1974; Sambuco and Whitehead 1976; Gill 1977). In this approach, the upstream and downstream states are linked by the Bernoulli equation (conservation of energy), potential vorticity along streamlines and a cross-stream geostrophic balance. The flow was assumed to be frictionless and in steady state and represented by the hydraulics of rotating fluids.

The next level of complexity is the two-layer open channel hydraulics equations, both steady and time varying, including all external and internal forces. For simplicity we assume that the flow is gradually varied; steady state exists within periods during which a suitable time averaging of the external and internal forces is made. Many studies have been carried out on stratified two-layer flow in open channels (e.g. Stommel and Farmer 1952; Schijf and Schonfeld 1953; Long 1954, 1965; Wood 1968, 1970; Lai and Wood 1975; Abraham et.al. 1980). A variety of such flow problems were identified in a literature review presented by Elsayed (1978).

Most of the work done is based on laboratory experiments and limited to ideal rectangular channels. Much work is still required before the concepts can be applied to real problems. However, these models might answer the question as to whether the flow variations are dominated by local effects or by large scale motions in the adjacent basins.

b) Estuary Models

Two-layer models help to establish the relative importance of various terms in the local force balance but cannot deal with the actual structure of the flow, particularly, the vertical distribution of velocity and temperature. This vertical structure can be investigated by parameterization of vertical turbulence, e.g. vertical eddy viscosity dependent upon the local Richardson's number (Mortimer 1972).

Flow in estuaries has been studied by many researchers, e.g. Ippen (1966), Officer (1976), Bowden (1959,1971), Pritchard (1956), Hamilton (1975), Blumberg (1977), Odd and Roger (1978), etc. Similar models may be applied to exchange flow between two basins.

c) Three-dimensional Hydrodynamic Models

The main problem here is the open boundaries of adjacent basins. The problem may be solved by applying the usual three-dimensional hydrodynamic lake models using two different grid-size resolutions. A nested grid system, consisting of fine-mesh domains embedded in large coarse-mesh domains may be used (Lick 1976; Simons 1978). The simplest method is: first calculate a solution for the whole lake with the coarse-mesh discretization, then use this solution only to specify the boundary conditions for the fine-mesh domain comprising the communicating channel.

Such models may be able to present the three-dimensionality of the flow pattern, but require large computing effort and are very expensive to run due to small computational time increments. These

models must also be supported by many observations which might not be available in many cases. In any case the first stage overall model is unlikely to adequately describe the densimetric hydraulics of the connecting channel, and thus the boundary values for the second model would remain unreliable.

In the present study, a two-layer, one-dimensional model is developed. The model was applied to Lake Erie interbasin flow, but it is general enough to treat other similar problems.

2. THE MATHEMATICAL MODEL

2.1 Introduction

The continuous interchange of water between two bodies of water largely is controlled by three factors:

(1) stratification in each basin,

(2) the depth and width of the passage between the two basins, i.e., the morphometry of the strait, and

(3) the wind.

The currents in the interconnecting channel or strait are a consequence of the difference in vertical stratification between the water masses in the adjacent basins. The interchange is also wind induced, and thus variable. In this study we will restrict ourselves to the exchange flow between two interconnected fresh-water lakes or two basins of a lake where the stratification is mainly due to temperature. However the approach can be applied to treat stratification due to salt intrusion, for example.

2.2 Two-layer Steady State Model

Consider a system of two homogeneous layers of water separated by a sharp interface. The difference in density is assumed to be small compared to the density itself, thus the effect of buoyancy can be neglected. Velocity and density in each layer are vertically averaged. Vertical accelerations are neglected and the pressure distribution is assumed to be hydrostatic. The steady flow equations are derived for an arbitrary geometry. The cross stream velocities and Coriolis effect are neglected, and the flow is one-dimensional and gradually varied.

a) Momentum equations:

With reference to Figure 5.1 and the definitions below, for the upper and lower layers:

$$\frac{dWL_1}{dx} + \frac{\alpha_1 u_1}{g}\frac{du_1}{dx} = S_{1E} \qquad (5.1)$$

$$\frac{\rho_1}{\rho_2}\frac{dWL_1}{dx} + \frac{\Delta\rho}{\rho_2}\frac{dWL_2}{dx} + \frac{\alpha_2 u_2}{g}\frac{du_2}{dx} = S_{2E} \qquad (5.2)$$

b) Continuity equation

$$\frac{d}{dx}(Au) = 0$$

or

$$A\frac{du}{dx} + u\frac{dA}{dx} = 0 \qquad (5.3)$$

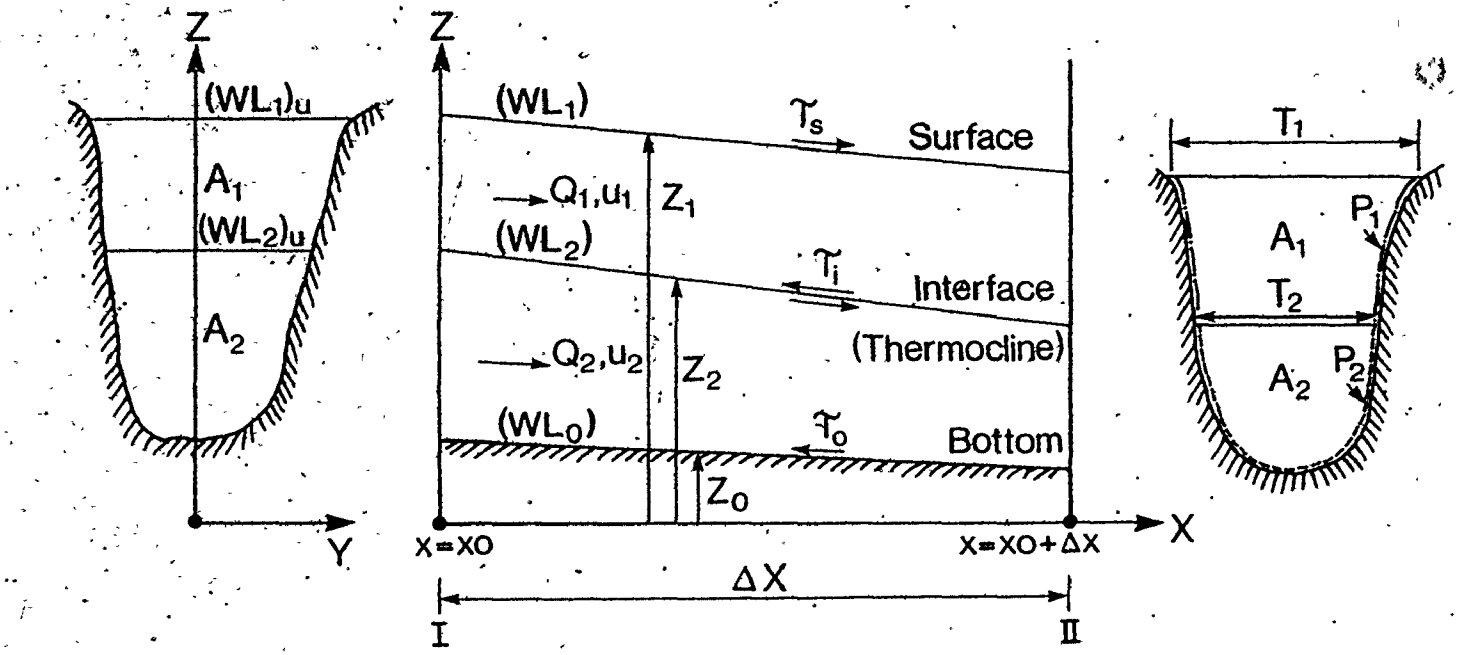

Figure 5.1 DEFINITION SKETCH OF TWO LAYER FLOW SYSTEM

For arbitrary (non-prismatic) channel

$$A = A(x, z)$$

Thus
$$\frac{dA}{dx} = \left(\frac{\partial A}{\partial z}\right)_x \frac{\partial z}{\partial x} + \left(\frac{\partial A}{\partial x}\right)_z \tag{5.4}$$

The first term on the right hand side represents the free surface term where $\partial A/\partial z$ = channel width at given distance x and $\partial z/\partial x$ is the slope of the water surface between two successive sections at distances x and $(x + \Delta x)$. The second is the topographic term (i.e. bottom slope, side walls, bottom configuration, etc.). For natural irregular channels of complex topography, this is difficult to determine. By replacing $\partial A/\partial x$ by the finite difference term $\Delta A/\Delta x$, where ΔA is the change of the cross-sectional area between two successive sections Δx apart for given water levels, it is not required to determine the bed slope (s_o), a parameter which is difficult to evaluate for irregular channels.

The term $\frac{dA}{dx}$ for the upper and lower layers may be expressed:

$$\frac{dA_1}{dx} = \left(\frac{\partial A_1}{\partial WL_1}\right)_x \frac{dWL_1}{dx} + \left(\frac{\partial A_1}{\partial WL_2}\right)_x \frac{dWL_2}{dx} + \left(\frac{\partial A_1}{\partial x}\right)_z$$

$$= T_1 \frac{dWL_1}{dx} - T_2 \frac{dWL_2}{dx} + \left(\frac{\partial A_1}{\partial x}\right)_z .$$

and

$$\frac{dA_2}{dx} = T_2 \frac{dWL_2}{dx} + \left(\frac{\partial A_2}{\partial x}\right)_z$$

Thus the continuity equation (5.3) becomes:

for upper layer:

$$A_1 \frac{d(\alpha_1 u_1)}{dx} + \alpha_1 u_1 \left[T_1 \frac{dWL_1}{dx} - T_2 \frac{dWL_2}{dx} + \left(\frac{\partial A_1}{\partial x}\right)_z\right] = 0 \qquad (5.5)$$

and for lower layer:

$$A_2 \frac{d(\alpha_2 u_2)}{dx} + \alpha_2 u_2 \left[T_2 \frac{dWL_2}{dx} + \left(\frac{dA_2}{\partial x}\right)_z\right] = 0 \qquad (5.6)$$

For the special case of a channel with constant width, Elsayed (1978):

$$\left(\frac{\partial A_1}{\partial z}\right)_z = 0 \text{ and } \left(\frac{\partial A_2}{\partial x}\right)_z = - T_2 \frac{\partial z_0}{\partial x} = - T_2 S_0$$

Neglecting the change of channel width might be serious when applying the model to channels with contractions or highly variable cross-sections.

S_{1E} and S_{2E} are the slopes of energy lines for the upper and lower layers respectively:

$$S_{1E} = \frac{-\tau_s T_1 - (\tau_i T_1 + \tau_{1b} P_1)}{\rho_1 g A_1} \qquad (5.7)$$

$$S_{2E} = \frac{\tau_i T_2 - \tau_{2b} P_2}{\rho_2 g A_2} \qquad (5.8)$$

where τ_s, τ_i and τ_b are surface, interface and bottom shear stresses.

u_1, u_2 are the average flow velocities.

ρ_1, ρ_2 are the densities.

$\Delta\rho = \rho_2 - \rho_1$.

Subscripts 1 and 2 denote the upper and lower layers respectively.

A, T and P are the cross-sectional area, top width and wetted perimeter of a given cross-section

α_1 and α_2 are kinetic energy correction factors.

g is the gravitational acceleration

The above equations may be written:

$$\frac{dWL_1}{dx} + \frac{\alpha_1 u_1}{g}\frac{du_1}{dx} = S_{1E} \tag{5.9}$$

$$\frac{\rho_1}{\rho_2}\frac{dWL_1}{dx} + \frac{\Delta\rho}{\rho_2}\frac{dWL_2}{dx} + \frac{\alpha_2 u_2}{g}\frac{du_2}{dx} = S_{2E} \tag{5.10}$$

$$\frac{dWL_1}{dx} - \frac{T_2}{T_1}\frac{dWL_2}{dx} + \frac{A_1}{u_1 T_1}\frac{du_1}{dx} = -\frac{1}{T_1}\left(\frac{\partial A_1}{\partial x}\right)_z \tag{5.11}$$

$$\frac{dWL_2}{dx} + \frac{A_2}{u_2 T_2}\frac{du_2}{dx} = -\frac{1}{T_2}\left(\frac{\partial A_2}{\partial x}\right)_z \tag{5.12}$$

These equations can be rearranged:

$$d/dx(\vec{y}) = \vec{C} \; ; \quad \vec{y} = (WL_1, WL_2, U_1, U_2)_t \tag{5.13}$$

or

$$\begin{bmatrix} 1 & 0 & 0 & 0 \\ 0 & 1 & 0 & 0 \\ 0 & 0 & 1 & 0 \\ 0 & 0 & 0 & 1 \end{bmatrix} \begin{bmatrix} \frac{dWL_1}{dx} \\ \frac{dWL_2}{dx} \\ \frac{du_1}{dx} \\ \frac{du_2}{dx} \end{bmatrix} = \begin{bmatrix} C_1 \\ C_2 \\ C_3 \\ C_4 \end{bmatrix} \tag{5.14}$$

The above equations are non-linear differential equations and can be solved for WL_1, WL_2, u_1 and u_2 for given boundary conditions using any suitable numerical technique. The numerical solution and computer algorithms are described in Section 3.

2.3 Shear stresses τ_s, τ_i and τ_b

2.3.1 Wind stress at water surface

It is well known that winds acting on the surface of a stratified lake give rise to large changes in the distribution of pressure, which in turn cause flows and changes in the positions of the interfaces. The wind shear stress τ_s may be written:

$$\tau_s = C_D \rho_{air} W_a^2 \tag{5.15}$$

where W_a is the component of wind speed along the channel's longitudinal axis at a standard anemometer elevation, ρ_{air} is the air density and C_D is the wind drag coefficient. The drag coefficient C_D is a function of wind and surface roughness characteristics (see Chapter II).

2.3.2 Interfacial shear stress τ_i

Assuming turbulent flow, internal shear stress may be expressed:

$$\tau_i = C_i \bar{\rho} |u_1-u_2| (u_1-u_2) \tag{5.16}$$

where $\bar{\rho} = (\rho_1+\rho_2)/2$ and C_i is the interfacial shear stress coefficient. The determination of the interfacial shear stress must necessarily be the subject of further research work (Lofquist 1960; Harleman 1961; French 1979; Dick and Marsalek 1972; Abraham et al. 1980).

2.3.3 Bottom shear stress

Bottom stress is written:

$$\tau_b = \rho_b C_o |u_\Delta| u_\Delta$$

$$u_\Delta = u(x,z,t) \quad \text{at } z = h - \Delta$$

Thus the bottom shear stress is related to the velocity at a distance Δ above the bottom. Δ can be considered to be representative of the frictional boundary layer just above the bottom (Eid 1976, James and Eid 1978a). For two-layer systems, $u_\Delta = u_b$, the average velocity in the bottom layer (Simons 1973). Thus the bottom shear stress for the upper and lower layers can be written:

$$\tau_{1b} = \rho_1 C_o |u_1| u_1 \tag{5.17}$$

$$\tau_{2b} = \rho_2 C_o |u_2| u_2 \tag{5.18}$$

The drag coefficient C_o may be assumed to be identical to that used in open channel flow (V.T. Chow 1959); e.g. Manning's roughness equation may be applied:

$$s_f = \frac{u^2 n^2}{(1.49)^2 R^{4/3}} \qquad \text{(English units)}$$

$$= \frac{u^2 n^2}{R^{4/3}} \qquad \text{(metric units)}$$

$$= \frac{\tau_b P}{\rho g A} = \frac{\tau_b}{\rho g R}$$

therefore $$\tau_b = \frac{g n^2}{R^{1/3}} \rho u^2$$

i.e.

$$C_o = \frac{g\, n^2}{R^{1/3}} \tag{5.19}$$

where R is the hydraulic radius A/p and "n" is Manning's roughness coefficient. Tables for different values of n for different kinds of soils and different channel conditions can be found in many text books (i.e. Chow). Manning's formula must be applied to a fully developed turbulent flow; it is unsatisfactory for channels so small that vicous effects predominate. Drag coefficients, C_o, or n may be varied not only from section to section along the channel axis but also within a given cross-section.

2.4 Averages from Distributed Parameters

In one dimensional theory flow characteristics which are distributed across complex sections in natural rivers and streams, must be spatially averaged. The velocities in (5.14) must be representative for each cross-section. Figure 5.2, for example, illustrates a case where the average velocity in the cross-section is not sufficiently representative to serve in the energy or momentum calculations. The velocity distribution factor, α, is used to account for the errors inherent in using the square of the mean velocity in such complex cross-sections.

Except in the very special case of a straight laboratory channel, cross-sections are seldom rectilinear or streamlines parallel to each other. It is important to have a solution technique that incorporates representative reach lengths in order to insure that the cross-sectional

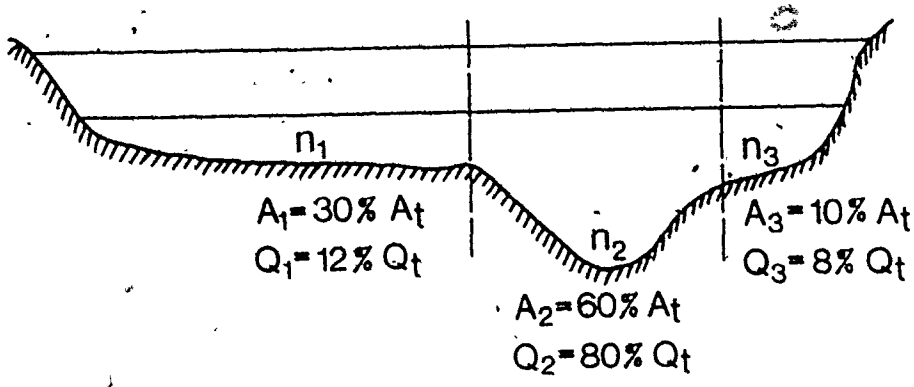

Figure 5.2 Irregular Distribution of Flow Parameters In a Complex Cross-section

data are appropriate for the entire range of discharges.

Another property that may vary across a channel section is the hydraulic roughness e.g., Manning's n-values. A technique to overcome this problem is to subdivide the cross-section into longitudinal sub-channels having similar hydraulic properties in the direction of the flow as shown in Figure 5.2.

Lateral discretization facilitates incorporating Coriolis forces especially necessary where the Rossby Radius of deformation $(g'h/f^2)^{1/2}$ is comparable to the channel width. Coriolis forces cause a transverse slope of the surfaces, obtained by applying the geostrophic balance equation (Defant: vol. I), under stationary conditions:

$$g \frac{\partial WL_1}{\partial y} = - fu_1 \quad \text{and}$$

$$g \frac{\partial WL_2}{\partial y} = -f \frac{\rho_2 u_2 - \rho_1 u_1}{\rho_2 - \rho_1} \qquad (5.20)$$

where f is the Coriolis parameter

$\frac{\partial WL_1}{\partial y}$ is the transverse inclination of the water surface, and

$\frac{\partial WL_2}{\partial y}$ is the transverse inclination of the interface (thermocline).

The latter inclination is considerably steeper than the former. The faster the currents and the wider the strait the greater this transverse slope.

2.5 Characteristics of Flow Profiles

Observed and computed flow profiles may be analysed in conformance with the general shape of two-layer densimetric flow profiles. In prismatic channels with one layer flow, the shapes of the water surface profiles are well established (see V.T. Chow). In natural channels carrying two-layer flow, the analysis of the flow profiles is complicated by the fact that the "control section" (section having critical flow) may occur at any point in the channel reach and its position cannot be determined easily. In this case, special features should be noted:

(1) The profile near or at critical depth cannot be predicted precisely by the gradually varied flow equations, since the flow is generally rapidly varied.

(2) When passing through critical depth, the flow profile should theoretically have a vertical slope. Since the flow is usually rapidly varied when passing through critical depth, the actual slope of the profile cannot be predicted precisely

by the above equations. Hence, and also due to friction, the critical depth may not occur above the break in the channel bottom profile or at the sill.

(3) The hydraulic jump may occur in either the upstream or downstream channel.

(4) If the upstream channel has an adverse slope, the discharge is not fixed by upstream channel conditions but by the elevation of the upstream pool level.

2.5.1 Dynamic equations of gradually varied flow.

Consider the profiles of gradually varied flow in the elementary length dx of an open channel. The water surface and interface slopes, with respect to x-axis, are obtained from Equation (5.14) as follows:

$$\frac{dWL_1}{dx} = C_1 = \frac{(1-F_{i2}^2)\, S_{1E} - (\frac{\rho_2}{\Delta\rho} F_{11}^2)\, S_{2E} + (1-F_{i2}^2)\, FF_1^2 - \frac{\rho_2}{\Delta\rho} FF_2^2}{(1-F_{i2}^2)\,(1-\beta\, F_{i1}^2) - \frac{\rho_1}{\Delta\rho} F_{11}^2} \qquad (5.21)$$

$$\frac{dWL_2}{dx} = C_2 = \frac{-\frac{\rho_1}{\Delta\rho} S_{1E} + \frac{\rho_2}{\Delta\rho}(1-F_1^2)\, S_{2E} - \frac{\rho_1}{\Delta\rho} FF_1^2 + \frac{\rho_2}{\Delta\rho}(1-F_1^2)\, FF_2^2}{(1-F_{i2}^2)\,(1-\beta\, F_{i1}^2) - \frac{\rho_1}{\Delta\rho} F_{11}^2} \qquad (5.22)$$

The above equations may be grouped:

$$S_1 = \frac{dWL_1}{dx} = \frac{\phi_{ns}(X,\ WL_1,\ WL_2,\ Q,\ \tau)}{\phi_c(X,\ WL_1,\ WL_2,\ Q)} \qquad (5.23)$$

$$S_2 = \frac{dWL_2}{dx} = \frac{\phi_{ni}(X,\ WL_1,\ WL_2,\ Q,\ \tau)}{\phi_c(X,\ WL_1,\ WL_2,\ Q)} \qquad (5.24)$$

Where:

$$F_1^2 = \frac{\alpha_1 Q_1^2 T_1}{g A_1^3} \quad , \quad F_{11}^2 = \frac{\alpha_1 Q_1^2 T_2}{g A_1^3} \quad , \quad F_{i1}^2 = \frac{\alpha_1 Q_1^2 T_1}{g' A_1^3}$$

$$F_2^2 = \frac{\alpha_2 Q_2^2 T_2}{g A_2^3} \quad , \quad F_{i2}^2 = \frac{\alpha_2 Q_2^2 T_2}{g' A_2^3}$$

$$FF_1^2 = \frac{\alpha_1 Q_1^2}{g A_1^3} \left(\frac{\partial A_1}{\partial x}\right)_z \quad , \quad FF_2^2 = \frac{\alpha_2 Q_2^2}{g A_2^3} \left(\frac{\partial A_2}{\partial x}\right)_z$$

$$\beta = \frac{\Delta\rho}{\rho_2} = \frac{\rho_2 - \rho_1}{\rho_2}$$

g' = reduced gravitational acceleration = $(g \cdot \beta)$

Equations (5.21) and (5.22) are solved for given discharges Q_1 and Q_2 and suitable parameterization of the shear stress coefficients, yielding the surface and interface profiles. The computer program "EXFLOW" was developed to solve the above equations using a Runge Kutta-Merson method. The process uses successive approximations and is known as the standard step method. The numerical solution is discussed in the next section.

Now consider Equation (5.24), setting each function to zero:

$$\phi_{ni}(X,\ WL_1,\ WL_2,\ Q,\ \tau) = 0 \qquad (5.25)$$

$$\phi_c(X,\ WL_1,\ WL_2,\ Q) = 0 \qquad (5.26)$$

As for one layer flow in an open channel, equation (5.25) represents the normal-depth profile in a prismatic channel. In nonprismatic channels, $\phi_{ni} = 0$ results in a "fictitious" normal-flow profile since uniform flow never occurs in non-prismatic channels. Similarly, Equation (2.26) represents the critical-depth profile. Since the critical discharge Q_c is independent of channel slope, the concept of the critical flow profile is valid in channels of variable slopes. Thus the critical flow condition is:

$$(1-F_{i2}^2)\,(1-\beta\, F_{i1}^2) - \frac{\rho_1}{\Delta\rho} F_{11}^2 = 0 \qquad (5.27a)$$

or:

$$F_{i1}^2 + F_{i2}^2 - \beta\, F_{i1}^2\, F_{i2}^2 - 1 = 0 \qquad (5.27b)$$

Equations (5.25) and (5.26) are solved using the Newton-Raphson method to produce respectively the fictitious normal-depth and critical-depth profiles along the channel reach.

In prismatic channels $\phi_{ni} = 0$ and $\phi_c = 0$ represent two parallel lines. In nonprismatic channels, however, the two profiles may intersect, say at point p (Fig. 5.3). At point p equation (5.24) gives $dWL_2/dx = 0/0$, an indeterminate form, or a "singular point". At this point the flow profile passes through the critical-depth and there exists a critical or "control" section. The slope of water at this point is equal to the limiting value of the indeterminate form $dz/dx = 0/0$ if this form is convergent. This value can be evaluated by:

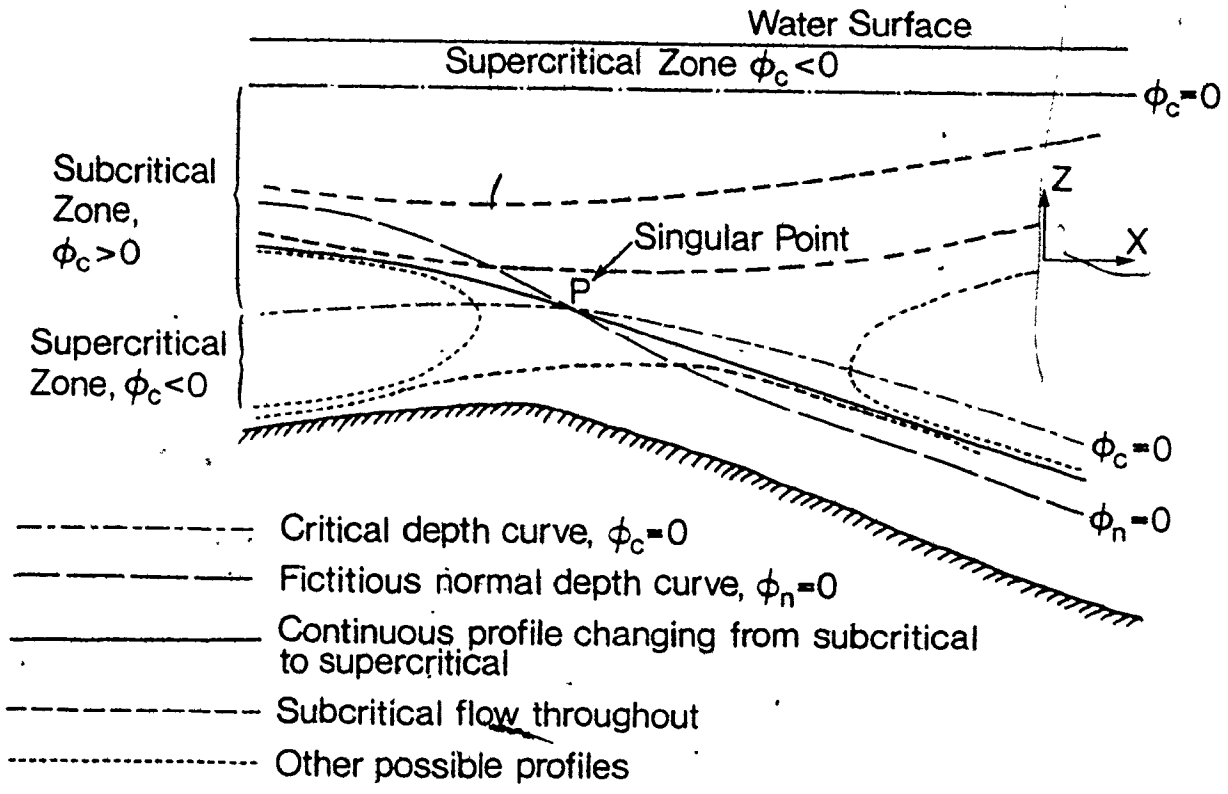

Figure 5.3 Flow Profiles in a Non-prismatic Channel

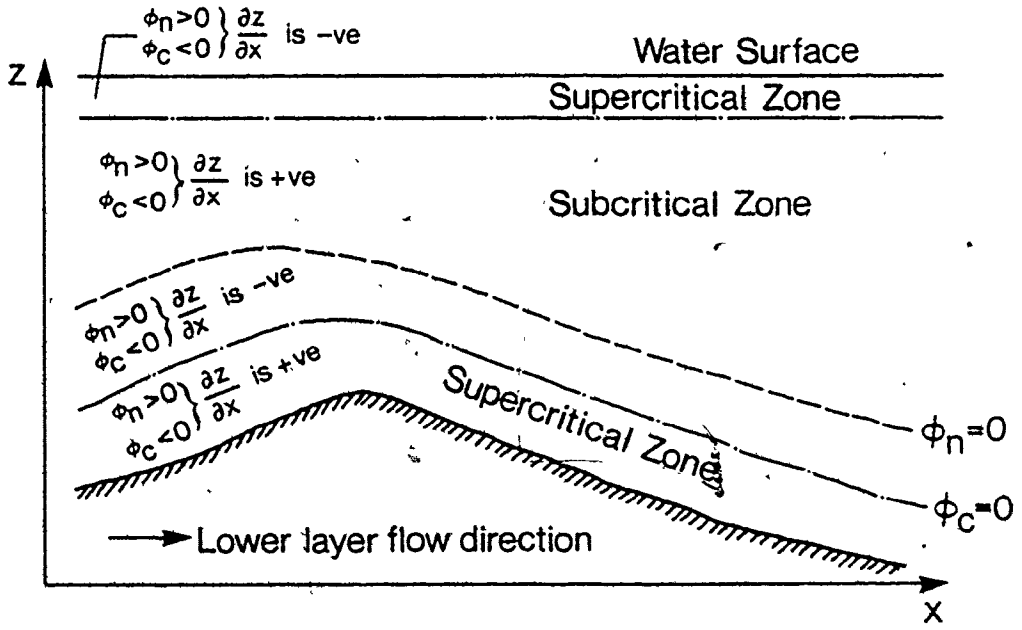

Figure 5.4 Characteristic Zones of Two-layer Open-Channel Flow Profiles

$$\frac{dz}{dx} = \left(\frac{dz}{dx}\right)_c = \left(\frac{d\,\phi_{ni}}{d\phi_c}\right)_c = \frac{d\,\phi_{ni}/dx}{d\,\phi_c/dx} \qquad (5.28)$$

$$\lim X \to X_c$$

A general solution of equation (5.28) for any kind of channel can be obtained mathematically by the method of singular points (T. Von Karman and M. Biot 1940). The position of the singular point (control section) can be determined graphically as shown in Figure 5.3.

2.5.2 Classification of Flow Profiles

For given discharge and channel conditions, the "normal"-depth and critical-depth lines divide the space in a channel into a number of zones where the interface profile can have different characteristics. In stratified flow, the water depth is divided into four zones as shown in Figure 5.4 and the slope and shape of the interface profile can be predicted accordingly. These characteristic zones can be used to check the computed profiles. It was found that for high interfacial shear stress coefficients and/or large discharges, there are two possible "normal depths" for a given discharge. This is similar to the flow in closed conduits (V.T. Chow 1959) under very small external pressure gradient.

3. THE COMPUTER MODEL

3.1 Development of the Computer Model

The computation of water surface profiles involves solving the stratified flow equations (5.21) and (5.22) to determine the shape of the surface and interface profiles between two (controlled) sections where the water levels are known. The most generally applicable procedure for steady flow profile calculation is called "the standard step method". In this method, the total channel reach is divided into smaller reaches by cross-sections at fixed locations along the channel. Starting from one end, where water levels and discharges in both layers are known, profile calculations proceed in steps from one section to another until the far end section is reached.

In the case of two-layer flow, model unknowns (i.e. water surface and interface levels as well as the discharges in both layers) may be given at either the upstream or downstream end section (initial-value problem). If the water levels only are given at two sections in the channel reach and it is required to determine the flow along the reach, this is termed a boundary-value problem. The solution of the boundary-value problem is more difficult, especially for irregular natural channels. In this case, the solution becomes sensitive to changes in bottom topography and water levels as there is more than one solution to equations (5.14) for the given water levels at the two end sections unless the discharges are properly constrained. Great care must be taken when modelling such problems.

On the other hand, solution of the initial-value problem is

useful when estimating the model parameters or when analysing the sensitivity of the solution to different variables and boundary conditions.

3.2 Numerical Solution of Initial-Value Problems

Water surface and interface profiles are computed along the connecting channel between the two basins for given water levels (WL_1 and WL_2) and discharges in both layers (Q_1 and Q_2) at one end. Equations (5.21) and (5.22) are integrated along the channel reach using the Runge Kutta-Merson method, (see Bull 1966; Elsayed 1978). The channel reach is divided into a number of cross-sections ΔX apart. The incremental distance ΔX, varies with the variation of channel topography (shorter at the sill). Each cross-section is described by a series of points whose coordinates are referred to arbitrary datums $x = y = z = 0$ as shown in Figure 5.5.

The computer program "EXFLOW" consists of a main program where the size of the arrays as well as the boundary values of the variables and the parameters are defined. The main program calls the computational subroutines. Information about the channel topography is given through subroutine XSEC. Critical and fictitious normal curves are calculated with the aid of subroutines CNCURVS, WLCRIT and NORMAL where equations (5.25) and (5.26) are solved using the Newton-Raphson method. Surface slopes given by equations (5.21) and (5.22) are integrated along an incremental reach of the channel using the Runge-Kutta-Merson method in subroutine FLPROF, originally written by E.

Elsayed (1978) and extended for the present study. More details and the listing of the computer program can be found in a recent publication (Eid 1980).

The present computer model is used to evaluate the flow profiles for given boundary conditions (water levels in either basin), discharge Q_2 in the lower layer (hypolimnetic flow) and different wind stresses at the surface. The discharge in the upper layer, Q_1, (epilimnetic flow) is determined from:

$$Q_{net} = Q_1 + Q_2 \tag{5.29}$$

where Q_{net} is the vertically integrated flow through the channel, set equal to the net flow into or out of either adjacent basin. In addition to the flow profile calculations, critical and "normal"-depth curves are determined. These curves are useful for determining the "critical" or "control" section where the singular point may be found. When a singular point exists, special treatment of the equations may be necessary. Plotting critical and normal curves throughout the channel reach, also aids interpretation of the possible flow profiles under different boundary conditions, (Fig. 5.4).

3.3 Numerical Solution Of Boundary-Value Problems

The initial-value problem model developed in Section 3.2 is modified to solve the boundary-value problems. The procedure may be carried out as follows: For given water levels at two sections in the channel reach calculate the average slope of the interface. Using

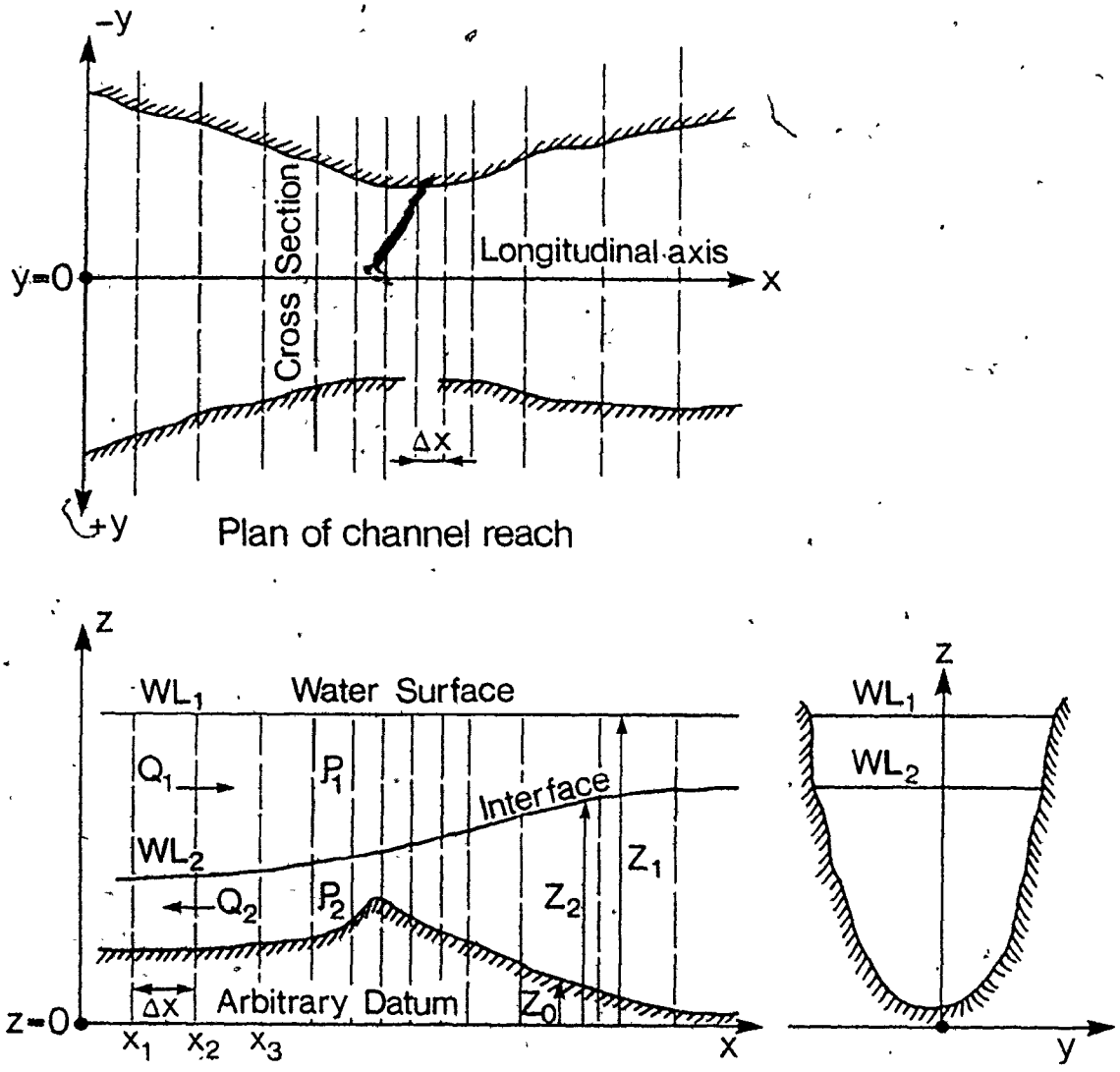

Figure 5.5: Numerical Discretization of the Exchange Flow Model

equations (5.9) and (5.10), eliminate the slope of the water surface S_1 and solve the resulting equation for Q_2 using a suitable numerical technique. Then use the calculated Q_2 as an input to the initial-value problem model "EXFLOW" and determine the surface and interface profiles. Compare the calculated profiles and flows with the observed data and repeat the procedures until the solution is obtained.

3.3.1 The Mathematical Algorithm

Equations (5.9) and (5.10) may be written in the form:

$$S_{1E} = S_1 - \frac{\alpha_1 Q_1^2}{gA_1^3}\left[T_1 S_1 - T_2 S_2 + \left(\frac{\partial A_1}{\partial x}\right)_z\right] \tag{5.30}$$

$$S_{2E} = \frac{\rho_1}{\rho_2} S_1 + \frac{\Delta\rho}{\rho_2} S_2 - \frac{\alpha_2 Q_2^2 T_2}{gA_2^3}\left[S_2 + \left(\frac{\partial A_2}{\partial x}\right)_z\right] \tag{5.31}$$

Eliminating S_1, Equation (5.31) becomes:

$$\begin{aligned}&(F_1 S_{2E} - \beta F_1 S_2 - \beta_1 F_{11} S_2 + \beta_1 FF_1) Q_1^2 \\ &- (F_2 S_2 + FF_2) Q_2^2 + (F_1 F_2 S_2 + FF_1 FF_2) Q_1^2 Q_2^2 \\ &+ (\beta_1 S_{1E} + \beta S_2 - S_{2E}) = 0\end{aligned} \tag{5.32}$$

where:

$$F_1 = \frac{\alpha_1 T_1}{gA_1^3}, \qquad F_2 = \frac{\alpha_2 T_2}{gA_2^3}, \qquad F_{11} = \frac{\alpha_1 T_2}{gA_1^3}$$

$$FF_1 = \frac{\alpha_1}{gA_1^3}\left(\frac{\partial A_1}{\partial x}\right)_z, \qquad FF_2 = \frac{\alpha_2}{gA_2^3}\left(\frac{\partial A_2}{\partial x}\right)_z$$

$\beta = \Delta\rho/\rho_2$ and $\beta_1 = \rho_1/\rho_2$

S_2 is the slope of the interface between two given cross-sections in the channel reach.

S_{1E}, S_{2E} are the slopes of energy lines of the upper and lower layers respectively (equations 5.7 and 5.8).

Equation (5.32) may be written in the short form:

$$y = f(Q_2) = 0 \qquad (5.32a)$$

which may be solved by using any suitable numerical technique. The method of interpolation or false position (Regula Falsi method; Scarborough 1966), was used in this study.

3.3.2 The Computer Model

Subroutine "BVPSOL" was written to solve equation (5.32) using the false position method (Eid 1980) and added to the previously developed program "EXFLOW". the program thus includes an option of choosing either the BVP or the IVP solution. Input for this subroutine includes the observed water levels at two sections in the channel reach (WL_1, WL_2). Subroutine BVPSOL calculates the corresponding value of the discharge in the lower layer Q_2 while the upper layer flow is determined from equation (5.29).

The computed values of Q_1 and Q_2 are then used to calculate the flow profiles and velocity distribution along the channel axis. The computed interface profile is further refined until it lies close to the observed profile. The model was applied to Lake Erie (Eid 1980). Model sensitivity analysis and verification is presented in Chapter VIII.

PART 2

PRACTICAL APPLICATIONS

PART 2

APPLICATION TO REAL LAKES

This part includes the practical application of the models developed in the previous chapters to a number of real lakes. The objective here is to illustrate the performance and validity of these models in practical problems. A wide range of lake sizes was selected in order to check the effect of each process or algorithm on the behaviour of these lakes. Each of these lakes is subjected to one or more of the processes or boundary conditions described previously. The field observations carried out in these lakes are described in the following chapters.

Although the algorithms are separately applied to lake transports under different boundary conditions, they are general enough to handle similar problems in different lakes. Calibration of key parameters and relating these to the lake and flow conditions will aid other studies.

The three-dimensional hydrodynamical lake transport model, described in Chapter I, is applied to a non-stratified small shallow lake with very rough bed (Valens reservoir) and to a stratified harbour (Hamilton harbour) during stagnation period. In these applications, the spatial and temporal variations of the boundary conditions at the surface and the bottom of the lake were studied (Chapter VI).

The transport and flux of a substance at the sediment-water

interface was studied in an ideal lake situation where the transports in the vertical direction dominate. A limo-corral or "test lake" was laid in a small, thermally stable, relatively deep lake in Switzerland (Baldeggersee). Vertical mixing in the hypolimnion is assumed to be mainly due to diffusion, and the vertical eddy diffusivity is determined as a function of depth and time using observed Radon-222 and temperature profiles (Chapter VII).

Finally, study of the exchange flow between the Central and Eastern basins of Lake Erie is presented in Chapter VIII. The interaction among winds, stratification, topography, river flow, etc. were studied. Field observations carried out by the National Water Research Institute, Canada Centre for Inland Waters were analyzed and used to calibrate and verify the model developed in Chapter V. This model is applicable to other interchange flow problems, e.g. between Hamilton harbour and Lake Ontario, where observations are currently lacking. The harbour - Lake Ontario interchange flow problem is not as complicated as that of Lake Erie and the present model can easily be applied there when the data becomes available.

CHAPTER VI

MODELING WIND-DRIVEN CURRENTS IN VALENS RESERVOIR AND HAMILTON HARBOUR

1. FIELD OBSERVATIONS

Valens reservoir is about 30 km northwest of Hamilton, Ontario, (about 185 acres; 0.75 sq.km). The maximum depth of the reservoir is about 4 m with an average depth of about 2.2 meters. Maximum wind fetch is close to 1 km and an average fetch is in the order of 0.3 to 0.4 km (Figure A-1 in the Appendix). The reservoir is characterized by extensive growth of bed weeds during summer months. Field observations were carried out through two summers in order to provide necessary data to verify the lake circulation model for different boundary conditions at the surface and the bottom of the reservoir.

Surface drift velocities were measured, using drogues, for various wind and bottom roughness conditions. Weed distributions throughout the lake were measured regularly. Wind speeds and directions, and water levels were continuously recorded. These field observations have been previously described in detail (Eid, 1976). A summary of field observations is presented in Table 6.1.

Hamilton harbour, on the other hand, is an enclosed body of fresh water connected to the western end of Lake Ontario by the Burlington ship canal (see the Appendix, Figure A-2). The harbour is approximately 8 by 4.8 km, maximum depth of 24 m and mean depth of about 13 m.

Table 6.1 Observed and Computed Surface Currents in Valens Reservoir with Weed Growth

Survey No.	Date	Wind speed m/sec	Wind Direction in degrees from North	V_{obs} cm/sec	V_{com} cm/sec	$\frac{V_{obs}}{V_{com}}$
1	June 5, 74	4.0	200 (S-W)	9.0	8.06	1.1
2	June 25, 74	3.8	45 (N-E)	6.3	6.30	1.0
3	June 26, 74	3.6	90 (East)	5.91	5.87	1.01
4	July 30, 74	4.1	245 (S-W)	7.46	7.33	1.02
5	May 21, 75	4.25	245 (S-W)	8.2	8.17	1.00
6	June 16, 75	4.9	250 (S-W)	8.0	8.02	0.99
7	June 26, 75	4.36	80 (N-E)	7.5	7.73	0.97
8	July 2, 75	3.6	300 (N-W)	8.0	6.43	1.24
9	July 22, 75	3.87	225 (S-W)	9.0	7.78	1.15
10	July 28, 75	3.4	270 (W)	7.2	6.45	1.10
11	July 30, 75	3.55	225 (S-W)	7.57	7.29	1.03
12	Aug. 11, 75	2.88	225 (S-W)	5.6	5.22	1.07
13	Aug. 18, 75	3.58	300 (N-W)	8.4	7.8	1.07
14	Aug. 26, 75	2.86	270 (W)	7.57	5.4	1.4

V_{obs}: is the average observed surface currents velocity

V_{com}: is the average computed surface currents velocity

Extensive water quality surveys have been carried out by the Ontario Ministry of the Environment since 1972. The results are summarized in the Ontario Ministry of the Environment Reports (1974, 1975, 1976). It was found that the harbour fails to meet the provincial criteria for fish, wildlife and recreation. Thus it was deemed important to develop a computer model to study the physical processes in the harbour under different boundary conditions.

Surface current velocities were measured (top 50 cm) using drogues (Figure 6.1), for various wind conditions. Continuous wind records were obtained at three stations around the harbour. Temperature profiles were taken from the Ministry of the Environment's reports. Details of the field observations in the harbour were presented in a previous publication (James and Eid 1976, 1978). A summary of the observations is presented in Table 6.2.

2. THE NUMERICAL MODEL

The three-dimensional (more accurately, a two-dimensional, multi-layered) hydrodynamic model, described previously in Chapter I was applied to Valens reservoir (non-stratified model) and Hamilton harbour (stratified model).

Figures 6.2 and 6.3 show the numerical discretization of the two lakes. The lakes are horizontally divided into equal squares (60 x 60 m in Valens and 305 x 305 m in the harbour). The mesh size has been chosen to adequately describe the boundaries, to reduce computation to manageable limits, and to correspond with our field data collection

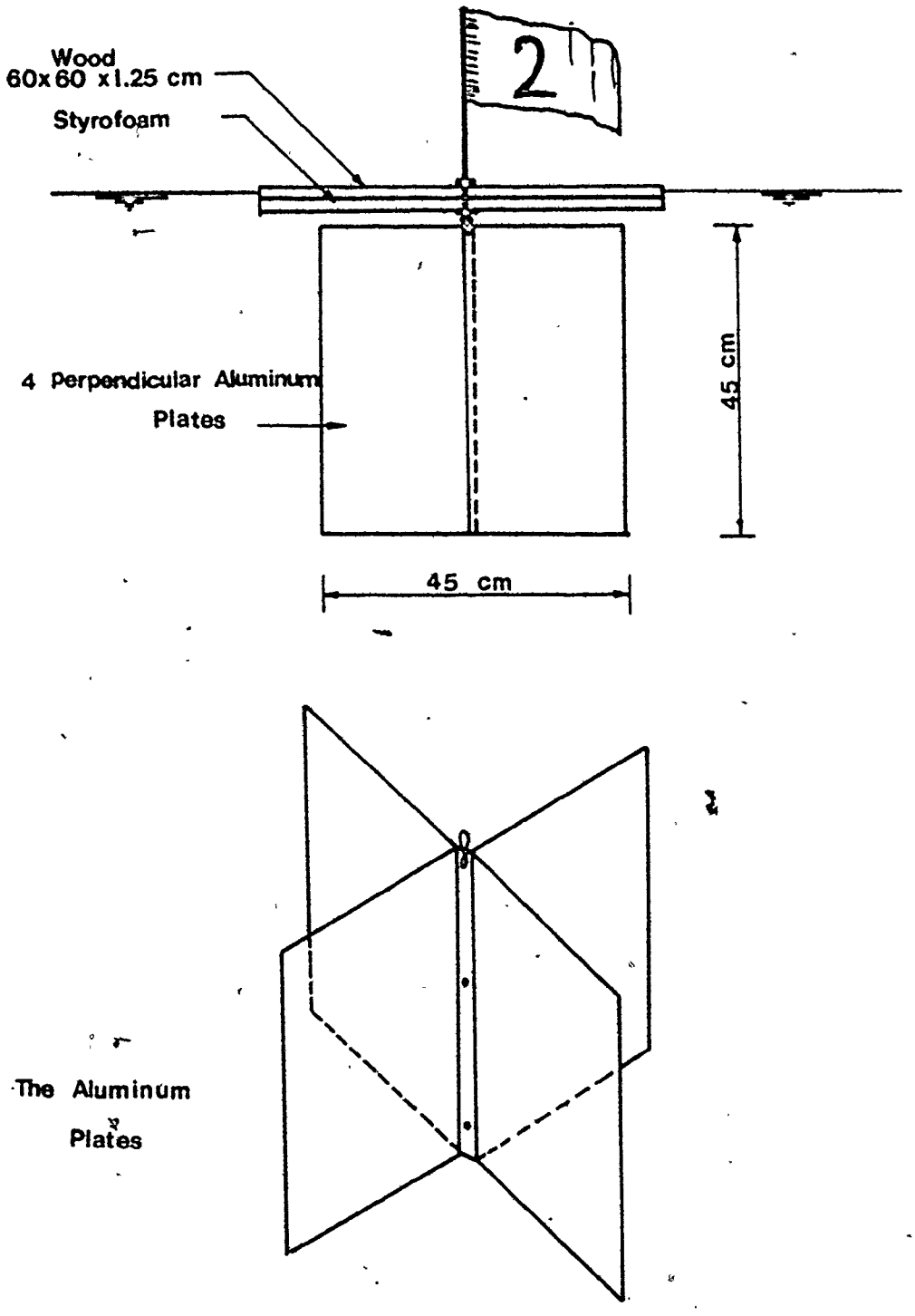

Figure 6.1: Typical drogue used to measure surface currents in Hamilton Harbour

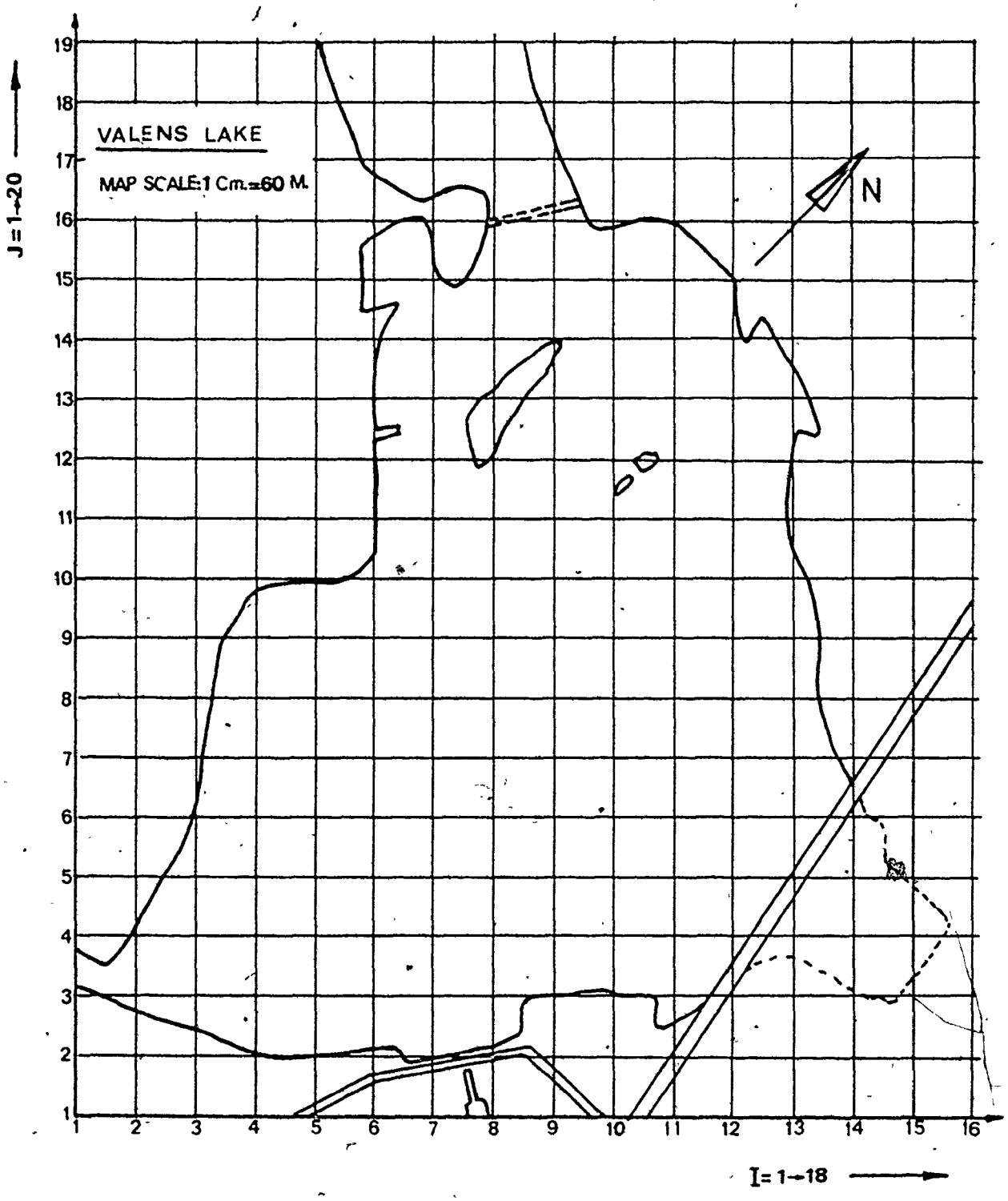

Figure 6.2: Numerical grid of streampoints superimposed on Valens Lake

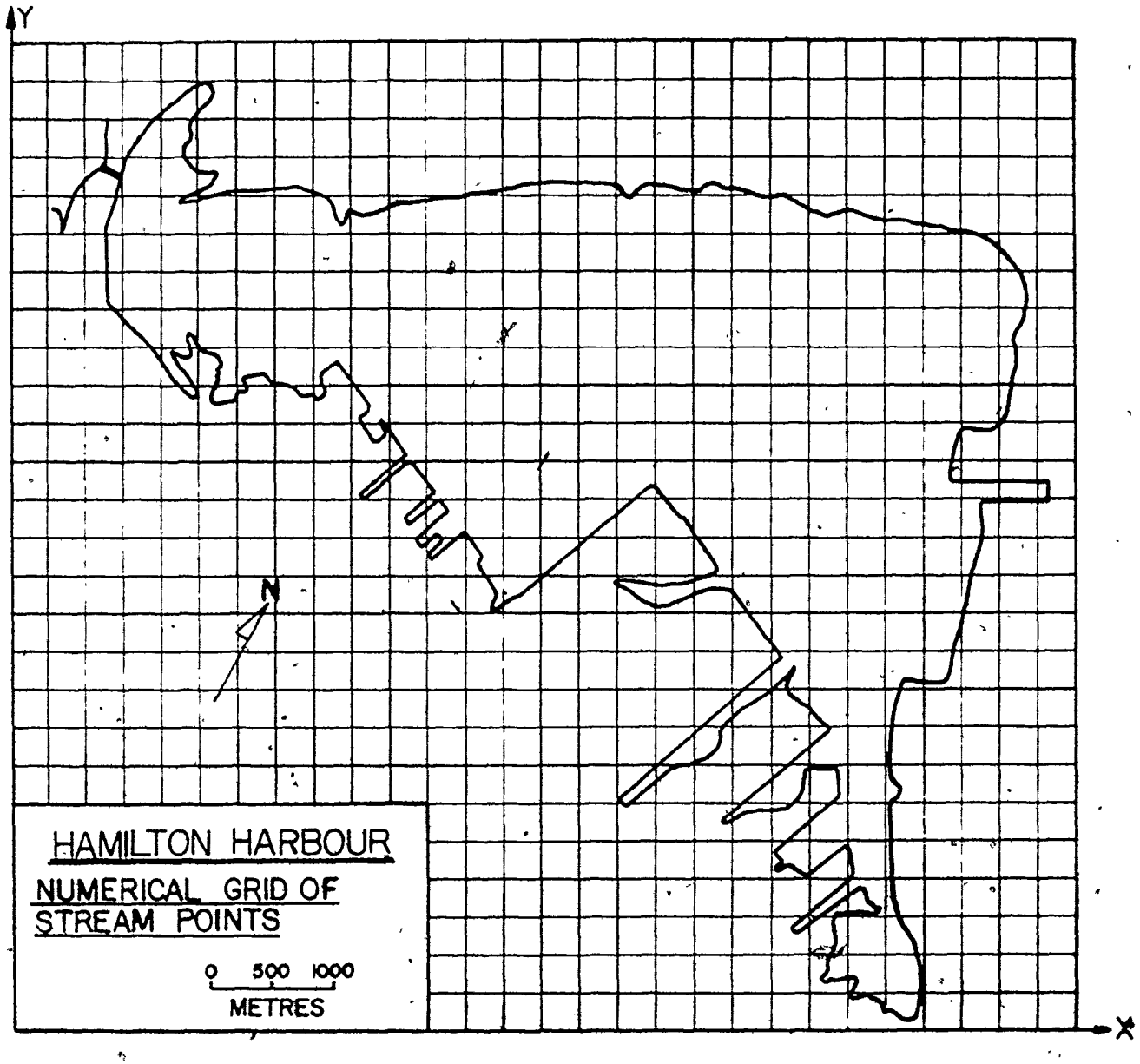

Figure 6.3: Hamilton Harbour numerical discretization

Table 6.2: Surface Current Observations in Hamilton Harbour

Survey No.	Date 1976	Wind Speed m/s	Wind direction in degrees from North	Average velocity cm/s	Average direction in degrees from North
1	July 16	6.52	310 (N-W)	20.3	312
2	July 30	3.42	110 (S-E)	13.0	115
3	Aug. 3	3.44	235 (S-W)	15.5	270
4	Aug. 4	3.53	225 (S-W)	12.1	260
5	Aug. 10	1.88	310 (S-W)	15.0	280 *
6	Aug. 11	3.95	225 (S-W)	12.1	235
7	Aug. 16	6.00	310 (N-W)	15.3	310
8	Aug. 17	2.82	300 (N-W)	10.3	250
9	Aug. 18	3.5	230 (N-E)	14.2	300 *

* Highly variable wind speed and direction were observed.

techniques. Two lattice-type numerical grids are arranged such that both components of the transport U and V are specified at the grid points (or streampoints) forming one lattice, while each point at the centre of each square is an elevation point at which ζ, T, P and W are defined, forming the second lattice. Water depths are given at streampoints (see Simons 1973 and Eid 1976).

In small lakes such as the two lakes under consideration, the variables can change rapidly over a short distance in the vertical direction. Consequently, a grid size is required that is much smaller in the vertical than the horizontal direction. In the vertical direction, six unequal-thickness layers are employed in the harbour such that the layer thickness decreases with increasing temperature gradient. In a non-stratified lake (Valens) however, the thickness of the layers are chosen to be smaller near the surface because of the extensive shallow zones and in order to have a sufficient number of layers for extrapolation to the surface.

Suitable time steps Δt were determined in each case such that the stability of the numerical solution is maintained as mentioned before in Chapter I.

The boundary conditions at the air-water interface were determined in both lakes by using the wind-wave coupling model developed in Chapter II. The local bed roughness due to variable weed distribution in Valens reservoir is determined with the aid of the model described in Chapter III. The following sections describe these applications.

3. WIND-WAVE COUPLING MODEL

3.1 Application to Hamilton Harbour

Surface drag coefficients were determined at each grid point using the two models (A and B) developed in Chapter II. Thus the drag coefficient is a function of wind-and-surface conditions. Different wind speeds ranging between 3 to 15 meters/sec were applied. The preliminary runs of the A-Model for one wind event (e.g., U_{10} = 6.52 m/s, north-west; Figure A.3 and A.4 in the Appendix) showed that the spatial variation of the drag coefficients (assuming a uniform wind over the lake) may have local effects on the computed velocity when compared to those computed using a constant drag equal to the average value (1.2×10^{-3}). This effect may be as high as $\pm$ 15% near the up or down-wind coast lines. On the average basis (and under a uniform wind condition), this effect may be small.

The B-Model, on the other hand, was applied to the same conditions and the results are shown in Figures A.5 and A.6 in the Appendix. As shown in Figure A-5, the values of the form drag coefficient change slightly with the location (or the fetch), ranging between 1.23×10^{-3} and 1.36×10^{-3} with a mean of 1.25×10^{-3}. Thus an average value of the drag coefficient calculated by the B-model may be sufficiently accurate.

Average values of the form drag coefficients computed in the harbour for wind speeds ranging between 3. and 15 m/s, using the two models, are presented in Figure 6.3a. These values are compared to those obtained from other studies (Smith and Banke 975, Wu 1969, Garratt

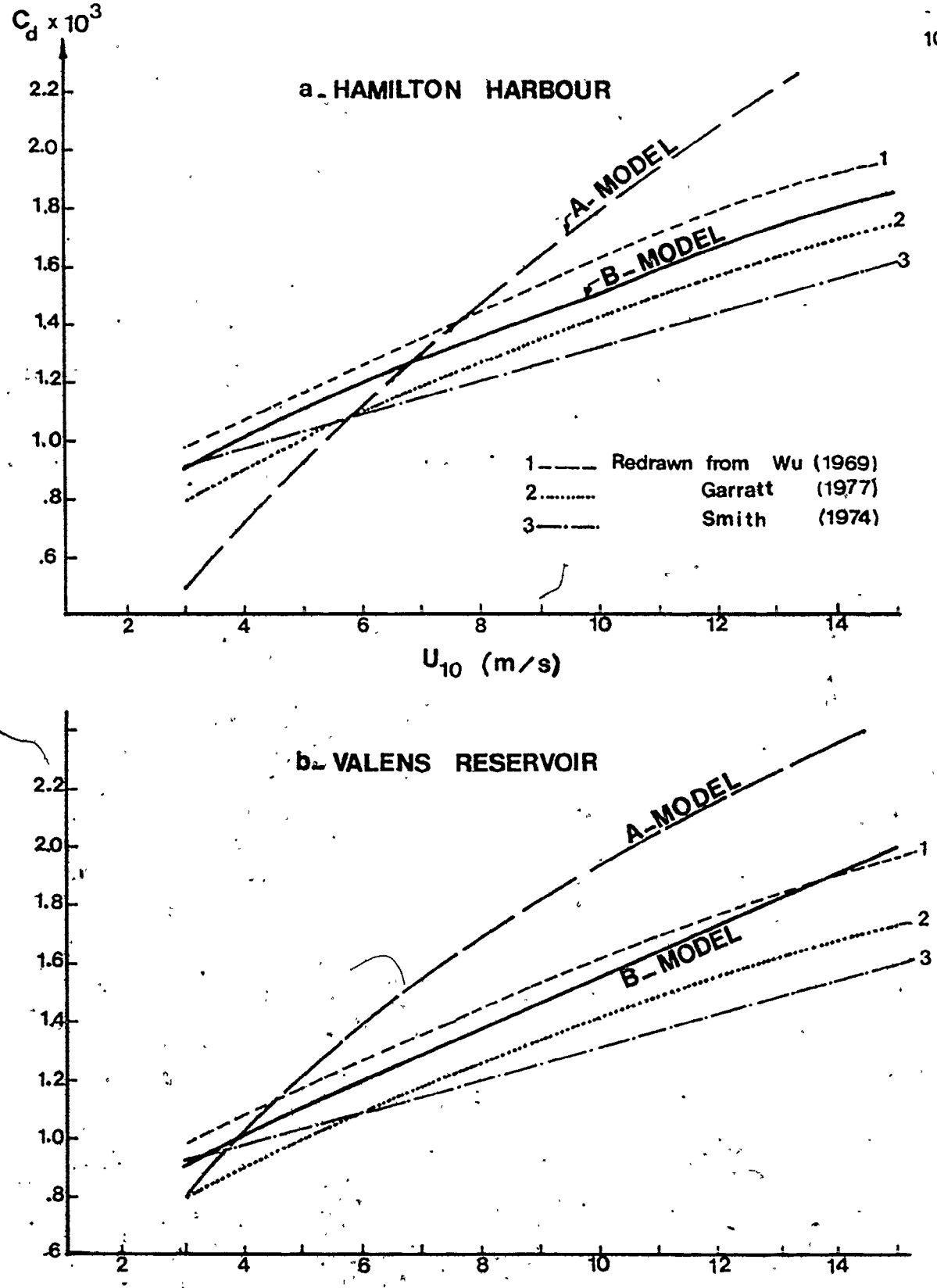

Figure 6.4 Computed Form Drag Coefficient as a Function of Wind Speed in Hamilton Harbour & Valens Reservoir

1977). As shown in Figure 6.4, the B-Model results are in good agreement with the reported results in other studies, while the A-Model gives lower values at slower wind speeds and higher values at higher speeds. Thus, and due to the lack of direct measurements of the drag coefficient in the harbour, the B-model is used in the hydrodynamical model to study wind-driven currents in the habour.

3.2 Application to Valens Reservoir

Similar computer runs were carried out to determine the drag coefficients at each grid point under different wind conditions in Valens lake. Samples of the results of the A and B-models are shown in Figures A.6 and A.7 respectively (see the Appendix). The effect of the spatial variation of the drag coefficient on the computed surface currents is smaller than that in Hamilton harbour. This is obviously because of the small size of the reservoir. Thus a spatially averaged drag coefficient may be sufficient for such small lakes.

The average drag coefficients calculated by the two models (A and B) for different wind speeds (3 to 15 m/s) at Valens are presented in Figure 6.4b. When compared with values obtained in the harbour, the average drag coefficients calculated in Valens reservoir are found to be slightly higher (due to the smaller fetches and the slower wave phase velocities). Again, the B-Model results were found to be in close agreement with the reported data. Accordingly the B-Model will be used in the following application of the hydrodynamical model (Section 6.1).

3.3 Conclusion

In summary, the present wind-wave coupling models may be used to determine the spatial variation of the form drag coefficient in a given lake. The larger the lake the more important it is to account for this variation. For smaller lakes (such as Valens) an average value may be used, and the present algorithm will give a good rational basis for calculating the spatially average drag coefficient as a function of wind speed, lake size and wave characteristics.

In the following applications of the three-dimensional hydrodynamic model, the B-model will be used to determine the form drag coefficients for different observed wind events. Adding the "skin" drag coefficient $C_s = 0.7 \times 10^{-3}$ to the calculated value of the form drag coefficient, we get the total drag coefficient C_D. Thus the shear stresses τ_o at the water surface are determined, from Equation (2.1), at each grid point in the numerical solution of the hydrodynamical equations (1.1 and 1.2).

4. SPATIAL DISTRIBUTION OF BED-ROUGHNESS IN VALENS RESERVOIR

4.1 Analysis of the Results

The computer model was run for all valid observed wind events (shown in Table 6.1) for two cases: a) with the existence of weeds, and (b) without weeds, in which the nonlinear bottom roughness coefficient was assumed to be constant all over the lake and approximately 2.5×10^{-3}. Samples of the model results are shown in Figures 6.5, 6.5 and 6.7. Figure 6.5 shows the computer plots comparing surface current

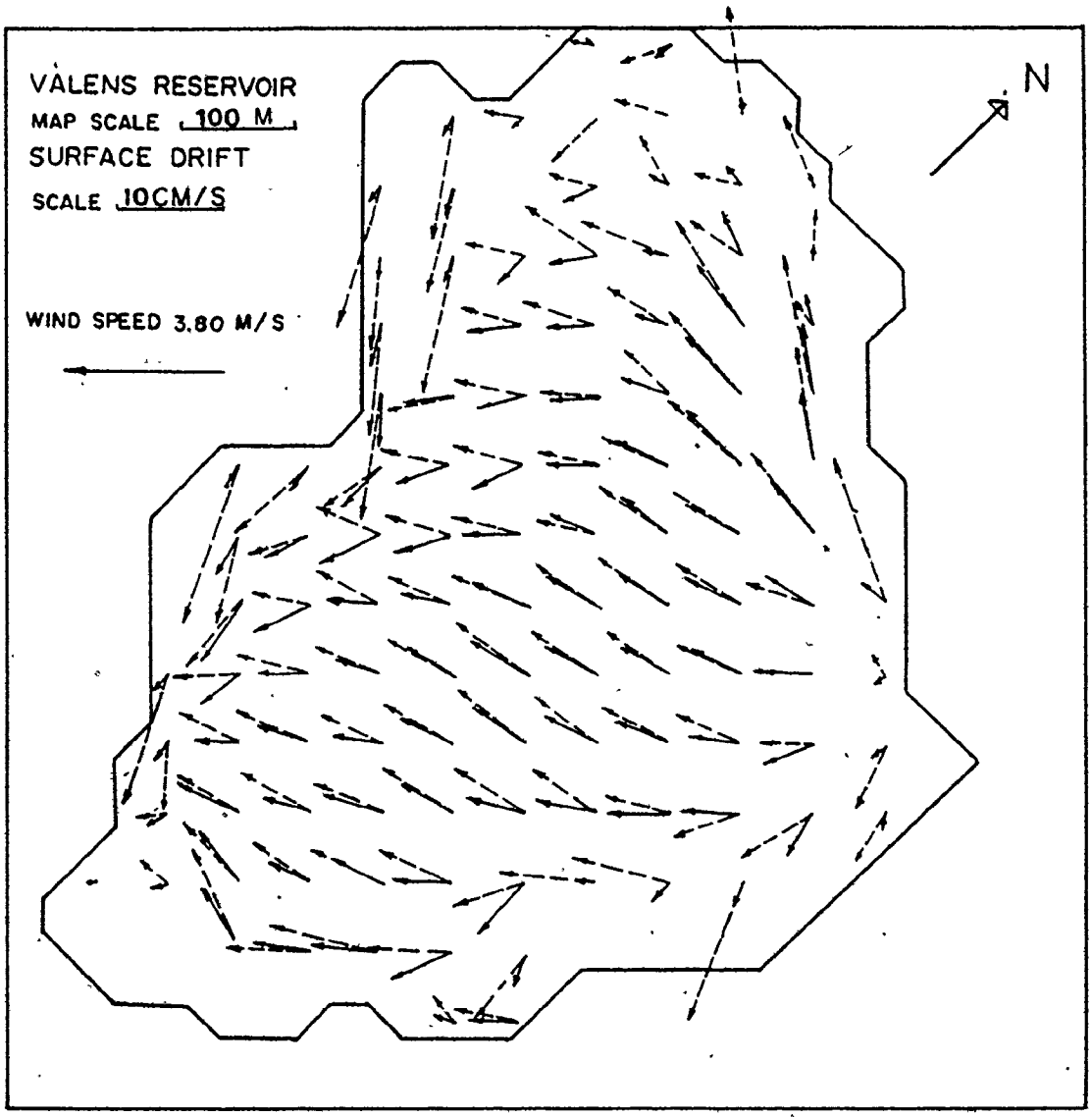

Figure 6.5: Effect of weeds on surface current pattern; with weeds (solid lines), without weeds (dashed lines).

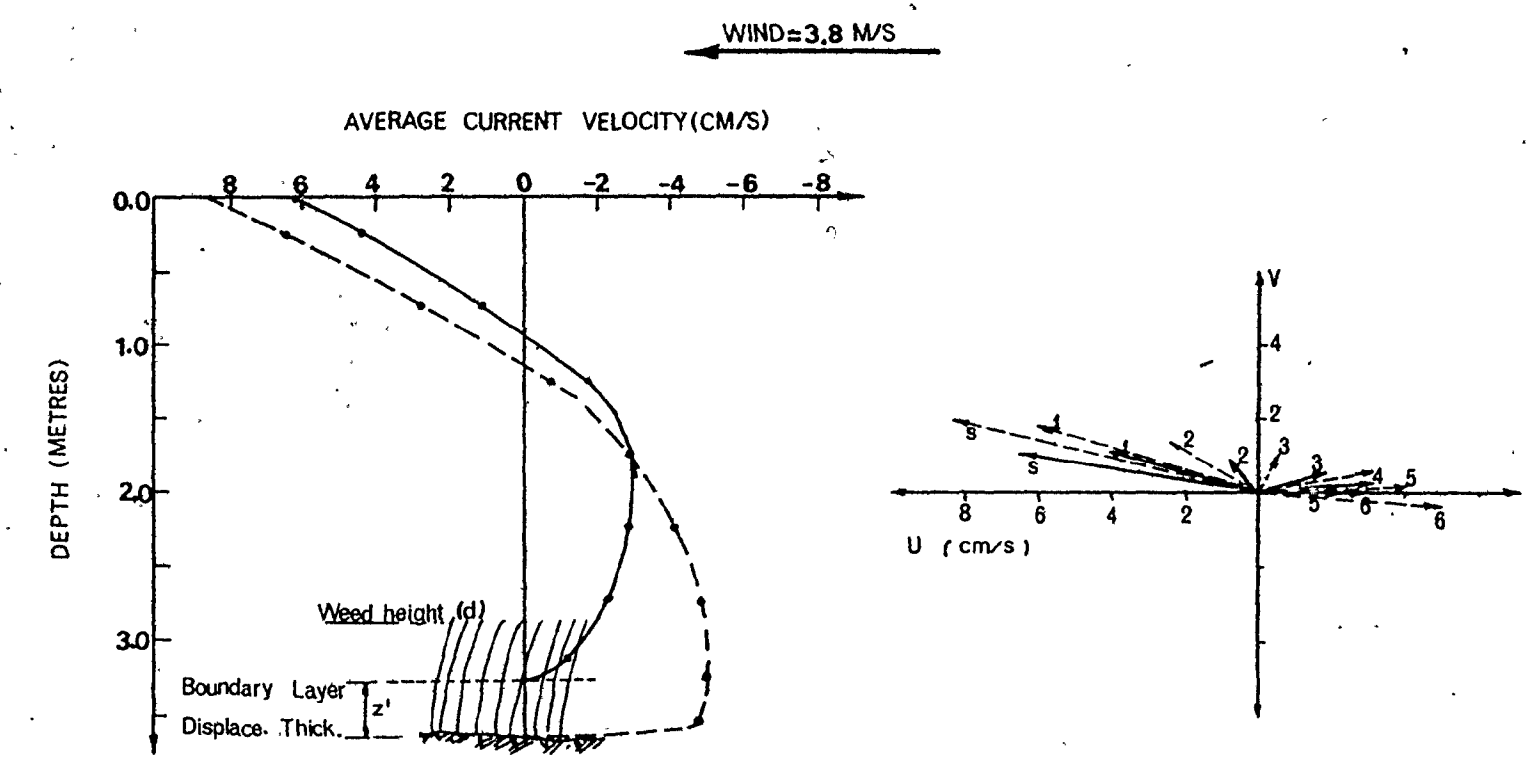

(a) VELOCITY PROFILES FOR TWO CASES OF ROUGHNESS

(b) PLAN SHOWING THE VELOCITY IN EACH LAYER 1,2,3 ..etc

Figure 6.6: Effect of bed weeds on velocity profiles; with weeds (solid lines), without weeds (dashed lines).

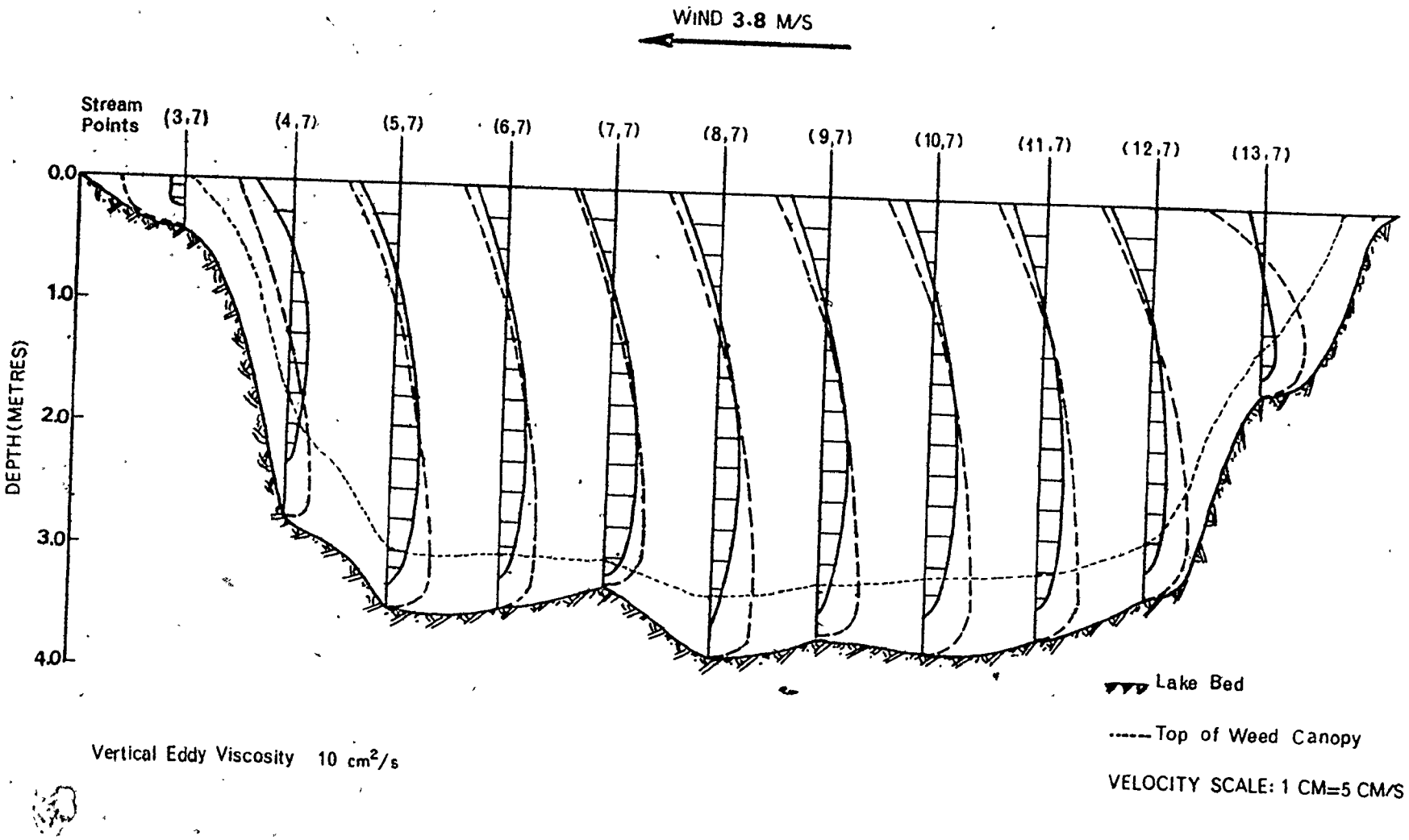

Figure 6.7: Schematic cross-section through Valens reservoir showing velocity profiles at the numerical grid points

patterns for the two cases of bottom roughness. It is clear that bottom shear stresses due to weeds generally affect the flow in both magnitude and direction. This influence depends on the stage of weed growth. Modeling weed growth might decrease the computed surface and bottom velocities. This reduction may be as high as 20%, but in shallow parts the reduction is greater because extensive weeds cause a considerable retardation of the flow. The effect of bottom roughness on the velocity profiles is shown in Figures 6.6 and 6.7. The velocity profile resulting from the assumption that the bottom roughness is areally constant was compared to that obtained by accounting for the spatially varying local bottom roughness due to weed growth. It was again found that spatially varying bottom stresses due to weeds cause a reduction in both surface and return currents. The reduction of the return flow near the bottom is much bigger than that of the horizontal flow near the surface. A comparison was made between the observed and computed average surface drifts for a narrow areal strip. The results are shown in Table 6.1, and presented in Section 6.1.

4.2 Discussion and Conclusion

Bottom roughness due to extensive weed growth in shallow lakes can be modeled using the formulation developed in Chapter III. The formulated bottom stress equation appears to incorporate the effect of weed height and distribution throughout the Lake. This formulation for bottom stresses can be conveniently incorporated into a three-dimensional transport model for wind-driven lake circulation. It

appears to account for the observed surface flow patterns.

In shallow lakes with prolific weed growth, the boundary condition at the bed is very important. Bottom shear stresses due to weeds greatly affect the currents in both magnitude and direction. This influence depends on the stage of weed growth and its distribution over the lake bed. It causes a reduction of flow velocities (both surface and return current). The effect of bottom roughness on the flow in shallow zones is much greater than that in deeper parts, as is to be expected.

5. OBSERVED SURFACE CURRENTS VERSUS WIND VELOCITY

Surface currents observed in Valens reservoir and Hamilton harbour at different wind velocities are summarized in Figure 6.8; each point indicates the value averaged from more than 20 measurements (see Eid 1976; James and Eid 1976). As shown, the observed surface drift increases with wind velocity and currents observed in Valens are much smaller than those observed in Hamilton harbour. This is obviously due to the shallowness of Valens lake and the effect of extensive bottom roughness due to weed growth.

The surface drift velocities as percentages of the measured wind velocities are plotted in Figure 6.8b. The percentage decreases as the winds increase. In Valens, an average value of about 2% was found for the observed wind events, while about 3.8% was found in the harbour. Wu 1968, in his laboratory experiment, found that an average value of 4% was observed. A value of the order 3.3% was reported by Keulegan

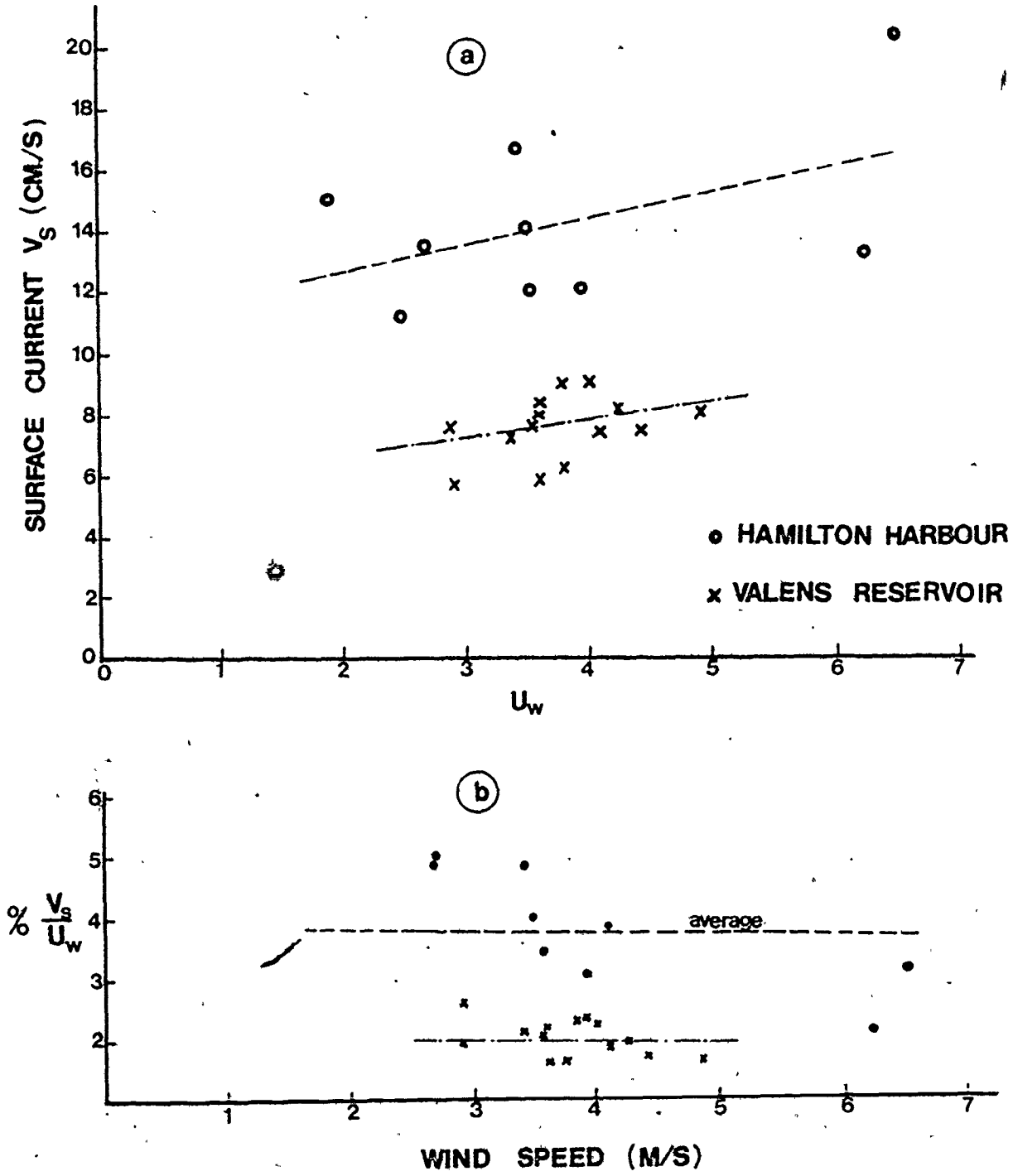

Figure 6.8 Observed Average Surface Currents vs. Wind Speed

(1951). These observed surface currents were used to verify the three-dimensional hydrodynamical lake circulation models of the Harbour and Valens reservoir.

6. ANALYSIS AND RESULTS OF THE HYDRODYNAMIC MODEL

6.1 Application to Valens Reservoir

As described in previous sections of this chapter, the three-dimensional hydrodynamic model was applied to determine surface currents in Valens reservoir for all valid wind events shown in Table 6.1. Due to its shallowness, the reservoir is considered to be homogeneous (i.e., thermally non-stratified lake) during summer time. Surface drag coefficients and consequently surface shear stresses were determined as a function of wind and wave characteristics as mentioned before. A spatially averaged value of the drag coefficient was determined for each wind event and used in the present application. Bottom roughness was computed for all measured weed distributions throughout the lake. Vertical eddy viscosity was determined as a function of wind speed and lake depth according to Equation 1.9, (Bengtsson 1973):

$$A_v = CHW_a$$

where C is a dimensionless constant = 2×10^{-5} for H < 15 m., H is the depth of the lake, was set to 400 cm, and W_a is the wind speed (cm/s). Samples of the computed and observed surface current patterns are shown in Figures 6.9 throughout 6.13. A comparison was made between the average computed and observed surface drifts for the same areal strips where measurements were taken (Table 6.1). As shown in Table 6.1 and

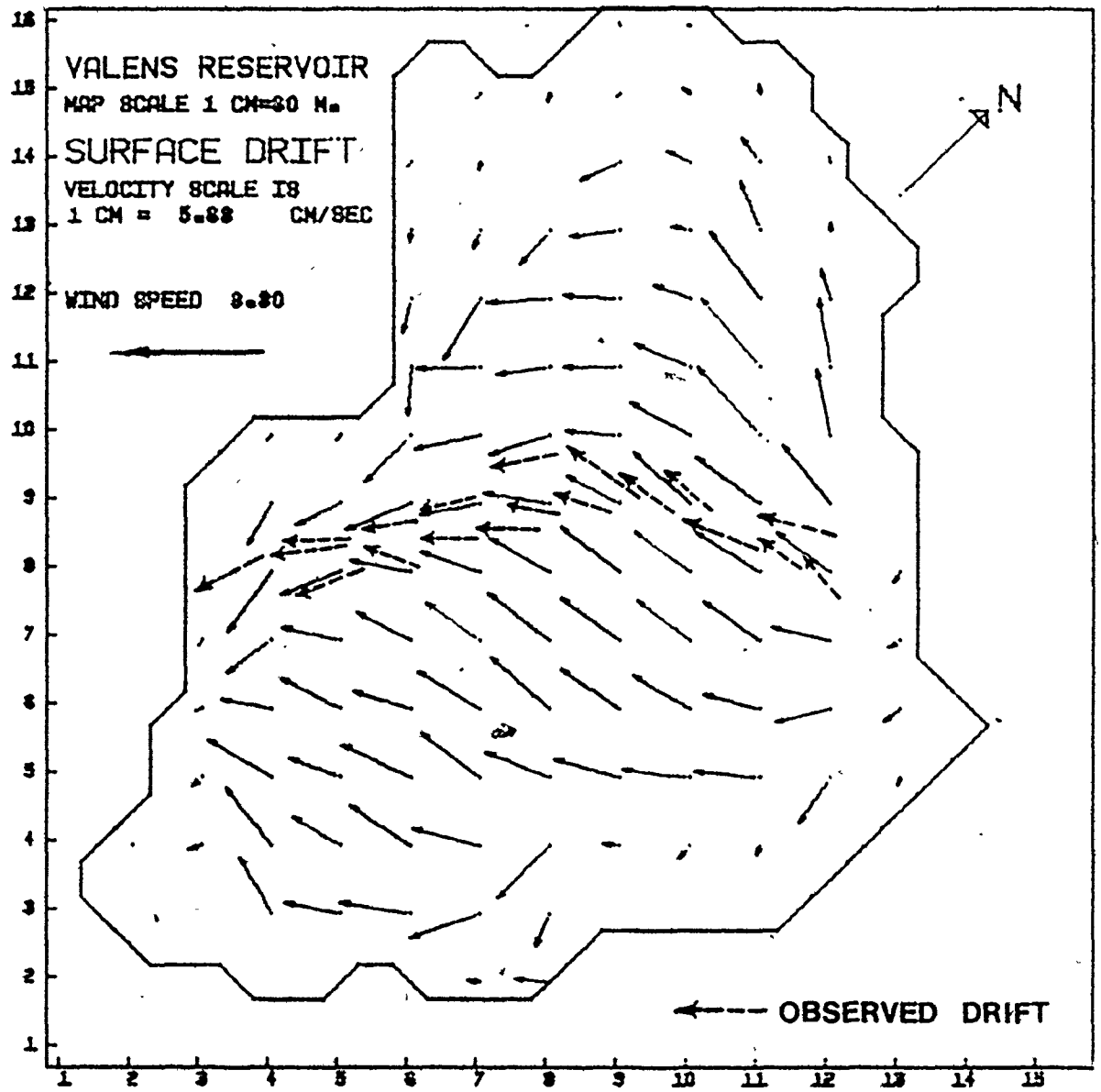

FIG.6.9:COMPUTED SURFACE CURRENTS

SURFACE CURRENT SURVEY : JUNE 25 , 74

WEED SURVEY JUNE 27, 74

VERTICAL EDDY VISCOSITY=3.0 CM/SEC

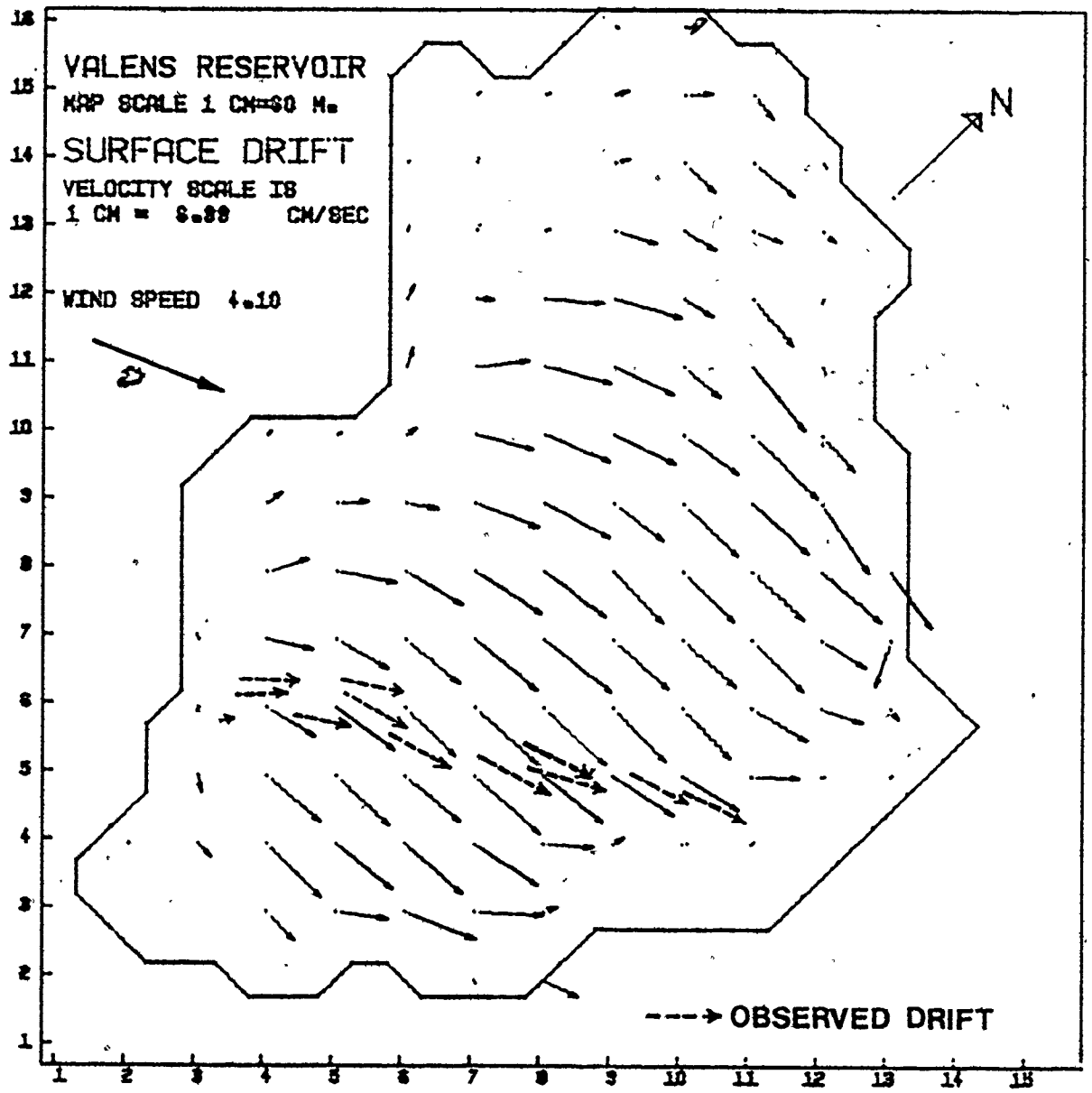

FIG. 6.30: COMPUTED SURFACE CURRENTS

SURFACE CURRENT SURVEY: JULY 30, 74

WEED SURVEY : AUG 6, 74

VERTICAL EDDY VISCOSITY=3.3 CM/SEC

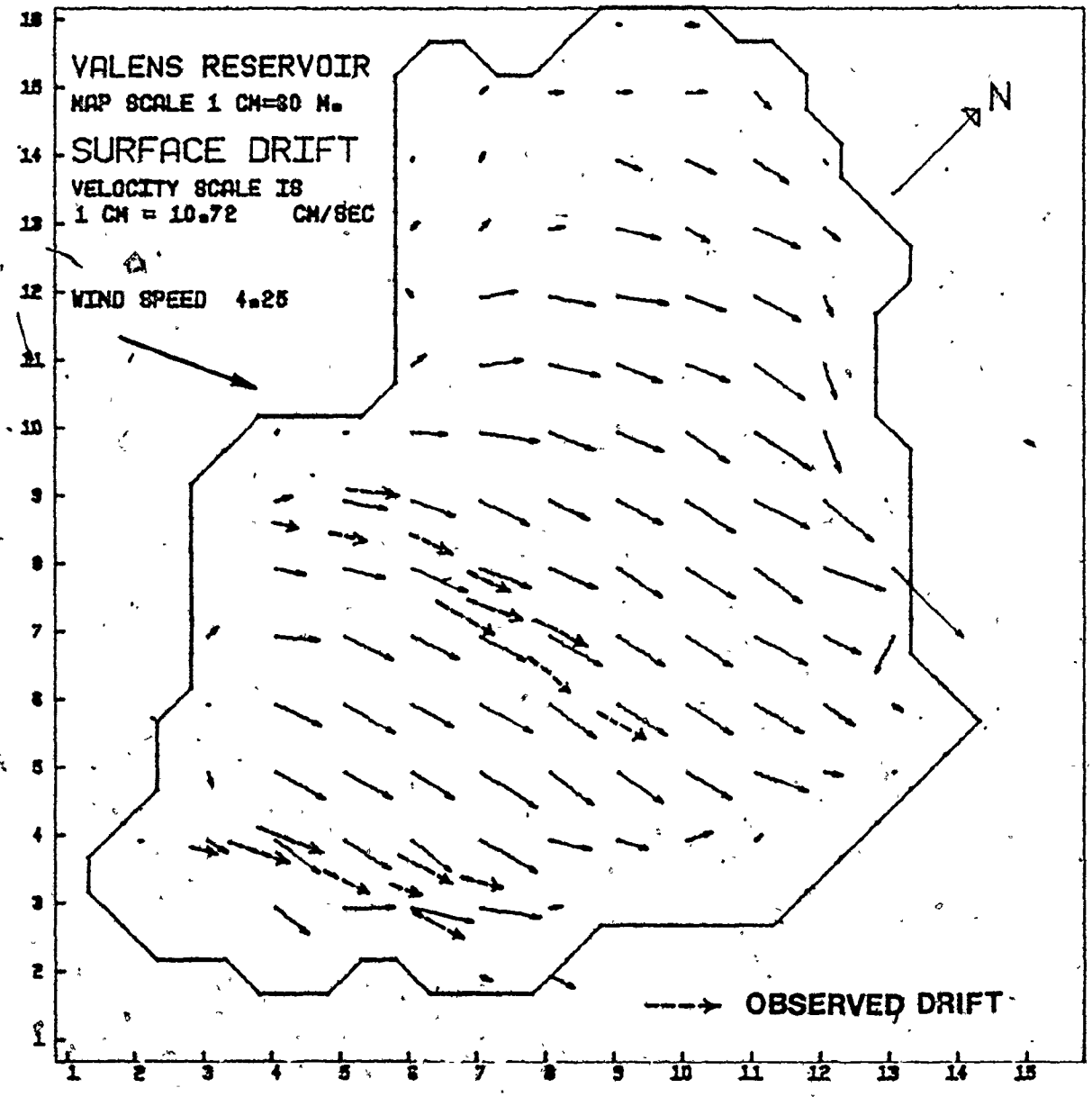

FIG.6.11 COMPUTED SURFACE CURRENTS

SURFACE CURRENT SURVEY: MAY 21,1975

WEED SURVEY : MAY 23, 75

VERTICAL EDDY VISCOSITY=3.4 CM/SEC

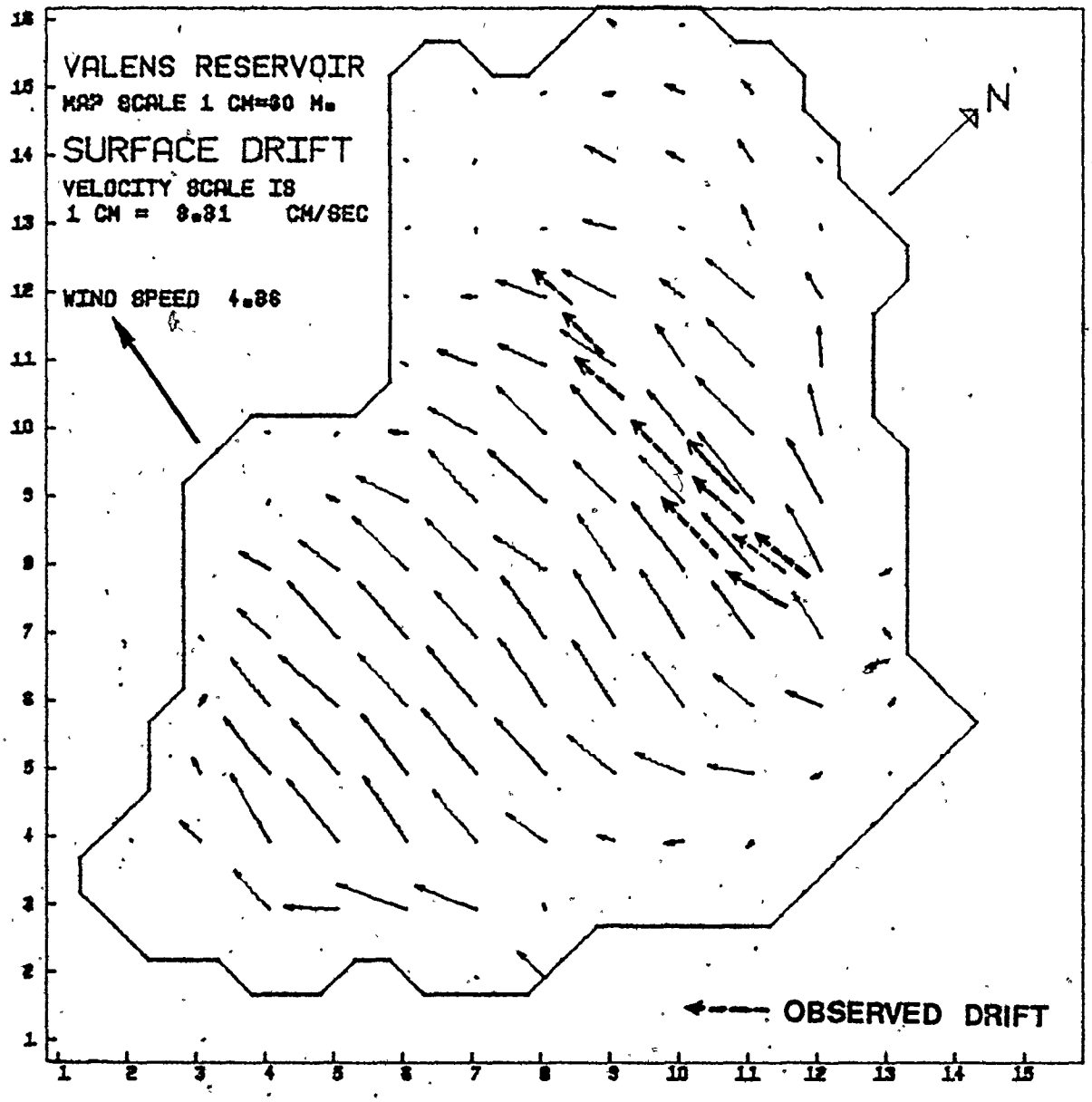

FIG.6.12 COMPUTED SURFACE CURRENTS

SURFACE CURRENT SURVEY : JUNE 26,75

WEED SURVEY : JUNE 20, 75

VERTICAL EDDY VISCOSITY=3.5 CM/SEC

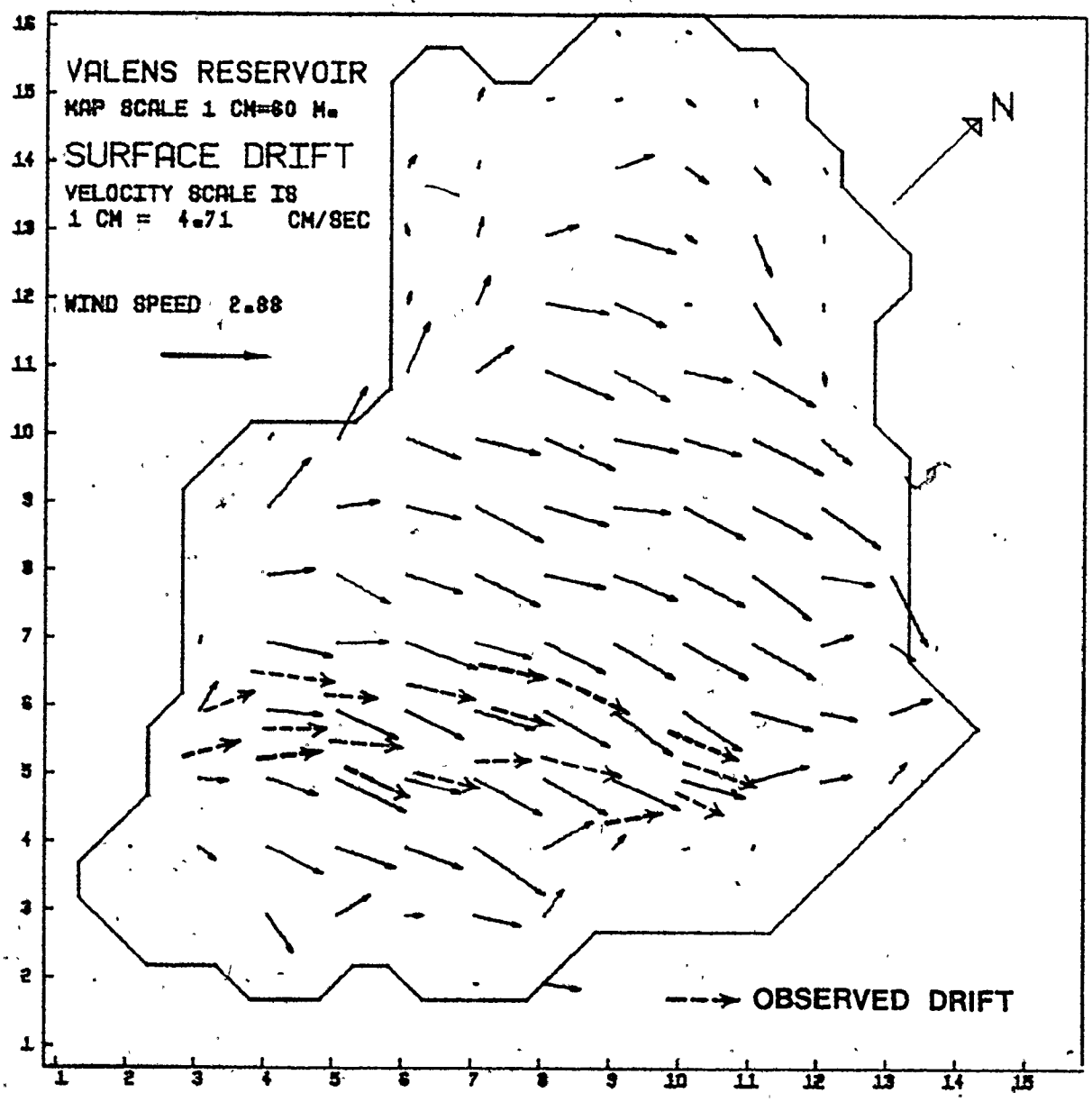

FIG.6.13:COMPUTED SURFACE CURRENTS

SURFACE CURRENT SURVEY: AUG 11, 75

WEED SURVEY: AUG 12,75

VERTICAL EDDY VISCOSITY=2.3 CM/SEC

Figures 6.9 to 6.13, the model results are in good agreement with the observations.

6.2 Application to Hamilton Harbour

The hydrodynamical model of the harbour was applied for various wind conditions. The model parameters were calibrated and the model performance was studied. Extensive field data are still needed to fully evaluate the methods developed in this study, but the model results were encouraging when compared with available observations of surface currents.

Computer runs were first carried out for a non-stratified harbour. The model reached a steady state, when a constant wind was applied, after about 5 hours as shown in Figure 6.14.

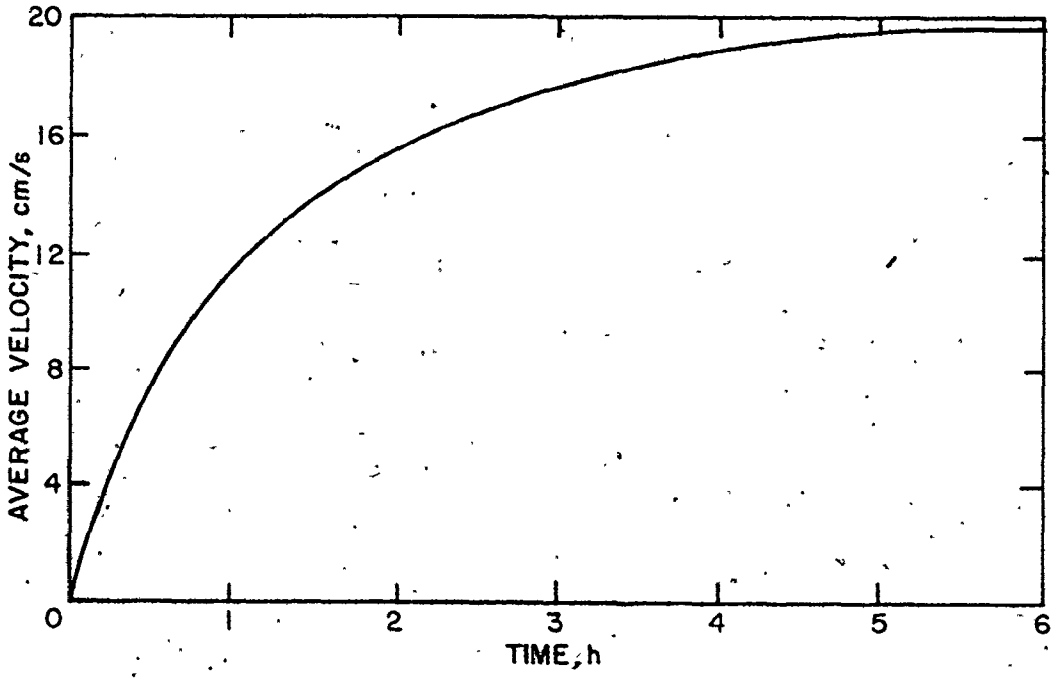

Figure 6.14: time to steady state (non-stratified lake)
wind speed = 6.52 m/s.

Taking stratification into account, the time to steady state is a little longer than that taken under non-stratification conditions. Most of the observations were taken under nearly steady wind conditions. Thus in following computer test runs, steady state was assumed, but of course the model can accept transient wind conditions.

The change of surface and bottom currents with time, as predicted by the model for a given wind event, is shown in Figure 6.15. As shown, the flow velocities change in both magnitude and direction with time till the model reaches steady state. The change of the direction is due to Coriolis forces.

The effect of temperature stratification on the model performance was studied. It was found that the harbour stratification should be considered when applying the model during stagnation period, as it has a significant effect on the model results, as shown in Figure 6.16.

The wind-wave coupling mode (B-Model) was included in the present hydrodynamic model. Thus the over-water wind stresses were determined for given wind conditions at each grid point. Bottom roughness coefficient was assumed to be constant throughout the lake and in the order of 2.5×10^{-3}. Vertical eddy viscosity is related to the thermocline depth and wind speed using equation (1.9) as mentioned previously in Chapter I.

$$A_v = C H W_a$$

where H is the depth of thermocline (cm) and $C = 1.5 \times 10^{-5}$, a value suggested by Bengtsson (1973). W_a is the wind speed (cm/s). Vertical eddy viscosity (A_v) is another important parameter affecting the model

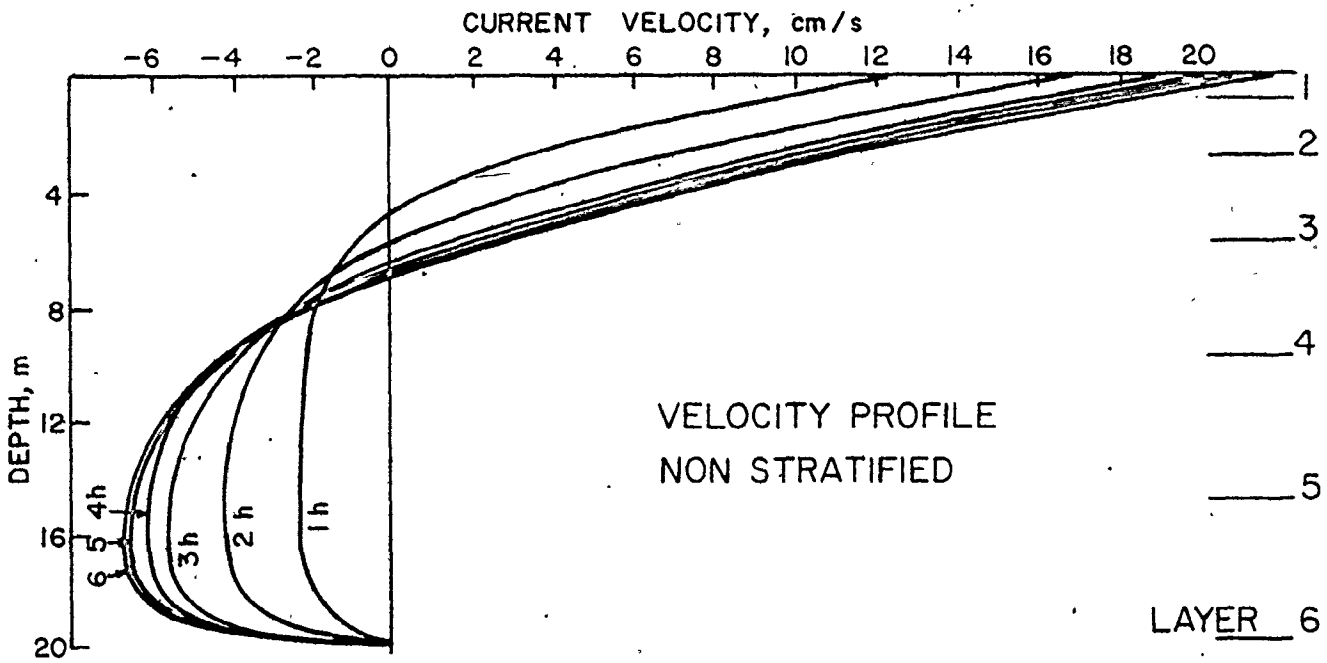

Figure 6.15a: Velocity profiles at the indicated simulation times

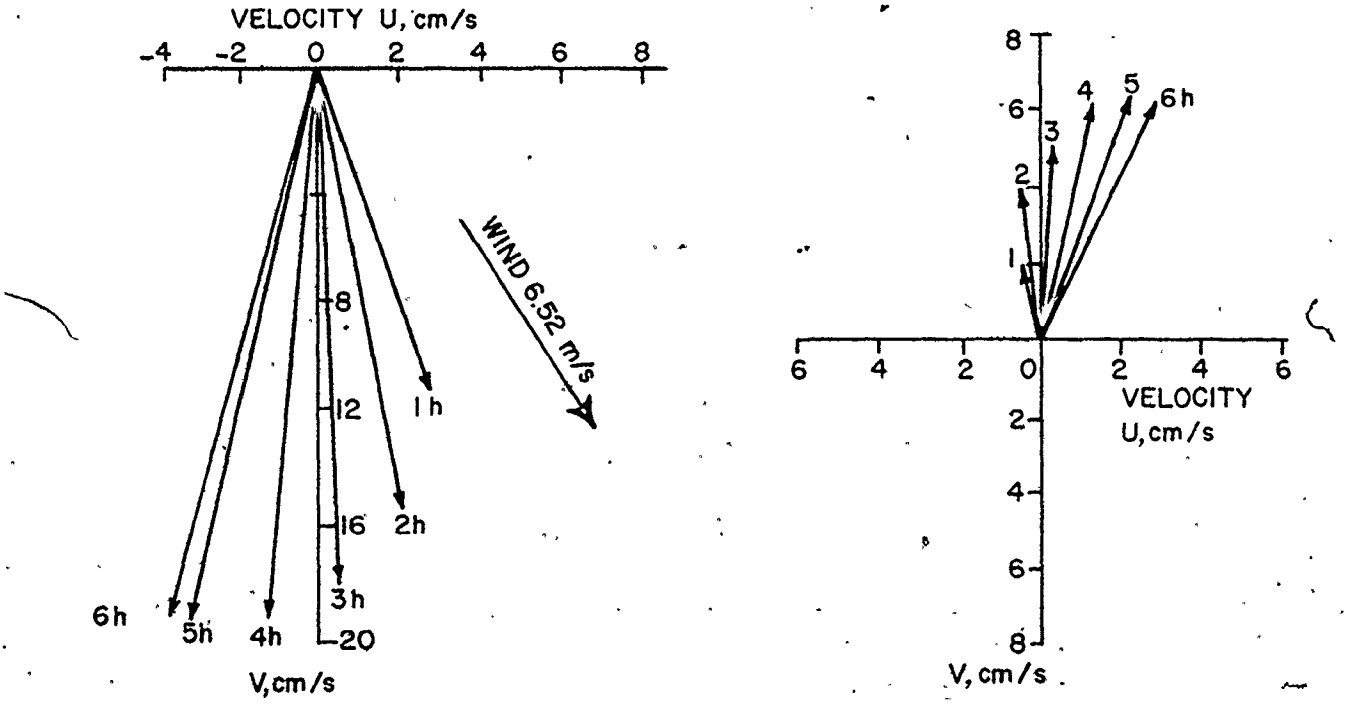

Figure 6.15b: Surface and bottom currents at a mid-harbour location at the indicated simulation time

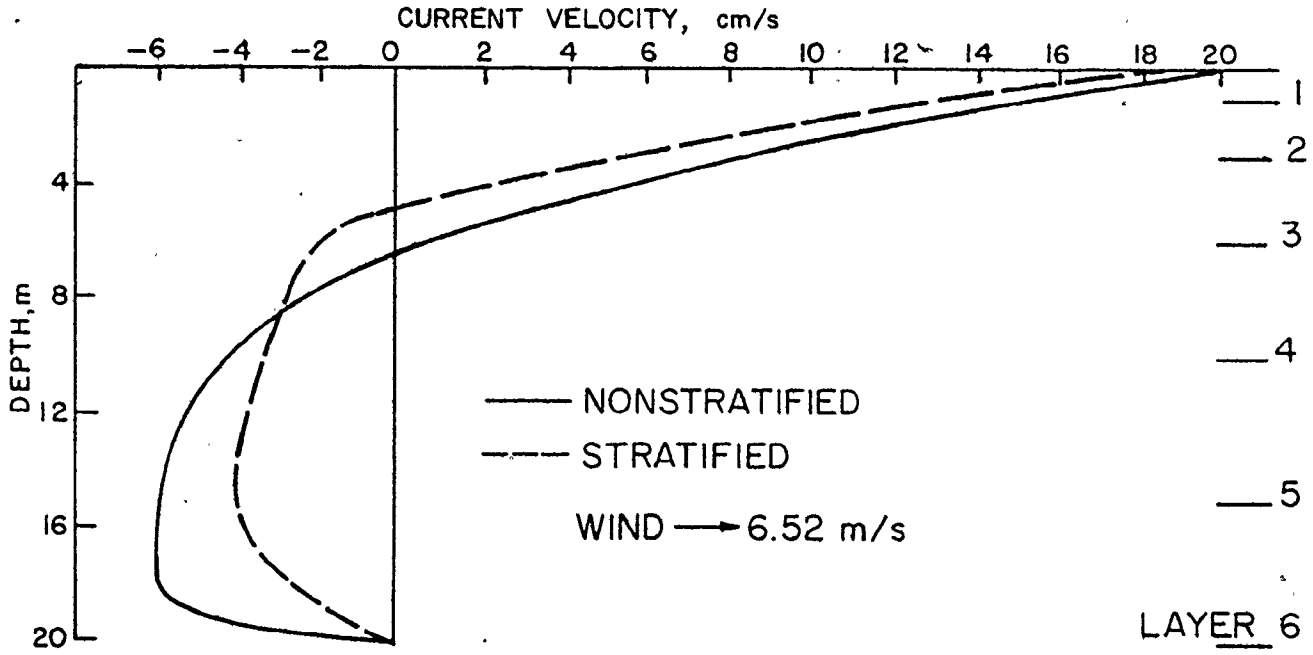

Figure 6.16: Effect of temperature stratification on the velocity profile (at grid point (16,16) after 3 hrs. simulation time).

results. As shown in Figure 6.17, different values of A_v were considered for a given wind event. As the coefficient of eddy viscosity increases, internal shear stresses and consequently turbulents increase, and the velocities of surface and return currents decrease.

The numerical model was applied for all valid wind observations. Some observations were discarded because of the uncertainty of the wind records, high variation of wind (e.g., surveys #5 and 9; Table 6.2) and unrealistio values of the measured velocities. The model results are shown in Table 6.3 and Figures 6.19 throughout 6.24. The observed surface currents (top 50 cm) were compared to those computed as shown in

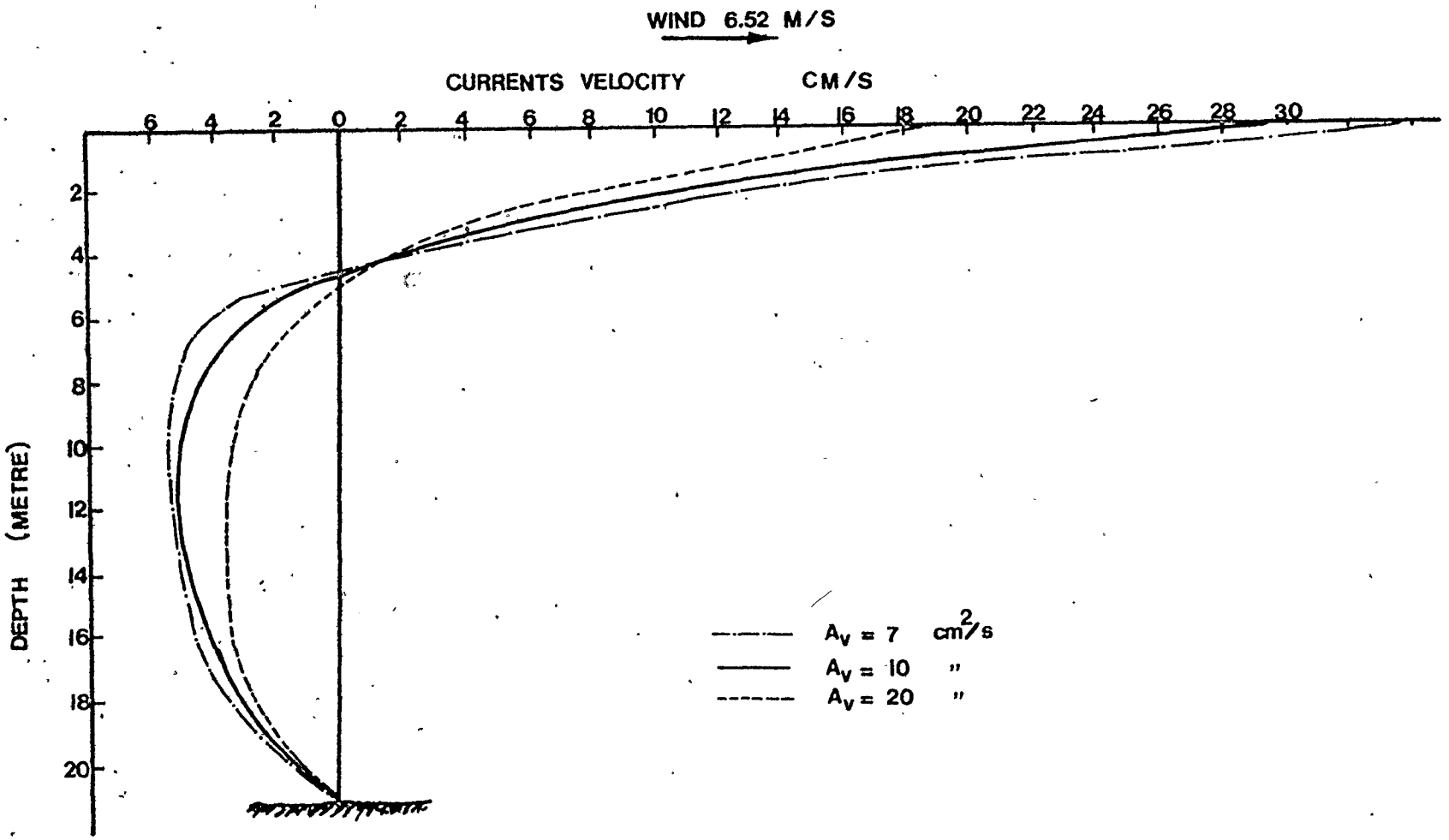

Figure 6.17: Effect of vertical eddy diffusivity of momentum (A_v) on the velocity profile

Table 6.3: Observed and Computed surface currents in Hamilton Harbour

Observation			Computer Results			
Survey No.	Wind Speed m/s	Average Velocity ($\bar{V}_{obs}$) cm/s	A_v c_m^2/s	Average $c_D \times 10^{-3}$	Average Velocity ($\bar{V}_{comp}$) cm/s	$\bar{V}_{obs}/\bar{V}_{comp}$
1	6.52	20.3	11.0	1.9	23.5	0.86
2	3.42	13.0	3.8	1.66	11.6	1.12
3	3.44	15.5	3.9	1.66	10.3	1.5
4	3.53	12.1	4.0	1.67	10.5	1.15
5	3.95	12.1	4.4	1.80	11.7	1.03
6	6.00	15.3	10.0	1.87	19.3	0.8
7	2.82	10.3	3.2	1.5	8.0	1.29

Table 6.3 and Figures 6.18 to 6.24. The values shown in Table 6.3 are the areally averaged velocities, the average drag coefficient and vertical eddy viscosity calculated for each wind event. As shown, the results are encouraging, however, they are not as good as those obtained in Valens reservoir due to several factors. The harbour was found to be a very dynamic lake where the physical processes are continually changing. The effect of Lake Ontario on the harbour should be considered, as the average exchange flow between the harbour and the lake was found to be about 1.0% of the harbour volume (Ontario Ministry of the Environment study 1975-1976). The instantaneous value of the exchange flow can be much higher than the above value. Due to the lack of observations, the exchange flow model (Chapter V) has not been applied in the present application. Another factor might have affected the observations is the ship movements in or out of the harbour.

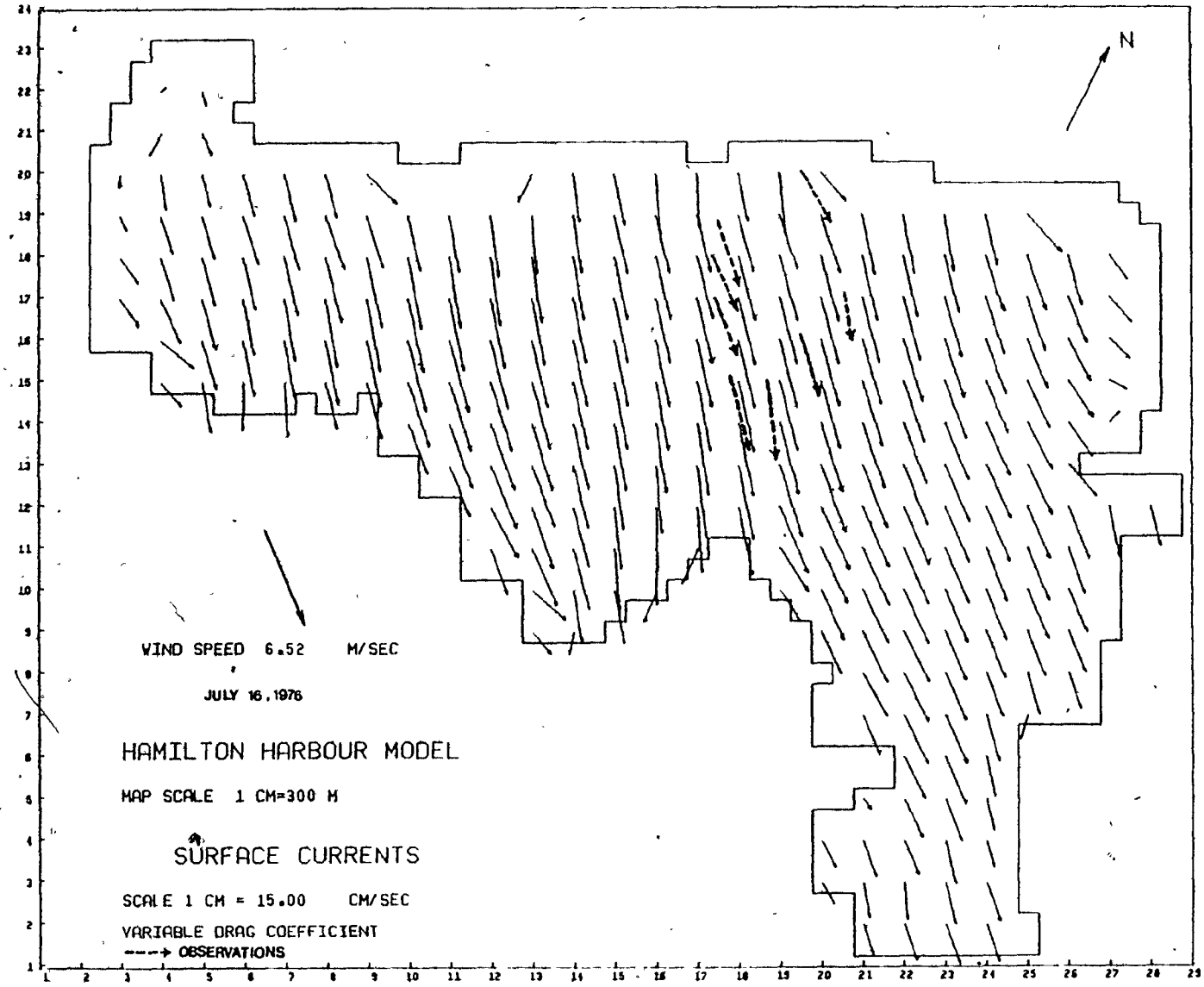

Figure 6.18 COMPUTED & OBSERVED SURFACE CURRENTS

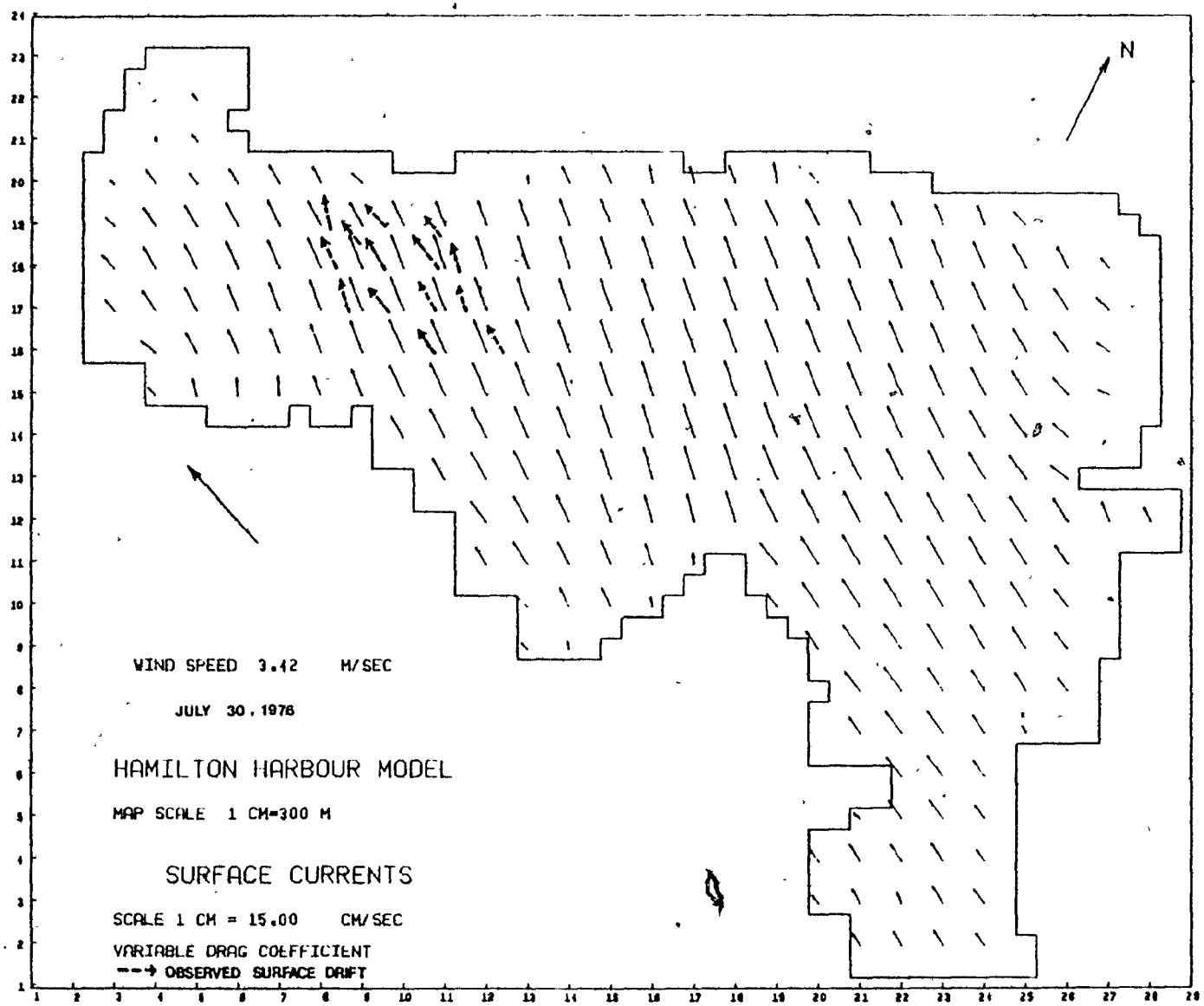

Figure 6.19 COMPUTED & OBSERVED SURFACE CURRENTS

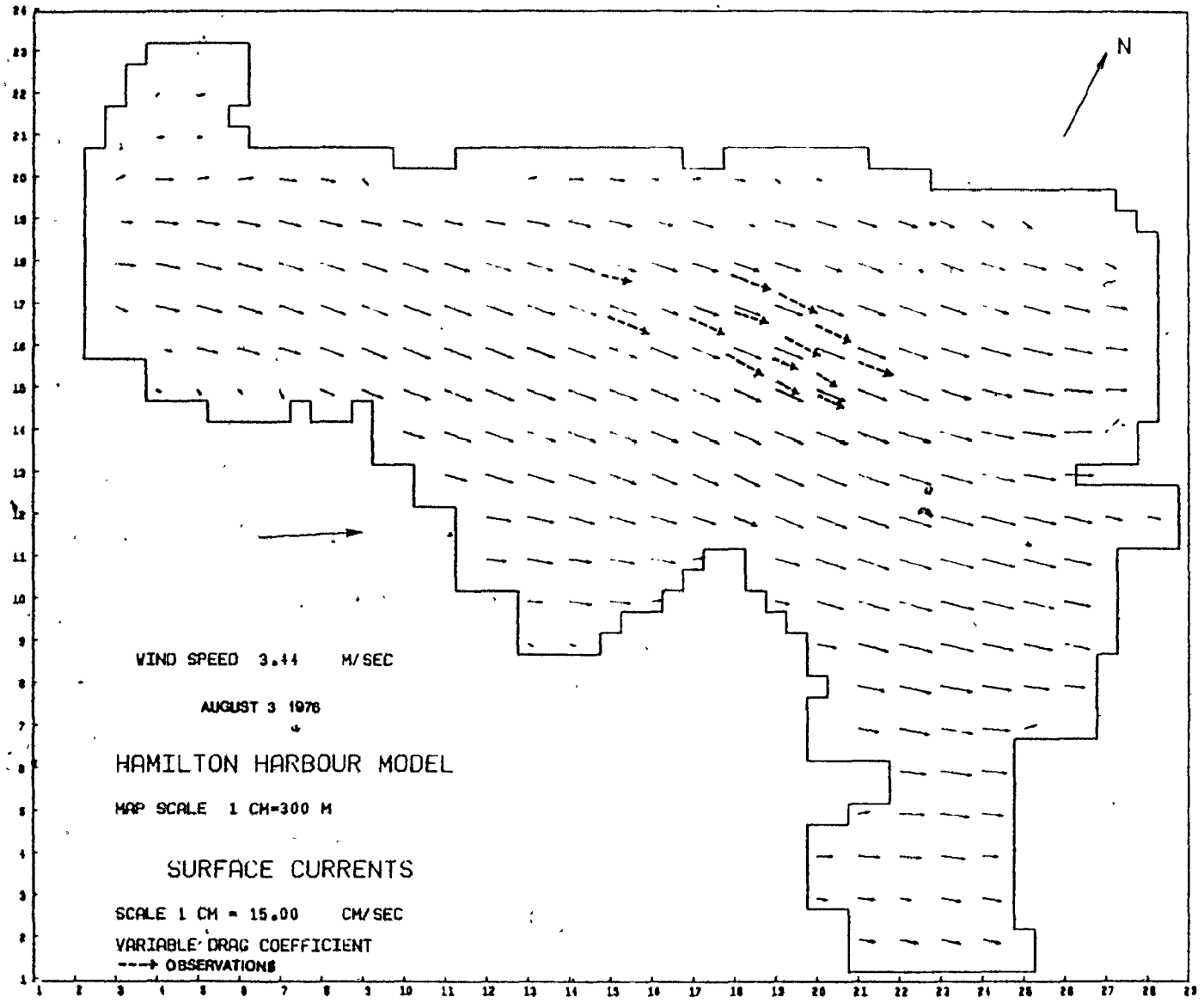

Figure 6.20 COMPUTED & OBSERVED SURFACE CURRENTS

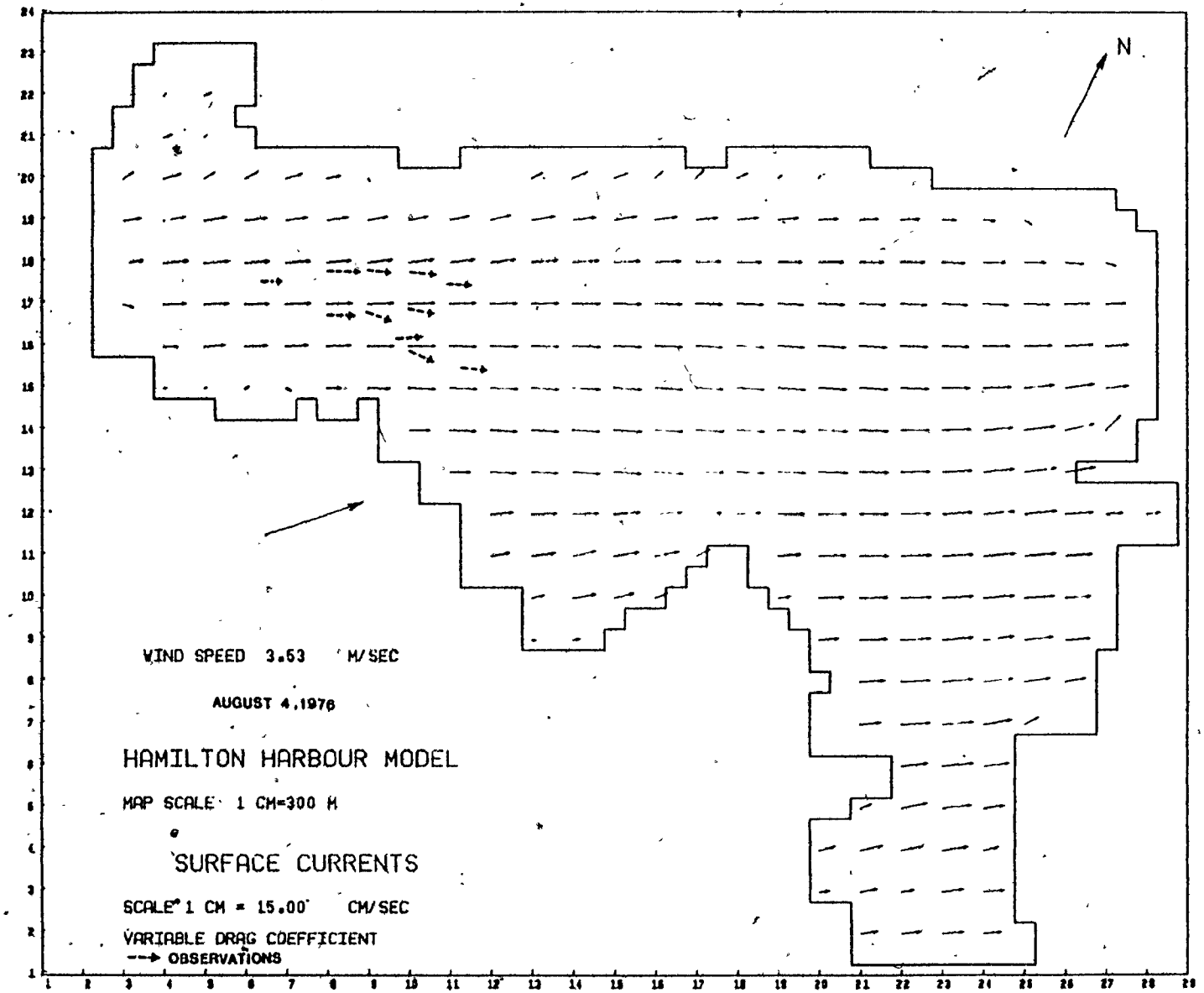

Figure 6.21 COMPUTED & OBSERVED SURFACE CURRENTS

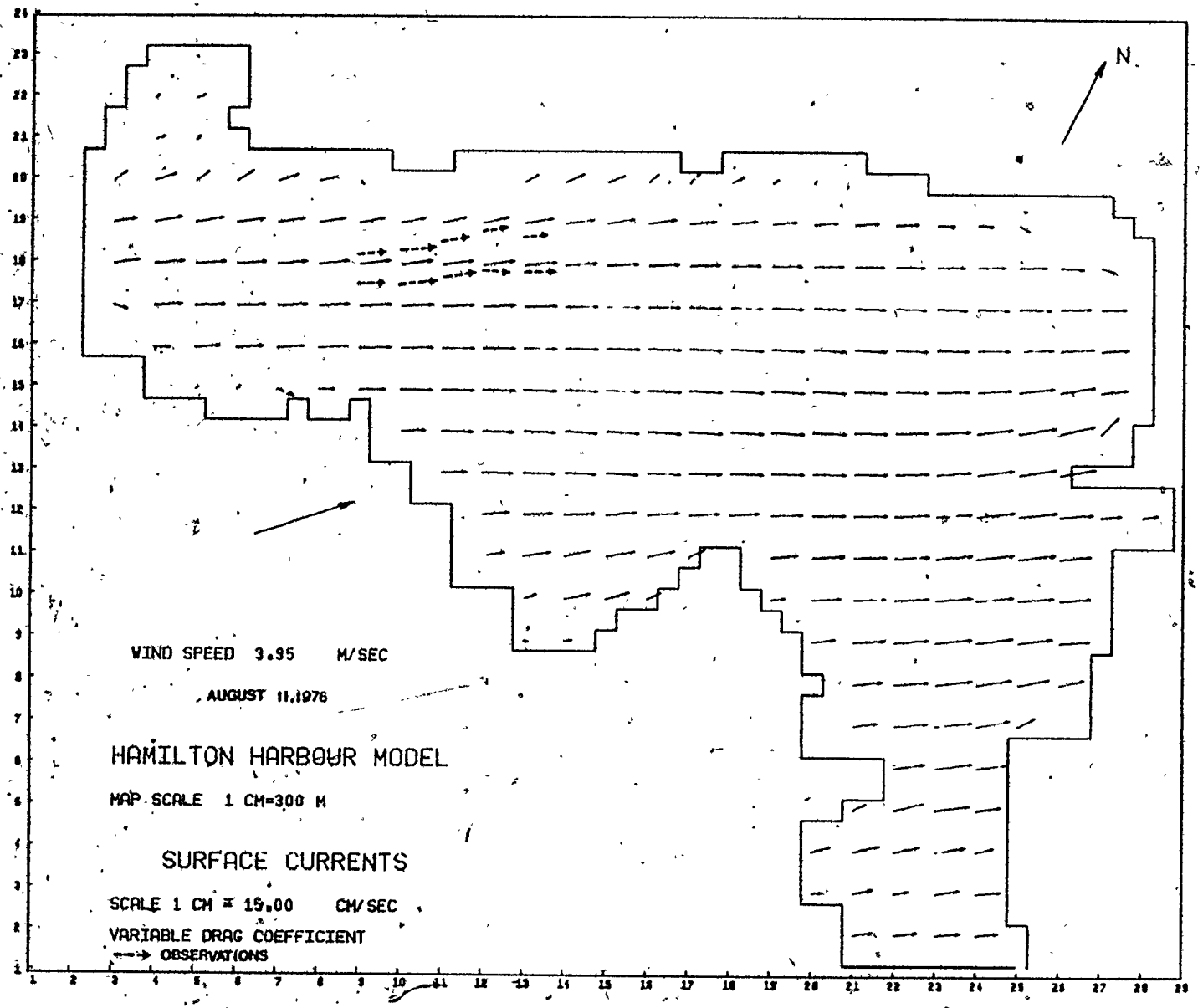

Figure 6.22 COMPUTED & OBSERVED SURFACE CURRENTS

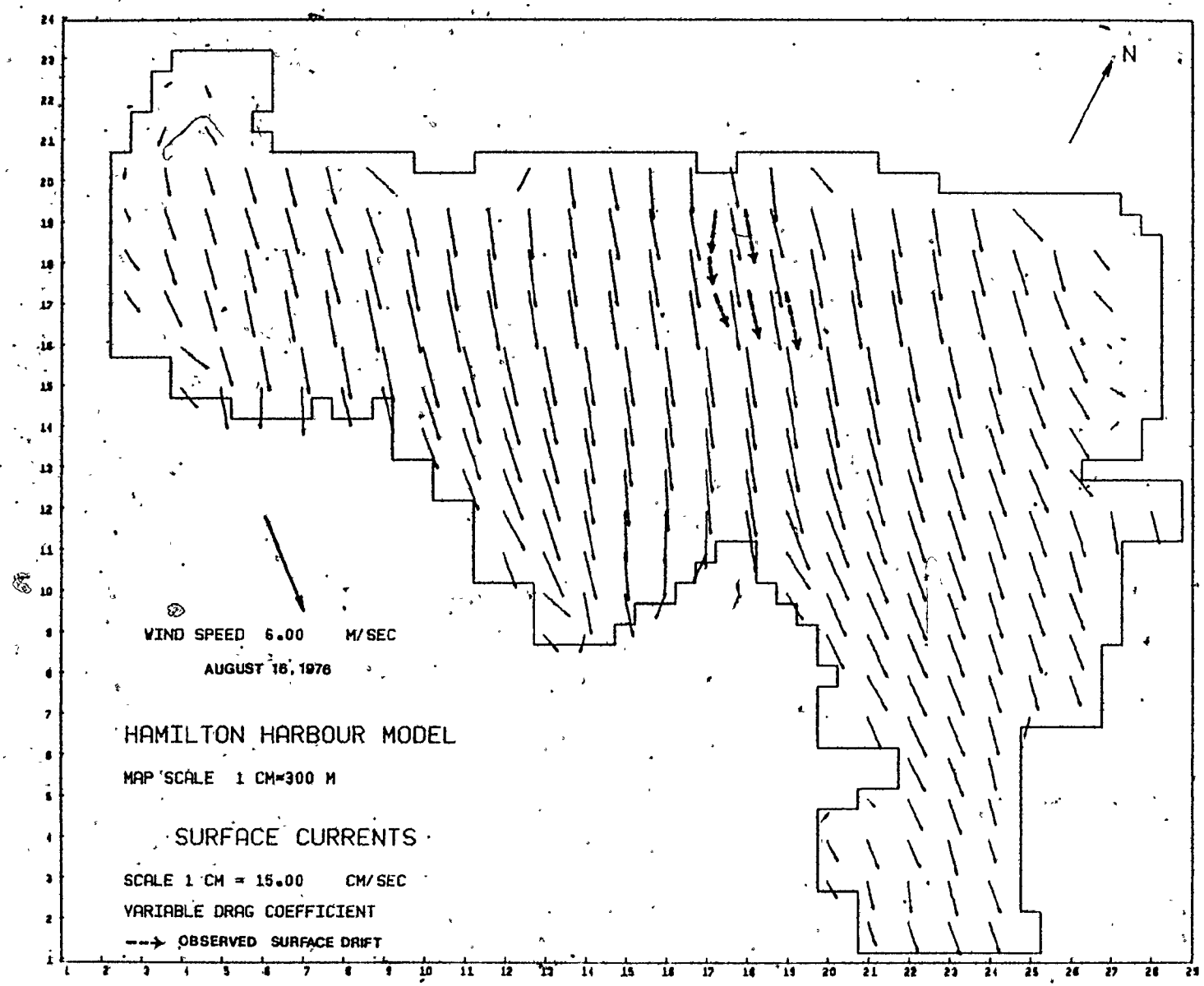

Figure 6.23 COMPUTED & OBSERVED SURFACE CURRENTS

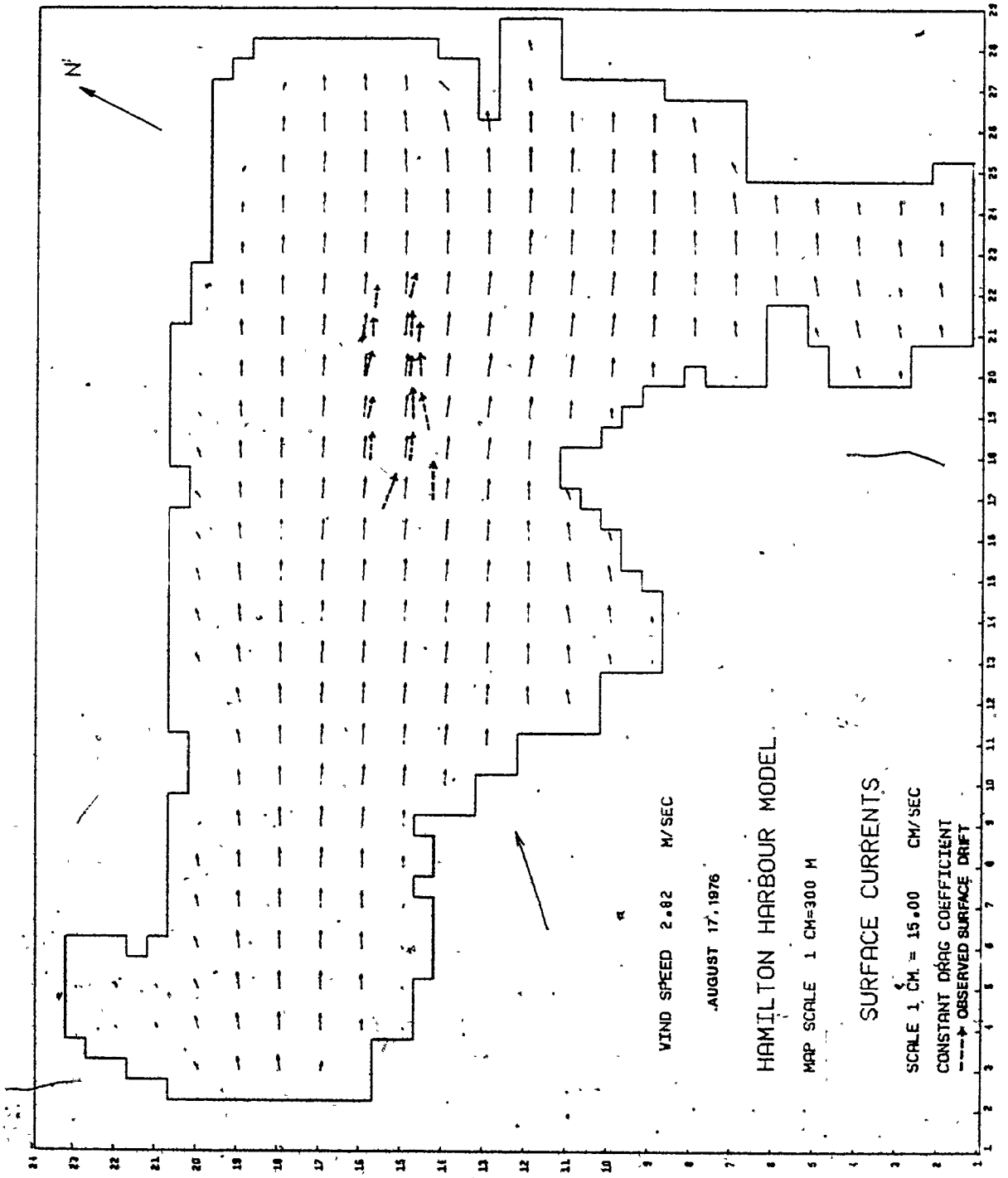

Figure 6.24 COMPUTED & OBSERVED SURFACE CURRENTS

CHAPTER VII

VERTICAL MIXING IN A LARGE LIMNO-CORRAL

1. INTRODUCTION

In a limno-corral (diameter 12 m, depth to sediment = 10m), located in Baldegersee (Switzerland), vertical mixing was measured over more than one year (1977-1978) and compared to the conditions in the open Lake. Baldegersee is a small, relatively deep lake (about 4.5 x 1.5 km; surface area is 5.3 km^2 and maximum depth of 65 m) (Figure 7.1). It is semi-sheltered and prolonged wind shears are likely to be minimal. The observed temperature profiles have shown a shallow depth of thermocline during the entire stratification period, which reflects the minor effect of winds on mixing. Also the sharp temperature gradient greatly reduces vertical advection through the thermocline.

Thus the limno-corrals in Baldegersee, used for experimental studies on heavy metal pollution (Gachter 1979), are idealized examples of horizontally well mixed and vertically stratified lakes. Similar studies have been applied to a number of Swiss lakes of similar characteristics (i.e. relatively deep and thermally stable where vertical mixing is more important as a transport mechanism) (e.g., Imboden and Emerson 1978). The major objectives of the present field programme may be stated as follows:

1) to test and verify the models previously developed in Chapter VI.
2) to determine the influence of the walls of the corrals on the

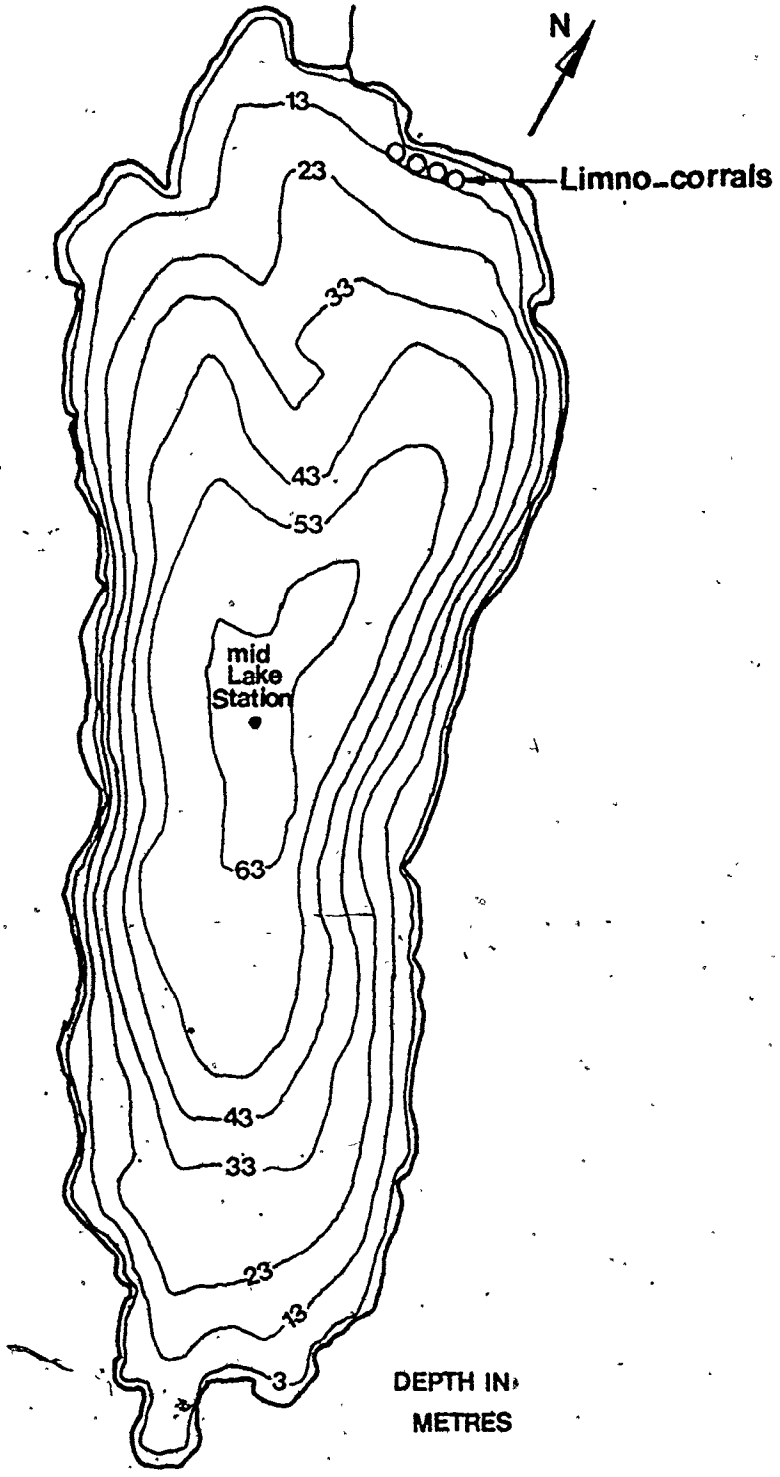

Figure 7.1 BALDEGGERSEE LAKE TOPOGRAPHY

mixing mechanism in comparison to that of the open lake.

3) to determine the absolute value of vertical eddy diffusion in the test lake (corral) as a function of depth and time.

2. FIELD OBSERVATIONS

Temperature profiles were observed biweekly inside and outside the corral and at a mid-lake station (Figure 7.1). A temperature/pressure sonde was used with a resolution of 2×10^{-3}°C and an accuracy of more than 10^{-2}°C. In Figure 7.2 the isothermals in the corral are compared to those of the upper 10 m. at the mid-lake station. Some systematic differences can be seen, especially in the shape and depth of the thermocline as shown in Figures 7.3a,b. These differences may be due to wind effect on the open lake, internal waves and also due to the fact that the observations are not synoptic. However, as shown in Figures 7.2 and 7.3, these differences were found to be small.

Radon and radium activities were measured monthly from water samples (20 liters each) taken at different depths above the water-sediment interface. The same technique as that described by Broecker (1965) was used. Briefly, from water samples, all gases are extracted by cycling helium through it and trapping the gases at liquid nitrogen temperature. CO_2 and H_2O is removed by passing the gases through ascarite and dryarite filters. The collected radon gas is then transferred to an alpha scintillation counter to determine its activity (R_n) (in decays per min.). After the first extraction of radon from the water samples, determination of the radium-supported radon (R_a) can

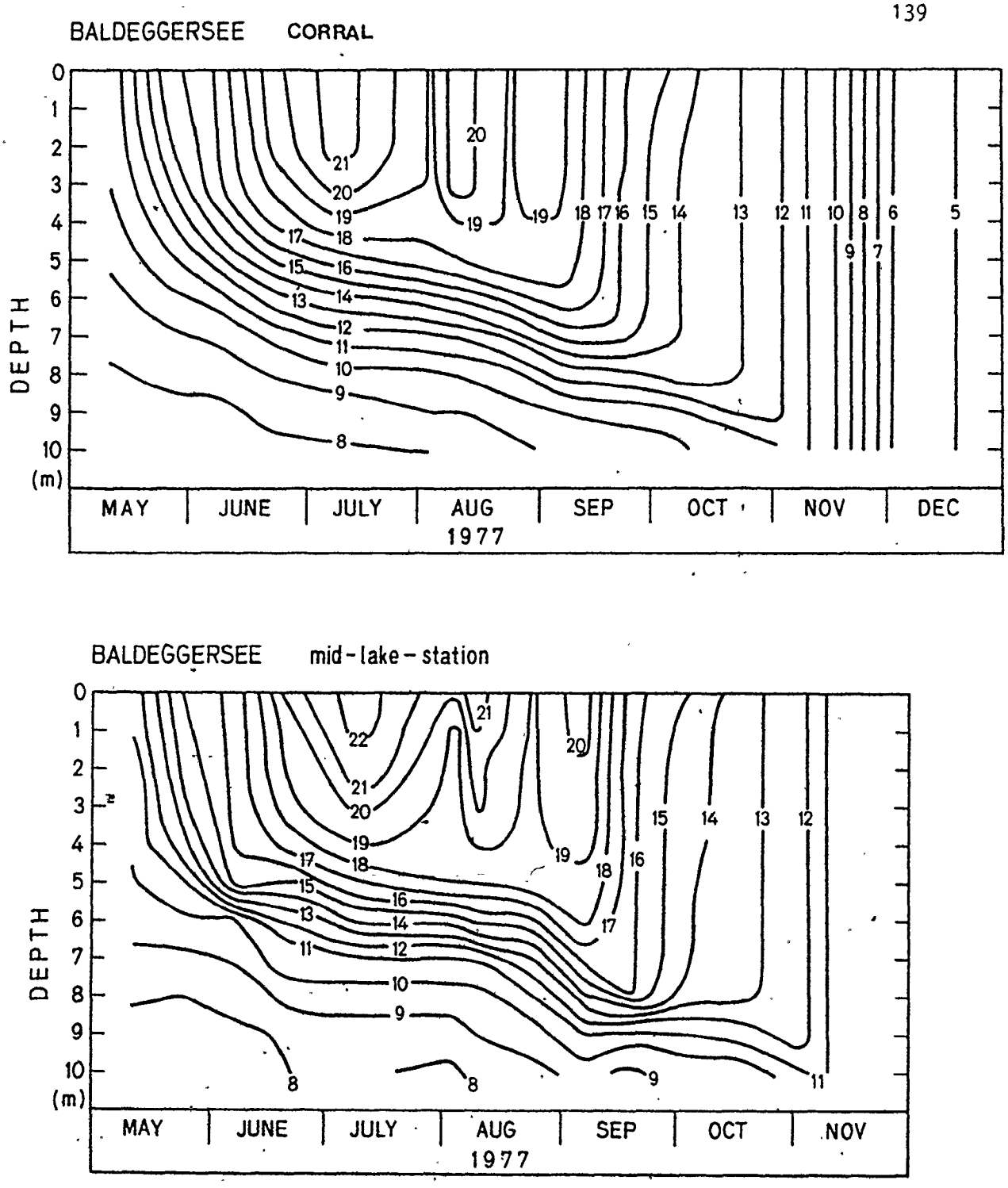

Figure 7.2 Isothermals in the corral and at mid-lake station

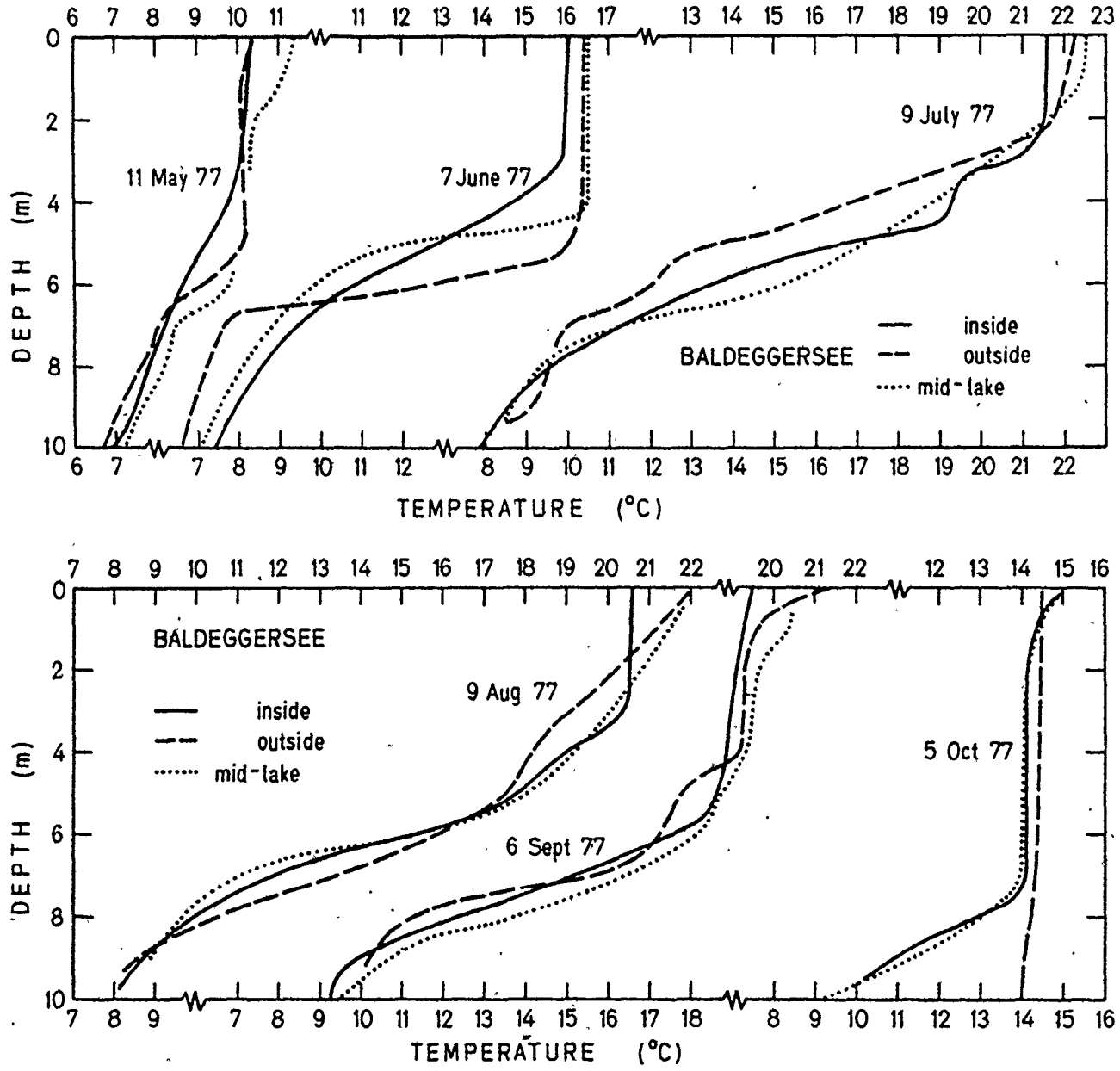

Figure 7.3a Comparison between the temperature profiles inside and outside the limno-corral and mid-lake station

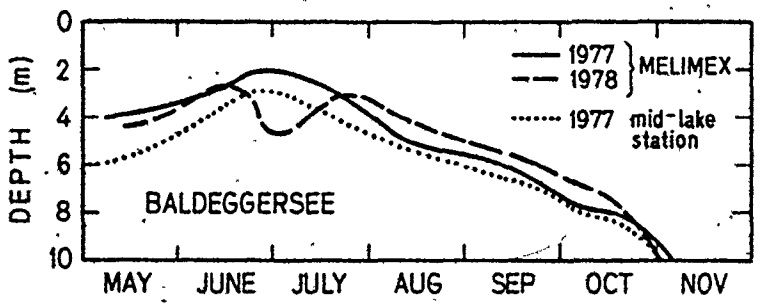

Figure 7.3b Depth of the thermocline inside the corral and at mid-lake station

be done by leaving the water samples sealed for ten or more days. Then the stripping of radon is repeated to determine the radium (R_a) activity. Thus the excess radon activity R_n' can be determined at a given depth by subtracting R_a from R_n activity.

The monthly radon profiles inside the corral are plotted in Figure 7.4. These profiles are interpreted as one-dimensional vertical eddy diffusion flux as previously mentioned in Chapter VI (Equ. 4.10). In order to determine K_z (vertical diffusion coefficient), the radon flux from the sediment (F_{RN}) should be determined independently of the measured radon profiles. This was done by taking samples from the sediment core, for different locations in the lake and the corral, and measuring radon flux from these samples. Details of the experimental methods are presented elsewhere (Imboden and Emerson 1976, 1978).

3. RESULTS AND DISCUSSION

From Figures 7.2 and 7.3 it appears that during the period extending from June to September the temperature regime in the corral below the mixed layer is fairly smooth and stable, a prerequisite to applying the temperature method (see Chapter VI). The vertical mixing, made visible by warming the hypolimnion, seems to be quite constant during this period.

The computer program (VERDI) was applied to calculate K_z from the measured temperature profiles of the limno-corral and the results are shown in Figure 7.5. From May to the end of June, K_z increases with time and is strongly depth-dependent. Near the bottom it reaches a

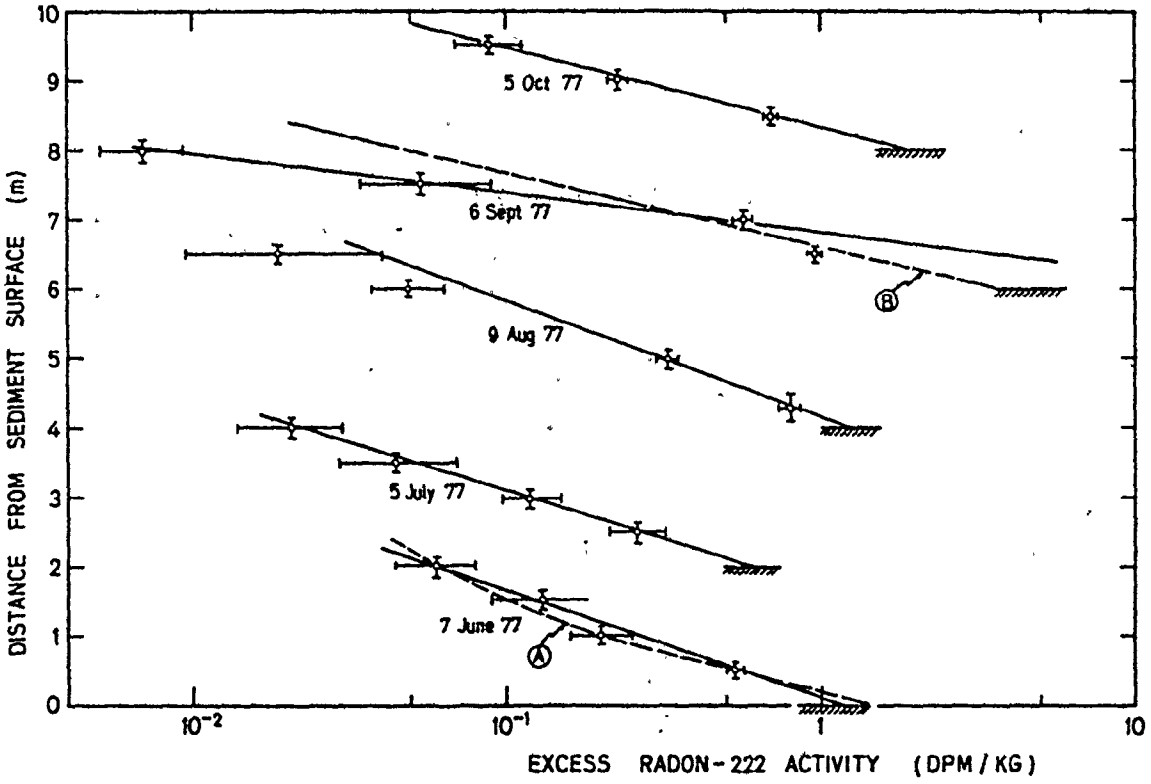

Figure 7.4 Profiles of excess radon inside the corral (error bars corresponds to one standard deviation

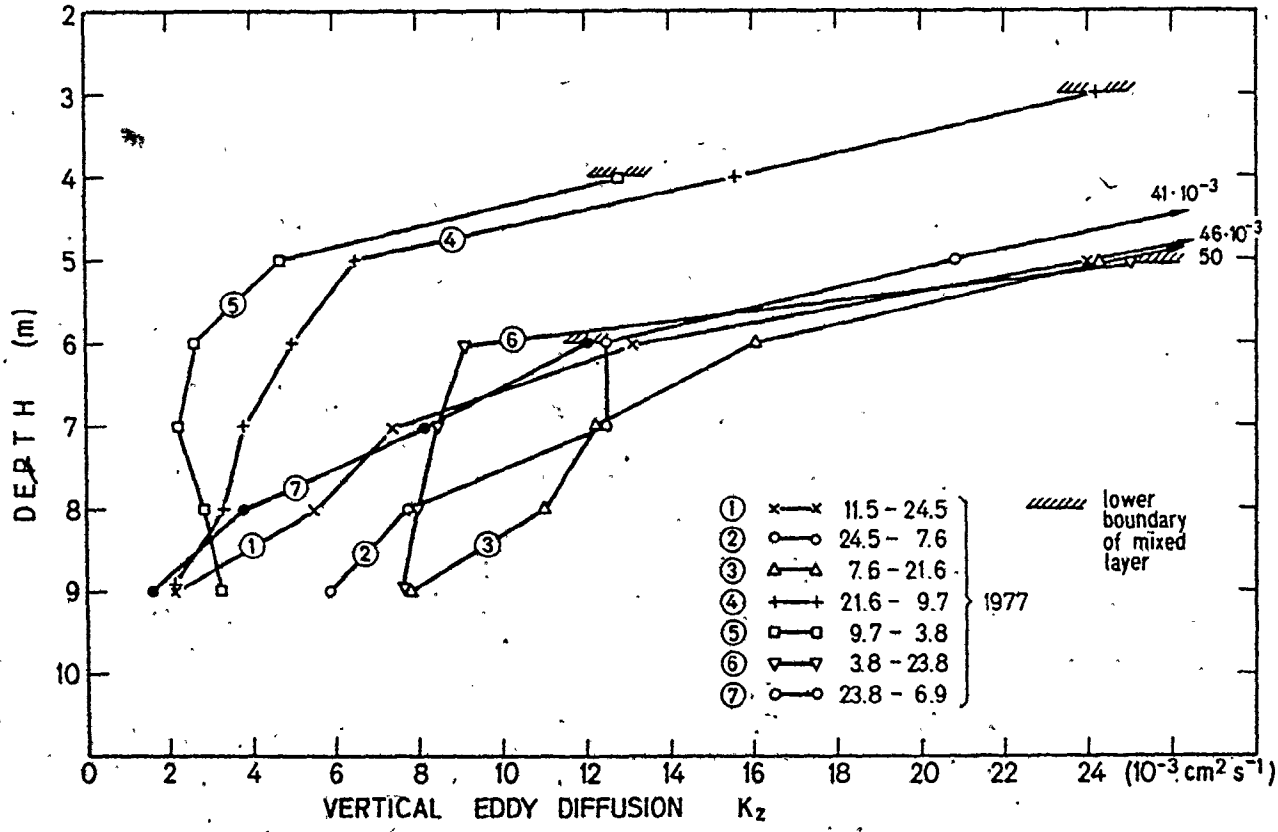

Figure 7.5 Vertical eddy diffusion K_z inside the corral claculated by the temperature method

value only slightly above the coefficient of molecular diffusion of heat at 4°C (1.36×10^{-3} $cm^2 s^{-1}$). Between 21 June and 3 August, K_z is relatively constant in the lowest 4 m of the corral and near its molecular value. Probably as a result of a meteorological perturbation, K_z is again larger in mid-August and reaches another minimum in September. Due to temperature drop of the surface waters, accompanied by convective turbulence, the eddy diffusion concept loses its validity in September.

Above the thermocline, vertical mixing is extremely time-dependent. The biweekly temperature profiles does not allow the temporal fine-structure of the near-surface vertical mixing to be described. However, the 'total mixing events' are frequent enough compared to the relevant chemical and biological reaction rates. Thus, the epilimnion can be treated as a permanently completely mixed system.

In 1978, the average vertical mixing was similar (Figure 7.6). Of course, the details of the mixing structure reflect the different meteorological conditions in the 2 years.

A possible error may be introduced into the one-dimensional temperature model by horizontal heat exchange across the walls of the corral. If the temperature at a given depth is higher inside the corral, it would lose heat through the walls leading to an underestimation of K_z calculated using the program VERDI. The situation may be most critical in June and July when temperature differences of more than 1°C exist across the wall. In fact, the double layer structure of the corral walls reduces the horizontal heat flux (see

Gachter 1979 for details of the wall structure). Also, due to internal waves and upwelling or downwelling at the shore line near the corral, the average horizontal temperature differences between the lake and corral are probably better represented by the mid-lake station, rather than the 'snapshot' profiles of the oscillating conditions outside the corral. It was found that the measured mid-lake temperature profiles are more similar to those measured in the corral. It is however, possible that the extremely small K_z values in June and July are underestimated by up to 30%, a presumption supported by the radon measurements plotted in Figure 7.4 (see also Figure 7.7).

Values of K_z were calculated from the radon profiles using Equation (4.10). The two independent methods for calculating K_z yield consistent results (Figure 7.7) despite the fact that different temporal and spatial averages were used. The only significant discrepancy occurred on 5 July 1977. The low average mixing between 21 June and 9 July may not have been representative of the few days preceeding the date of radon sampling (5 July). Also, due to horizontal heat flux through the corral walls, the temperature method may yield low values for K_z during this period.

The inhibiting effect of the limno-corral on vertical mixing will depend on whether wind-induced turbulence, internal waves and advection are more important than thermal stability. This evaluation will be different for every lake due to its particular morphometry, surroundings, etc. Observed thermal stratification, which was found to be similar inside the corral and the open lake, has shown that thermal

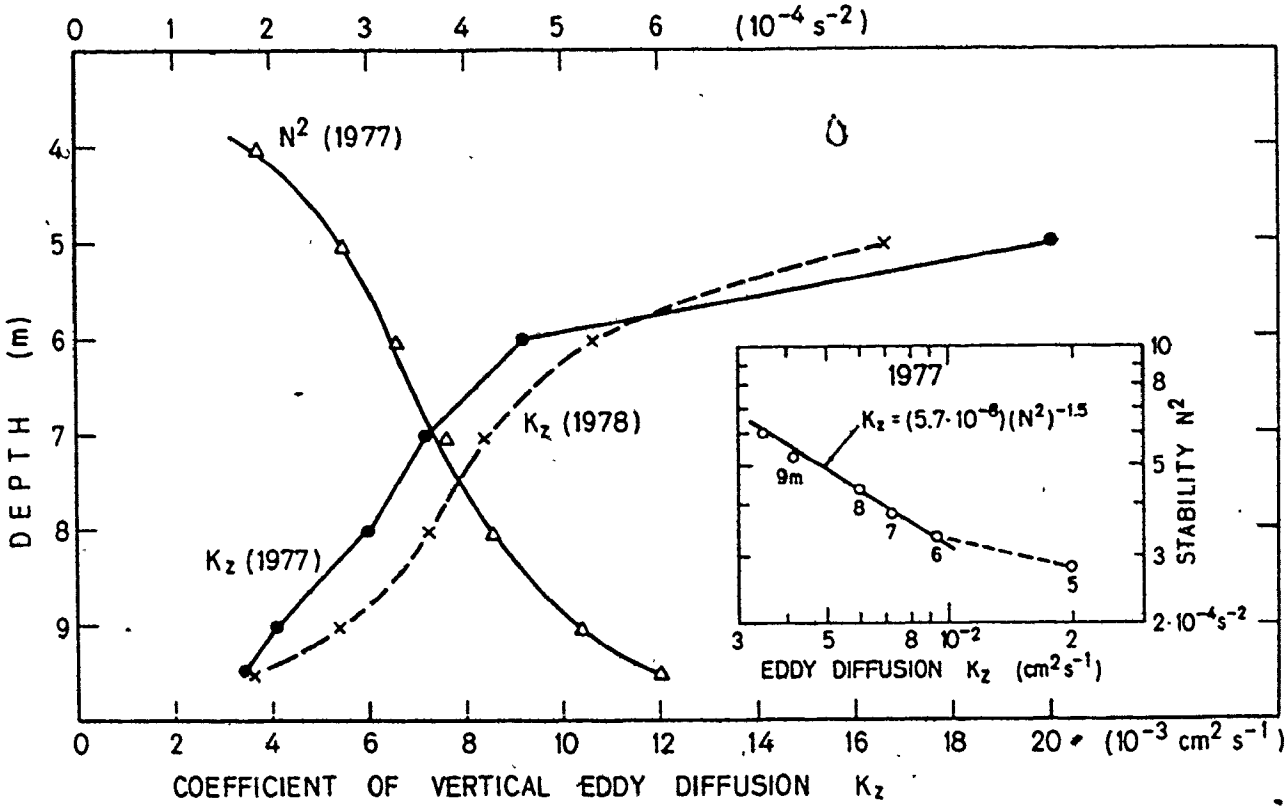

Figure 7.6 K_z averaged over stagnation periods of 1977 and 78 (in the corral) as function of depth. K_z is correlated to N^2 (see insert).

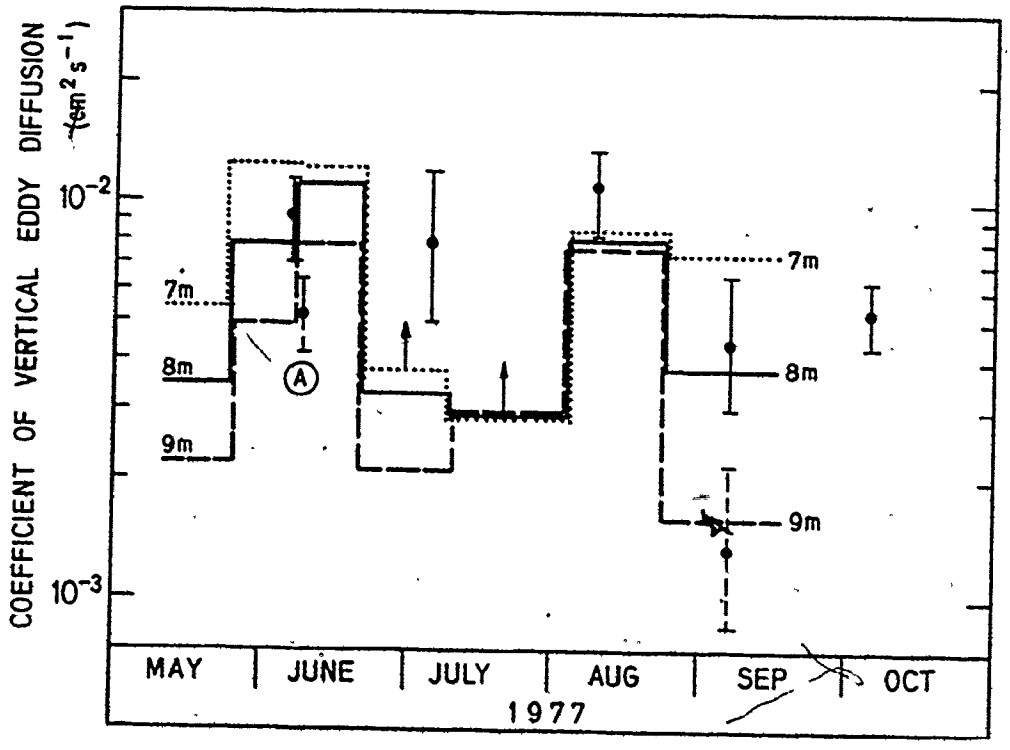

Figure 7.7 Comparison of K_z values in the corral calculated by the temperature (step curve) and radon (points with error bars) methods.

structure has a major influence on vertical mixing in the Baldegersee. Indeed, during quiet wind conditions, K_z can be calculated in the open lake from the bottom up to the lower boundary of the mixed surface layer using the method developed here, and the values will be similar to those determined inside the corral. However, a heavy storm may disturb the temperature structure down to a depth of over 10 m in the open lake, whereas the same event may leave the layers below 5 m in the corral practically unaffected.

The average K_z in the corral is related to the Brunt-Vaisala stability number N^2 through equation (4.8):

$$K_z = 5.7 \times 10^{-8} \, (N^2)^{-1.5} \ cm^2/s$$

Whereas the exponents b (in equation 4.8) for real lakes are usually smaller than 1 rather than 1.5 for the corral, i.e. the average K_z in the corral drops faster with stability number N^2 than that under open lake conditions (Figure 7.6). On the other hand, the corrals are more sensitive to the heat exchange at the surface due to their smaller depth.

4. SUMMARY AND CONCLUSIONS

Vertical mixing in a limno-corral (10 m deep), located in Baldegersee (Switzerland) has been measured and compared to conditions in the surrounding open lake (maximum depth 65 m). The temperature method of McEwen (1929) and Hutchinson (1957) yields K_z values between 5×10^{-2} $cm^2 \ s^{-1}$ at the upper boundary of the thermocline and 2×10^{-3} $cm^2 s^{-1}$ at the bottom, a value near the molecular diffusion of heat at 4°C (1.36×10^{-3} $cm^2 s^{-1}$). During the period of largest heating (June, July)

horizontal heat conduction across the walls of the corral may lead to an underestimation of K_z of 30% at most. Vertical eddy diffusivity K_z is found to be strongly depth-dependent and also time variable.

K_z calculated from the excess radon profiles generally agreed with those calculated from temperature data. It is suggested that the radon method is an excellent tool for monitoring vertical mixing near the sediment-water interface because of the simplicity of the measurements and their sensitivity to very low rates of mixing changes which may become very difficult to detect using other methods (e.g., temperature method).

Compared to the open lake, the corral has a shallower epilmnion. Turbulent energy input from wind does not significantly affect the temperature structure below 5 m, whereas at a mid-lake station turbulence penetrates to more than 10 m. During calm conditions, vertical mixing in the upper 10 meters is similar inside and outside the corral.

Finally we conclude that the present methods (temperature and radon) can be used to determine vertical mixing in the hyplimnion of Baldeggersee, which may be considered a typical small, relatively deep and thermally stable lake. The present model can be applied to any lake with similar conditions where mixing is mainly due to turbulent diffusion.

The results of the present model can be used to determine the concentration of a dissolved substance in the hypolimnion (e.g., dissolved oxygen, phosphorus, etc.), by solving the diffusion equation (see Chapter VI).

CHAPTER VIII

EXCHANGE FLOW BETWEEN EASTERN AND CENTRAL BASINS OF LAKE ERIE

1. INTRODUCTION

The computer model "EXFLOW" was applied to the Eastern and Central basins of Lake Erie at Pennsylvania ridge north of Erie during the stratification period (Figure 8.1). A stretch 50 km long (about 25 km from each side of the ridge) is taken to represent the interconnecting channel between the two basins, as shown in Figure 8.2. The ridge, which separates the shallow Central Basin from the deep Eastern Basin, is about 48 km wide and about 15 m deep at the northern end and 22 m below the water surface at the southern end (Pennsylvania channel). The X-axis runs along the channel (or the lake) longitudinal axis. The 50 km stretch is divided into 20 incremental unequal reaches represented by 21 cross-sections Δx apart as shown in Figure 8.3. Each cross-section is described by number of pairs of coordinates (y,z). Δx is smaller near the ridge where the change of bottom topography is more rapid.

A detailed description of the field observations, analyses of observed data and model results were reported in a recent publication (Eid 1980).

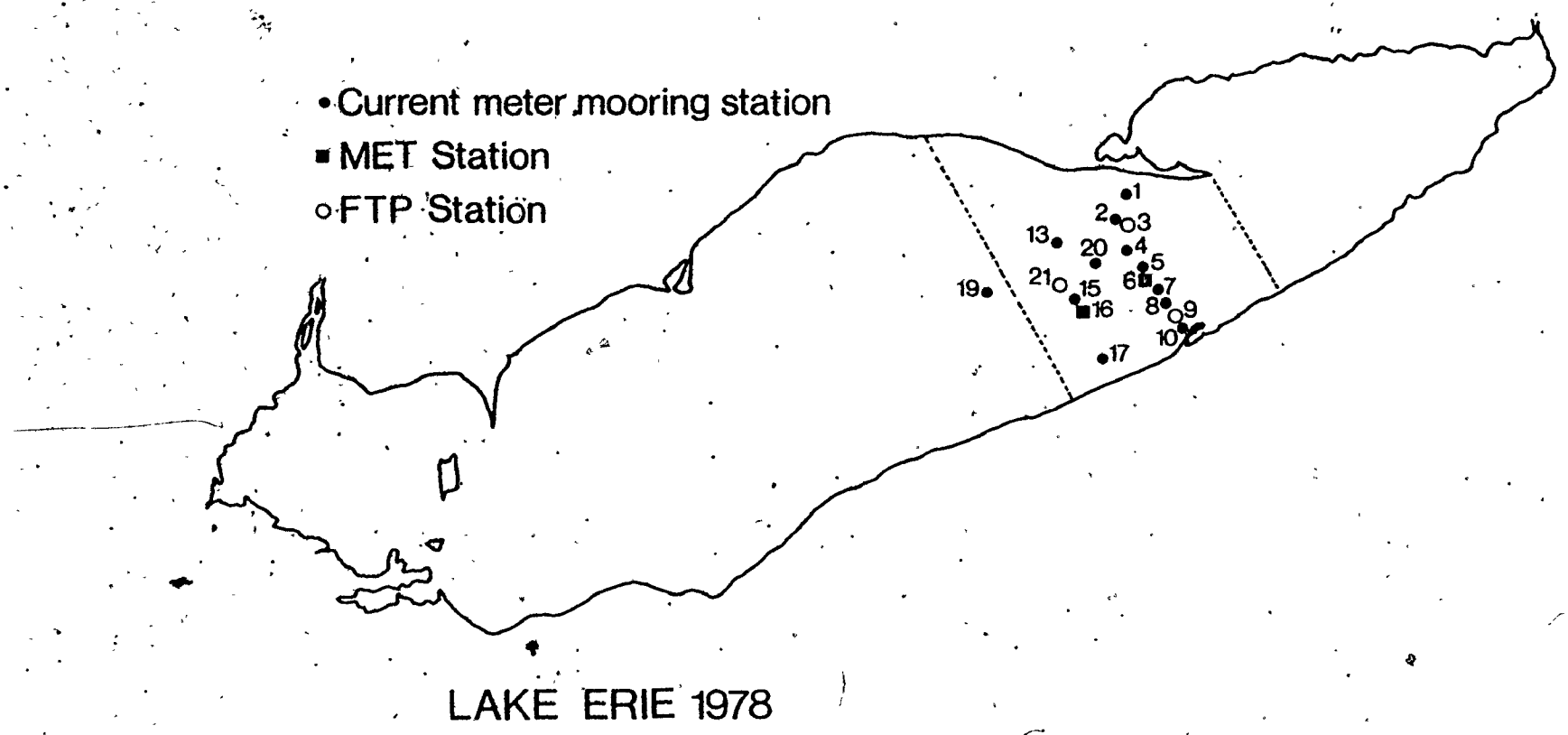

Figure 8.1 LAKE ERIE FIELD STATIONS IN THE STUDY AREA

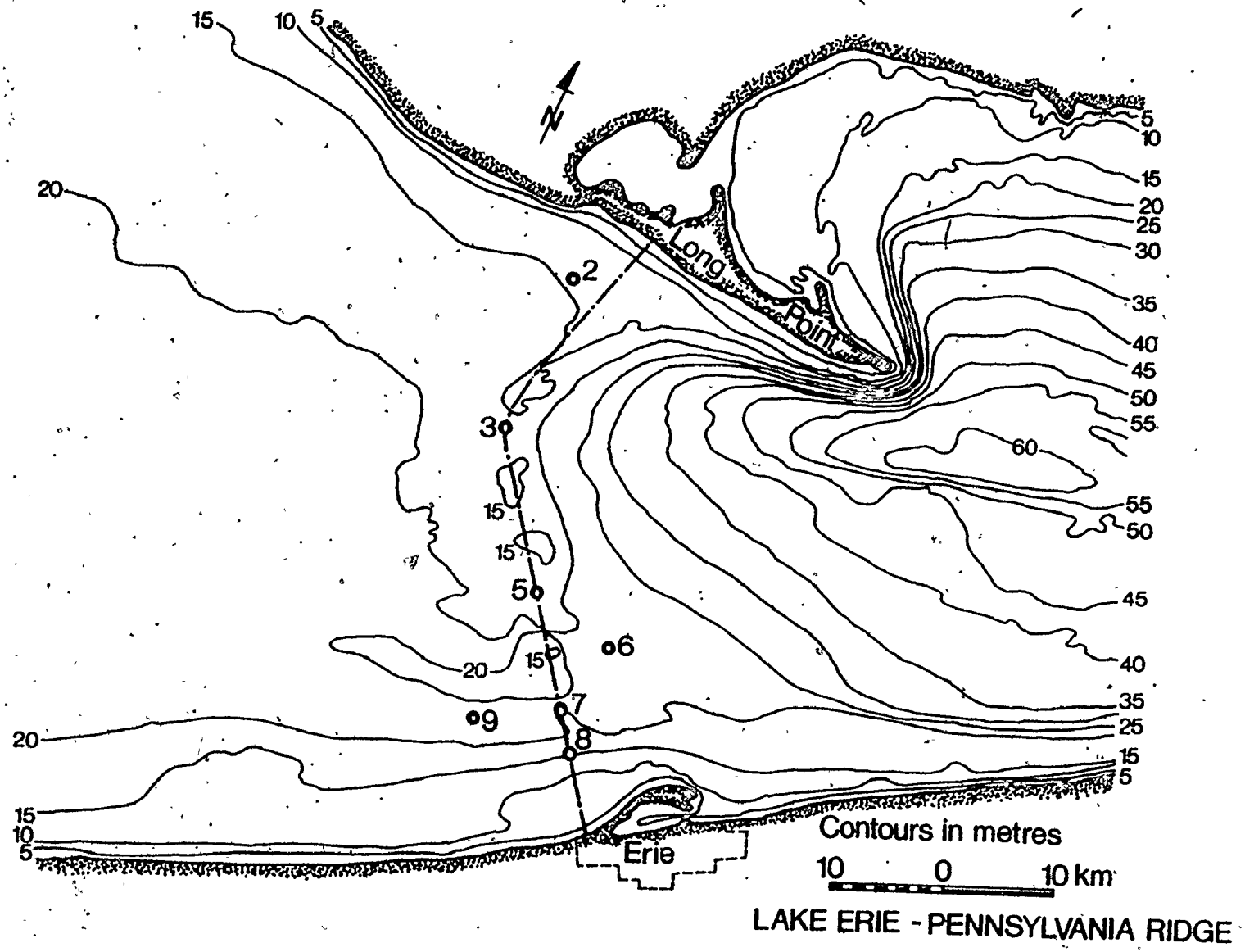

Figure 8.2 BOTTOM TOPOGRAPHY

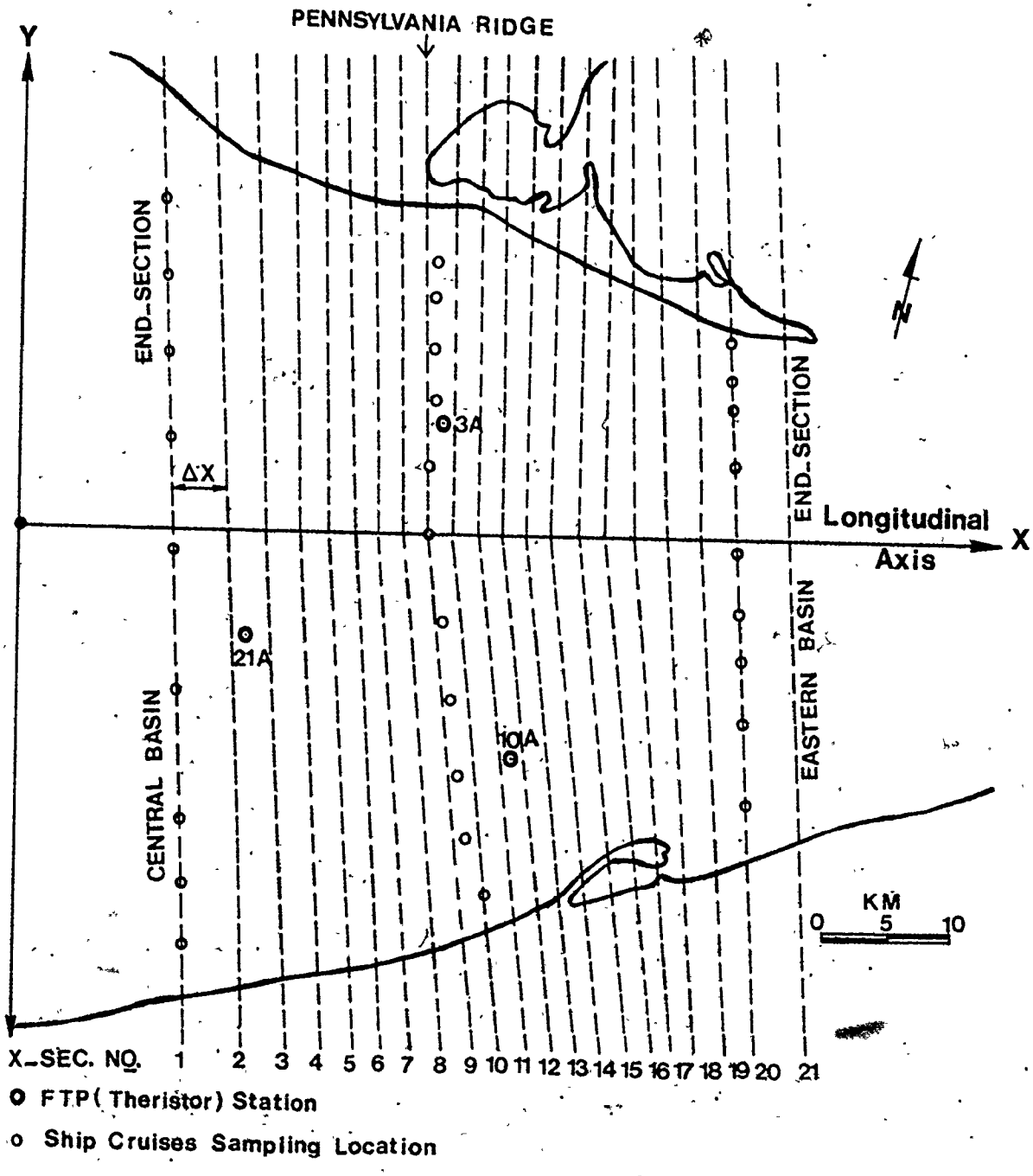

Figure 8.3 NUMERICAL DISCRETIZATION

2. FIELD DATA 1977-1978

During the months May to November 1977, 1978, CCIW carried out an extensive field observation program in the study area. A network of 23 current meters in 10 moorings and 2 meteorological buoys were employed (Figures 8.1 and 8.3). In addition, three FTP (fixed temperature profilers) stations were used to record temperature profiles in 1978. Two FTP's (3A and 10A) were located at the ridge and the third is located near the ridge in the Central Basin as shown in Figure 8.1.

Basic data sets

1. Temperature cross-sections obtained from ship data (bi-weekly observations). For the present study, the cross-section temperature profiles at the ridge and the two end sections of the "connecting channel" were used (Figures 8.1 and 8.3).
2. Time series of wind vectors: hourly average records are available from the meteorological (MET) data.
3. Time series of hourly average values of air and surface water temperatures.
4. FTP 1978 data: the hourly temperature profiles recorded at the three thermistor arrays (21A, 03A and 10A) are available for the boundary value problem model.
5. Time series of current meter data.

The time series data (wind, temperature and current) were averaged over 48 hour intervals. The components of wind and current parallel to the main longitudinal axis of the channel were taken. This

48 hour interval was found to be a convenient average period as it extends over 3 (16 hours) inertial cycles and also filters out other undesired periodicities (e.g. longitudinal oscillation, seiches, ... etc.).

The mean hypolimnion flow velocities were estimated from the current meter records (Figures 8.4 and 8.5). Analyses of field data and estimation of the flow are presented in detail elsewhere (Boyce, Chiocchio, Eid, Penicka and Rosa 1980; Eid 1980). In addition to the above data, the mean surface water elevation and the average daily flow into the Niagara River are required.

The 48-hour averages of the wind show dominant south-west winds (along the lake axis), with occasional and relatively weak reversed east winds. As a result of this dominant wind direction, a dominant mean normal flow pattern was observed along the channel's longitudinal axis (Figures 8.4 and 8.5). Data collected in summer of 1977 (Figure 8.4) were used for the model sensitivity analysis as shown in the next section, while the 1978 data (Figure 8.5) were used for model verification (section 4).

3. SENSITIVITY ANALYSIS

The first step in computing the interchange flow is to extract the components of current and wind normal to the boundary cross-section and to average them over consecutive 48-hour periods. These observations will be used to study the sensitivity of the model to different external forces and boundary conditions.

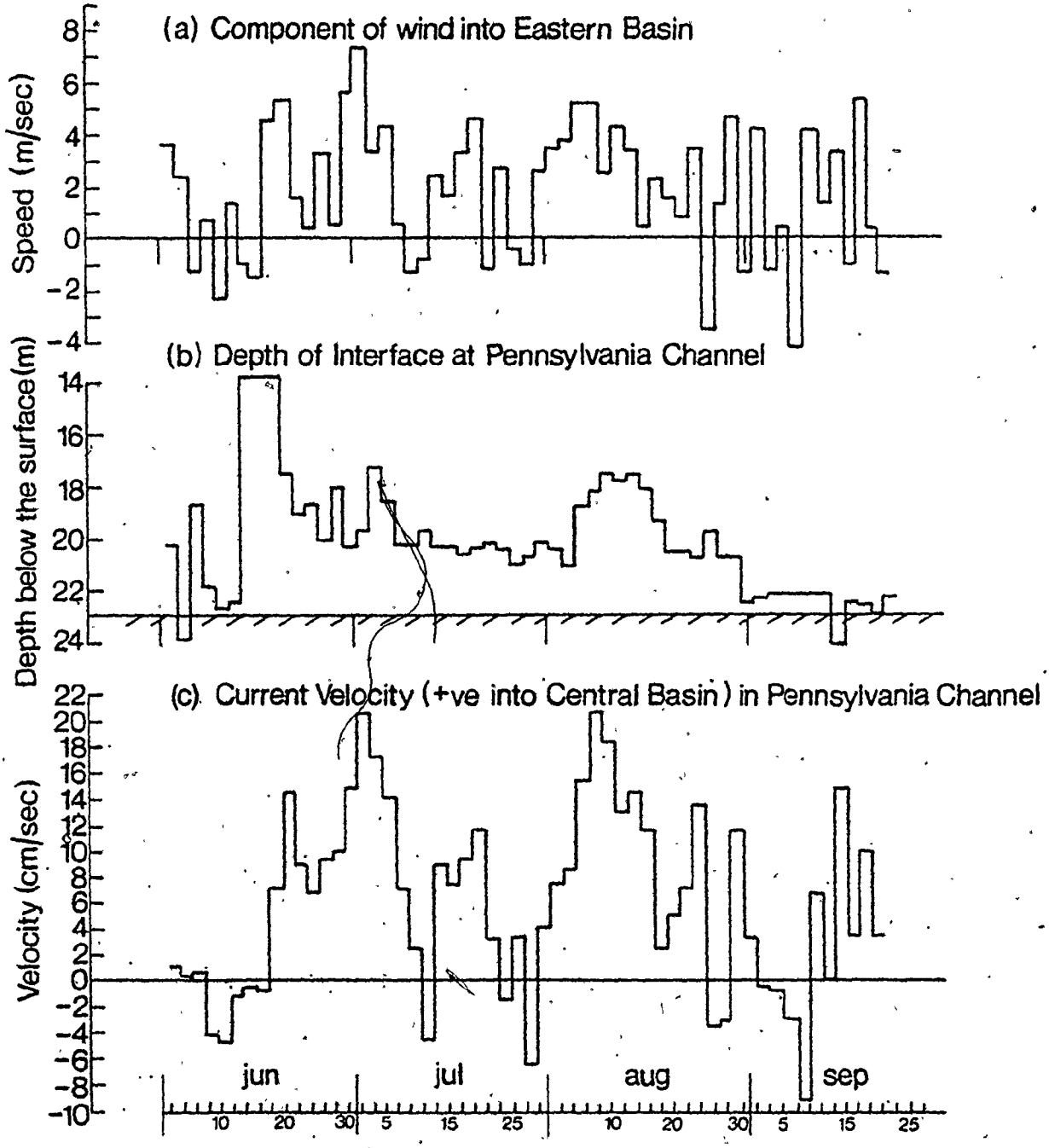

Figure 8.4: Lake Erie 1977 field data

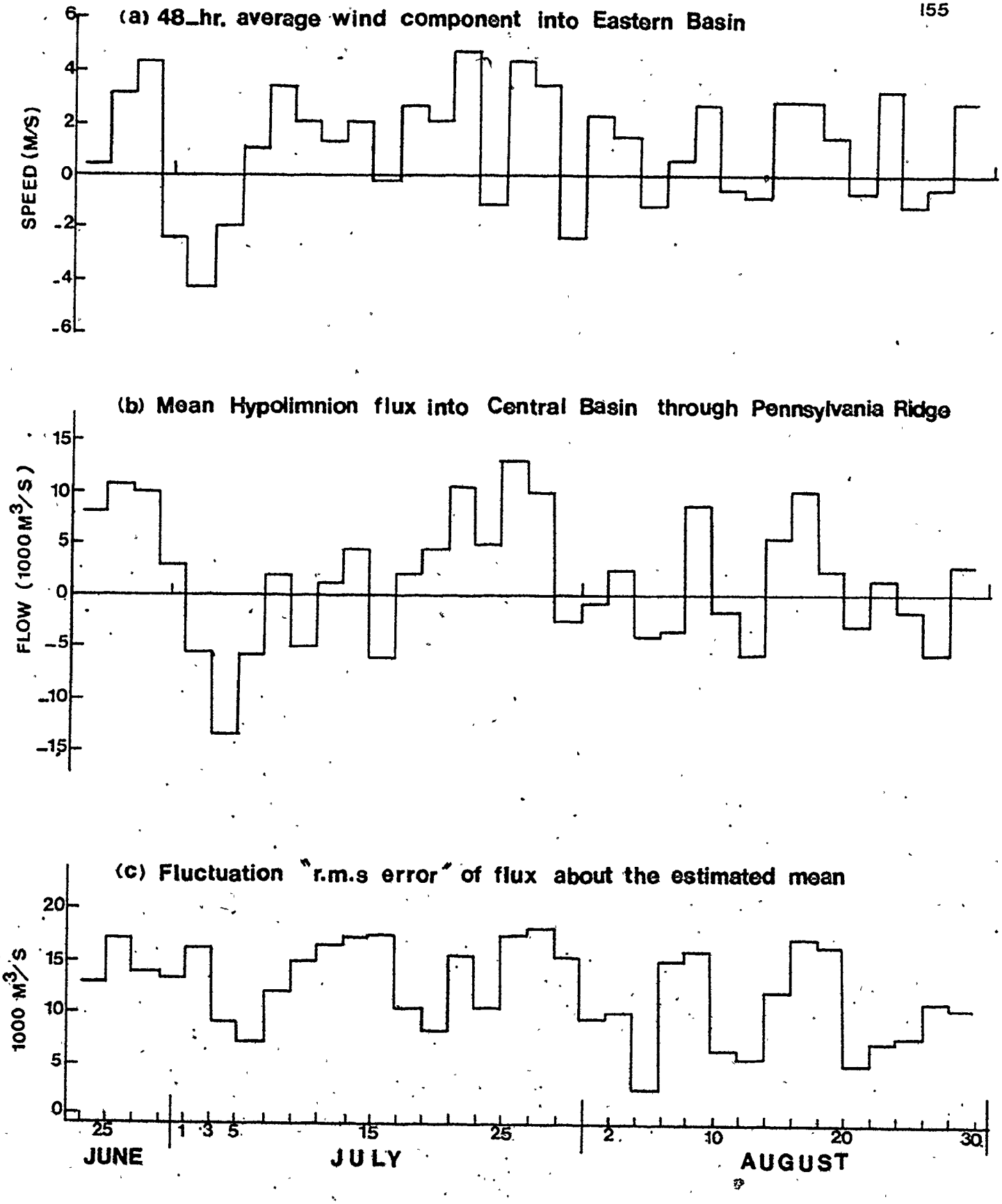

Figure 8.5 LAKE ERIE 1978: Averages of wind & current_meters Observations

We assume at first that the flow is steady during each 48-hour interval. This seems reasonable, since the time scale for internal adjustments in the sill (ridge) area, based on the internal wave speed, is about 30 hours, and the observations show that many episodes of exchange flow persist over several 48-hour periods. With this model, the discharges and water levels in both layers are specified at one end, and the integration of the equations is carried out stepwise along the channel with friction parameters being adjusted until a match is obtained with the known boundary conditions at the sill and at the other end.

Two main types of computer runs were carried out: (1) sensitivity analysis for external (wind and flow) and internal (shear stresses) forces, and (2) calibration of the model parameters, giving the "permissible" range of water levels and "physically" correct interface profiles for the given range of wind speeds and bottom layer flows.

3.1 Effect of External and Internal Forces on the Model Results

The computer model was run for different values of wind speed and hypolimnion flow, keeping the model parameters constant. Different values of interfacial shear stress coefficient and bottom friction coefficient were employed while wind speed and discharges were kept constant. The results of these runs are summarized as follows:

a) Effect of Changing the Hypolimnion Flow

The net flow through the ridge cross-section Q_{net} was set to be equal to the average flow into Niagara River (6000 m^3/s; 215,000 cfs)

and wind speed (eastward) to 3 m/s. Three hypolimnion discharges, estimated from 1977 observations, were applied (Q_2 = 2500, 5000 and 7500 m^3/s). As shown in Figure 8.6 for same up-stream water levels, as the hypolimnion flow increases, the interface rises. The corresponding change of the surface elevation is very small and may be neglected (e.g. 0.7 Cm in 50 Km). When the bottom flow (Q_2 = 2500 m^3/s) direction is reversed, keeping other variables the same, the computed interface elevation drops to very close to the bed just before the ridge, indicating that this flow is totally inconsistent with the driving forces.

b) Effect of Wind

Figure 8.7 shows the computed surface and interface profiles for different wind speeds (eastward wind) and constant flow (Q_2 = 5000 m^3/s into the central basin hypolimnion, and Q_1 = 11000 m^3/s into the Eastern Basin epilimnion). As shown in Figure 8.7, the mean flow velocities and the interface level correlate with the wind. The return flow velocity (Q_2) entering the Central Basin hypolimnion increases as the wind speed increases. It is interesting to notice that there can be strong hypolimnion flow into the Central Basin even when the thermocline in the Eastern Basin is much lower than the thermocline in the Central Basin.

We conclude that the exchange flow is strongly related to meteorological factors, namely the strength and persistence of the eastward component of the wind. This correlation has been observed in the field data (Figures 8.4 and 8.5).

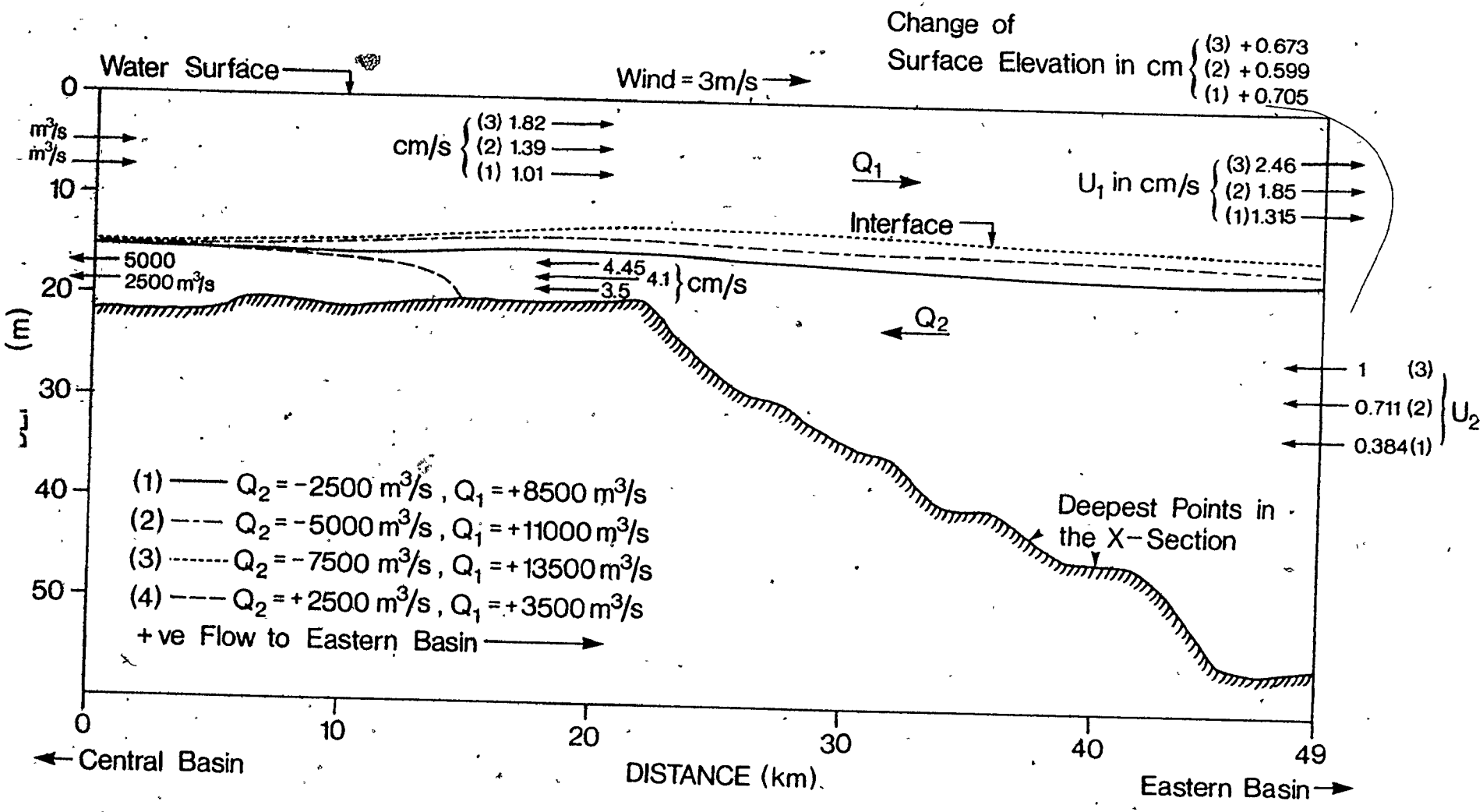

Figure 8-6. EFFECT OF CHANGING THE HYPOLIMNION FLOW ON FLOW REGIME

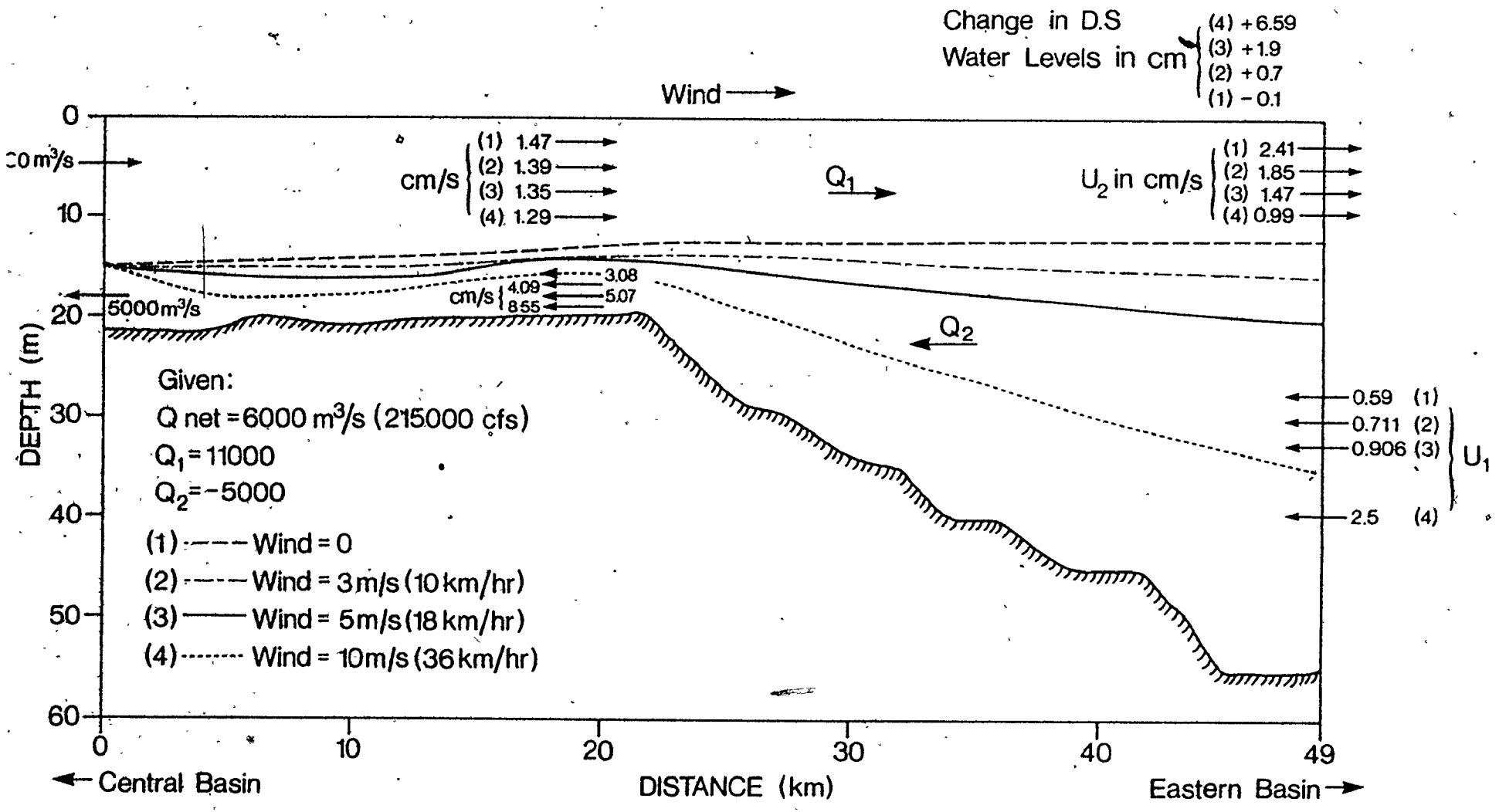

Figure 8-7 . EFFECT OF WIND SPEED

c) Effect of Bottom Roughness Coefficient

The observed structure of the subsurface flow, with the maximum velocity occurring some distance above the bottom indicates that bottom friction is an important term in the force balance. Figure 8.8 shows the effect of bottom roughness coefficient on the flow regime in the Pennsylvania channel. As the friction coefficient increases the flow velocity in the lower layer decreases while the upper layer flow velocity slightly increases and the interface rises. The internal pressure gradient increases at the vicinity of the sill as the friction coefficient increases.

d) Effect of Interfacial Shear Stress

For constant discharges (Q_1 = 11000, Q_2 = 5000 m^3/s) and wind speed (5 m/s), different interfacial shear stress coefficients (C_i = 0.0, 0.0025 and 0.005) were applied. As shown in Figure 8.9, increasing the interfacial shear stress would result in appreciable decrease of the return (hypolimnion) flow velocity and slight increase of the surface layer velocity. This is combined with a rise of the interface. The interfacial shear stress term is likely to be as important as the bottom friction term and produces a comparable effect.

3.2 Model Parameterization

The objective of this analysis is to evaluate the model parameters, namely; bottom roughness coefficient (C_o), interfacial shear stress coefficient (C_i) and surface drag coefficient (C_D). This has

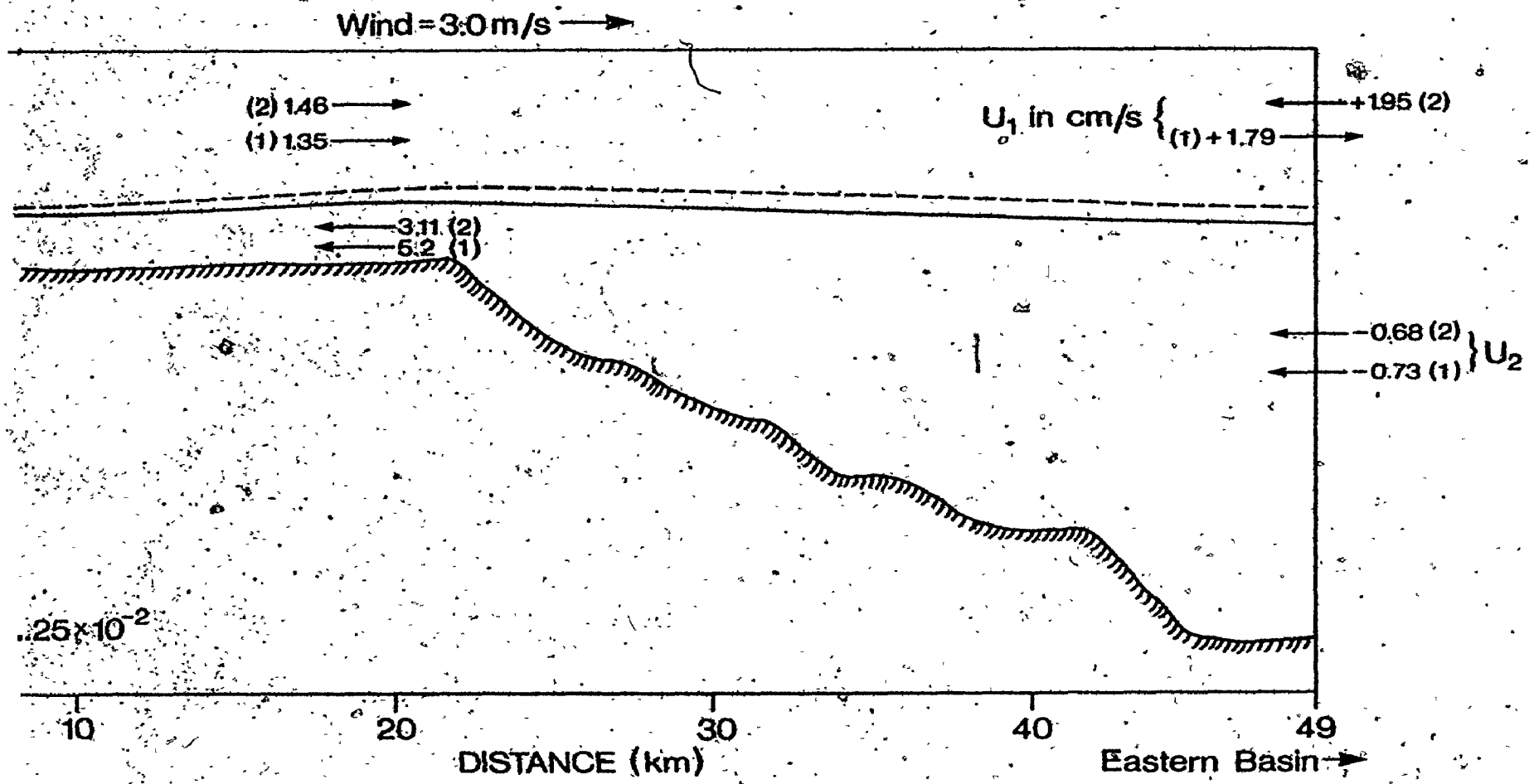

FECT OF BOTTOM ROUGHNESS COEFFICIENT

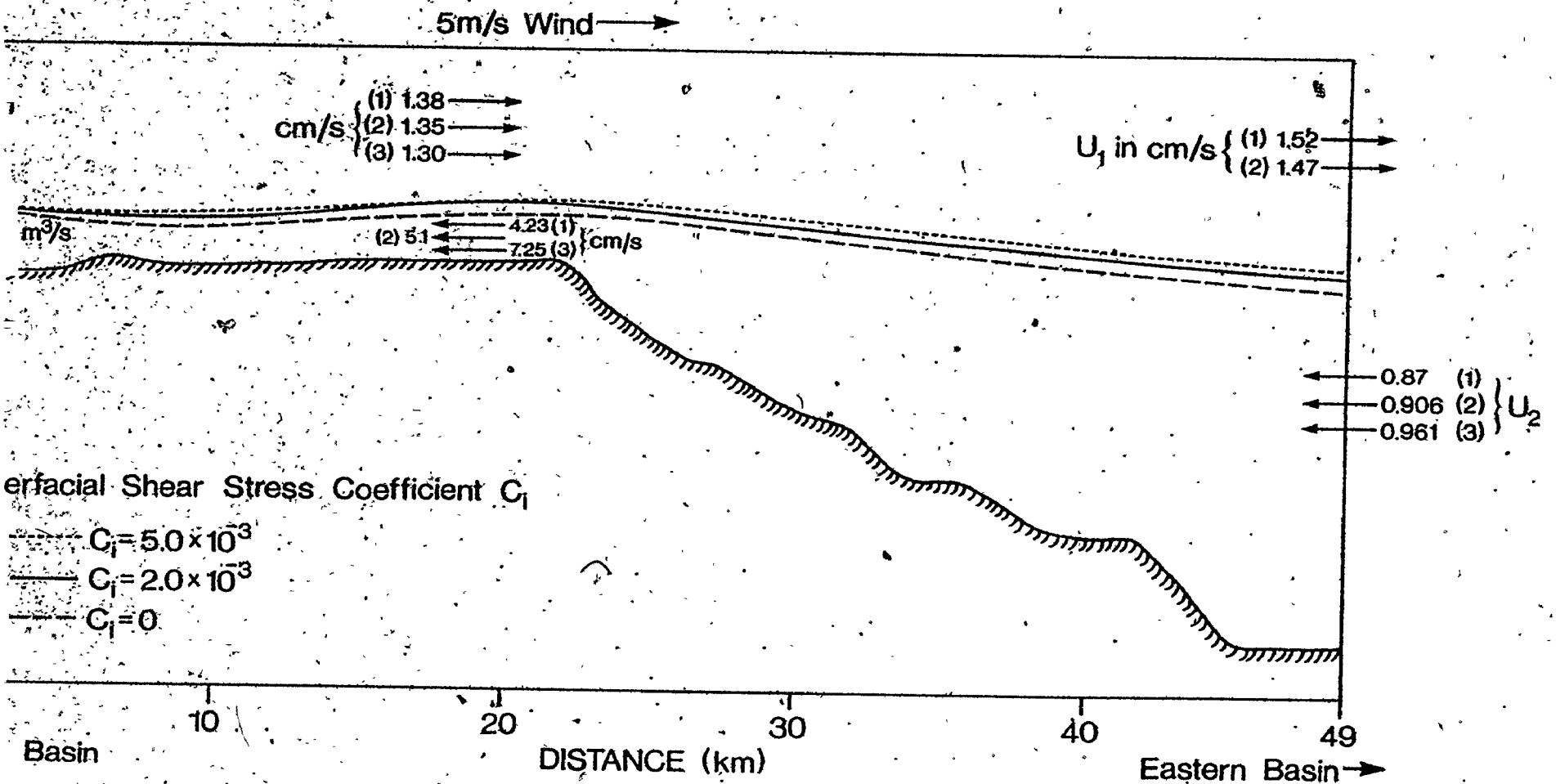

e 8-9. EFFECT OF INTERFACIAL SHEAR STRESS

been done by running the model for the observed values of wind speed and the corresponding estimated hypolimnion flow. A sample of the results is shown in Figures 8.10, 8.11 and 8.12.

Now, a comparison between the computed interface profiles and the observed thermocline would give the range of shear stress coefficients (Eid 1980). The significant results obtained from this analysis are:

1) The interfacial shear stress coefficient which gives close agreement with observations ranges between 0.0 and 2.5×10^{-3} (average 1.25×10^{-3}). This value is comparatively high indicating that interfacial shear is an important term in the force balance equations.
2) Bottom shear stress coefficient ranges from 1.25×10^{-3} to 3.75×10^{-3} with an average 2.5×10^{-3}. This value agrees with values used in 3-D hydrodynamical models for wind-driven lake circulation (Simons 1973, Eid 1976).
3) An average value of wind drag coefficient C_D of the order $2. \times 10^{-3}$ was found suitable for the present model. This value is close to those used in other studies (e.g., Wilson 1960; Donelan 1975; Eid 1976; James and Eid 1978).
4) Wind drag coefficient C_D may be determined as mentioned in chapter II using the wind-wave coupling model. In the present application, however, the wind is averaged over a rather large period and the use of the wind-wave coupling model may result in underestimating C_D.

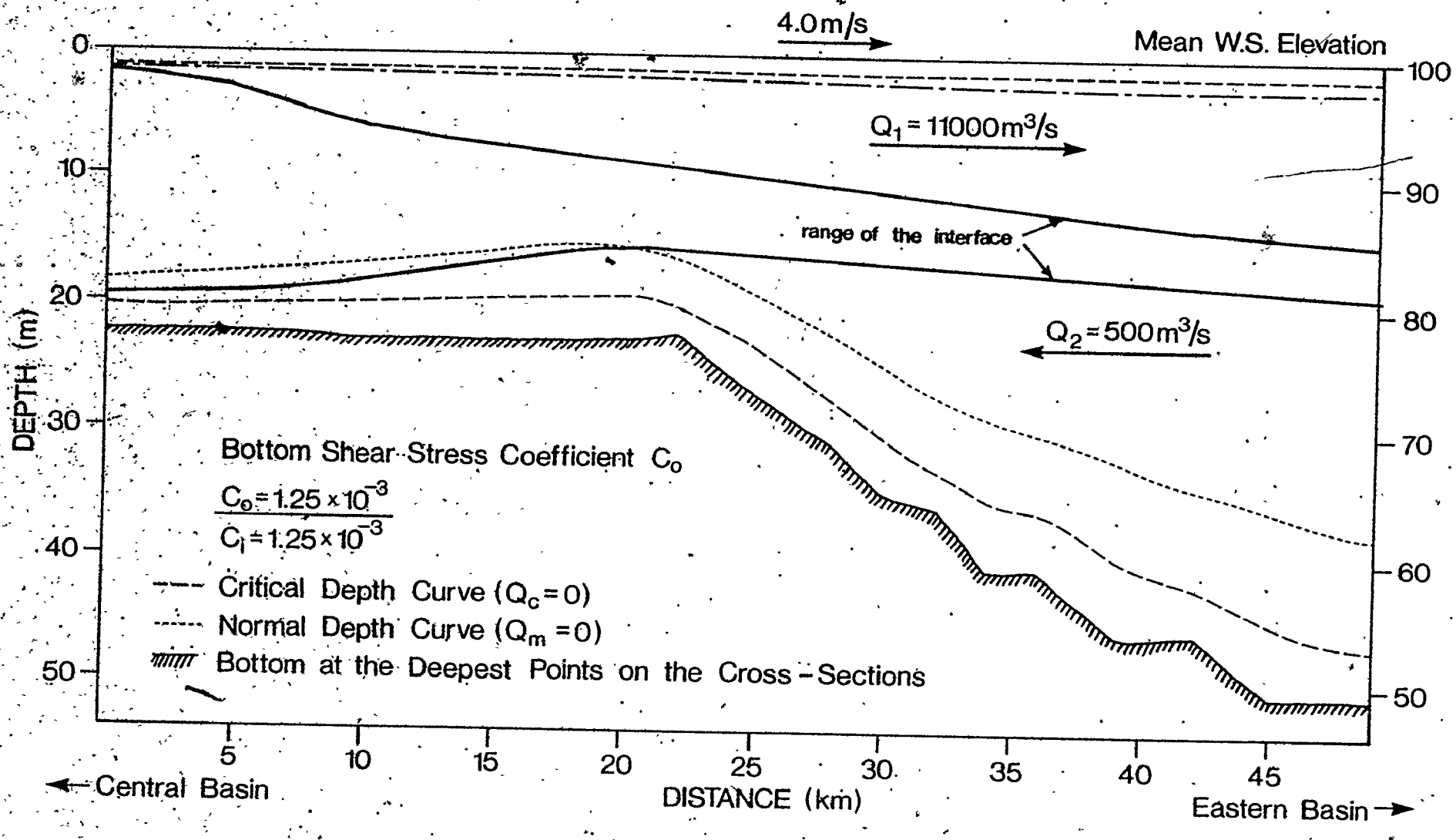

Figure 8.10 MODEL PARAMETERIZATION : BOTTOM ROUGHNESS COEFFICIENT

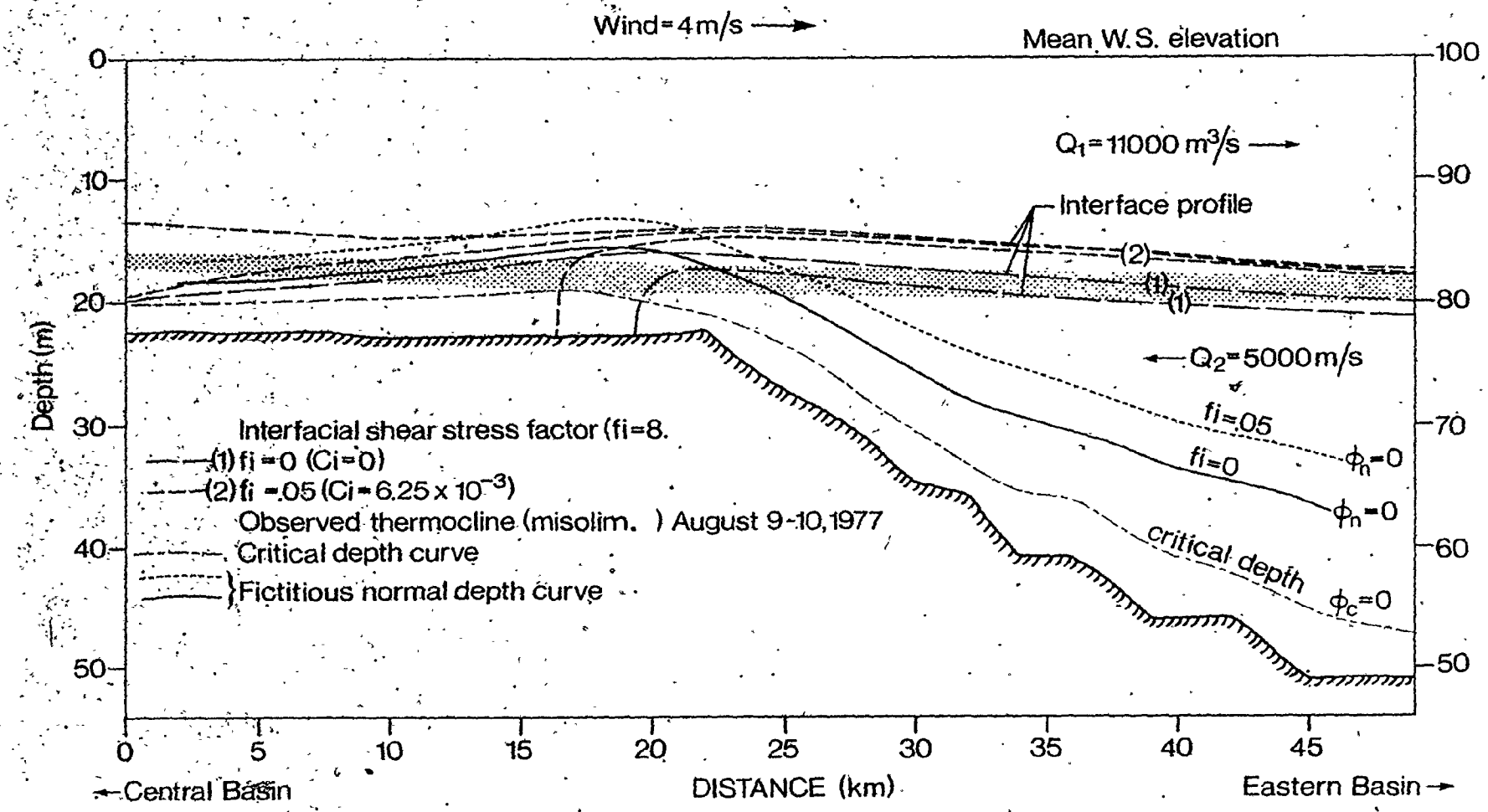

Figure 8.11 MODEL PARAMETERIZATION ; INTERFACIAL SHEAR COEFFICIENT

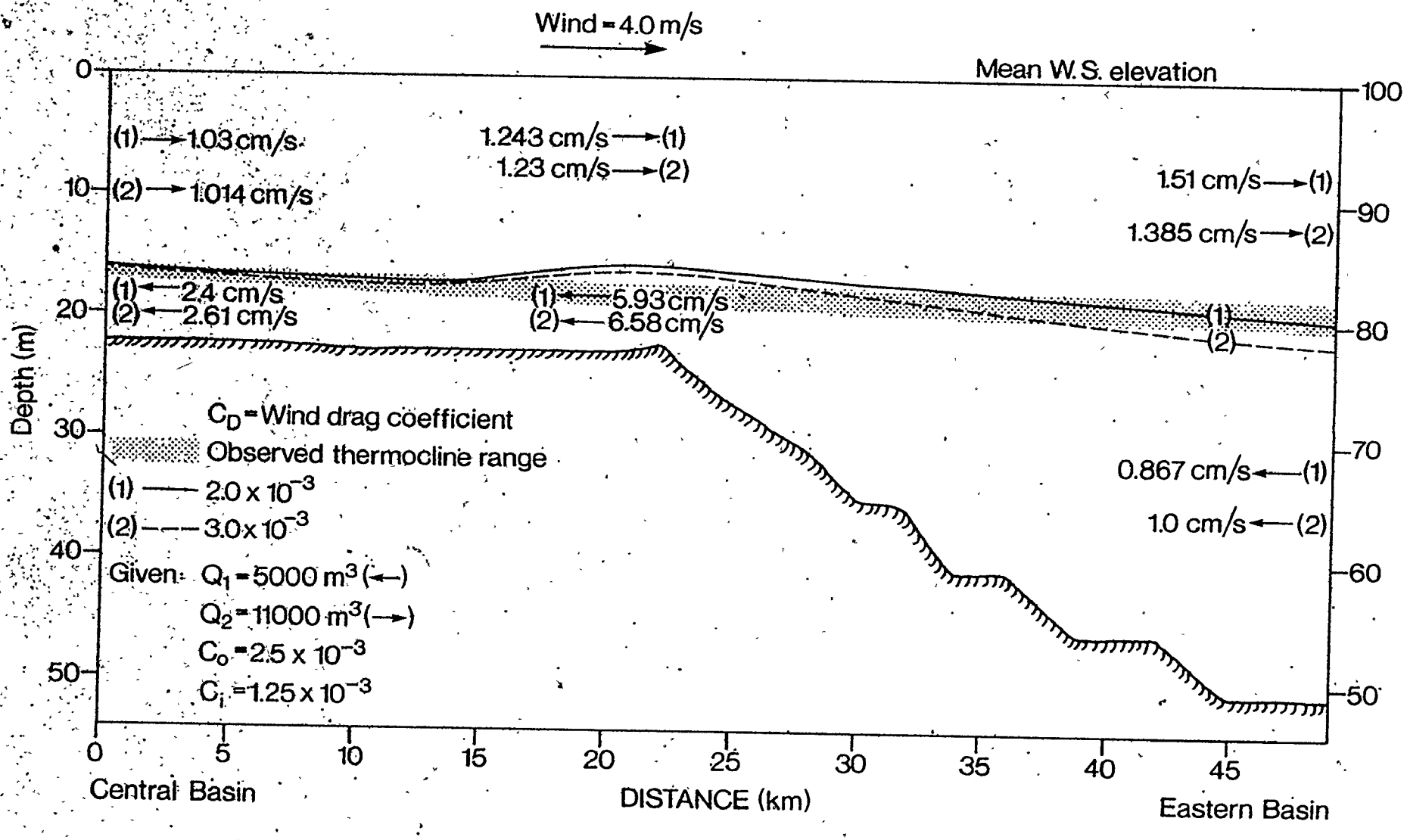

Figure 8.12 MODEL PARAMETERIZATION: WIND DRAG COEFFICIENT

5) The computation of the interface profile is more sensitive to the changes in the interface elevation at the deeper Eastern Basin end-section than that at the Central Basin end-section. As shown in Figures 8.10, 8.11 and 8.12, for example, a very small change (<10 cm) of the interface elevation at Eastern Basin end-section causes a large change at the other end-section (more than 3.0 metres). This indicates that the thermal structure of the deep Eastern Basin is an important factor affecting the exchange flow between the two basins.

6) It is interesting to notice that there can be strong hypolmnion flow into the Central Basin even when the thermocline in the Eastern Basin is much lower than that in the Central Basin. This indicates the strength of wind as the main driving force. When there is no wind, however, the flow in the lower layer is mainly due to the internal pressure gradient (i.e., density flow). The combined effect of the external and internal forces on the flow regime is shown in Figure 8.13.

4. MODEL VERIFICATION

The 1978 observations were used to check the validity of the model as a tool of predicting the interbasin exchange flow under given meteorological conditions. For more details see Eid (1980).

In general, the temperature data have shown strong stratification during the months of July and August. Figure 8.14 presents the 48-hour average depths of the interface (i.e., the line of maximum temperature

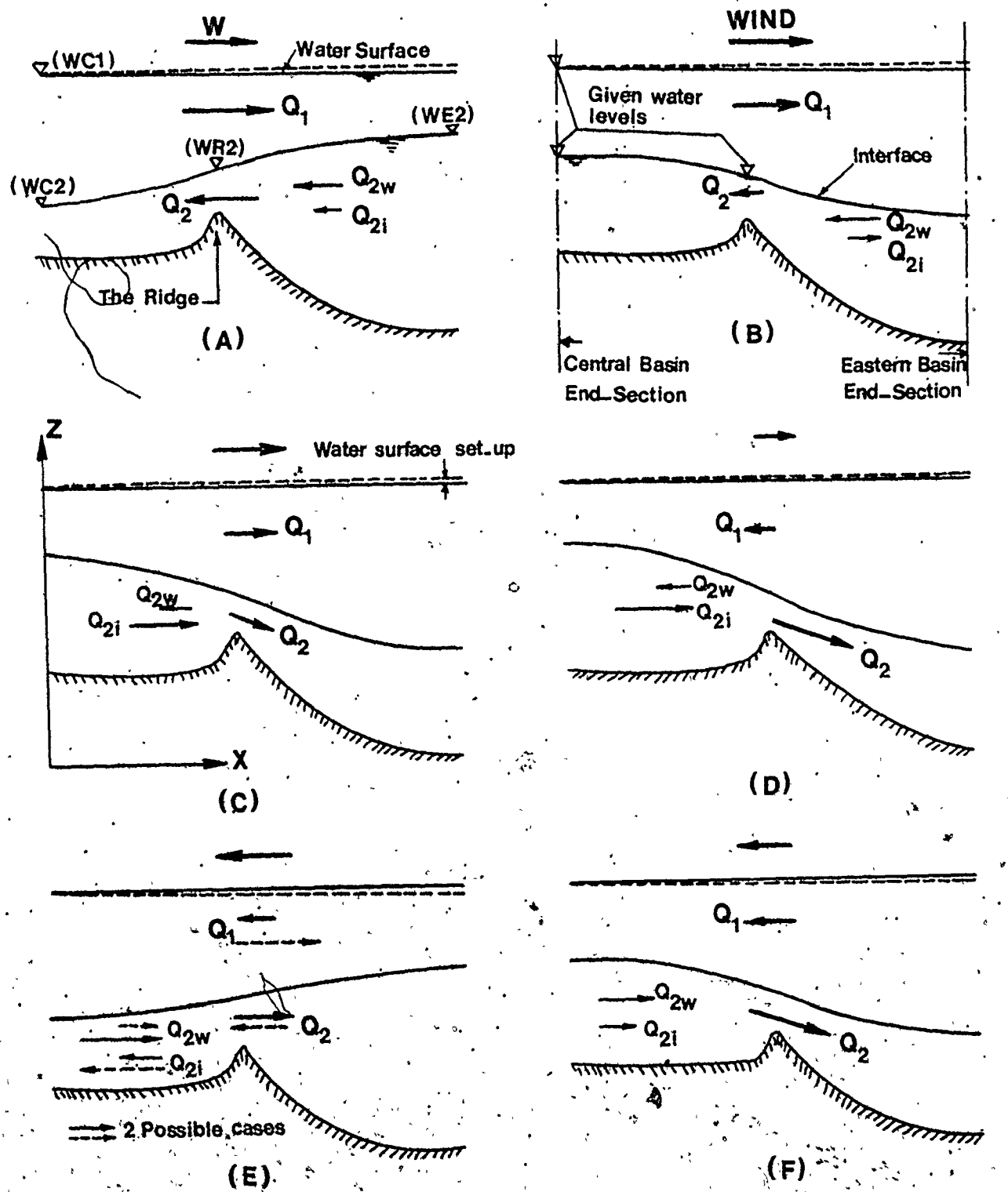

Q_1 = Epilimnion Flow

Q_2 = Hypolimnion Flow

$= Q_{2w} + Q_{2i}$

$Q_{2w} = Q_2$ Due to surface Pressure gradient

$Q_{2i} = Q_2$ Due to internal pressure gradient

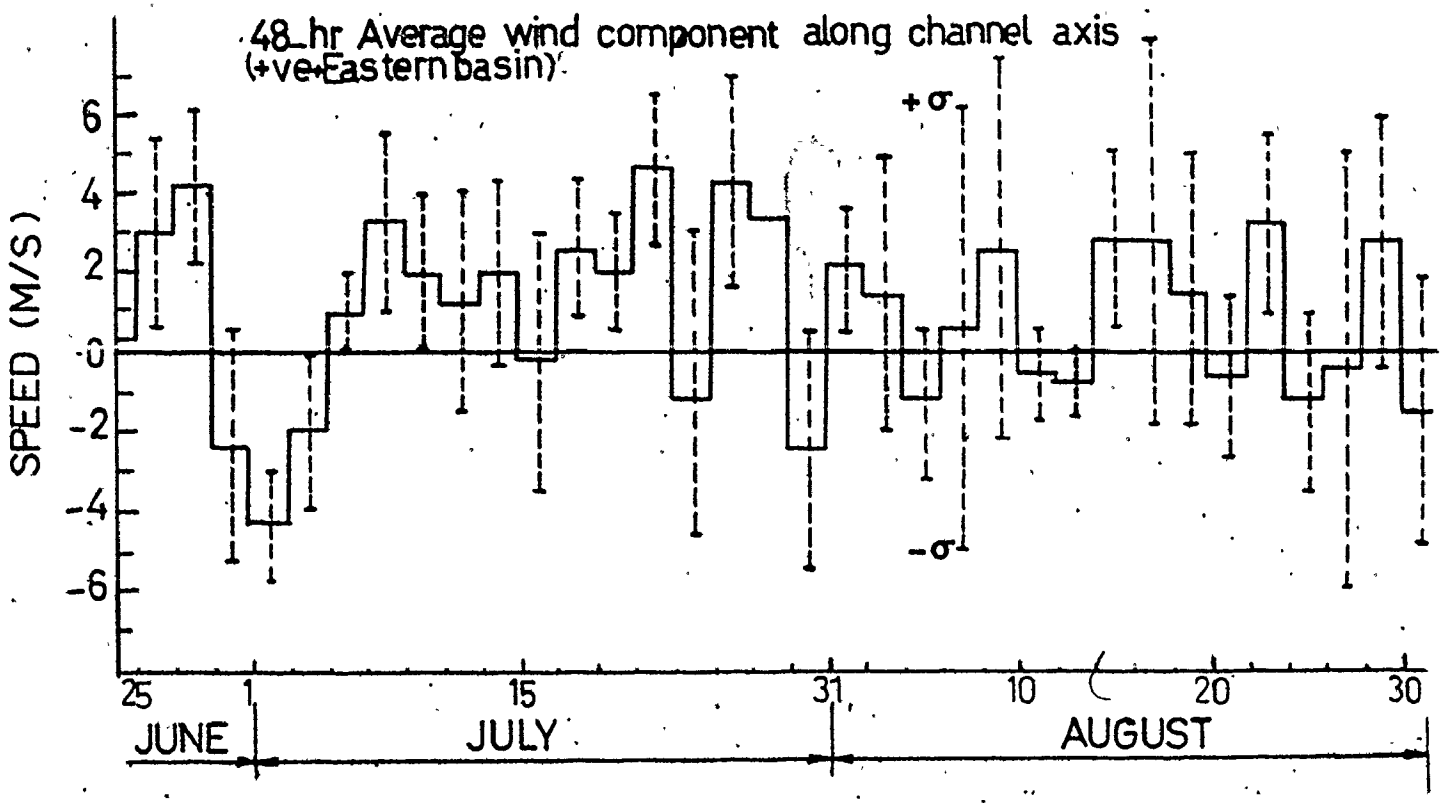
48 hr Average wind component along channel axis
(+ve Eastern basin)
SPEED (M/S)
6
4
2
0
-2
-4
-6
+σ
-σ
25
1
15
31
10
20
30
JUNE
JULY
AUGUST

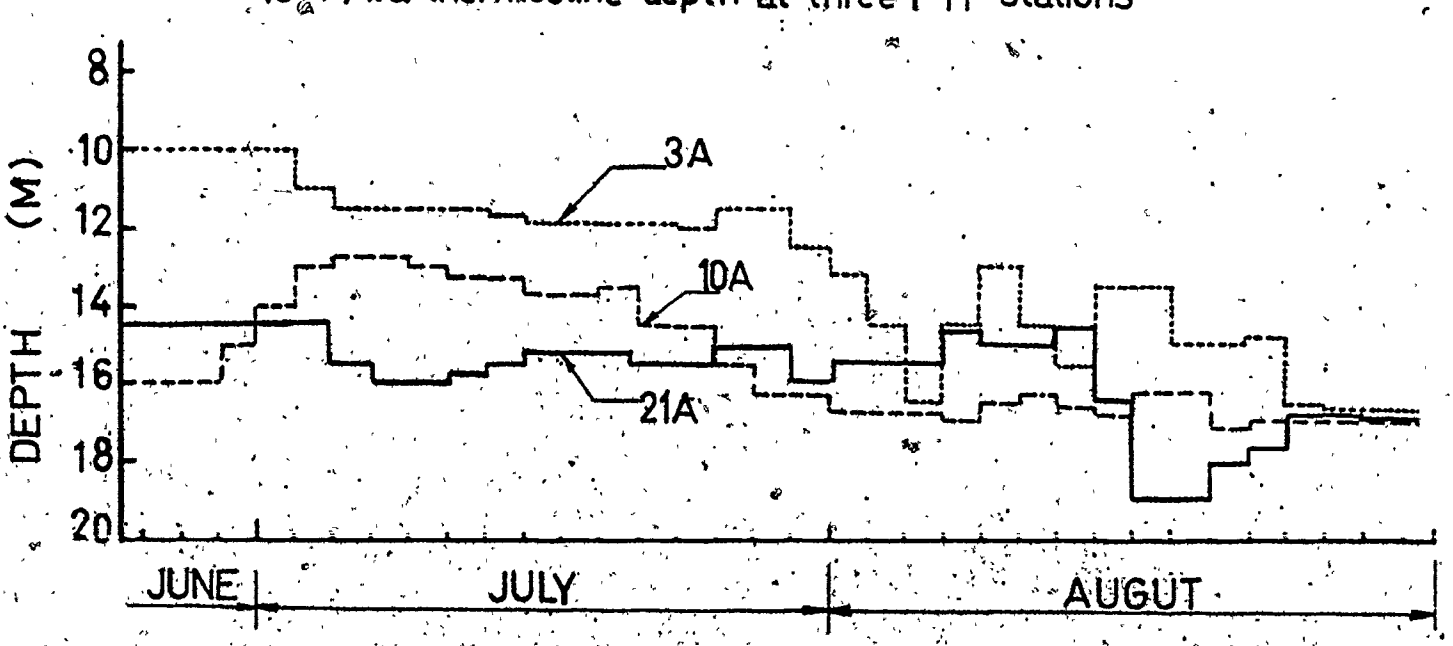
48 hr Ave. thermocline depth at three FTP stations
DEPTH (M)
8
10
12
14
16
18
20
3A
10A
21A
JUNE
JULY
AUGUT

gradient) and wind component along the channel axis. These time series data are used as input to the BVP model. The hypolmnion flows into Central Basin were estimated (Eid 1980) and summarized in Table 8.1 (Figure 8.5).

The following parameters and constants were used from the previous sensitivity analysis (section 3):

1 - wind drag coefficient $C_D = 2.0 \times 10^{-3}$

2 - interfacial shear stress coefficient $C_i = 1.25 \times 10^{-3}$ (f_i=0.01)

3 - bottom shear stress coefficient $C_o = 2.5 \times 10^{-3}$ (f_o=0.02)

4 - Average surface water elevations (from U.S. Dept. of Commerce, NOAA, 1978) were taken to be 174.42, 174.33 and 174.23 m for the months of June, July and August respectively.

5 - Kinetic energy correction factors $\alpha_1 = \alpha_2 = 1.0$

The input variables to the model are:

1 - the component of wind speed (cm/s) along the channel axis (+ve towards Eastern Basin), Figure 8.14.

2 - depth of the interface at two cross-sections in the channel reach (Figure 8.14).

4.1 Computer Analysis And Model Results

In this section the results of the computer runs of the Boundary-Value Problem (BVP) model are presented.

The first set of runs was carried out to check the effect of using longer periods on the model prediction. This is useful to determine a suitable time scale for the model. In order to do this, the

Table 8-1: Hypolimnion flow estimated from 1978 current meter observations at Pennsylvania Ridge (48-hr average)

Date	Interface depth (m)	Area $\times 10^3$ m^3	Average Flow m^3/s +ve to C.B.	$\bar{u}_2$ cm/s	$V^*_{s.d}$	Error* E m^3/s
June 25	13	315.5	+ 7895	2.5	± 4.15	± 13109
27	13	315.5	+ 10877	3.5	± 5.5	± 17377
29	13	315.5	+ 10230	3.4	4.48	14135
July 1	13	315.5	+ 2880	0.91	4.32	13618
3	14	217.5	- 5072	- 1.87	5.07	16418
5	14.25	262.5	- 13830	- 5.28	3.5	9216
7	14.5	253.5	- 5655	- 2.16	2.9	7345
9	14.5	253.5	+ 1679	+ 0.67	4.8	12236
11	14.5	253.5	- 4798	- 1.9	5.97	15133
13	14.0	371.5	+ 1473	+ 0.54	6.16	16728
15	13.5	282.5	+ 4051	+ 1.43	6.19	17488
17	14.0	271.5	- 5859	- 2.16	6.46	17554
19	13.75	279.5	+ 2246	+ 0.81	3.76	10499
21	13.5	282.5	+ 3866	+ 1.37	2.96	8360
23	14.0	271.5	+ 9618	+ 3.55	5.8	15747
25	14.0	222.5	+ 4484	+ 1.65	4.73	10516
27	14.0	271.5	+ 12356	+ 4.56	6.55	17772
29	14.5	256.5	+ 10000	+ 4.0	7.08	18167
31	15.0	228	- 2368	- 1.05	6.76	15415
Aug. 2	16.0	191	- 677	- 0.36	5.08	9707
4	16.0	191	+ 2560	1.26	5.25	10021
6	16.5	172.5	- 3825	- 2.24	3.87	2811
8	15.75	197.5	- 3511	- 1.8	7.75	15303
10	14.75	238	+ 8688	+ 3.68	6.77	16104
12	16	191	- 1054	- 0.56	3.4	6518
14	16	191	- 5818	- 3.08	2.95	5637
16	15	215	+ 5679	+ 2.51	5.57	11982
18	15	228	+ 10123	+ 4.48	7.5	17100
20	15.5	200	+ 2312	+ 1.13	8.3	16602
22	17.5	135.5	- 2971	- 2.22	3.69	5009
24	17	152	+ 1327	+ 0.87	4.88	7423
26	17	152	- 1642	- 1.7	4.96	7536
28	17	152	- 6456	- 4.3	7.4	11251
30	17	152	+ 3142	+2.1	7.0	10617

$$V_{s.d} = \left(\frac{\sum_{i=1}^{n} A_i \sigma_i^2}{n}\right)^{1/2} \quad ; \quad E = \sum_{i=1}^{n} A_i \cdot V_{s.d}$$

48-hr averages of wind and interface depths were grouped into number of longer periods which have similar wind and/or thermal conditions, as shown in Figure 8.15. As we are not certain of the depth of the interface, the upper and lower bounds of the interface levels were estimated from the observations as shown in Figure 8.15b. The results of these runs are presented in Figure 8.15c. The computer results were compared with the estimated average hypolimnion flow calculated from current meter data observed for the same periods. As shown in Figure 8.15c, the model results differ greatly from the observations. This leads to the conclusion that a longer time scale (say one week) is not appropriate for this problem.

The second set of computer runs was carried out using the 48-hour average wind speeds (shown in Figure 8.14) and different values of the interface depths at the ridge and Central Basin end-sections. Again as we are not certain about the depth of the interface, an average depth was assigned, using all available temperature data in the study area. An error band on the depth of the interface was assumed to range between ± 1 m to $\pm$ 2.0 m depending on the temperature gradient. The results of these runs are shown in Figure 8.16a.

As shown in Figure 8.16a, the mean flow into the Central Basin hypolimnion is strongly correlated, as one might expect, with wind speed and direction. It is also clear that the depth or the slope of the interface between the two control sections (e.g. the ridge and upstream sections) has a considerable effect on the exchange flow between the two basins.

(a) Average wind component into Eastern Basin

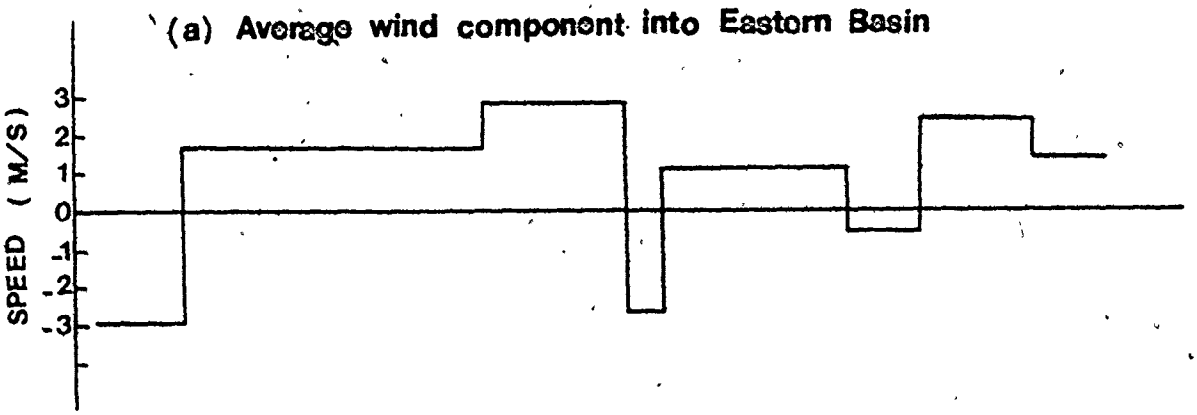

(b) Average depth of the interface

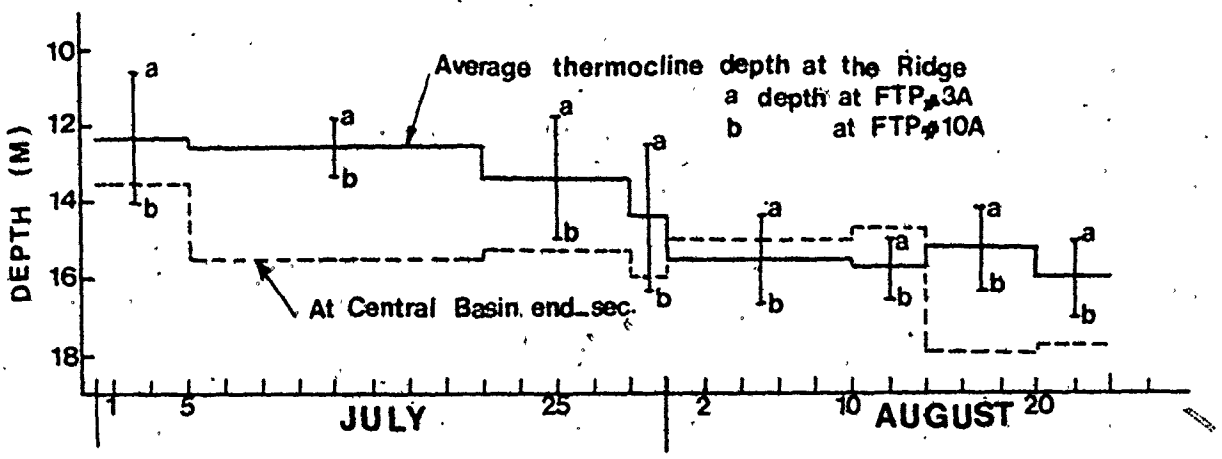

(c) Computed average hypolimnion flow into Central Basin

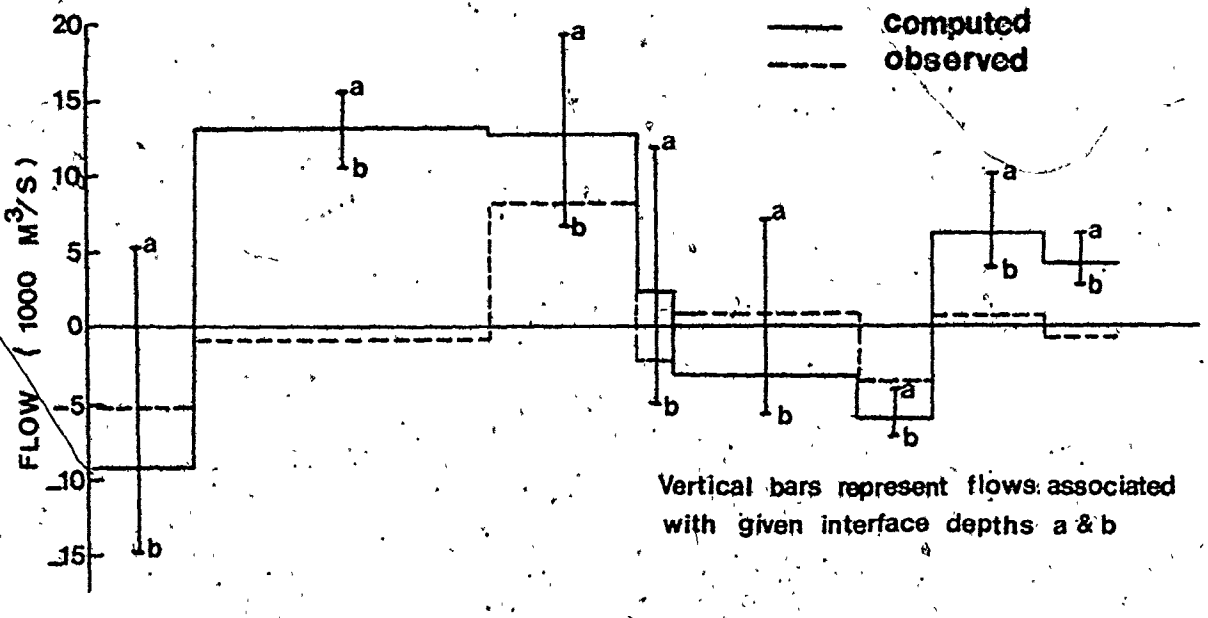

(a) Range of flow due to the range (error) of interface depth

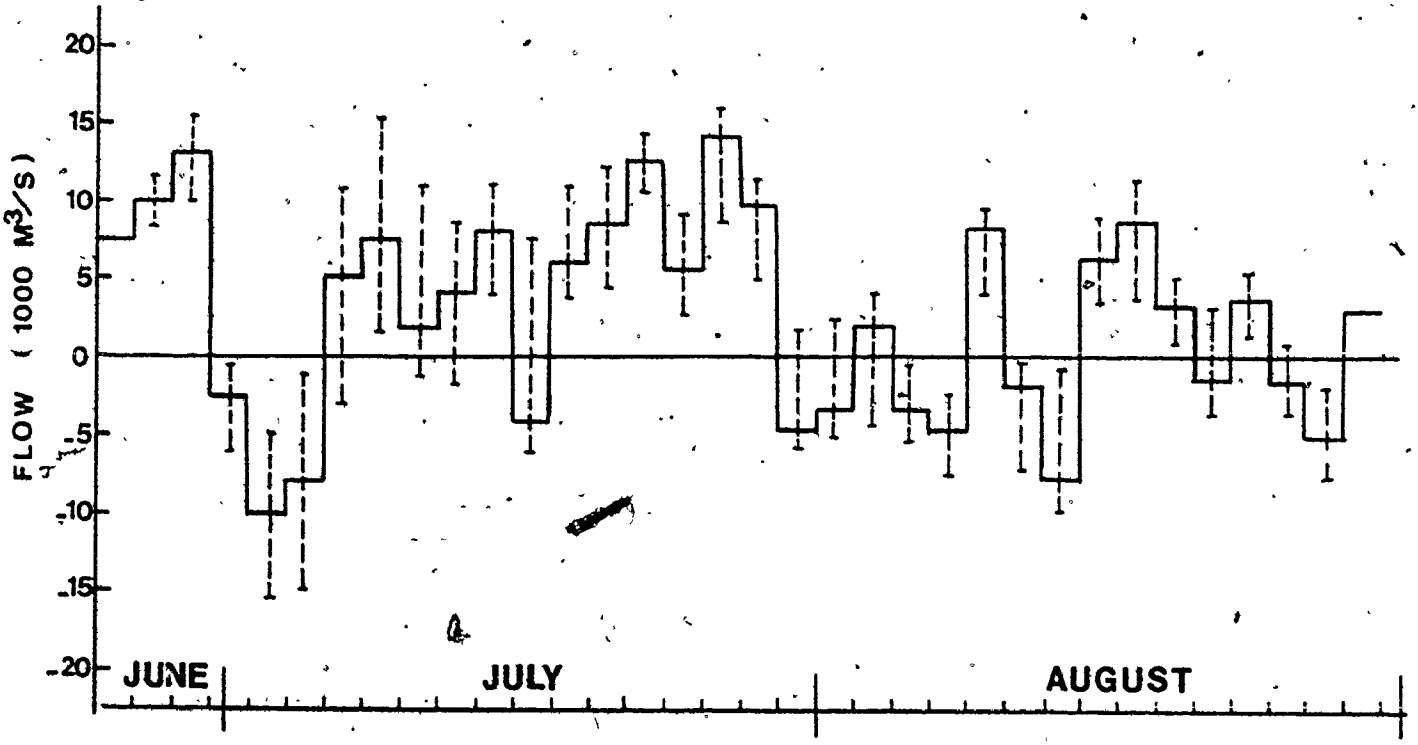

(b) Variation of flow due to variation of wind about the mean

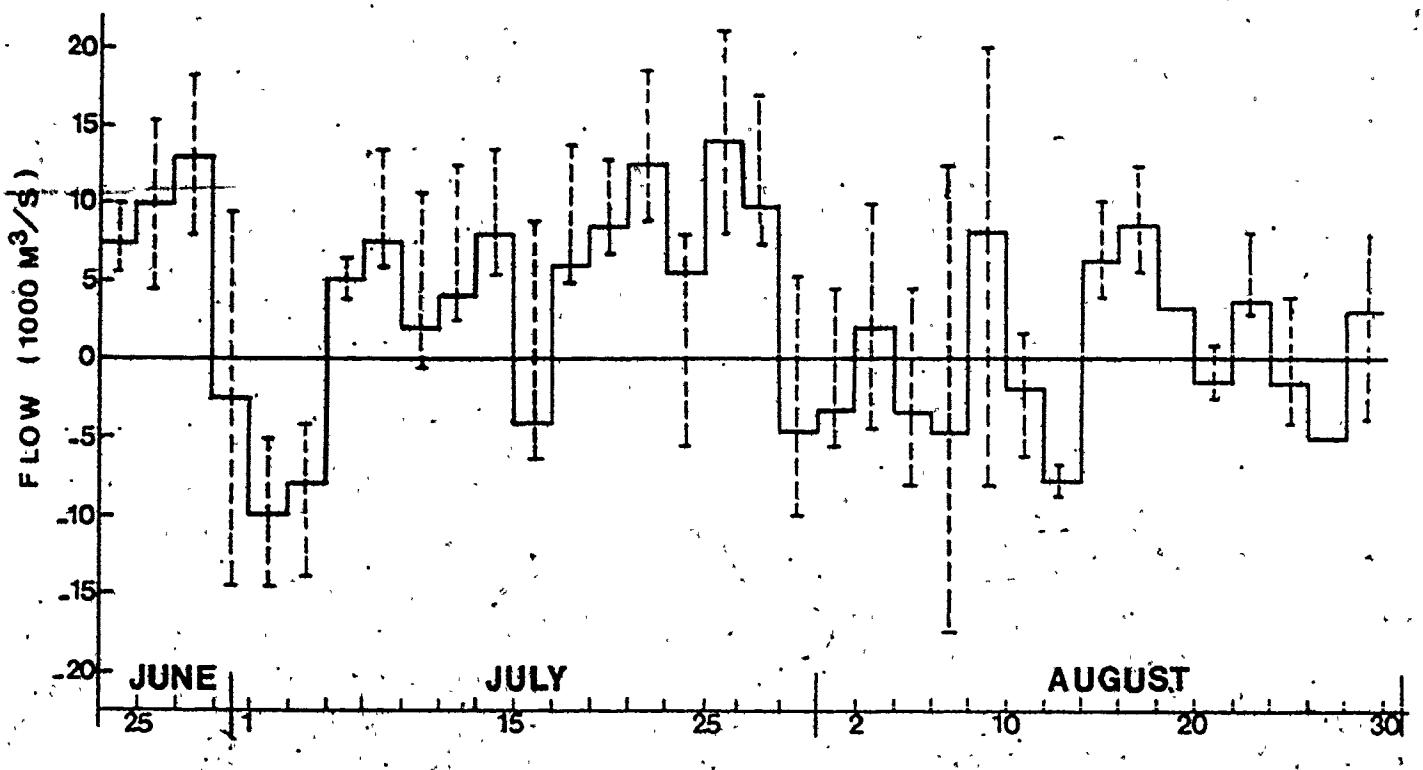

Figure 8.16 MODEL RESULTS: 48-HR. AVERAGE HYPOLIMNION FLOW (+ve.

Another source of error is the variation of the component of wind speed about the mean. The variance of wind speed about the mean produces an error in the steady state model results. The variance about the 48-hour mean (shown in Figure 8.14) may be viewed as a measure of the sensitivity of the model to such variations in wind speed. The model was run for the average wind speeds $\pm$ standard deviation (σ) of wind speed about the mean, and the results are shown in Figure 8.16.b. It is obvious that the model results are very sensitive to variations in mean wind speed.

The 48-hour average hypolimnion flow estimated from the current meter observations were compared with those computed by the model. As shown in Table 8.2 and Figure 8.17, encouraging agreement was found. This suggests that a 48-hour period is a suitable averaging interval for the model, for predicting exchange flow between the Central and Eastern Basins of Lake Erie during a stratification period.

4.2 Effect of Neglecting Coriolis Forces

As mentioned before, Coriolis force may cause a transverse slope of both the water surface and the interface, which can be determined from equation (5.20). In the present model, however, the flow is assumed to be along the channel axis, e.g., the velocity component perpendicular to the channel axis is zero. Thus the Coriolis term vanishes in the momentum equations (5.1) and (5.2). The Coriolis force is then balanced by the "geostrophic" pressure gradient resulted from the transverse slope of water. This effect may only cause a

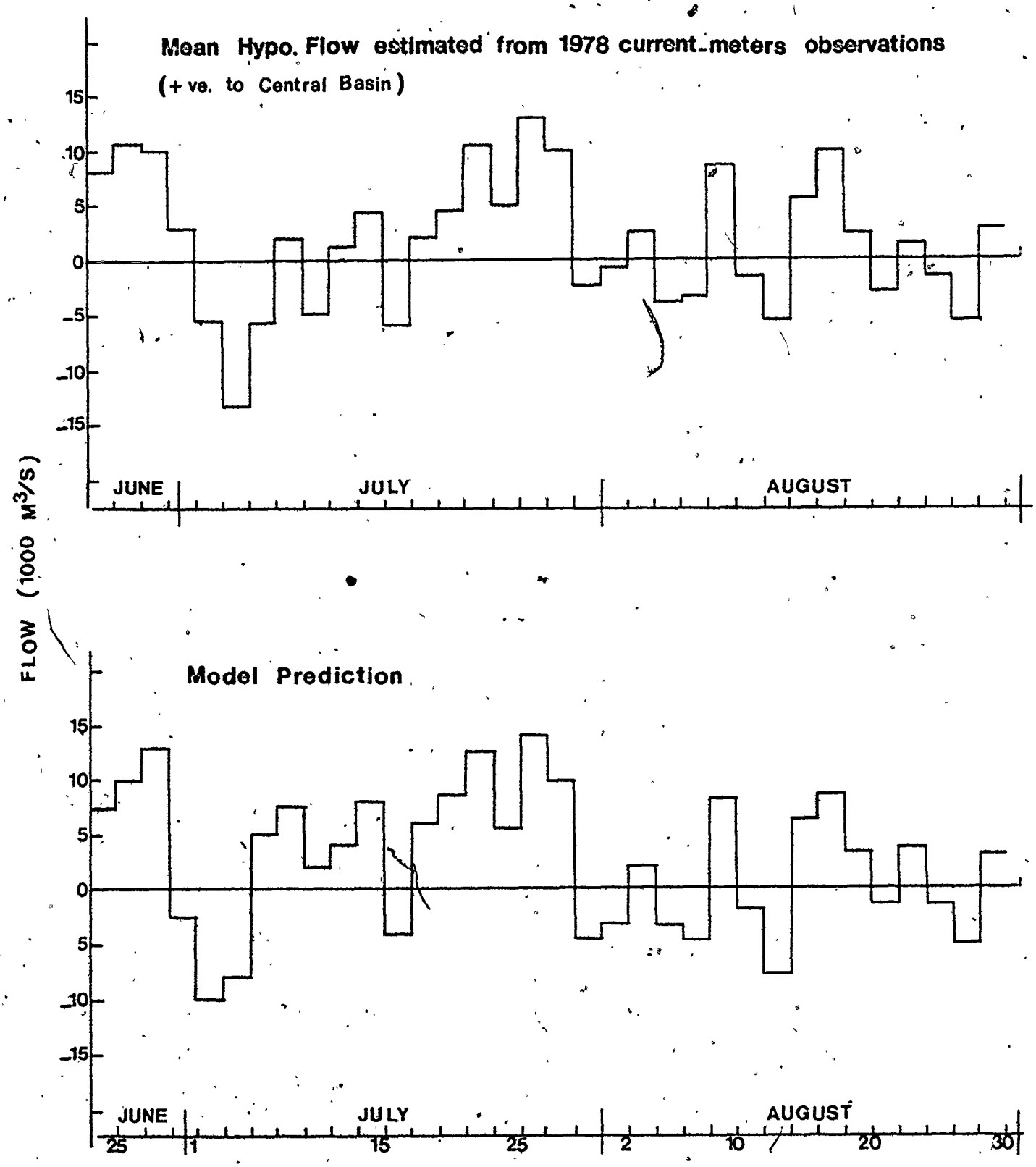

Figure 8.17 COMPARISON BETWEEN OBSERVATIONS AND THE COMPUTER MODEL RESULTS

Table 8.2: Comparison between model results and 1978 observations

Date		Wind* m/s	Model Results Q_1** m^3/s	Model Results U_1 cm/s	Model Results Q_2 m^3/s	Model Results U_2 cm/s	Observations WE_2 m	Observations Q_2 m^3/s	Observations U_2 cm/s
June	25	- 0.29	- 13500	-1.88	+ 7500	2.5	12.4	+ 7895	2.5
	27	- 3.03	- 15540	- 2.06	+ 9540	3.11	16.0	+ 10877	3.5
	29	- 4.24	- 18870	- 2.5	+ 12870	5.0	17.6	+ 10230	3.4
July	1	+ 2.41	- 3270	- 0.5	- 2730	- 0.8	10.0	+ 2880	0.91
	3	+ 4.38	+ 4000	+ 0.6	- 10000	- 2.5	--	- 5072	- 1.87
	5	+ 2.00	+ 2040	+ 0.27	- 8040	- 3.3	13.2	- 13830	- 5.28
	7	- 0.93	- 11330	- 1.45	+ 5330	+ 2.4	14.4	- 5655	- 2.16
	9	- 3.29	- 15240	- 1.95	+ 9240	+ 4.0	16.2	+ 1679	0.67
	11	- 1.95	- 8150	- 1.0	+ 2150	+ 1.2	16.3	- 4798	- 1.90
	13	- 1.20	- 10000	- 1.25	+ 4000	+ 2.0	15.1	+ 1473	0.54
	15	- 2.00	- 10420	- 1.30	+ 4420	+ 2.18	15.7	+ 4051	1.43
	17	+ 0.28	- 1730	- 0.21	- 4270	- 2.4	15.6	- 5859	- 2.16
	19	- 2.64	- 12050	- 1.51	+ 6060	+ 2.9	16.0	+ 2246	0.81
	21	- 2.04	- 10530	- 1.3	+ 4530	+ 2.2	15.6	+ 3866	1.37
	23	- 4.68	- 17200	- 2.2	+ 11200	+ 5.1	17.7	+ 9618	3.55
	25	+ 1.28	- 11560	- 1.5	+ 5560	+ 2.2	14.0	+ 4484	1.65
	27	- 4.36	- 19960	- 2.6	+ 13960	+ 5.5	16.25	+ 12356	4.56
	29	- 3.38	- 15700	- 2.0	+ 9700	+ 4.2	16.0	+ 10000	4.0
	31	+ 2.74	- 1130	- 0.14	- 4870	- 2.7	14.2	- 2368	- 1.05
Aug.	2	- 2.19	- 2700	- 0.3	- 3300	- 2.1	16.2	- 677	- 0.36
	4	- 1.48	- 8000	- 1.0	+ 2000	+ 1.2	16.0	+ 2560	1.26
	6	+ 1.26	- 2400	- 0.3	- 3600	- 2.1	14.0	- 3825	- 2.24
	8	- 0.61	- 1200	- 0.14	- 4800	- 2.9	16.0	- 3511	- 1.80
	10	- 2.76	- 14400	- 1.9	+ 8400	+ 3.42	15.0	+ 8688	3.68
	12	+ 0.53	- 4500	- 0.45	- 1500	- 0.7	16.0	- 1054	- 0.56
	14	+ 0.68	+ 1000	+ 0.15	- 7000	- 5.0	16.5	- 5818	- 3.1
	16	- 2.87	- 12450	- 1.5	+ 6450	+ 3.4	16.4	+ 5679	2.51
	18	- 2.87	- 14700	- 1.8	+ 8700	+ 4.2	15.8	+ 10123	4.48
	20	- 1.57	- 9360	- 1.1	+ 3360	+ 2.4	17.0	+ 2312	1.13
	22	+ 0.56	- 4600	- 0.5	- 1400	- 1.4	17.6	- 2971	- 2.22
	24	- 3.31	- 9500	- 1.1	+ 3500	+ 2.9	18.5	+ 1327	0.87
	26	+ 1.23	- 4350	- 0.5	- 1650	- 1.3	16.7	- 1642	- 1.10
	28	+ 0.43	- 1000	- 0.12	- 5000	- 3.6	16.7	- 6456	- 4.30
	30	- 2.76	- 9000	- 1.1	+ 3.000	- 2.4	18.0	+ 3142	2,10

* Wind speed +ve to Central Basin

** Flow and velocity are +ve towards Central Basin

modification of the calculated axial velocity using the continuity and momentum equations alone.

To measure the effect of neglecting Coriolis forces on the model results, slopes of the interface are determined by substituting the computed velocities U_1 and U_2 (Table 8.2) into equation (5-20). The computed interface slopes were then compared to those observed between the two themistor arrays (3A and 10A) at the ridge (Figure 8.14). This may provide only a rough indication of Coriolis effect due to the fact that bottom topography might affect this slope. This effect of the topography was observed in all temperature observations at the ridge. As shown in Figure 8.18, the interface inclination was found to be towards the notch south of the ridge during the stratification period even when the flow reverses its direction, which indicates the minor effect of Coriolis term.

When compared to the observed Δh (Figure 8.14), it was found that the calculated Δh is about one order of magnitude less than the observed value. For example, the slope of the interface was found to be in the order of 5×10^{-5} (in average) and Δh is about 1.25 m, while the observed Δh was averaged between 2 and 3 m. this shows the combined effect of Coriolis forces and bottom topography. In addition, observations in the study area have shown that during most of the stratification period the thermocline depth is close to 15 meters and most of the hypolimnion flow is confined to the arrow notch in the shallow sill between the two basin. Thus, the effect of Coriolis term appears to be small.

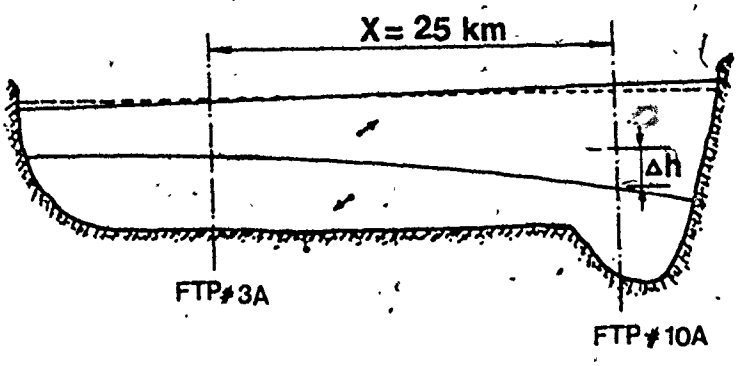

Figure 8.18 Typical interfacial inclination at ridge cross-section (Coriolis effect)

In general we found that the effect of Coriolis is minor in the present model as the averaging of the velocities and thermocline elevations in the cross-section direction may have reduced this effect.

5. DISCUSSION AND CONCLUSION

The computer model "EXFLOW" was applied to the connection between the Central and Eastern basins of Lake Erie using 1977-1978 observations. The model is one-dimensional (along the channel); this assumption was found applicable as the dominant wind and consequently the flow are mainly along the longitudinal axis of the lake.

Strong stratification during summer period suggests that two-layer densimetric flow model may be used.

Although the present model assumes steady flow, the model is applied to the time series of wind speed and interface depth, and the model results are in the form of time series of the flow in both layers. This is done by applying the model for each time-averaging interval.

The choice of the proper time scale is an important factor which sould be carefully considered. In the present application, the spectral analysis of the current meter records has shown that most of the kinetic energy of the spectra is confined in the lower frequencies, i.e., periods more than 48 hours (Boyce et.al. 1980).

The effect of Coriolis forces, which might cause tilting of the interface and water surface in the transverse direction, is neglected. Thus the free surface and the interface are assumed horizontal in the cross-section direction. In the present application, the connecting channel is wide and the Rossby radius of deformation may be comparable to the channel width and Coriolis term might affect the calculated flow velocities. The tilt of the interface at the ridge is a combined effect of Coriolis forces and the topography of the sill. On the other hand, the tilts at the two end sections were found to be much smaller than that at the ridge, indicating the effect of the topography. Generally, it was found that the effect of Coriolis term is small and it may have been cancelled through the averaging of the velocity over the cross-sectional area of the channel.

The model was calibrated using 1977 observations and the model parameters, namely; bottom, interface and surface drag coefficients were found to be: 2.5×10^{-3}, 1.25×10^{-3} and 2.0×10^{-3}, respectively. The model was verified using 1978 observations and good agreement was obtained between the model results and the observations.

The present analysis has shown that the wind is the most important driving force in the exchange flow mechanism. The principle

dynamic balance of the return flow into the Central Basin hypolimnion appears to be the direct action of wind stress through the tilt of the free surface, which is modified by te effect of internal pressure gradient due to stratification and opposed by the bottom friction. Bottom topography of the interconnecting channel plays an important role in the exchange mechanism.

The thermal structure of the adjacent basins close to the sill and within the connecting channel has a considerable effect on the local exchange between the two basins. The model has shown that most of the flow variations are caused by local effects rather than by large scale adjustments of the whole lake. For example, we found that there are hypolimnion flows into Central Basin although the isothermal surfaces of the thermocline lie about two meters deeper in the Eastern Basin during 1977 and 1978 stratification seasons. We conclude that the internal pressure gradients at the basin-wide state are not a major factor in the interbasin flow mechanism. On the other hand, the present model has shown that the local inclination of the interface at the sill is an important term in the driving forces.

Finally, we may conclude that a rather simple, two-layer, one-dimensional model can be used to study the complex exchange flow mechanism between the two basins of Lake Erie through suitable averages of the external and internal forces. The model can be applied to predict the flow of water to the hypolimnion of Central Basin under differnt meteorological conditions. The model is general enough to be applied to other similar interchange flow problems.

CHAPTER IX

SUMMARY AND CONCLUSIONS

This chapter presents a brief summary and the general findings of the study. It also includes recommendations for future research work.

The dissertation describes a number of boundary conditions and related physical processes necessary in the numerical modeling of lake transports. This includes the determination of various important parameters and relates them to the lake and flow characteristics. These key parameters are: surface drag coefficient, vertical eddy diffusion and eddy viscosity coefficients, and bottom roughness coefficient.

Thus, this thesis defines a framework of numerical modeling of lake transports against which a variety of boundary conditions and the related physical processes are studied.

Momentum transfer at the air-water interface, shear stresses due to a very rough lake bed, vertical transports at the sediment-water interface and in the hypolimnion layer as well as the exchange flow between two interconnected stratified basins were studied. The theoretical background and computational algorithms were laid out and numerical models were developed to study these processes and boundary conditions. These models were applied to real lakes of various sizes and characteristics. Field observations were collected at several lakes: Valens Reservoir, Hamilton harbour, Baldeggersee (Switzerland),

and Lake Erie. The significant results obtained in each of the four research areas studied, were as follows:

a) Wind-induced shear stresses at the air-water interface:

The wind drag coefficients and consequently shear stresses at the water surface are determined as a function of wind speed at standard anemometer elevation. Water surface characteristics are represented by significant wave height and phase velocity. Thus, temporal and spatial variations of wind shear stress over a lake surface can be determined when solving the hydrodynamic equations of wind-driven lake transport. For small lakes, however, a spatially averaged value of the drag coefficient may be sufficient for model computations and the present approach gives a good rational basis for determining this average as a function of wind speed and lake size. The wind-wave coupling model was applied to two lakes (Valens and Hamilton harbour) and the results were tested against data collected from other studies in the literature. This algorithm has been incorporated in the general three-dimensional wind-driven hydrodynamic model of lake circulation.

b) Spatial variation of bottom shear stresses in a vegetated shallow lake:

Bottom roughness due to very rough, flexible weeds in shallow lakes can be modeled using the formulation described in a previous thesis by the author. The developed bottom roughness equation incorporates the effect of weed height and its distribution throughout

the lake. This formulation of bottom shear has been conveniently included in the three-dimensional, wind-driven lake circulation model derived in the present study. This model was applied to a shallow recreational lake (Valens reservoir). In such a shallow lake, the boundary conditions at the bed were found to be very important. It greatly affects the currents in both magnitude and direction. This influence depends on the stage of weed growth and its distribution throughout the lake. Field observations were carried out in Valens reservoir in the previous study to measure weed heights, wind speed and direction, and surface currents. These observations were used to calibrate and test the numerical model developed in this study.

c) Vertical mixing near the sediment-water interface and in the hypolimnion:

A one-dimensional diffusion model has been developed to study vertical transports and thermal structure in the lower layers of a stratified lake, where the mixing is mainly due to turbulent diffusion in the vertical direction. The temperature and natural radon-222 profiles were measured and used to study the transport mechanism. The model was developed and tested in an ideal "test lake", a limno-corral located in a typical deep, thermally stable lake where mixing is mainly due to diffusion. The vertical eddy diffusion coefficient was found to be strongly depth-dependent and also time variable. Vertical mixing in the limno-corral was compared to that in the open lake. The present model provides insight into the transport mechanism in the lower layers

of stratified lakes. It is suggested that natural radon-222 is an excellent tool for monitoring vertical mixing near the sediment-water interface. This is due to the simplicity of measurements and their sensitivity to very low rates of mixing changes which may become very difficult to detect using other traditional methods. The model can be used to determine vertical eddy diffusivity which in turn is used to study the transport of any other substance near the sediment-water interface (e.g. dissolved oxygen, methane, phosphorus, etc.).

d) Exchange flow between two interconnected stratified bodies of water:

This phenomena was initially studied through a literature survey of possible hydrodynamical models. A numerical model was then developed for the local exchange flow in the "channel" connecting two stratified basins. The open boundaries at the two ends of the communicating channel were treated such that the effect of the adjacent basins were properly modeled. A one-dimensional, along the channel, two-layer densimetric flow model was developed. Since the model assumes a steady state, the input data are in the form of discrete time series of average wind speeds and depths of the thermocline. Solutions of initial-value problems as well as boundary-value problems were presented for channels of arbitrary geometry. The effects of wind as the main driving force, stratification, river flow, interfacial and bottom shear stresses were considered. The model was successfully applied to study the interchange flow between the Central and Eastern Basins of Lake Erie, where

extensive field observations were collected. These observations were used to calibrate and verify the numerical model. Good agreement was obtained between the observed and computed hypolimnion flow into the Central basin of Lake Erie.

The present study has shown that wind is the most important driving force in the exchange flow mechanism. Thermal structure in the adjacent basins close to and within the comunicating channel has a considerable effect on the local exchange mechanism. Most of the flow variations were found to be caused by local effects rather than by large scale adjustments of the whole lake. Bottom topography of the strait (or connecting channel) plays an important role in the exchange flow.

We conclude that a rather simple, one-dimensional, two-layer stratified flow model an be used to study the complex interchange flow between two basins through suitable averages of the external and internal forces. The choice of the proper time scale for such a "steady-state" model is an important task which should be carefully determined.

In addition to the above models, a two-dimensional, multi-layered hydrodynamical model of wind-driven lake circulation was applied to a homogeneous lake and a stratified harbour during the stagnation period. Some of the above algorithms were incorporated in this model. Field observations were carried out in the two lakes, and the computed surface currents were found to be in good agreement with these observations.

An important aspect of the present study is the practical application of these new numerical models to a variety of real lakes of

various sizes and characteristics. Since each model was developed separately to study a specific boundary condition or a key parameter related to modeling of lake transports, each model was applied to a different lake where this particular parameter or process is dominant.

Recommendations For Future Research

This thesis represents a step towards a comprehensive study of the transport phenomena in lakes of different sizes and characteristics. An important aspect in the numerical modeling of lake transports is the treatment of various boundary conditions and the determination of model parameters by relating them to the lake and flow characteristics. More research efforts are still needed to fully account for all interfacial transports, such as transports across the thermocline of a stratified lake or entrainment.

Development of a numerical model to determine the concentration of a substance (dissolved or suspended, conservative or non-conservative, radio-active or stable) incorporating of the models developed in the present study should be the next step. More investigations should be carried out to study lake responses for the unsteady nature of external forces such as wind.

The momentum transfer from the air to water surface and consequently down to lower layers still requires substantial research to account for heat transfer, stratification and stability of the air above the water surface. More field observations are still needed to refine the wind-wave coupling model developed in the present study.

The vertical mixing model developed in this thesis is essentially a one-dimensional diffusion model which can be applied under very restricted conditions. More general, three-dimensional models of mixing in the hypolimnion may be necessary in many lakes.

The exchange flow between two interconnected stratified basins still requires more research work to include the two dimensionality of the densimetric flow conditions and to include the effect of Coriolis forces especially for wide straits. Further investigations are needed in two areas where there is still uncertainty: interfacial shear stresses for different stratified flow conditions and the entrainment across the interface. In addition, an equation of the transport of a substance, e.g. dissolved oxygen, should be added to the present exchange flow model to account for the fluxes of all materials between the two basins.

Further work is needed to include the exchange flow model in the general three-dimensional hydrodynamical model of a lake transport, e.g., Lake Erie and Hamilton harbour where the interchange flow may affect the transport or mixing mechanisms. This will particularly require more field and numerical experiments and careful analysis is needed to include different time scales in one model.

BIBLIOGRAPHY

1. Abraham, G., M. Karelse, and A. Van Os, 1980: "On the Magnitude of Interfacial Shear in Subcritical Stratified Flows in Relation With Interfacial Stability", Delft Hydraulic Lab. Publication, No. 225, February 1980.

2. Barnett, T.P., E. Bouws, H. Carlson, D. Cartwright, and others, 1973: "Measurements of Wind-Wave Growth and Swell Decay During the Joint North Sea Wave Project (JONSWAP)", Woods Hole Oceanographic Institution Contribution, No. 2911, 95 pp.

3. Bengtsson L., 1973: "Mathematical Models of Wind-Induced Circulation in a Lake", Proceeding International Symposium On Hydrology of Lakes, Helsinki, pp. 312-320.

4. Bengtsson, L., 1973: "Conclusions About Turbulent Exchange Coefficient from Model Studies", Hydrology of Lakes Symposium, Proceedings of the Helsinki Symposium, pp. 306-312.

5. Bennett, J.R., 1974: "On the Dynamic of Wind-Driven Lake Circulations", J. of Physical Oceanography, Vol. 4, pp. 404-414.

6. Blanton, J.O., 1973: "Rates of Vertical Entrainment in Stratified Lakes", Proceedings International Symposium on Hydrology of Lakes, Helsinki, pp. 301-305.

7. Blumberg, A.F., 1977: "Numerical model of Estuarine Circulation", J. Hydraulic Division, ASCE, Vol. 103, HY3, pp. 295-310.

8. Bowden, K.F., L.A. Fairbairn, and P. Hughes, 1959: "The distribution and shearing stress in a tidal current", Geophys. J. Royal Astr. Soc., Vol. 2, pp. 288-305.

9. Bowden, K.F., and P.M. Gilligan, 1971: "Characteristic features of estuaries circulation as presented in the Mersey estuary", Limn. Oceanogr., Vol. 16, pp. 490-502.

10. Boyce, F.M., 1974: "Some aspects of Great Lakes physics of importance to biological and chemical processes", J. Fish Res. Board of Canada, Vol. 31, pp. 689-730.

11. Boyce, F., F. Chiocchio, B. Eid, F. Penika, and F. Rosa, 1980: "Hypolimnion Flow Between the Central and Eastern Basins of Lake Erie During 1977", J. of Great Lakes Research, Vol. 6, No. 4, 290-306.

12. Brocks, K. and L. Krugermeyer, 1970: "The Hydrodynamic Roughness of the Sea Surface", Report No. 14 of the Institute for Radiometeorology and Marine Meteorology, University of Hamburg, 55 pp.

13. Broeker, W.S., 1965: "An application of natural radon to problems in ocean circulation", Symposium on Diffusion in Oceans and Fresh Waters, Lamont Geological Observatory, Palisades, N.Y.

14. Broeker, W.S., J. Cromwell, and Y.H. Li, 1968: "Rates of vertical eddy diffusion near the ocean floor based on measurement of the distribution of excess 222 R_n", Earth Planet. Sci. Let. 5, pp. 101-105.

15. Chow, V.T., 1959: "Open-Channel Hydraulics", McGraw-Hill Book Company, New York.

16. Csanady, G.T., 1967: "Large-Scale Motion in the Great Lakes", Journal of Geophysics Research 72, pp. 4151-4162.

17. Csanady, G.T., 1968: "Wind-Driven Summer Circulation in the Great Lakes", Journal Geophysics Research 73, pp. 2579-2589.

18. Csanady, G.T., 1972: "Response of Large Stratified Lakes to Wind", Journal Physical, Oceanography 2, pp. 3-13.

19. Cionco, R.M., 1965: "A Mathematical Model for Air Flow in a Vegetative Canopy", J. of Applied Meteorology, No. 4, pp. 517-522.

20. Cionco, R.M., 1972: "A Wind-Profile Index For Canopy Flow", Boundary-Layer Meteorology, No. 3, pp. 255-263.

21. Chung, Y. and H. Craig, 1972: "Excess-Radon and Temperature Profiles from the Eastern Equatorial Pacific", Earth Planet. Sc. Lett. 14, pp. 55-64.

22. Charnock, H. 1955: "Wind stress on a Water Surface", Quart. J. Roy. Meteor. Soc., 81, p. 639.

23. Davidson, K.L., 1974: "Observational results on the influence of stability and wind-wave coupling on momentum transfer and turbulent fluctuation over ocean waves", Boundary Layer Meteor., Vol. 6, pp. 305-331.

24. Deacon, G.R., 1957: "Wind Profiles and the Shearing Stress - an anomaly resolved", Quart. J. Roy. Meteor., Soc., No. 83, pp. 537-540.

25. Deacon, G.R. and E.K. Webb, 1962: "Interchange of properties between sea and air", The Sea, Vol. 1, Interscience, pp. 43-87.

26. Deardorff, J.W., 1972: "Parameterization of the Planetary Boundary Layer for Use in General Circulation Models", Monthly Weather Review, 100, pp. 92-106.

27. Defant, M., 1961: "Physical Oceanography", Vol. 1, Pergamon Press, New York.

28. Dobson, F.W., 1971: "Measurements of atmospheric pressure of wind-generated sea waves", J. Fluid Mech., 48, pp. 91-127.

29. Donelan, M.A., 1975, "Are Aquatic Micrometeorologists Delivering the Goods or is the Over-Water Drag Coefficient far from Constant?", Symposium on Modeling of Transport Mechanisms in Oceans and Lakes, October 1975.

30. Donelan, M.A., 1978: "A Simple Numerical Model for Wave and Wind Stress Prediction", Physical Limnology Section, Hydraulic Res. Div., Canada Centre for Inland Waters, Burlington, Can., Report No. 13.

31. Dunckel, M., L. Hasse, L. Krugermeyer, D. Schriever and J. Wucknite, 1974: "Turbulent Fluxes of Momentum, Heat and Water Vapor in the Atmospheric Surface Layer at Sea During Atex", Boundary-Layer Meteorology, 6, pp. 81-106.

32. Eid, B., 1976: "Wind-Driven Surface Currents on a Small Lake with Weed Growth", M.Eng. Thesis, McMaster University, Hamilton, Ontario.

33. Eid, B., 1979: "Review of the Physical Mechanisms of Exchange Flow Between Two Stratified Basins", Report, Dept. of Civil Eng., McMaster University, Hamilton, Ont., March 1979.

34. Eid, B., 1980: "Exchange flow between two interconnected stratified bodies of water; Part II: Model development and application to the exchange flow between Eastern and Central Basins of lake Erie", Sci. Report, Canada Centre for Inland Waters, Burlington, Ontario, June 1980.

35. Elsayed, E., 1978: "Towards a Problem-Oriented Library for the Computer Analysis of Stratified Flow Phenomena", Ph.D. Thesis, McMaster University, Hamilton, Ontario.

36. Gachter, R., 1979: "MELIMEX, an experimental heavy metal pollution study: Goals, experimental design and major findings", Schweiz. Z. Hydrol. (Swiss J. Hydrology), 41, pp. 169-176.

37. Garratt, J.R., 1977: "Review of Drag Coefficients over Oceans and Continents", Monthly Weather Review, Vol. 105, pp. 916-929.

38. Gedney, R.T. and Lick, W., 1972: "Wind-Driven Currents in Lake Erie", J. of Geophys. Res., Vol. 77, No. 15, pp. 2714-2723.

39. Gill, A.E., 1977: "The hydraulics of rotating-channel flow", J. Fluid Mech., Vol. 80, Part 4, pp. 641-671.

40. Graf, W.H., and J.P. Prost, 1980: "Aerodynamic Drag and its Relation to the Sea State: with data from Lake Geneva", Arch. Met. Geoph. Biokl., Ser. A, pp. 67-87.

41. Hamilton, P., 1975: "A numerical model of the vertical circulation of tidal estuaries and its application to the Rotterdam Waterway", Geophys. J. Royal Astr. Soc., 40, pp. 1-21.

42. Harleman, D., 1961: "Stratified Flow", in Chapter 26 in "Handbook of Fluid Dynamics", (Ed. V. Streeter), McGraw-Hill Book Company, N.Y.

43. Hesslein R., and P. Quay, 1973: "Vertical eddy diffusion studies in the thermocline of a small stratified lake", J. Fish. Res. Board of Canada, 30, pp. 1491-1500.

44. Hicks, B.B., 1972: "Some evaluations of drag and bulk transfer coefficients over water bodies of different sizes", Boundary-Layer Meteorology, Vol. 3, pp. 287-297.

45. Hicks, B.B., R.L. Drinkrow and G. Grauze, 1974: "Drag and bulk transfer coefficients associated with shallow water surface", Boundary-Layer Meteorology, Vol. 6, pp. 287-297.

46. Hsu, S.A., 1974: "A dynamic roughness equation and its application to wind stress determination at the air-sea interface", J. Physical Oceanography, 4, pp. 116-120.

47. Hutchinson, G.E., 1957: "A Treatise in Limnology", Vol. 1, J. Wiley, New York.

48. Imboden, D.M. and S. Emerson, 1976, "Study of Transport Processes Through the Sediment-Water Interface in Lakes Using Natural Radon-222", Proceedings SIL-Symposium, Amsterdam, Sept. 1976.

49. Imboden, D.M. and S. Emerson, 1978: "Natural Radon and Phsophorus as Limnologic Tracers: Horizontal and Vertical Eddy Diffusion in Greifensee", Limnol. Oceanogr., 23, pp. 23-77.

50. Imboden, D.M., B. Eid, T. Joller, M. Schurter and J. Wetzel, 1979: "Mixing in a Large Limno-Corral", Schweiz. Z. Hydrologic (Swiss J. Of Hydrology), vol. 41, No. 2, pp. 177-189.

51. Ippen, A.T., 1966, "Estuary and Coastline Hydrodynamics", Engineering Societies Momographs, McGraw-Hill Book company, N.Y.

52. James W., and Eid, B., 1976: "Hamilton Harbour Study: 1976 Field Programme", Department of Civil Engineering, McMaster University, Hamilton, Ontario, Research Report.

53. James, W., and Eid, B. 1978 a: "Spatial Distribution of the Transient Bed Boundary Condition For Small Lakes With Weeds", Canadian Journal of Civil Eng., CSCE, Vol. 5, No. 3, pp. 442-448.

54. James, W. and Eid, B., 1978 b, "A Three-dimensional Model of Hamilton Harbour Incorporating Spatial Distribution of Transient Surface Drag", Canadian J. of Civil Eng. CSCE, Vol. 5, No. 4, pp. 479-488.

55. Jassby, A., and T. Powell, 1975: "Vertical patterns of eddy diffusion during stratification in Castle Lake, California", Limnol. Oceanogr. 20, p. 530.

56. Kitaigorodiskii, S.A., 1968: "On the calculation of aerodynamic roughness of the sea surface", Izv. Atmos. Oceanic Phys., 4, pp. 498-502.

57. Kitaigorodiskii, S.A. and M.M. Zaslaviskii, 1974: "A dynamical analysis of the drag coefficients at the sea surface", Boundary Layer Meteorology, Vol. 5, pp. 53-61.

58. Kondo, J., 1975: "Air-sea bulk transfer coefficients in diabatic conditions", Boundary-Layer Meteor., Vol. 9, pp. 91-112.

59. Kouwen, N., Unny, T.E. and Hill, H.M., 1969: "Flow Retardance in Vegetated Channels", J. of the Irrig. and Drainage Div., ASCE, 95, No. ER2, pp. 6633.

60. Kouwen, N. and Unny T.E., 1973, "Flexible Roughness in Open Channels", J. Hyd. Div., ASCE 99, HY5, May 1973, pp. 9723.

61. Kraus, E.B., 1972: "Atmosphere-Ocean Interaction", Oxford Monogr. on Meteorology, Clarendon Press, 195 pp.

62. Lai, K. and I.R. Wood, 1975: "A two-layer flow through a contraction", J. of Hydraulic Res., Vol. 13, No. 1, pp. 19-33.

63. Leendertse, J.J., 1973, A Three-Dimensional Model for Estuaries and Coastal Seas", Vol. I: Principles of Computation, The Rand Corporation, R-1417-OWRT, December, 1973.

64. Leendertse, J.J., 1975: "A Three-Dimensional Model for Estuaries and Coastal Seas", Vol. II: Aspects of Computation, the Rand Corporation, R-1764-OWRT, June 1975.

65. Li, Y.H., 1973: "Vertical eddy diffusion coefficient in Lake Zurich", Schweiz. Z. Hydrol., Vol. 35, p. 1.

66. Lick, W., 1976: "Numerical Models of Lake Currents", Ecological Research Series, EPA-600/3-76-020.

67. Liggett, J.J. and C. Hadjitheodorn, 1969", Circulation in Shallow Homogeneous Lakes", J. of Hydr. Div., ASCE, 95, HY2, pp. 609-620.

68. Lith, G. and L. Bengtsson, 1971: "Wind-induced Circulation in a Lake", First International Conference on Port and Ocen Eng. Under Arctic Conditions", Trondheim, Norway 1971, pp. 893-908.

69. Long, R.R., 1954: "Some aspects of the flow of stratified fluids: Experiments with a two-fluid system", Tellus 5, No. 2, pp. 97-115.

70. Long, R.R., 1956: "Long waves in a two-layer fluid system", J. of Meteorology, Vol. 13, pp. 70-74.

71. Longuet-Higgins, M.S., 1969, "A non-linear mechanism for the generation of sea waves", Proc. Roy. Soc. London, A311, pp. 371-389.

72. McEwan, G.F., 1929: "A mathematical theory of the vertical distribution of temperature and salinity in water under the action of radiation, conduction, evaporation and mixing due to resultant convection", Bull. Scripps Inst. Oceanogr., 2, p. 197.

73. Miyake M., and M. Donelan, G. McBean, C. Paulson, F. Badgley and E. Leavit, 1970, "Comparison of turbulent fluxes over water determined by profile and eddy correlation techniques", Quart, J. Roy. Meteor. Soc., Vol. 96, pp. 132-137.

74. Mortimer, C.H., 1972: "Advances in Lake Hydrodynamics - a Selective Review", The University of Wisconsin, Milwakee, 53201, U.S.A.

75. Odd, N.V. and J.G. Rodger, 1978: "Vertical mixing in stratified tidal flows", J. Hyd. Div,, ASCE, vol. 104, HY3, pp. 337-349.

76. Officer, C.B., 1976: "Physical Oceanography of Esturaires and Associated Coastal Waters", John Wiley, N.Y.

77. Ontario Ministry of the Environment, 1974, 1975, 1976: "Hamilton Harbour Study", Technical Reports.

78. Pernir, E.R., J.M. Robertson, and R.J. Millington, 1972: "Spatial and Temporal Variation of Wind Above and Within a Soybean Canopy", Agricultural Meteorology, 10, pp. 443-465.

79. Phillips, O.M., 1966: "Dynamics of the Upper Ocean", Cambridge University Press, Cambridge, England.

80. Plate, E.J. and A. Quraishi, 1965: "Modeling of Velocity distribution Inside and Above Tall Crops", J. Applied Meteorology, Vol. 4, p. 400.

81. Platzman, G.W., 1963: "The Dynamic Prediction of Wind Tides on Lake Erie", Meteorological Monogr. 4(26), 44 pp.

82. Pritchard, D.W., 1956: "The dynamic structure of a coastal plain estuary", J. Har. Res., Vol. 15, pp. 33-42.

83. Rouse, H., 1965: "Critical Analysis of Open Channel Resistance", J. of Hydro Division, ASCE, 91, HY4, pp. 4387.

84. Sambuco, E., and J.A. Whitehead, 1976: "Hydraulics control by a wide weir in a rotating fluid", J. Fluid Mech., Vol. 73, Part 3, pp. 521-528.

85. Sayre, W.W. and M.L., Albertson, 1961: "Roughness Spacing in Rigid Open Channels", J. Hyd. Div., ASCE, 87, HY3, p. 2823.

86. Scarborough, J.B., 1966: "Numerical Mathematical Analysis", John Hopkins Press, 6th ed.

87. Schijf and Schonfeld, 1954: "Theoretical considerations on the motion of salt and fresh water", Proc. Minnesota Inter. Hydraulics Convention, Minneapolis.

88. Schlichting, H., 1968: "Boundary Layer Theory", McGraw-Hill Book Company, N.Y.

89. Schmidt, W., 1917: "Wirkungen der ungeordneten Bewegungen inn Wasser de Meere und Seen", Ann. Hydrogr. Marit. Meteorol., Vol. 45, pp. 367-431.

90. Sheppard, P.A., O.T. Tribble and J.R. Garratt, 1972: "Studies of Turbulence in the Surface Layer Over Water (Lough Neagh), Part I", Quart. J. Roy. Meteor. Soc., Vol. 98, pp. 627-641.

91. Simons, T.J., 1971: "Development of numerical models of Lake Ontario", Proc. 14th Conf. Great Lakes Res. Int. Assoc. Great Lakes Res., pp. 654-669.

92. Simons, T.J., 1972: "Development of numerical model of Lake Ontario, Part 2", 15th Conf. Great Lakes Res. Int. Assoc. Great Lakes Res.

93. Simons, T.J., 1973: "Development of Three-Dimensional Numerical Models of the Great Lakes", Scientific Report No. 12, Canada Center for Inland Waters, Burlington, Ontario.

94. Simons, T.J., 1976: "Continuous dynamical computations of water transports in Lake Erie for 1970", J. Fish. Res. Board of Canada, Vol. 33, No. 3, pp. 371-384.

95. Simons, T.J., 1978: "Wind-driven circulations in the southwest Baltic", Tellus, Vol. 30, pp. 272-283.

96. Smith, S.D., 1973: "Thrust-anemometer measurements over the sea re-examined", Rep. 73.1, Bedford Inst. Oceanogr., 23 pp.

97. Smith, S.D. and E.G. Banke, 1975: "Variation of the sea surface drag coefficient with wind speed", Quarterly Journal of the Royal Meterological Society 101, pp. 665-673.

98. Stewart, R.W., 1974: "The air-sea momentum exchange", Boundary Layer Meteor., Vol. 5, pp. 151-167.

99. Stommel, H. and H. Farmer, 1952: "Abrupt change in width in two-layer open channel flow", J. Marine Res., Vol. 11, No. 2, pp. 205-214.

100. Taylor, G.I., 1916: "Skin Friction of the Wind on the Earth's Surface", Proc. Roy. Soc. London, A92, pp. 196-199.

101. Taylor, P.A., P.R. Gent, 1976: "Some numerical solutions for turbulent boundary layer flow above fixed, rough wavy surfaces", Geophys. J. Roy. Astron. Soc., Vol. 44, pp. 177-201.

102. Taylor, P.A., and P.R. Gent, 1978: "A numerical investigation of variation in the drag coefficient for air flow above water surface", Quart. J. Roy. Met. Soc., Vol. 104, pp. 979-988.

103. U.S. Army Coastal Engineering Research Centre, "Shore Protection Manual", Vol. I, 1973.

104. Von Karman, T., and M.A. Biot, 1940: "Mathematical Methods in Engineering", McGraw-Hill Book Company, New York.

105. Wellander, P., 1957: "Wind action on shallow sea, some generalizations of Ekman's Theory", Tellus 9, pp. 47-52.

106. Wellander, P., 1968: "Wind-driven circulation in one and two-layer oceans of variable depth", Tellus 20, pp. 1-15.

107. Wellander, P., 1968: "Theoretical forms for the vertical exchange coefficients in a stratified fluid with application to lakes and seas", Acta Reg. Soc. Sci. Litt., Gothoburgensis, Geophys. 1, 26 pp.

108. Whitehead, J.A., A. Leetma and R.A. Knox, 1974: "Rotating hydraulics of strait and sill flows", Geophys. Fuild Dyn., Vol. 5, pp. 101-126.

109. Wood, 1968: "Selective withdrawal from a stably stratified fluid", J. Fluid Mech., Vol. 32, pp. 209-223.

110. Wood, 1969: "The analysis of the flow of layered fluids", 13th Congress IAHR, Kyoto, Japan, Vol. 2, pp. 271-280.

111. Wu, J., 1968: "Laboratory studies of wind-wave interactions" J. Fluid Mechanics, ASCE, Vol. 34, Part 1, pp. 91-111.

112. Wu, J., 1969: "Wind stress and surface roughness at air-sea interface", J. Goephys. Res., Vol. 74, No. 2, pp. 444-445.

113. Zubkovskii, S.L., and T.K. Kravchenko, 1967: "Direct measurements of some turbulence in the near-water layer", Izv. Atmos. Oceanic. Phys., Vol. 3, pp. 127-135.

APPENDIX

Wave Prediction in Deep and Shallow Waters

In this study we have used the significant wave method originally introduced by Sverdrup and Munk in 1947 and revised by Bretschneider in 1952 and 1958 with additional empirical data. This predictive relationship is now called the Sverdrup–Munk–Bretschneider (SMB) method (U.S. Army, 1973).

This simplified wave prediction scheme is based on the assumption that the waves being considered are entirely due to a wind blowing at constant speed and direction for a specific fetch and duration.

SMB method for Prediction of waves in deep water:

The significant wave height H, and significant wave period T for given wind speed, fetch and duration are given by:

$$[1'] \qquad \frac{gH}{U^2} = 0.283 \tanh \left[0.0125 \left(\frac{gF}{U^2}\right)^{0.42}\right]$$

$$[2'] \qquad \frac{gT}{2\pi U} = 1.2 \tanh \left[0.077 \left(\frac{gF}{U^2}\right)^{0.25}\right]$$

$$[3'] \qquad \frac{gt}{U} = K \exp\left\{\left[A \left(\ln \frac{gF}{U^2}\right)^2 - B \ln \frac{gF}{U^2} + C\right]^{1/2} + D \ln \frac{gF}{U^2}\right\}$$

The above equations are dimensionally consistent.

where: H = wave height

T = wave period (sec)

U = wind speed

F = wind fetch (the distance from the forecasting point to the opposite shore, measuring along the wind direction)

t = minimum duration required to establish steady-state generation for a particular wind speed and length of fetch

K = 6.5882

A = 0.0161

B = 0.3692

C = 2.2024

D = 0.8798

g = gravitational acceleration

In order to use equations (1) and (2) correctly, the actual wind duration ta should be more than or equal to the minimum duration. If ta<t, the significant wave parameters are functions of wind speed and the limiting duration t, rather than functions of wind speed and fetch length. In this case calculate the corresponding fetch ($F_{\quad}$) from equation (3'), then use this fetch to calculate wave height and period from equations (1') and (2').

For simplification, the wind is assumed to blow over the lake for a time long enough so that the wind durations are bigger than minimum durations required to satisfy the above equations. The above assumption seems reasonable especially when dealing with small lakes (fetchs<10 km.) and for small wind speed (less than 10 meters/sec).

Wave prediction for shallow water

If $d/T < 2.5$ ft/sec^2, where d is the water depth, then the wave effectively "feels the bottom" and the depth and bottom friction should enter as additional factors in the wave forecasting equations. Bretschneider found that the best agreement between wave data and numerical methods was obtained when a bottom friction factor of $f = 0.01$ was selected (Ippen 1966). This f is also called "a calibration friction factor" which would take into account other influential factors not normally included in the friction factor term. The quasi-empirical-quasi-theoretical relationships established by Bretschneider in 1953 are used for wind-wave generation in shallow water with constant depth:

$$[4'] \quad \frac{gH}{U^2} = 0.283 \tanh\left[0.578\left(\frac{gd}{U^2}\right)^{0.75}\right] \tanh \frac{0.0125\left(\frac{gF}{U^2}\right)^{0.42}}{\tanh 0.578\left(\frac{gd}{U^2}\right)^{0.75}}$$

$$[5'] \quad \frac{gT}{2\pi U} = 1.20 \tanh\left[0.520\left(\frac{gd}{U^2}\right)^{0.375}\right] \tanh \frac{0.077\left(\frac{gF}{U^2}\right)^{0.25}}{\tanh 0.520\left(\frac{gd}{U^2}\right)^{0.375}}$$

The above equations can be extended to a bottom of constant slope or irregular bottom topography, by segmenting the bottom into elements, each element having a mean depth assumed to be constant.

In the present numerical model wave characteristics (H & T) are first calculated for deep water (equation 1', 2'). If d/T^2 is greater than 2.5 ft/sec^2, then the computed wave height and wave period are

correct, otherwise apply equations (4') and (5') for shallow water wave prediction.

Then the procedure is to calculate wave clerity c:

[6'] $$c = L/T$$

The wave length L can be obtained from the implicit equation:

[7'] $$L = \frac{gT^2}{2\pi} \tanh \frac{2\pi d}{L}$$

for deep water

$$\tanh \left(\frac{2\pi d}{L}\right) = 1$$

[8'] $$L_o = \frac{gT^2}{2\pi}$$

Thus, we have a complete set of equations for estimating wave characteristics in both deep and shallow water. These can then be used in computing wind shear stress over the water surface in a lake as previously mentioned.

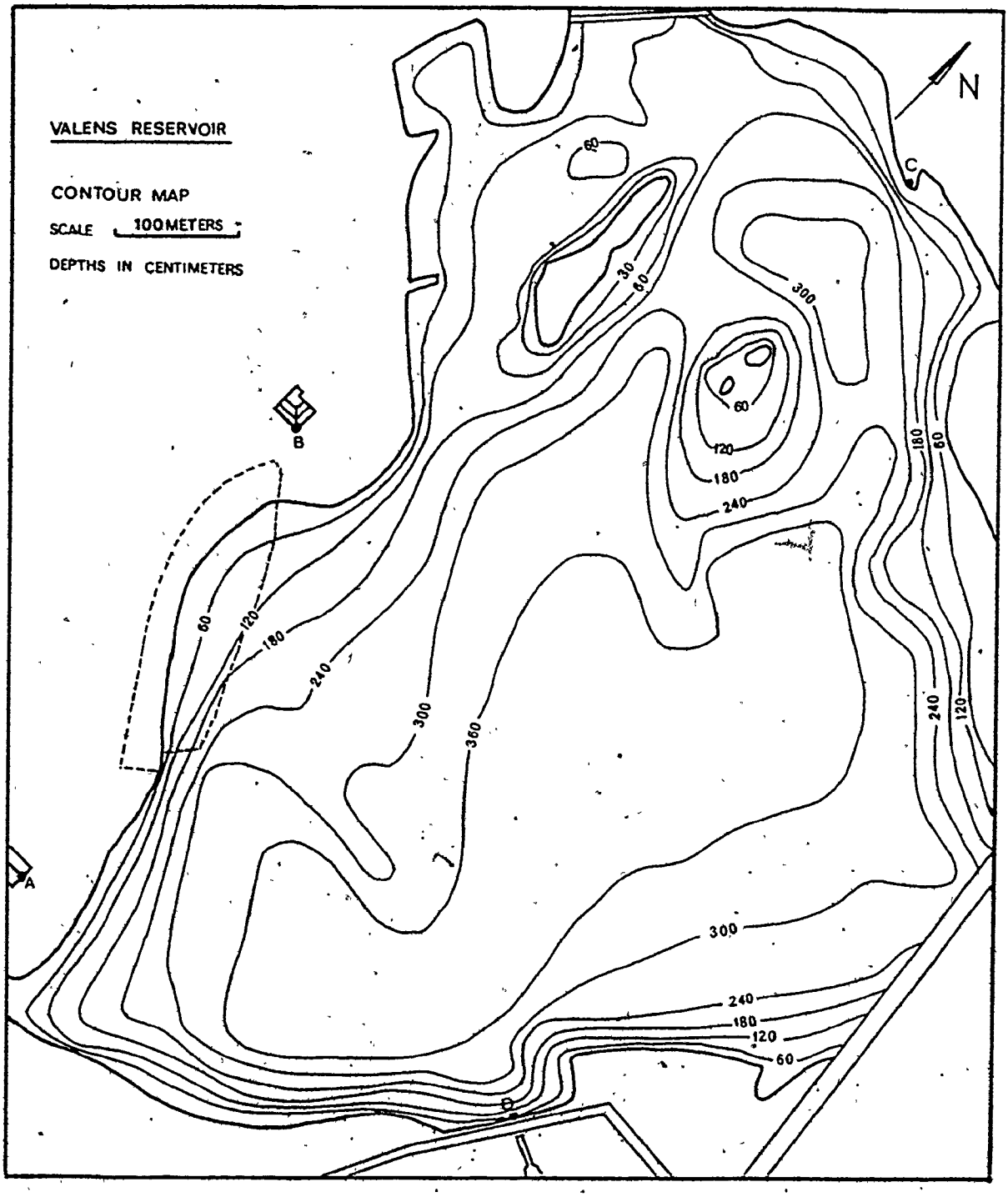

Figure A.1: Valens Reservoir bottom topography

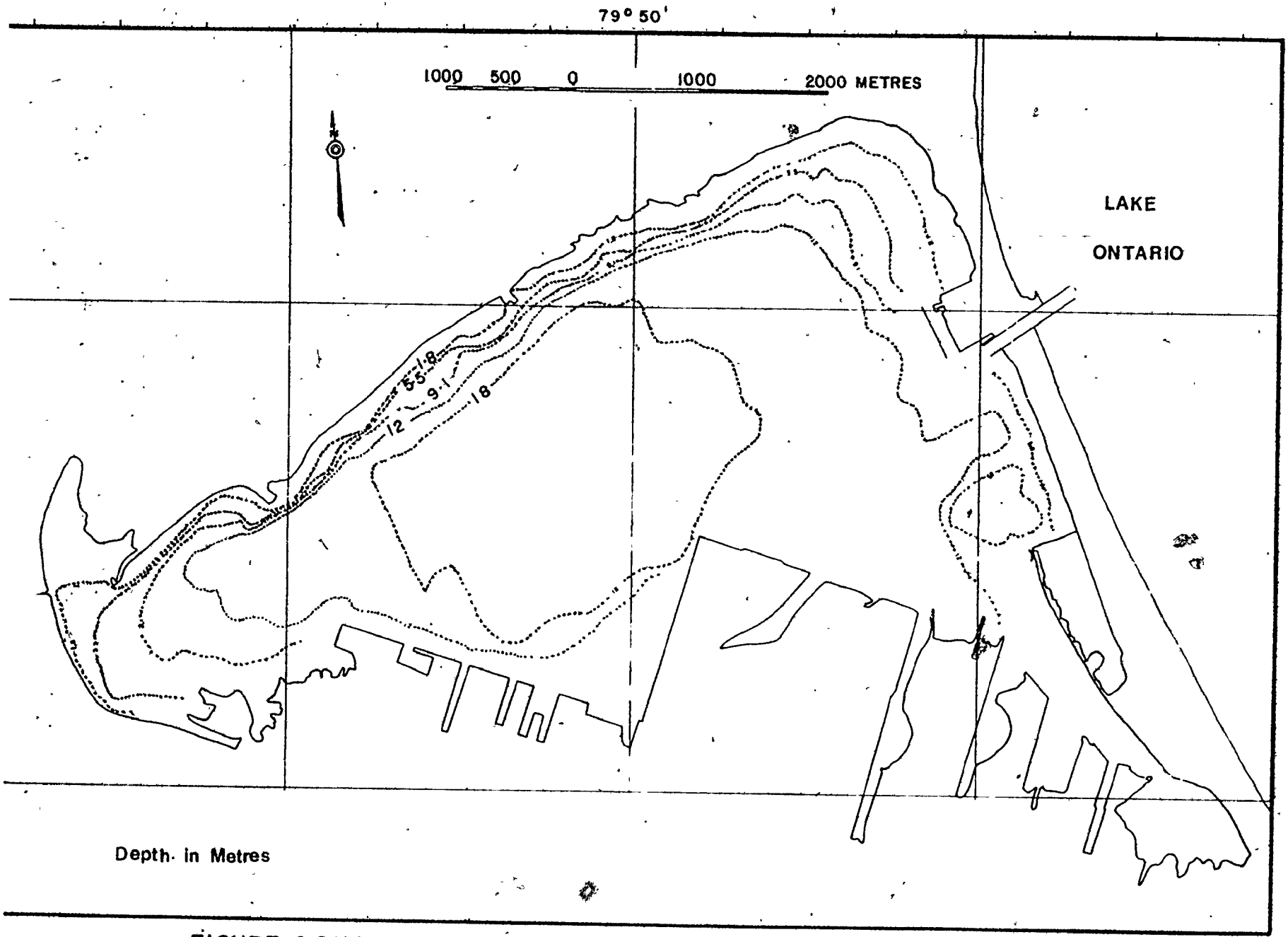

FIGURE A.2 HAMILTON HARBOUR

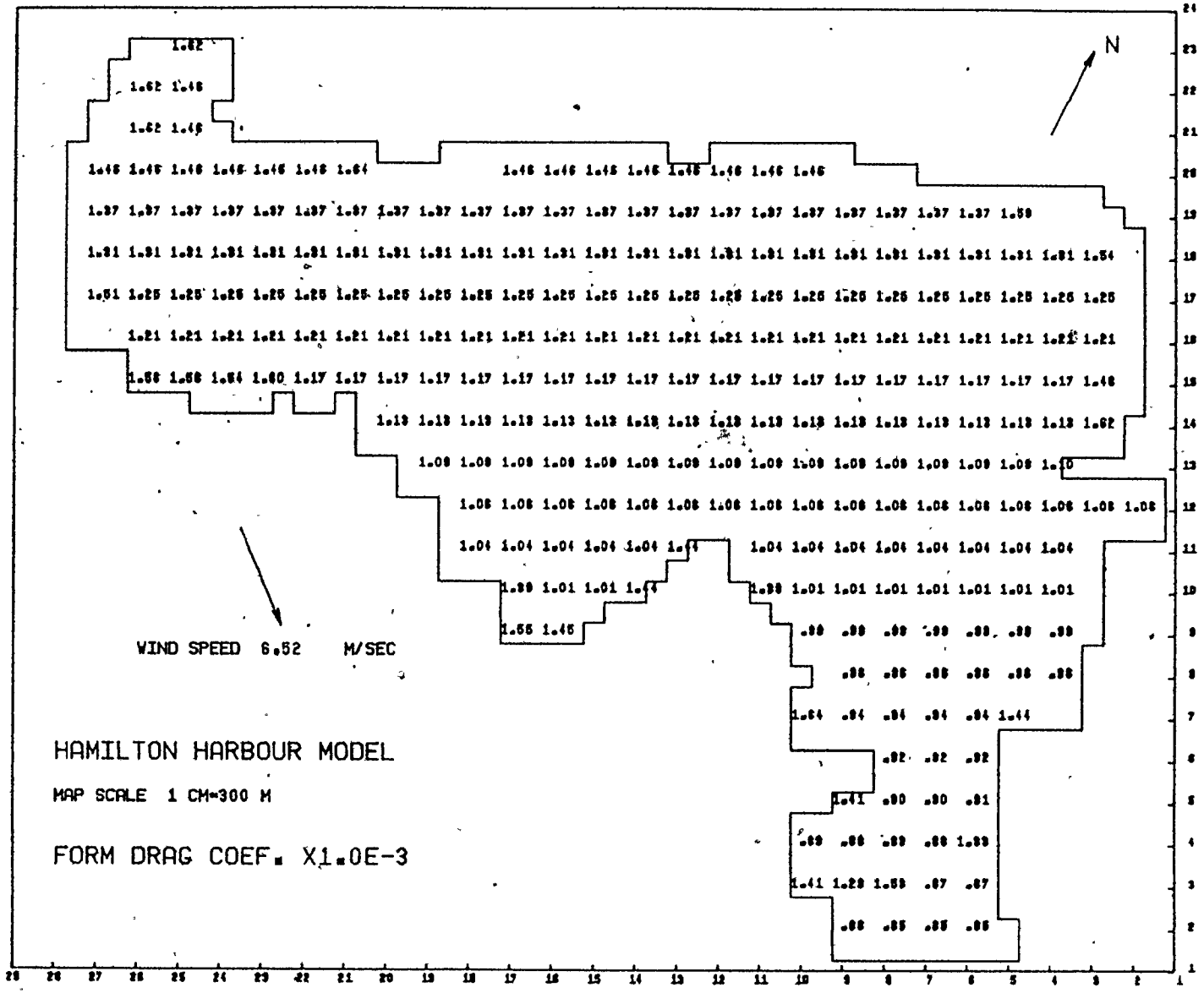

Figure A.4: Spatial variation of form drag coefficient in Hamilton Harbour (A-Model)

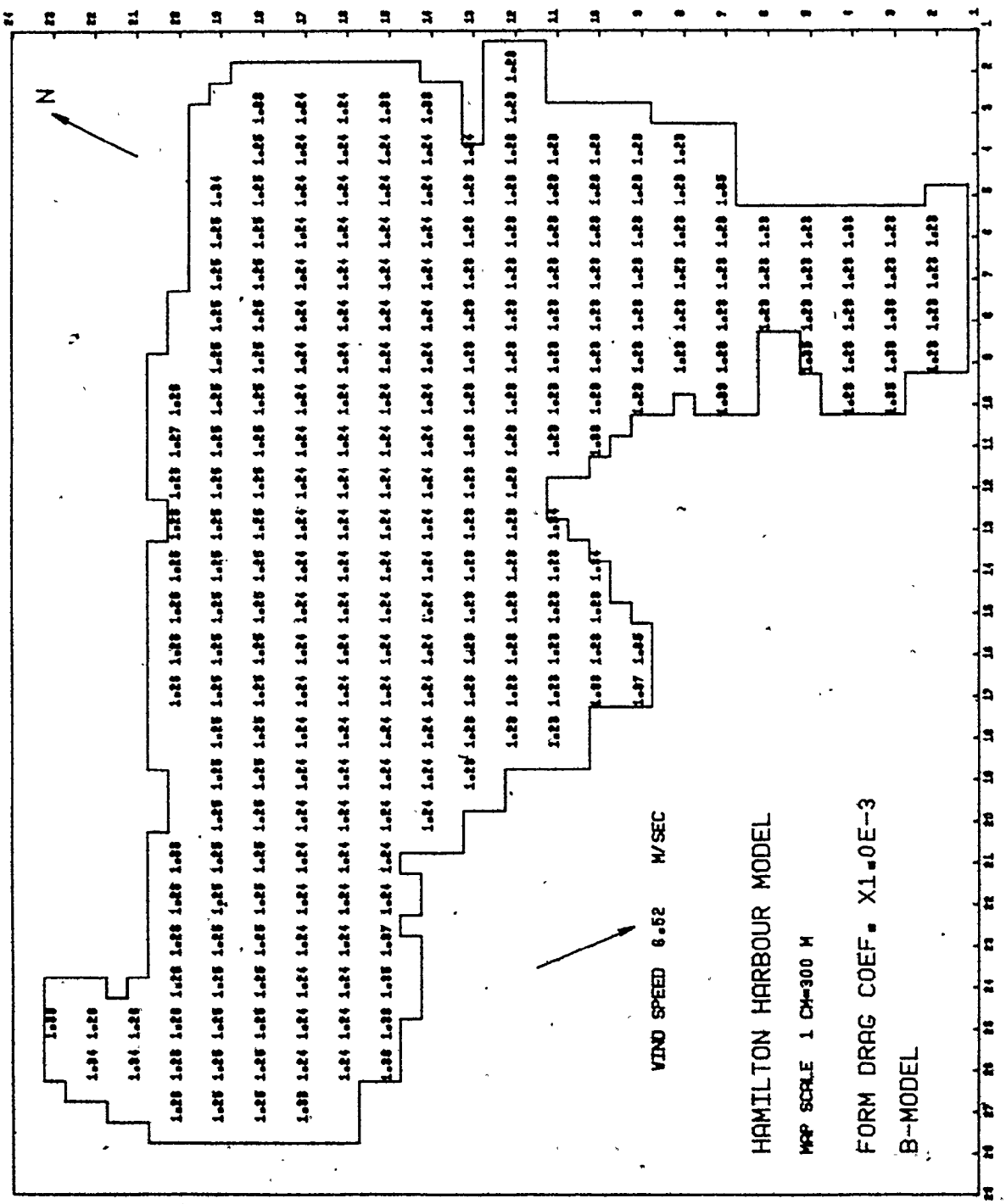

Figure A.5: Form drag coefficient in Hamilton Harbour (B-Model)

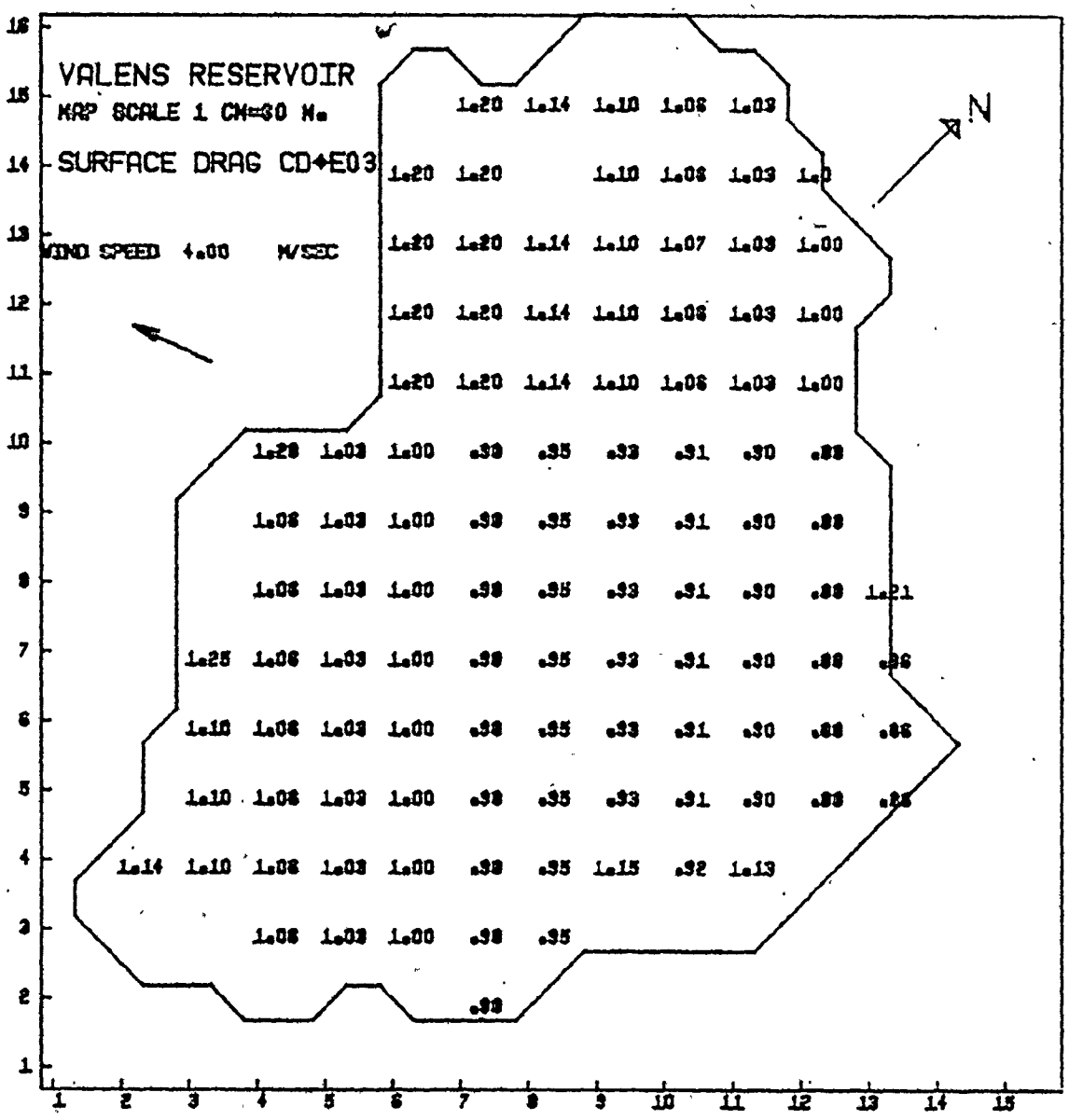

Figure A.6: Form drag coefficient in Valens Reservoir (A-Model)

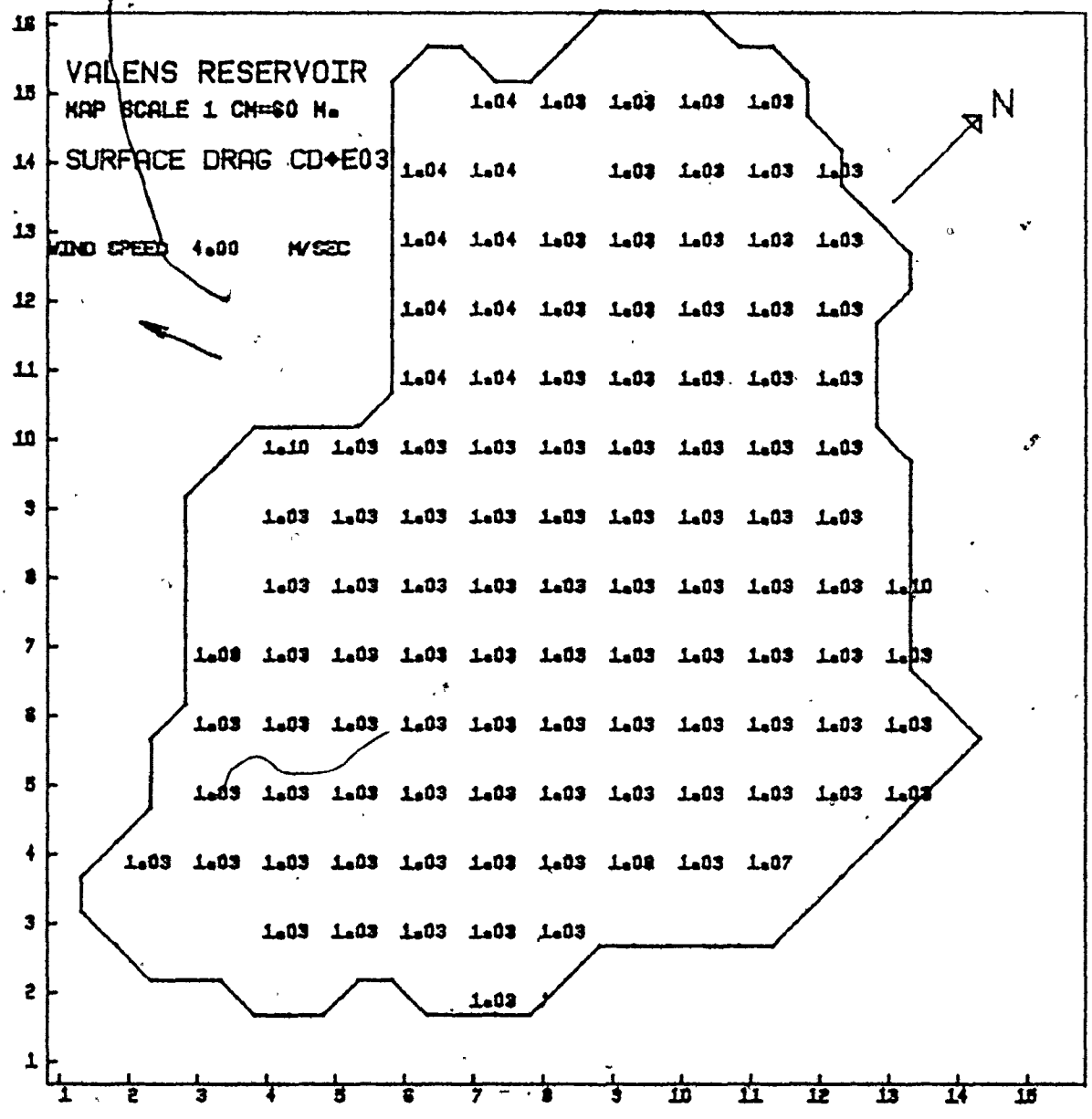

Figure A.7: Form drag coefficient in Valens Reservoir (B-Model)